Universität Stuttgart

Institut für Wasser- und Umweltsystemmodellierung

Mitteilungen

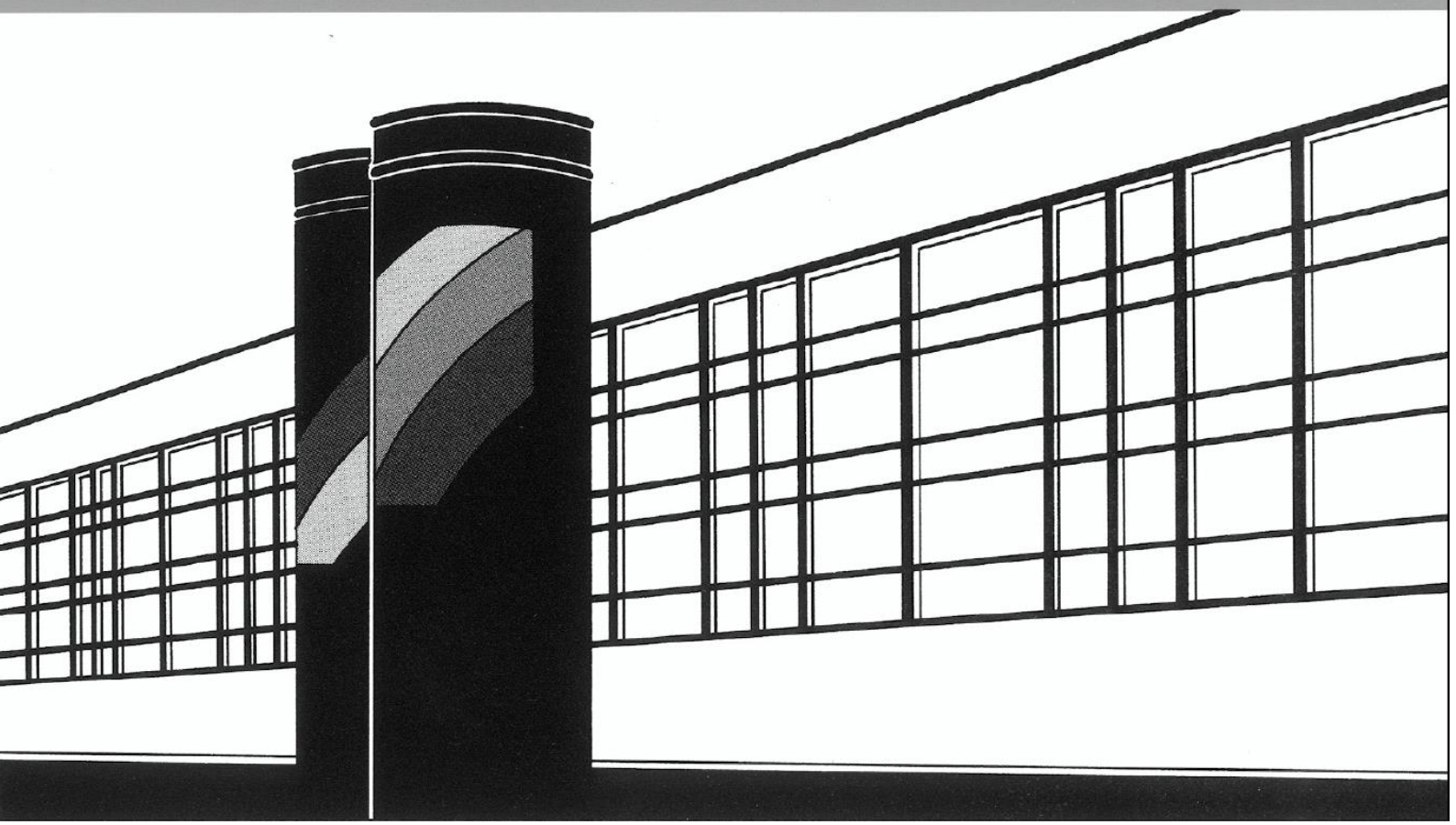

Heft 301 Dhiraj Raj Gyawali

Development and parameter estimation of conceptual snow-melt models using MODIS snow-cover distribution

Development and parameter estimation of conceptual snow-melt models using MODIS snow-cover distribution

von der Fakultät Bau- und Umweltingenieurwissenschaften
der Universität Stuttgart zur Erlangung der Würde eines
Doktor-Ingenieurs (Dr.-Ing.) genehmigte Abhandlung

vorgelegt von
Dhiraj Raj Gyawali
aus Kathmandu, Nepal

Hauptberichter:	Prof. Dr. rer. nat. Dr.-Ing. András Bárdossy
Mitberichter:	Prof. Dr. Jan Seibert

Tag der mündlichen Prüfung: 01. August 2023

Institut für Wasser- und Umweltsystemmodellierung
der Universität Stuttgart
2023

Heft 301

Development and parameter estimation of conceptual snow-melt models using MODIS snow-cover distribution

von
Dr.-Ing.
Dhiraj Raj Gyawali

Eigenverlag des Instituts für Wasser- und Umweltsystemmodellierung
der Universität Stuttgart

D93 Development and parameter estimation of conceptual snow-melt models using MODIS snow-cover distribution

Bibliografische Information der Deutschen Nationalbibliothek
Die Deutsche Nationalbibliothek verzeichnet diese Publikation in der Deutschen Nationalbibliografie; detaillierte bibliografische Daten sind im Internet über http://www.d-nb.de abrufbar

Gyawali, Dhiraj Raj:
Development and parameter estimation of conceptual snow-melt models using MODIS snow-cover distribution, Universität Stuttgart. - Stuttgart: Institut für Wasser- und Umweltsystemmodellierung, 2023

(Mitteilungen Institut für Wasser- und Umweltsystemmodellierung, Universität Stuttgart: H. 301)
Zugl.: Stuttgart, Univ., Diss., 2023
ISBN 978-3-910293-05-2
NE: Institut für Wasser- und Umweltsystemmodellierung <Stuttgart>: Mitteilungen

Herausgegeben 2023 vom Eigenverlag des Instituts für Wasser- und Umweltsystem-modellierung

Druck: P+K Solutions GmbH & Co. KG, Stuttgart

Acknowledgement

I would like to express my sincere gratitude to all those who have been instrumental in the successful completion of my doctoral journey.

First and foremost, I extend my deepest appreciation to my supervisor Prof. Dr. rer. nat. Dr.-Ing. András Bárdossy, whose unwavering trust, guidance, and expertise have been invaluable throughout this research. His mentorship has shaped not only the trajectory of my academic work but also my personal growth as an independent researcher. I am also grateful to him for providing the resources and environment conducive to scholarly exploration at the Department of Hydrology and Geohydrology, nurturing an atmosphere of intellectual curiosity and discussion, which helped me a lot in refining my work.

I am very thankful to Prof. Dr. Jan Seibert for thoroughly and critically going through my dissertation and providing insightful feedback and constructive criticism, which has significantly enriched the quality of this study.

I am very thankful to Prof. Dr.-Ing Holger Steeb for his valuable time and patience as the doctoral committee chair and his unwavering support despite his busy schedule.

I would like to acknowledge the International Doctoral Program Environment Water (ENWAT) at the University of Stuttgart for providing an academic framework for my doctoral research. Furthermore, sincere thanks to Dr.-Ing. Gabriele Hartmann, the course director of the ENWAT program, for her continued support since the beginning of my PhD journey.

I extend my appreciation to Dr. rer. nat. Jochen Seidel for his lead in facilitating scientific discussion and maintaining a healthy working aura in the department. Sincere thanks to Ms. Astrid Lemp, as my unofficial 'stress counsellor' and admin-/bureaucratic support throughout my study.

I express special gratitude to my colleagues Faizan Anwar, Masoud Mehrvand, Abbas El Hachem, Dr.-Ing Dirk Schlabing and Dr.-Ing Ehsan Modiri, for all the stimulating discussions regarding science, philosophy and life. Sincere thanks to my colleagues Micha Eisele, Bushra Amin, Fahad Ejaz, Iman Fatehi, Claudia Teutsch, Ning Wang and others for the camaraderie and shared experiences. Your support has been a source of inspiration and motivation. I also extend my thanks to Dr.-Ing Pawan Thapa for introducing me to the world of Prof. Bárdossy and for his constant encouragement.

Heartfelt thanks go to my wife and my best friend Prativa Khanal, and our darling daughter Nyrah Gyawali for their patience, unwavering support, encouragement, and understanding throughout and especially during the challenging moments of this academic pursuit. Your belief in me has been my pillar of strength.

I am very grateful to my mother Anju Dixit, my father Dhruba Raj Gyawali and my brother Dr. Bigyan Gyawali, who have always and forever taught and encouraged me to persevere, yearn for more and aim high.

Last but not the least, I want to express my gratitude to the German Academic Exchange Service (DAAD) whose financial support made this research possible. Furthermore, thanks to the International Office of the University of Stuttgart for awarding me the Christian Bürkert Stipendium to support my PhD towards the end.

This journey would not have been possible without the encouragement, guidance, and support of these individuals and institutions. Thank you all for being an integral part of this significant chapter in my academic life.

Contents

List of Figures

List of Tables

List of Abbreviations

AVHRR	Advanced Very-high-resolution Radiometer
BS	Brier Score
BW	Baden-Württemberg
DEM	Digital Elevation Model
E-OBS	European Observations
ECA&D	European Climate Assessment and Dataset
EDK	External Drift Kriging
ET	Evapo-transpiration
FAO-LCCS 2	Food and Agriculture Organization - Land Cover Classification System
fSCA	Fractional Snow Cover Area
GLS	Generalized Least Squares
HBV	Hydrologiska Byråns Vattenbalansavdelning
HRU	Hydrologic Response Unit
LAI	Leaf Area Index
LIDAR	Light Detection and Ranging
LOOCV	Leave-one-out cross validation
LST	Land Surface Temperature
MLR	Multiple Linear Regression
MODIS	Moderate-resolution Imaging Spectroradiometer
NDSI	Normalized Difference Snow Index
NOAA	National Oceanic and Atmospheric Administration
NSE	Nash-Sutcliffe Efficiency
OLS	Ordinary Least Squares
RK	Residual Kriging
RMSE	Root Mean Square Error
ROPE	Robust Parameter Estimation
RS	Remote Sensing
SAR	Synthetic Aperture Radar
SCA	Snow Cover Area
SCD	Snow Cover Duration
SCMD	Snow Cover Melt Date
SCOD	Snow Cover Onset Date
SDC	Snow Depletion Curve

SRM	Snowmelt Runoff Model
SWE	Snow Water Equivalent
TI	Temperature Index
TIR	Thermal Infrared
TVX	Temperature Vegetation Index
USGS	United States Geological Survey
VIIRS	Visible Infrared Imaging Radiometer Suite
WClim	WorldClim

Abstract

Snow is one of the most important components of the hydrological cycle, providing temporary reservoir of available water during accumulation phase to be released for the downstream during ablation, thereby governing the hydrological variations in the mountainous regions. Given the crucial relevance to mountain hydrology and high sensitivity to climate change, it is highly pertinent to have a solid understanding of the seasonal snow evolution and subsequent estimation of the available water for not only the water resources development trajectories, but also to better plan against snow-related disasters. However, with a high spatio-temporal variability observed in the inherent snow-related processes owing to the complex topographical and climatological variations in the snow-dominated regions, reliable representations of spatial distribution of seasonal snow and subsequent snow-melt remain critical challenges for monitoring the seasonal evolution of snow and in turn for any hydrological estimations in these regions.

Though snow-dominated regimes are often associated with data scarcity, different measurement and monitoring techniques ranging from expanded observational station network and dedicated research sites, to Remote Sensing (RS) based snow-cover monitoring are currently in place to understand and quantify the snow-related processes. However, the spatio-temporal heterogeneity in the mountains limits the reliable extrapolation of observational data, which is also the case with experimental sites, rendering these data as non-representative as they are highly prone to localized influences. Likewise, lack of snow-depth information and persistent cloud cover often limit the standalone usage of RS data. Snow-melt modeling approaches, thus remain the widely accepted tools in practice to simulate the snow processes and the resulting contribution to discharge. Depending upon the simulation strategy, these models are also constrained with data availability and the degree of detail required for simulation to represent the underlying processes. Complex, data intensive physically based models are more accurate but are often restricted by the lack of detailed input, whereas conceptual models are more prone to uncertain predictions due to simplistic representation of the underlying processes driven by non-representative meteorological data. The trade-off between the model complexity given the data unavailability, especially in snow-melt modeling, thus requires a flexible model structure that can accommodate different details of model complexities in regimes with different levels of data availability.

Furthermore, to deal with the uncertainties associated with the estimated model parameters, it is very important to critically select a calibration variable that offers spatio-temporal representation and reasonable amount of information at an implementable spatial detail. Given the data limitations, the choice of the calibration data and the appropriateness of calibration routine can further help avoid parameter compensation. This compensation normally happens in the absence of a dedicated calibration routine and a representative calibration

variable, where the calibration approach tries to match the whole simulation to the non-representative data by imparting compensation within the parameter subsets representing the sub-processes. Remote sensing based snow-cover images have been increasingly incorporated into modeling context in recent years that provide a plausible alternative to ground based data especially in the data scarce mountain regions as they contain a very relevant information on the spatio-temporal distribution of snow. A crucial research gap was thus identified on how to best utilize the pixelwise qualitative information from these images to improve the snow-melt modeling approaches thereby reducing the uncertainties in snow-processes simulation.

This thesis introduces a **novel standalone calibration technique** using MODIS snow-cover images for calibration of independent conceptual snow-melt models, thereby estimating model parameters from individual or sets of MODIS images. The aim was to exploit the **pixel-wise binary ('snow', 'no snow') information** that MODIS snow-cover images offer on a daily scale at a reasonable spatial resolution. Switzerland and Baden-Württemberg were selected as study snow regimes, with the former representing partly longer duration snow and the latter associated with a shorter duration. The standalone calibration approach was evaluated on different extensions of conceptual snow-melt models in different layers of scrutiny. The extended snow-melt models were devised incorporating factors governing the different aspects of snow accumulation and ablation processes to evaluate the improvement in the simulation of snow-cover distribution with minimal data input for future implementation in data scarce regions. All the calibrated models adeptly simulated the snow-cover distribution and the best performing model, i.e. the radiation-based model, was identified. An upside to this approach is that it allows future implementation in conjunction with any snow-melt models that can simulate snow-cover distribution, in reliably identifying the model parameters. Furthermore, the selection of binary MODIS information as calibration variable permits relatively complex snow-melt modules to be calibrated with **more robustness** as a result of **reduced uncertainty** associated with the calibration data.

Different simulation thresholds were also identified for defining the calibration data (NDSI thresholds), selecting the images for calibration (cloud cover thresholds), and reclassifying the snow water equivalent (SWE) outputs to snow-cover information (SWE thresholds). The results of the sensitivity analysis of this calibration algorithm align with various studies carried out in snow-melt modeling. The approach was found to exhibit lesser sensitivity towards cloud thresholds, meaning the flexibility to calibrate on patches of snow and no-snow in the images. This thesis further discusses the selection of images or a set of images representing a period during snow season for calibration in different regimes. It was observed that the estimated parameters based on calibration in different periods within the season were transferable to other periods, with the ones estimated from melt season images in longer duration snow conditions and the ones from onset season images in shorter duration snow conditions observed to be more robust.

Similarly, another important goal of this thesis was to evaluate the efficacy of the calibration approach on the resulting SWE and its implications on the hydrological discharge at catchment level. For this five catchments namely Reuss at Seedorf, Thur at Andelfingen and Aare at Brienzweiler in Switzerland, and Neckar at Rottweil and Horb in Baden-Württemberg,

were selected. The hydrological simulation and the comparison was done based on two hydrological models; the standard HBV model calibrated solely on discharge and a modified HBV model designed to receive the melt from the snow-melt model calibrated on MODIS images, as standalone input. It was observed that the standalone approach reduced the uncertainty in the representation of snow-accumulation and melt processes, HBV calibrated solely on discharge exhibited parameter compensations with other non-snow parameters in the snow routine, thereby leading to uncertain snow processes simulation. This uncertainty becomes very critical in reliably understanding the underlying sub-processes, as even if the discharge simulation is found to be reliable, it leads to **right for wrong reasons** conclusion. The estimation of the parameters solely from any MODIS information not only eliminated the reliance on a single calibration variable 'discharge' which is already an availability constraint in the higher altitudes but also preserves the spatial heterogeneity at a more regional level.

In addition, the standalone melt outputs to the modified HBV was found to further increase the reliability of discharge prediction and for **a right reason** as the snow processes are adeptly represented by process-informed parameters. Moreover, the individual calibration parameter space is also reduced for both snow-melt and the truncated hydrological models, which favors a reduced equifinal parameter space, thereby contributing to reduced modeling uncertainties in either cases. This further allows additional relevant parameterization aided by better computational efficiency while calibrating the snow-melt models in contrast to increased complexities when done with a hydrological model calibrated on discharge alone. The independent calibration thus, facilitates a dedicated simulation of snow processes without passing the snow simulation through a more complex hydrological model. This further holds a crucial relevance for discharge simulation in areas with episodic days of snow, where the snow processes can be calibrated quickly on images without having to calibrate the entire hydrological model.

The whole concept was replicated in mimicking a data scarce scenario in the Bavarian state of Germany. The snow-melt model was driven by freely available global meteorological inputs downscaled to match MODIS resolutions. In this case as well, the snow-cover distribution was well simulated and the resulting melt improved the hydrological predictions at catchment level. This highlights the applicability of the MODIS based calibration in data scarce regions.

The thesis concludes that the addition of snow-cover information in estimating the parameters of snow-melt models utilizing the snow/no-snow information and a modest and globally available input data demand, facilitates a simple, spatially flexible approach to calibrate snow-cover distribution in mountainous areas with reasonably accurate precipitation and temperature data, especially in data scarce regions. Furthermore, this also allows the possibility for immediate verification with point measurements, especially crucial during episodic days of snow. The uncertainty reduction with snow-cover estimation and subsequently discharge prediction is a critical value addition in improving the conceptualization of snow-melt model routines which in turn complements the distributed hydrological modeling framework.

Kurzfassung

Schnee ist eine der wichtigsten Komponenten des Wasserkreislaufs, da er während der Akkumulationsphase ein temporäres Reservoir an verfügbarem Wasser bildet, das während der Ablation für den Abfluss freigegeben wird und so die hydrologischen Schwankungen in Bergregionen bestimmt. Angesichts der entscheidenden Bedeutung für die Hydrologie in Gebirgsregionen und der hohen Empfindlichkeit gegenüber dem Klimawandel ist ein solides Verständnis der jahreszeitlichen Schneeentwicklung und der anschließenden Abschätzung des verfügbaren Wassers nicht nur für die Entwicklung der Wasserressourcen, sondern auch für eine bessere Planung gegen schneebedingte Katastrophen von großer Bedeutung. Da jedoch aufgrund der komplexen topografischen und klimatologischen Variationen in den schneedominierten Regionen eine hohe räumlich-zeitliche Variabilität bei den schneebezogenen Prozessen zu beobachten ist, bleiben zuverlässige Darstellungen der räumlichen Verteilung des saisonalen Schnees und der anschließenden Schneeschmelze eine kritische Herausforderung für die Überwachung der saisonalen Entwicklung des Schnees und damit für alle hydrologischen Schätzungen in diesen Regionen.

Obwohl schneedominierte Regime oft mit Datenknappheit verbunden sind, werden derzeit verschiedene Mess- und Überwachungstechniken eingesetzt, die von einem erweiterten Netz von Beobachtungsstationen und speziellen Forschungsstandorten bis hin zur fernerkundungsbasierten Überwachung der Schneedecke reichen, um die schneebezogenen Prozesse zu verstehen und zu quantifizieren. Die räumlich-zeitliche Heterogenität in den Bergen schränkt jedoch die zuverlässige Extrapolation von Beobachtungsdaten ein, was auch bei Versuchsstandorten der Fall ist, so dass diese Daten nicht repräsentativ sind, da sie sehr anfällig für lokale Einflüsse sind. Ebenso schränken das Fehlen von Informationen über die Schneehöhe und die anhaltende Bewölkung die eigenständige Nutzung von Fernerkundungsdaten ein. Modellierungsansätze für die Schneeschmelze bleiben daher die in der Praxis weithin akzeptierten Werkzeuge zur Simulation der Schneeprozesse und des daraus resultierenden Beitrags zum Abfluss. Je nach Simulationsstrategie sind diese Modelle auch durch die Datenverfügbarkeit und den für die Simulation erforderlichen Detaillierungsgrad zur Darstellung der zugrunde liegenden Prozesse eingeschränkt. Komplexe, datenintensive physikalisch basierte Modelle sind genauer, werden aber oft durch den Mangel an detaillierten Eingangsdaten eingeschränkt, während konzeptionelle Modelle aufgrund der vereinfachten Darstellung der zugrunde liegenden Prozesse, die durch nicht repräsentative meteorologische Daten gesteuert werden, anfälliger für unsichere Vorhersagen sind. Der Kompromiss zwischen der Modellkomplexität und der Nichtverfügbarkeit von Daten, insbesondere bei der Modellierung der Schneeschmelze, erfordert daher eine flexible Modellstruktur, die verschiedene Details der Modellkomplexität in Regimen mit unterschiedlichem Grad der Datenverfügbarkeit berücksichtigen kann.

Darüber hinaus ist es für den Umgang mit den Unsicherheiten, die mit den geschätzten Modellparametern verbunden sind, sehr wichtig, eine Kalibrierungsvariable kritisch auszuwählen, die eine räumlich-zeitliche Darstellung und eine angemessene Menge an Informationen in einem implementierbaren räumlichen Detaillierungsgrad bietet. Angesichts der Datenbeschränkungen können die Wahl der Kalibrierungsdaten und die Angemessenheit der Kalibrierungsroutine dazu beitragen, eine Parameterkompensation zu vermeiden. Diese Kompensation erfolgt normalerweise in Ermangelung einer speziellen Kalibrierungsroutine und einer repräsentativen Kalibrierungsvariablen, wobei der Kalibrierungsansatz versucht, die gesamte Simulation an die nicht repräsentativen Daten anzupassen, indem eine Kompensation innerhalb der Parameterteilmengen, die die Teilprozesse darstellen, vorgenommen wird. In den letzten Jahren wurden zunehmend fernerkundungsbasierte Schneedeckenbilder in die Modellierung einbezogen, die insbesondere in den datenarmen Gebirgsregionen eine plausible Alternative zu bodengestützten Daten darstellen, da sie sehr relevante Informationen über die räumlich-zeitliche Verteilung von Schnee enthalten. Es wurde daher eine wichtige Forschungslücke identifiziert, wie die pixelweisen qualitativen Informationen aus diesen Bildern am besten genutzt werden können, um die Modellierungsansätze für die Schneeschmelze zu verbessern und dadurch die Unsicherheiten bei der Simulation von Schneeprozessen zu verringern.

In dieser Arbeit wird eine **neuartige, eigenständige Kalibrierungstechnik** vorgestellt, die MODIS-Schneedeckenbilder zur Kalibrierung unabhängiger konzeptioneller Schneeschmelzmodelle verwendet und dabei Modellparameter aus einzelnen oder mehreren MODIS-Bildern schätzt. Das Ziel war es, **die pixelweise binäre Information ('Schnee', 'kein Schnee')** zu nutzen, die MODIS-Schneedeckenbilder auf täglicher Ebene bei einer angemessenen räumlichen Auflösung bieten. Als Schneeregime wurden die Schweiz und Baden-Württemberg ausgewählt, wobei erstere teilweise länger andauernde und letzteres eine kürzer andauernde Schneebedeckung aufweist. Der eigenständige Kalibrierungsansatz wurde an verschiedenen Erweiterungen konzeptioneller Schneeschmelzmodelle in unterschiedlichen Betrachtungsebenen evaluiert. Die erweiterten Schneeschmelzmodelle wurden unter Einbeziehung von Faktoren entwickelt, die die verschiedenen Aspekte von Schneeakkumulations- und Ablationsprozessen berücksichtigen, um die Verbesserung der Simulation der Schneedeckenverteilung mit minimalem Dateninput für die künftige Implementierung in datenarmen Regionen zu bewerten. Alle kalibrierten Modelle simulierten die Schneedeckenverteilung sehr gut, wobei das Modell mit der besten Leistung, d. h. das strahlungsbasierte Modell, ermittelt wurde. Ein Vorteil dieses Ansatzes besteht darin, dass er eine künftige Implementierung in Verbindung mit beliebigen Schneeschmelzmodellen, die die Schneedeckenverteilung simulieren können, ermöglicht, indem die Modellparameter zuverlässig bestimmt werden. Darüber hinaus ermöglicht die Auswahl binärer MODIS-Informationen als Kalibrierungsvariable eine **robustere Kalibrierung** relativ komplexer Schneeschmelzmodule, da die mit den Kalibrierungsdaten verbundene **Unsicherheit geringer** ist.

Es wurden auch verschiedene Simulationsschwellenwerte für die Definition der Kalibrierungsdaten (NDSI-Schwellenwerte), die Auswahl der Bilder für die Kalibrierung (Wolkenbedeckungsschwellenwerte) und die Reklassifizierung der SWE-Ausgaben in Schneedeckeninformationen (SWE-Schwellenwerte) ermittelt. Die Ergebnisse der Sen-

sitivitätsanalyse dieses Kalibrierungsalgorithmus stimmen mit verschiedenen Studien überein, die im Bereich der Schneeschmelzmodellierung durchgeführt wurden. Es wurde festgestellt, dass der Ansatz eine geringere Empfindlichkeit gegenüber Wolkenschwellenwerten aufweist, was bedeutet, dass die Kalibrierung auf schneebedeckten und schneefreien Flächen in den Bildern flexibel ist. Es wurde festgestellt, dass die geschätzten Parameter, die auf der Kalibrierung in verschiedenen Perioden innerhalb der Saison beruhen, auf andere Perioden übertragbar sind, wobei die Parameter, die aus Bildern der Schmelzsaison bei länger anhaltenden Schneeverhältnissen geschätzt werden, und die Parameter, die aus Bildern der Zeit des Schneebeginns bei kürzer anhaltenden Schneeverhältnissen geschätzt werden, sich als robuster erweisen.

Ein weiteres wichtiges Ziel dieser Arbeit war es, die Wirksamkeit des Kalibrierungsansatzes auf die resultierende SWE und ihre Auswirkungen auf den hydrologischen Abfluss im Einzugsgebiet zu bewerten. Der Vergleich wurde anhand von zwei hydrologischen Modellen durchgeführt: dem HBV-Standardmodell, das ausschließlich auf der Grundlage des Abflusses kalibriert wurde, und einem modifizierten HBV-Modell, das die Schmelze aus dem auf MODIS-Bildern kalibrierten Schneeschmelzmodell als eigenständigen Input erhielt. Es wurde festgestellt, dass der eigenständige Ansatz die Unsicherheit bei der Darstellung von Schneeakkumulations- und Schmelzprozessen reduzierte, während HBV, das ausschließlich auf der Grundlage des Abflusses kalibriert wurde, Parameterausgleiche mit anderen Nicht-Schnee-Parametern in der Schneeroutine aufwies, was zu einer unsicheren Simulation von Schneeprozessen führte. Diese Unsicherheit ist für ein zuverlässiges Verständnis der zugrundeliegenden Teilprozesse sehr kritisch, denn selbst wenn sich die Abflusssimulation als zuverlässig erweist, führt sie zu einer **'richtigen Schlussfolgerung aus falschen Gründen'**. Durch die Schätzung der Parameter allein aus MODIS-Informationen entfällt nicht nur die Abhängigkeit von einer einzigen Kalibrierungsvariablen für den Abfluss, die in den höheren Lagen bereits eine Verfügbarkeitsbeschränkung darstellt, sondern es bleibt auch die räumliche Heterogenität auf regionaler Ebene erhalten.

Darüber hinaus wurde festgestellt, dass die eigenständigen Schmelzausgaben des modifizierten HBV die Zuverlässigkeit der Abflussvorhersage weiter erhöhen, und zwar **aus gutem Grund**, da die Schneeprozesse durch prozessinformierte Parameter angemessen dargestellt werden. Darüber hinaus wird der individuelle Kalibrierungsparameterraum sowohl für die Schneeschmelze als auch für die abgeschnittenen hydrologischen Modelle reduziert, was einen reduzierten äquifinalen Parameterraum begünstigt und damit in beiden Fällen zu einer Verringerung der Modellierungsunsicherheiten beiträgt. Dies ermöglicht außerdem eine zusätzliche relevante Parametrisierung, die durch eine bessere Recheneffizienz bei der Kalibrierung der Schneeschmelze-Modelle unterstützt wird, im Gegensatz zu der erhöhten Komplexität bei der Kalibrierung eines hydrologischen Modells, das auf eine einzige Variable, d.h. den Abfluss, kalibriert ist. Die unabhängige Kalibrierung begünstigt somit eine dedizierte Simulation von Schneeprozessen, ohne dass die Schneesimulation durch ein komplexeres hydrologisches Modell geleitet wird.

Das gesamte Konzept wurde in einem datenarmen Szenario im Freistaat Bayern in Deutschland nachgebildet. Das Schneeschmelzmodell wurde durch frei verfügbare globale meteorologische Daten angetrieben, die auf die MODIS-Auflösung heruntergerechnet wurden.

Auch in diesem Fall wurde die Schneedeckenverteilung gut simuliert, und das Schmelzergebnis verbesserte die hydrologischen Vorhersagen auf Einzugsgebietsebene. Dies unterstreicht die Anwendbarkeit der MODIS-basierten Kalibrierung in datenarmen Regionen.

Die Dissertation kommt zu dem Schluss, dass die Hinzunahme von Schneedeckeninformationen bei der Schätzung der Parameter von Schneeschmelzmodellen unter Verwendung von Schnee/Nicht-Schnee-Informationen und einem bescheidenen und global verfügbaren Bedarf an Eingabedaten einen einfachen, räumlich flexiblen Ansatz zur Kalibrierung der Schneedeckenverteilung in Gebirgsregionen mit einigermaßen genauen Niederschlags- und Temperaturdaten ermöglicht, insbesondere in Regionen mit wenigen Daten. Darüber hinaus bietet dies auch die Möglichkeit einer sofortigen Verifizierung mit Punktmessungen, was insbesondere bei episodischen Schneetagen von entscheidender Bedeutung ist. Die Verringerung der Unsicherheit bei der Schätzung der Schneedecke und der anschließenden Abflussvorhersage ist ein entscheidender Zusatznutzen bei der Verbesserung der Konzeptualisierung von Schneeschmelzmodellroutinen, die wiederum die verteilte hydrologische Modellierung ergänzen.

1. Introduction

1.1. Motivation

Snow is one of the most important components of the hydrological cycle providing a reservoir for available water lagged for subsequent discharge in downstream reaches. Snow portrays a very complex dynamics with high spatio-temporal variability observed in the inherent processes in the mountainous regimes. The temporal variability is controlled by variability associated with the accumulation process such as the amount and distribution of solid precipitation, and with the ablation process such as the ambient air temperature, humidity and incident radiation. The spatial variability is explained by topography and land cover in the mountains which in turn govern the temporal variability [Clark et al., 2011]. Due to this high spatio-temporal variability, reliable representations of spatial distribution of seasonal snow and subsequent snow-melt still remain critical challenges for monitoring the seasonal evolution of snow and in turn for any hydrological estimations despite the crucial relevance in mountainous regimes in determining the available water for the human settlement and operational management [Gyawali and Bárdossy, 2022]. The snow-cover distribution holds very important information on snow accumulation and melt in the mountainous regimes, and can add a crucial detail, especially for simulation of the snow-melt and accumulation processes and reasonably predict the spatial distribution of snow-water equivalent and its partition from evapotranspiration, runoff and percolation and spring discharge. This work is motivated by the challenge to accurately account for the contribution of snow-cover evolution in mountain hydrology.

1.2. Challenges in snow estimations

Highly localized point measurements, snow-melt models and to some extent Remote Sensing (RS) based observations, are currently being employed to estimate and analyze the accounting of snow-processes. Owing to the inherent large scale spatial variability of the snow characteristics, widespread measurement of snow-depth as well as the simulation of the snow processes is very challenging. Limitation of reliable snow-melt estimation via modeling in mountainous regions is, also, further exacerbated by data scarcity. This lack of highly pertinent data severely impacts the reliable understanding of snow-related processes in the mountainous regions in different layers, namely reliability and representativeness of the available data, choice of model complexity, and appropriateness for a reliable calibration and model evaluation [Tarasova et al., 2016]. In addition to the complex climatic and physiographic conditions, the limitations of the snow-melt models can also be inferred as a

function of the modelling approach, and the model application. A general case is that the models are limited by data whereas a case-by-case unique problems are generally the functions of the model choice and the climatic characteristics of the regions [Leavesley, 1989]. Following sections briefly explain these limitations.

1.2.1. Non-representative case of measurements

The widely used point measurements of snow provide an accurate measure of snow-depth and the water equivalent, however, these in-situ measurements can seldom cover a wider spatial extent and are prone to be non-representative due to local influences. These point measurements of Snow Water Equivalent (SWE) such as the snow-pillows have the tendency to not represent the spatial and temporal variability in the mountainous areas [Rittger et al., 2016] as these primary sources of snow-related data are often located in the valleys and often lack the information about areas above them and along the slopes. Interpolation of the SWE and snow-depth data are often limited by the fact that the spacing distance between these measurements are often greater than the correlation-length scale of measurements [Molotch and Margulis, 2008].

In the context of snow-melt modeling, the mountainous areas are mostly characterized by a very low density of rainfall and climate observation stations. Among all the climatic variables, the precipitation exhibits a very complex behaviour with topography and is highly prone to be underestimated due to under-catch even at the gauging stations. The extrapolation of this uncertain precipitation to higher altitudes is more non-representative as this important driver is very prone to local climatic patterns, thereby rendering the simulation very uncertain.

1.2.2. Model complexities and data limitations

Various modeling and measurement techniques are in practice to account for the snow processes but these methods hold their own limitations. Prior studies on the comparison of snow models [Feng et al., 2008; Rutter et al., 2009] have highlighted the better reliability of complex model structures in simulating the snow processes. However, depending upon the complexities of the models, there exists big differences in model results. Relatively accurate and process based physically based models are highly data intensive, which is often a big limitation in mountainous catchments around the world. More widely used conceptual snow-melt model applications are either lumped (mean basin/regional parameters/inputs) or distributed (dividing the region into smaller areas with distributed inputs/parameters) to define the physical and hydrological features of the basin. Distributed models somewhat take the spatial heterogeneity into account, however the model complexities increases with added layer of detail thus straining the model with more data requirement.

The simplified energy-balance and temperature index based approaches are popular owing to their simplistic representation of the snow-processes. The former uses a simplified energy budget for a snowpack to calculate the snow-melt. However, limited availability of required input data such as wind speed, net solar radiation, vapour pressure, and the techniques

to extrapolate these information on a distributed scale further restricts the energy-balance models usage in a larger scale [Anderson, 1976]. The temperature-index models are more empirical in nature, where a melt factor and the air temperature are used to account for the energy-interactions in the snow-pack. These models, owing to their simplistic algorithm and less data requirement have been widely used around the world in snow-melt modeling and as a core component in hydrological models.

The trade-off between the model complexity given the data unavailability, however, remains a critical question especially in snow-melt modeling. Tarasova et al. [2016] argues that the discharge from ablation processes in snow-dominated catchments are often more predictable than, for instance, the discharge from small-scale stochastic rainfall events, which often allows a more simplistic and better prediction with less complex (lumped, or semi-distributed) models than with distributed models with high data requirement. Depending upon the regimes with different levels of data availability, it is thus very important to have a flexible structure that can accommodate different details of model complexities without much loss in model performance, thereby reducing the model uncertainties.

1.2.3. Uncertainties in snow parameters estimation

The uncertainties associated with the calibration technique of a model is a multi-pronged effect of the data scarcity and the resulting implementation of unrepresentative input data; model complexities and the appropriateness of the calibration routine and the reference data given these conditions. The parameter related uncertainties, though to some extent are unavoidable, given the data limitations, the choice of the calibration data remains a critical deciding factor that can further determine the complexities of the model structure. In hydrological modeling, the snow-processes are generally calibrated on a single variable, i.e the discharge at the outlet. Due to this, the snow processes are impacted by a compensating effect with other non-snow parameters, leading to a possible accurate discharge but a very uncertain representation of the underlying snow processes. This is further described in subsequent chapters in detail. Furthermore, the SWE and snow-depth based calibration also often lack the spatial detail as the extrapolation of these variables is highly uncertain owing to the complex spatio-temporal variability in these catchments. Multiple data set modeling has gained traction in recent years to identify and target the specific modules inside these models but the question remains on to what level the model complexities in terms of added parameterization can be allowed for better simulation given the data-scarcity constraints. These uncertainties thus highlight the need in critically selecting a calibration variable that offers reasonable amount of information at a implementable spatial detail.

1.2.4. Limitations of standalone usage of satellite imageries

With the advances in space technology, various satellite based snow-products have been made available to researchers and other end-users for snow-cover monitoring. However, the lack of snow-depth information and persistent cloud cover in the mountains severely limit the standalone usage of Remote-sensing images in snow-cover estimation [Tran et al.,

2019]. Another limitation of the satellite based information is also associated with the complexities in converting the qualitative pixel-level data to quantitative information required for hydrological modeling [Corbari et al., 2009].

The Remote Sensing images can, however, provide a plausible alternative to ground based data especially in the data scarce mountain regions, since their resolution and availability do not depend on the mountainous terrain [Parajka and Blöschl, 2008(a)]. In particular, the snow-cover distribution from these images not only hold a crucial information on the spatial distribution of snow, but also contain the proxy information on accumulated snow precipitation during the snow season, which can be further analysed to update the existing SWE estimates. The snow-cover depletion rate showcases an inverse relationship to the the available snow water equivalent and the resulting snow-melt discharge [Rango and Itten, 1976]. This information is very relevant for simulating snow-melt and accumulation processes and the spatial detail offered by freely available satellite images of snow-cover distribution provides a solid foundation for distributed snow-melt modeling. This research aims to exploit this crucial information from freely available images of snow-cover distribution to understand and analyze the snow processes in data scarce snow-dominated regimes.

1.2.5. Sensitivity to climate change

Considering the snow effect on land and atmospheric processes which is further exacerbated by high sensitivity to climate change, accurate representation of seasonal snow evolution is thus highly imperative to strengthen and better plan the competing priorities of water resources development trajectories in these regions [Kirkham et al., 2019; Schmucki et al., 2014; He et al., 2014]. Climate change, in particular the increasing trend of temperature, complicates the problem with snow-estimation in the data scarce regions as the temperature fluctuations impart uncertainty in terms of timings and volume of snow accumulation and melt. The temperature changes alter the regional atmospheric circulation patterns, which further has a cascading effect on the distribution and phases of precipitation resulting in less snow precipitation in the accumulation season and accelerated melt well before spring with early onset of spring discharge. This has been observed in most of the mountainous areas around the world which raises a crucial question for the water resources strategies, particularly on spatiotemporal distribution of snow accumulation, the rate and timing of depletion and resulting availability to the downstream reaches. The spatio-temporal snow cover variation provides a pertinent information on this aspect, as these changes strongly correlate with changing climatic trends. Global and regional snow-cover monitoring based on the RS based snow cover information have been in place and highly prioritized in recent years to assess these spatiotemporal changes. However, a robust snow assessment technique that can capture the influence of the change including changing precipitation and temperature, at a regional scale, to (a) reconstruct a snow cover time series (b) to accurately quantify the volume of water stored in the snowpack, (c) to locate precisely where the snow is accumulated and (d) to estimate the timing and quantity of melt for downstream availability, is very crucial, under a changing climatic regime, for better snow estimation and adequate management of the downstream water demand for different socio-economic needs.

1.3. Research objectives and questions

As discussed above, with the topographical complexities and various limitations of data in the mountainous terrain, it is imperative to develop a simplistic, less data-intensive and an adaptive methodology applicable in mountainous regimes. In general, this research aims to develop a standalone calibration technique with which conceptual and parsimonious snow-melt models can be calibrated on spatial snow-cover distribution from the satellite images at a pixel level using reasonably accurate precipitation and temperature model forcings, thereby formulating a flexible snowmelt model useful for distributed hydrologic modeling. In this context, following specific objectives were envisioned and these try to address the questions that follow:

(a) To develop and extend different variants of distributed temperature-index snow-melt incorporating different aspects governing snow hydrology such as the elevation, aspect, solar radiation

- This will address the question on how well the increasing model complexities with modifications concerning aspects of the underlying snow-processes impact the mimicry of snow-cover distribution.

(b) To develop and evaluate a pixel-based binary calibration methodology to calibrate the snow-melt model variants with parameters estimated from a single or a set of Moderate-resolution Imaging Spectroradiometer (MODIS) images during the snow season.

- The research question addressed here is if the binary calibration on snow ('1') or no snow ('0') spatial distribution is able to simulate the MODIS snow-cover distribution well. This will also analyze if the uncertainty in model simulation is reduced with the selection of a robust binary information used for calibration.
- How will the model performance vary in different elevation zones? Which is the best model to use?

(c) To identify and recommend different thresholds used for calibration using MODIS images. The research questions that would be addressed are:

- What NDSI threshold should be used to demarcate between snow/no-snow pixel for the observed MODIS snow-cover?
- What is the minimum cloud percentage threshold for the observed MODIS imageries to be used for the proposed calibration?
- What is the minimum SWE threshold value to demarcate between snow/no-snow pixel for the simulated snow-cover distribution?

(d) To assess the spatio-temporal transferability of the parameters estimated with the proposed calibration technique.

- This will answer the pertinent question on how well the calibrated parameters perform in different phases of the snow season and within different regions.

(e) To investigate the performance of the SWEs from the snow-melt models calibrated on MODIS snow-cover distribution in a modified hydrological model.

- How does the distribution-based calibration reduce uncertainties related to snow-processes simulation in hydrologic modeling?

(f) To evaluate the methodology in a data scarce scenario. This evaluates the methodology in the absence of observed precipitation and temperature inputs.

(g) To investigate the model inversion to obtain seasonal estimates of accumulated snow in a semi-distributed manner.

1.4. Scope and structure of this thesis

This thesis aims to address the research objectives and is structured as following sections.

Chapter two gives a brief introduction of the Remote Sensing concept. This chapter provides the background on how snow-cover monitoring is being done with optical satellite sensors along with the overview of existing space-borne snow products. Further discussed is the problems associated with the cloud obscurity in remote sensing images. The chapter then details the literature review on Remote Sensing integration in hydrological modeling as well as assimilation in snow-modeling context.

Chapter three provides an overview of the study regions selected for snow-melt modeling along with the justification for selection in terms of snow-cover regime, topography and climate. The section then introduces the different hydrometeorological dataset used in the study to drive the snow-melt and the hydrological models. Finally, the chapter describes in detail about the MODIS snow-cover product and the cloud removal methodology as a data preparation step.

Chapter four discusses the geostatistical interpolation of the meteorlogical inputs employed in the study. The chapter first provides a brief introduction on the concept of Kriging. It further provides a detailed introduction of ordinary Kriging along with the limitations of the intrinsic hypothesis, external drift Kriging and residual Kriging methodologies. The chapter then discusses the Kriging methodologies employed in the study regions along with a description of the directional smoothing methodology used in conjunction with a multiple linear regression based residual Kriging approach for precipitation interpolation in the mountains. Furthermore, results of Kriging in the study regions in the form of leave-one-out cross validation statistics are also presented in this chapter.

Chapter five starts with a introduction to snow-melt modeling along with the types of models commonly used for snow estimation. This chapter then highlights the different extensions to the simplistic degree-day model devised and used in this study. The extended models show a gradual added model parameterization with different aspects governing the snow evolution in the mountains. The chapter also discusses about the data input requirement for the snow models. The overall methodological approach of the study is also

presented. The chapter then describes different components and the schematics of a hydrological model, Hydrologiska Byråns Vattenbalansavdelning (HBV).

Chapter six is the backbone of this thesis. This chapter focuses on the novel calibration methodology proposed in this study in detail. The chapter discusses the problem statement on how traditional snow-routine calibration is being done and the novelty of this study to tackle this challenge. The calibration methodology, along with the objective functions used are also described in detail. The Robust Parameter Estimation (ROPE) methodology is also discussed briefly. Finally, the results of snow-cover simulations in both the study regions are also compared and discussed in different layers of detail. The best performing model variant is identified in this chapter.

Chapter seven explains the sensitivity analysis carried out in terms for identifying the best thresholds regarding snow/no snow differentiation (Normalized Difference Snow Index (NDSI) threshold for MODIS and SWE threshold for simulated series), selection of images (cloud threshold). The sensitivity in relation to the selection of periods within a snow season is also discussed in this section along with calibration and validation in different seasons. This chapter further explains the results of validation of the calibration methodology in terms of hydrological modeling. The snow-cover simulation from the snow-routine of HBV calibrated on discharge and the snow-cover simulation from MODIS are compared and described in detail. Furthermore, the translation of MODIS calibrated melt to discharge is also analysed and compared against HBV modeled discharge. The chapter is concluded with a discussion on hydrological model uncertainties and how it can be reduced with the proposed methodology.

Chapter eight describes two practical extensions of the research methodology using MODIS snow-cover data. The first section covers the snow-melt modeling and MODIS based calibration in a data scarce scenario, using freely available global data. Likewise, a MODIS snow-cover based SWE reconstruction at Hydrologic Response Unit (HRU) level is also discussed in this chapter.

Chapter nine concludes the thesis with a summary of the approach comparing the findings in line with the set research objectives.

2. Remote Sensing (RS) in snow estimation

2.1. Brief concept of Remote Sensing

Remote sensing is the science and art of acquiring the information pertaining to an object, area or a phenomenon via abstraction of the information obtained by a sensor without direct contact with the concerned target. Generally, the remote sensing information refers to the information coming in from the electromagnetic spectrum acquired via airborne or space-borne sensors, generally classified as the active and passive sensors [Ritchie and Rango, 1996]. Despite the niche of potential information, remote sensing missions were historically driven by political and technological motives [Wagner et al., 2009], rather than the needs of the scientific community. However, in the recent years, the need to close the gap between the scientific user groups and the remote sensing providers have been identified and accordingly followed up by increasing space-based missions. Remote sensing data now has found its application particularly in environmental sector including, hydrology, snow-cover monitoring, agriculture, forestry, oceanography, meteorology, geology as well as for planning purposes [Gafurov, 2010].

Both the active sensors (sending a pulse and measuring the reflected backscatter) and passive sensors (measuring the reflected sun light from natural surfaces) provide valuable information about reflective, thermal and dielectric properties of the Earth's surface [Engman and Gurney, 1991]. This information, particularly in hydrology, can be used as a proxy for different hydrological variables, later transformed into hydrologically relevant information empirically or with different transfer functions. With ever-evolving Remote sensing missions, this data has been a valuable alternative or supplement to existing operational and research hydrology sector. The major advantage of the RS data is pronounced in the ungauged areas (especially inaccessible high mountains) where this valuable information can act as a driver for various hydro-meteorological operations, as the resolution and availability of these data do not depend on the terrain.

2.2. Snow-cover monitoring with optical satellite observations

Remote sensing offers a very effective option to monitor the snow-cover distribution, at a reasonable spatio-temporal detail, with the value more highlighted in the topographically inaccessible regions, which are characterized by low density of monitoring observation stations [Huang et al., 2017]. The areal extent of snow is a very pertinent hydrological variable and this spatial information needs to be 'judiciously' integrated into snow-melt and in turn hydrological modeling in order to improve seasonal streamflow forecasts in the data scarce

mountainous regimes. Snow can be considered as one of the most 'colorful' natural surface covers [Dozier et al., 2009] as the inherent spectral reflectance can range from high (albedo) in a visible wavelength spectrum with minimal sensitivity to the grain size, to low in the mid- InfraRed spectrum [Kongoli et al., 2012] where it becomes sensitive to the grain size. This unique spectral response in different wavelengths allows snow to be distinguished from other natural surfaces such as the soil, water as well as vegetation. Due to this high albedo of snow presenting a good contrast with most other natural surfaces and the need to effectively map the snow distribution in the mountains, the spatial monitoring of snow-covered area has been carried out with the help of space-borne sensors since the inception of the satellite based remote sensing. Prior to the availability of these satellites, there was no efficient way of identifying the snow-cover extents [Rango and Itten, 1976; Dozier et al., 2009]. Various RS based techniques and their satellites are currently in operation to monitor the condition of snow. A summary of different examples of space-borne instruments or satellites generally used in snow cover monitoring related studies, along with their general properties classified by type of sensors is shown in table 2.1.

The optical sensor based observations are more useful in providing information on snow-cover extents. Passive optical sensors utlilize a multi-spectral imaging system in the visible and infrared domain to detect the snow, with spatial resolutions ranging from 1m to 1 km and a temporal revisit of 1 day to 16 days [Largeron et al., 2020]. MODIS, Advanced Very-high-resolution Radiometer (AVHRR), Proba-V, Sentinel-3, and Visible Infrared Imaging Radiometer Suite (VIIRS) are the examples of this category. MODIS and AVHRR products are widely favored due to their reasonable spatial temporal resolution and a longer time-series of snow-cover data. Satellites with higher spatial resolution such as the SPOT 6/7, Sentinel 2 and Landsat 8 are limited by a longer revisit. Active optical sensors i.e. Light Detection and Ranging (LIDAR) based observations are more useful in regional scale snow-depth mapping. However, these observations highly depend on the availability of an accurate DEM and are susceptible to long revisit times (as high as 91 days with Ice Sat-2) which limits the practical integration of these observations into hydrological context.

Similarly the thermal infrared sensors monitoring the snow and ice surface temperatures MODIS also provide a basis to couple the surface temperature amplitude at daily scales for SWE prediction. However, based on the satellites, they are also limited by either high spatial resolution and low revisit (Landsat 30m), or low spatial resolution (1km with MODIS) and higher revisit frequency. The passive microwave sensors have been used monitoring snow cover at global and regional scales but among other limitations, the spatial resolution of these sensors (upto 25km) limit the applicability in the mountains where finer processes are more relevant, though the concept of estimation of brightness temperature and in turn snow-depth via the measurement of spectral luminance energy is very suitable to get information under all atmospheric conditions [Largeron et al., 2020]. The Active microwave radar such as the active imaging Synthetic Aperture Radar (SAR) sensors measure the backscatter signal to estimate snow cover roughness and in turn snow-depths at very high resolution which makes them very well-suited to snow hydrological applications [Leinss et al., 2014]. The Airborne observations offer another possibility for snow cover monitoring but the high spatial resolution offered compared to satellite-based observations is again limited by restricted domain and less-frequent revisit schedule.

Due to the reasonable spatial resolution and a shorter temporal resolution, this study concerns with passive optical sensor-based monitoring, more so with MODIS products. This satellite-based snow monitoring basically identifies the snow-covered land masses from snow-free areas and to an extent from clouds. The snow is detected on a pixel-by-pixel basis by automated algorithms based on different spectral thresholds using different indices via analysis of the reflectance and brightness temperature in different spectral bands measured by on-board sensors. The widely used NDSI is calculated as the normalized difference between reflectance of the visible and middle InfraRed Spectra and is used to detect snow-pixels in MODIS [Hall et al., 2002] as shown in Eq.2.1. The reflectance of the majority of clouds is higher in the short-wave Infra-red spectra, where the snow reflectance remains low. In contrast, the snow and ice reflectance is more in the visible spectrum. Based on this high contrast in reflectance between the two wavelengths, NDSI becomes very useful tool in better identifying the snow-extents as it offers a better demarcation with clouds. The snow-covered area can then be defined based on NDSI thresholds for snow-detection. The snow-covered fraction is estimated using a linear relationship with NDSI value [Salomonson and Appel, 2004].

$$NDSI = \frac{R_{band4} - R_{band6}}{R_{band4} + R_{band6}} \tag{2.1}$$

where,
R_{band4} = Reflectance from visible spectrum (green), and
R_{band6} = Reflectance from Middle IR spectrum

Table 2.1.: Examples of widely used space-borne instruments and satellites classified by the sensor type along with their properties; Source: Largeron et al. [2020]

	Types of Sensors				
	Mono. optical	**Stereo. optical**	**Active optical**	**Passive mw**	**Active mw**
	Examples of Space Missions				
	MODIS Landsat-8 Sentinel-2/3 Meteosat 8-11 GOES-16-17 VIIRS	SPOT-6/7 Pleiades 1a/1b WorldView 1-4	ICESat ICESat-2	SSM/I SMMR AMSR-E AMSU-A/B	ALOS 2 Sentinel 1 RADARSAT-2 TerraSAR-X
	Properties				
Spatial Res.	High (10-500 m)	Very High (1 m)	High (10-100 m)	Coarse (km)	Very High (1-20 m)
Temporal Res.	High (daily to 5 days)	On request	Very low	High (daily)	High (daily)
Limits	Day/no cloud	Day/no cloud	Revisit time	Coarse res.	Geometrical distortion
Retrieve data	SCF/SCA/Albedo No direct SWE	SD No direct SWE	SD	Snow depth/SWE SWE with To Only dry snow	Snow depth/Snow wetness No direct SWE
Accuracy	10% for SCA/SCF 5-15% for albedo	0.8 at 3 m res. 0.4 at 20 m res.	0.15-0.6 m for aggregated data	Highly variable	0.31 m for Snow depth

2.2.1. The problem of clouds in snow-cover images

Well identified problem in this satellite-based approach is the obscurity due to cloud contamination. One of the major drawbacks with the optical sensors stems from their inability to measure the land surface reflectance through clouds [Mullen et al., 2021]. This cloud contamination hinders the true identification of what lies beneath and is regionally and seasonally dependent [Parajka and Blöschl, 2008(a)]. In case of snow-cover, the winter season images are more prone to be obscured with clouds. Apart from the case by case requirement of the spatio-temporal resolution of satellite images, the obscurities due to clouds limit the direct integration of the satellite products into hydrological research and/or operations.

Several studies have been carried out using different methodology to reduce the cloud contamination from the images. This section focuses more on the context of snow-related studies as snow and cloud exhibit similar colour and textural properties and it is deemed very important to correctly and reliably distinguish between the two features for the subsequent interpretation and assimilation for different purposes. The cloud removal techniques in practice, can generally be categorized as spatial (spatial patterns of snow), temporal (temporal changing correlation), spatio-temporal (combination of the former two), and multi-source fusion (combining complementary information from stations or other RS observations)[Li et al., 2019]. Parajka and Blöschl [2008(a)] introduced a three-step (Aqua-Terra combination, spatial filter based on 8-pixel neighbourhood search, and a temporal filtering method) cloud-removal method to reduce the cloud coverage of snow cover using a spatio-temporal combination of MODIS data. They found a remarkable reduction in cloud-covered pixels. Gafurov and Bárdossy [2009] also used a six step filtering MODSNOW algorithm to reduce the cloud-covered pixels from the MODIS snow-cover data in Kokcha River Basin. The technique utilizes a subsequent and gradual removal of cloud pixels from MODIS including spatial combination of Terra and Aqua images followed by different temporal combinations for the composite images from the first image. The later steps use a more spatial setup comparing highest and lowest pixel elevations with and without snow followed by a spatial neighbourhood search in a four and eight pixels neighbourhood. The results suggest that validation accuracy differed from step to step but the overall methodology was able to fully remove the cloud pixels from snow-cover time-series. A more detailed review of studies related to cloud-cover removal can be read from Li et al. [2019].

2.3. RS Integration in hydrological modeling

Remote sensing integration in hydrological sciences has made important strides in recent years. The critical observation on spatio-temporal alterations in hydrological states and variables has historically been crucial for hydrological studies [Ritchie and Rango, 1996]. The relevance of RS integration in hydrology has surpassed the usage of traditional geophysical air/space borne products such as the land cover, DEMs to a more widened realm of dynamic land surface variables such as the skin temperature, soil moisture, snow-cover, vegetation cover and so on [Wagner et al., 2009]. Increasing number of studies now attempt to exploit the novelty of the advances in RS technology to better understand and complement the traditional concepts of hydrological applications.

Majority of these studies employ these data in constraining the calibration of the hydrological models or for assimilating the RS information into land surface models. The question on to what extent remote sensing information can complement hydrological modeling is highlighted in Parr et al. [2015] in which they investigated the effect of satellite based Leaf Area Index (LAI) to drive the evapotranspiration ET simulation in a hydrological model and later combine the simulated ET with a satellite based ET to propose a bias-correction algorithm. They concluded that the LAI driven ET routine significantly improved the simulation of temporal variability of discharge. They also conclude that this integration into modeling context helps characterize the model-related uncertainties in simulating the underlying process. Sirisena et al. [2020] used remote sensing-based evapotranspiration data along with discharge to calibrate hydrological models and concluded that the multi-variable calibration with globally available remote sensing data along with traditionally used discharge based calibration can lead to better representation of the hydrological processes, especially in data scarce regions. Sun et al. [2015] used satellite observations derived river width to calibrate a hydrological model in an ungauged basin leading to good agreement with monthly discharge data. Mattia et al. [2009] proposed a promising approach to merge SAR data with hydrological modeling to use the simulated soil moisture fields at coarse spatial scale as a priori information for the retrieval algorithm to transform into multi-temporal and high spatial resolution soil moisture maps. Parajka et al. [2009] implemented a calibration for a conceptual hydrological model in Austria using ERS scatterometer derived surface soil moisture data and discharge. They concluded that the combined use of discharge and soil moisture improves the simulation of soil moisture while maintaining the discharge performance of the model. They further discussed that the augmentation of satellite data allows for a more robust parameter estimation. Liu et al. [2012] investigated the applicability and significance of RS data (precipitation, ET and LAI) in a distributed hydrological model in data scarce scenario. MODIS Snow Cover Area (SCA) was also used for model initialization and validation. They concluded that the differences in model results (between station based and RS based simulations) were very small and thus, the RS data holds a very good potential as the required model inputs in data scarce regions as well as provide a reliable ground for model initialization and validation.

Similarly increasing number of studies have been carried out by coupling satellite-based snow related state variables such as the snow-cover in hydrological and snow-melt modeling. Parajka and Blöschl [2008(b)] implemented a snow-cover (MODIS) and discharge constrained calibration to simulate flows in 148 catchments in Austria and concluded that this multi-objective calibration scheme improved the snow-model performance though the overall performance of the hydrological model was similar or improved in validation period. MODIS snow-cover was used by He et al. [2014] to estimate distributed degree-day factors for snow-melt modeling. Udnæs et al. [2007] discussed the operational application of MODIS SCA in the Hydrologiska Byråns Vattenbalansavdelning (HBV) [Bergström, 1995] model for spring flood prediction. They concluded that the combined calibration with SCA and discharge resulted in better prediction of the snow-cover distribution, albeit a similar performance with discharge. Tekeli et al. [2005] used MODIS products in identifying the snow duration curve to be used in a snow-melt model and concluded that the coupling provides crucial information on snow-melt timing and magnitude. Rodell and Houser [2004]

evaluated a updating routine for snow-water storage in a land surface model using MODIS snow cover observations and concluded that the updated simulations were characterized by more reliable snow coverage comparing in favor with in situ time series. Gan et al. [2022] also assessed an assimilation technique with blended in-situ SWE products for improving snow and streamflow forecasts in two basins in the US. Thirel et al. [2013] conclude that the particle filter based assimilation of MODIS SCA products into a distributed hydrological model yielded better snow-cover simulation and in many cases improved the modeled discharge.

These studies suggest that the integration of remotely sensed information to modeling led to a better representation of the hydrological processes, reduced uncertainty, and to some extent improved hydrological predictions.

3. Study area and data

The overview of the areas considered and data used in this research is presented in this chapter.

3.1. Study area

In this research, the study area was split into two distinct snow-regimes, to develop and test the extended degree-day models.The domain selection was done on the basis of the average availability of snow over the season, namely (a) characterized by intermittent snow and (b) characterized by partly longer-duration snow. For the former, the southern German state of Baden-Württemberg (BW) and for the longer duration regime, whole of Switzerland were considered. Figure 3.1 shows the study domain.

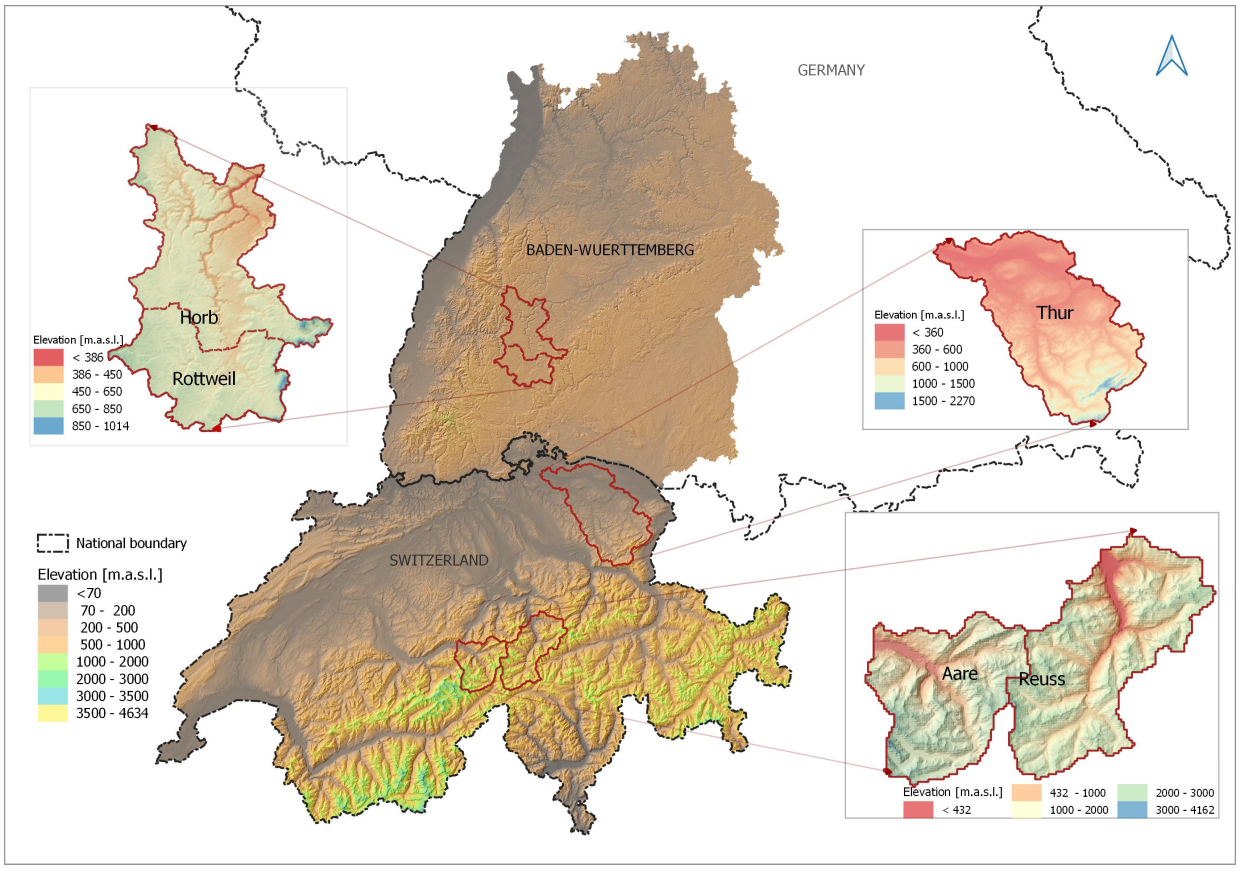

Figure 3.1.: Study area domain with elevation

3.1.1. Baden-Württemberg

The federal state of Baden-Württemberg is located in the south-west of Germany with an area of around 35,751km^2. The region includes the Swabian Alps and the Black Forest and is characterized by an accentuated topography with elevation ranging from a low of 88 m.a.s.l in the Rhine valley to 1465 m.a.s.l. at Feldberg in the Black Forest. The forested mountain range, Black forest, lines the south-western border of the state with the Rhine basin to the west. The Neckar river originates from these ranges and drains the majority of the region of BW. The Swabian Jura (Alps) extends from southwest to northeast with a peak elevation of around 1000 m.a.s.l. Furthermore, low mountain ranges such as the Odenwald mountain range in the north and a pre-alpine range in the south-eastern tip further add diversity to the topography of the region. Figure 3.2 shows the topographical map of Baden-Württemberg.

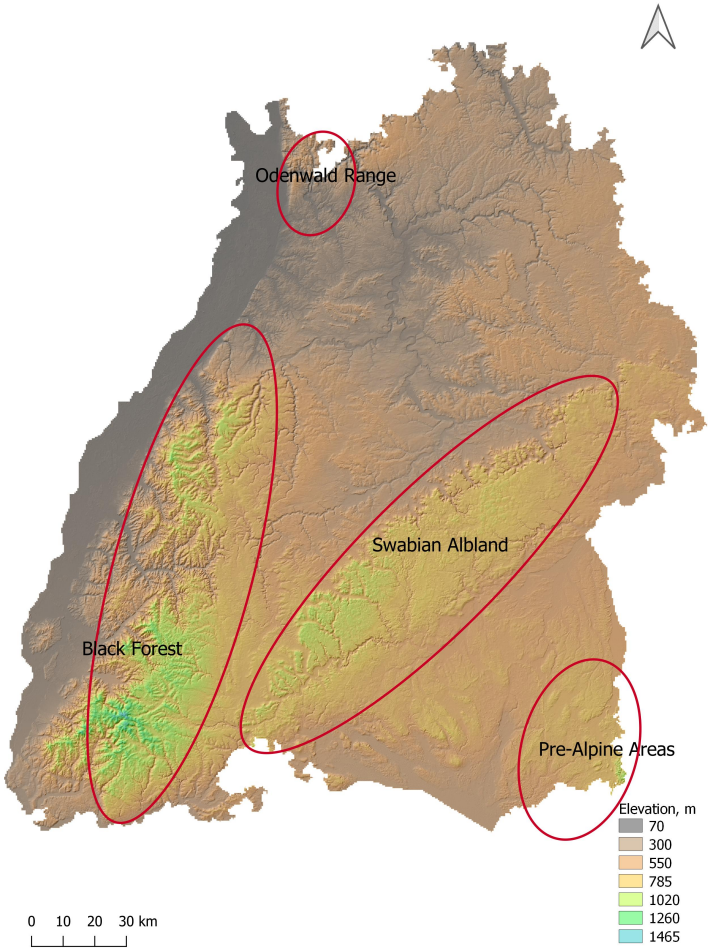

Figure 3.2.: Topographical map of the Baden-Württemberg region

Strongly influenced by the Atlantic Westerlies, the mean annual precipitation in BW ranges from 1800-2200mm in the Black forest. However, the mean annual amount reduces to less than 700mm in the Rhine valley. Precipitation in BW is strongly influenced by orographic

effects due to high altitude differences, but with non-uniform distribution of rain with increasing elevation. The precipitation increase is disproportionately higher on the western side of the mountains where it rains more. The highland regions receive regular rainfall throughout the year but the lowlands on the lee-side such as Stuttgart experience higher intra-annual variations, with the highest amount in June and the lowest in March.

Temperature variability is also very strong in BW because of the differences in altitude. The average annual temperature is around 4°C at Feldberg in the Black Forest which rises to more than 10 °C in the Neckar Valley. The highlands in the Black Forest exhibit a relatively lower temperature fluctuation throughout the year and are characterized by subdued extreme temperature due to higher frequency of winds and heavy clouds in the summer. The coldest month is February with an average minimum temperature of around -12 °C which increases to a average maximum of around 22 °C in July. In the Swabian Alps, the average minimum temperature fluctuates from -12°C in February to almost 30°C in July. In the flatter regions of Stuttgart, the maximum temperature ranges from around 14°C in the winter to above 30°C in July/August. The minimum temperature also reaches upto -10°C in these regions.

The average number of days with mean air temperature less than 0°C for BW is around 46. A more detailed elevation zone-wise description can be referred from table 3.1.

Table 3.1.: Elevation zone-wise characteristics in BW

Zones, m.a.s.l	% of total area	Mean annual temperature,°C	Avg. no. of days, $T_{mean}<0°C$
<300	21%	11	26
300-600	47%	9	40
600-900	28%	8	52
>900	4%	7	68

Due to this unique elevation dependent precipitation and temperature phenomena, BW region observes a uniform increase in snow duration and accumulation with increasing elevation. The snow season starts from October and with the snow ablation completed by mid-May in the higher areas of the Black Forest. However, in the lower regions, the snow season is more sporadic with snow season starting from November till April. These regions are characterized by episodic snowfall events. The melting water exiting the snow-regimes feeds the Neckar river which drains a large area in the BW region. This snow-melt is very imperative to the water supply for this region as well as for flood risk management. The case of 1862 flood is one such example, when a drastic temperature increase by 10°C within 24 hours from 25 to 26 December, in addition to a persistent rain the succeeding day, incited a rapid melting of the accumulated snow. This triggered a severe flooding in the tributaries of and subsequently the Rhine River [Bárdossy et al., 2020]. Prior to the melt triggering event, heavy snowfall was recorded in the Black forest region. Owing to these unique characteristics, this region was thus selected as a shorter duration snow regime to assess the potential of the proposed methodology in terms of snow-cover simulation.

In addition, to assess the performance of the snow-melt modeling in hydrological simulation, two catchments in the upper-Neckar River Basin were considered in this study, namely

Neckar at Rottweil and Neckar at Horb. Figure 3.1 shows the location of these catchments in the study domain. These catchments are henceforth termed as Rottweil and Horb in this thesis. They are relatively higher elevation catchments in the Black Forest region and are snow-fed in nature. The elevation in the bigger Horb catchment ranges from 390 to around 1000 m.a.s.l, whereas the elevation in Rottweil ranges from about 750 to around 1000 m.a.s.l. The mean annual precipitation amount hovers around 1200mm and the mean temperature is about 8°C. The mean annual flow (1981-2018) is about 5.2 cumecs for Rottweil and 15 cumecs for Horb. Further details about these catchments are provided in table 3.2.

Table 3.2.: Properties of selected catchments

River	Outlet	Catchment Area, km^2	Catchment Elevation, m.a.s.l.			Glaciation,%
			Max	Min	Mean	
Neckar	Rottweil	412	1006	555	705	0
Neckar	Horb	1110	1006	386	656	0
Reuss	Seedorf	837	3416	437	2010	6.4
Thur	Andelfingen	1702	2217	372	770	0
Aare	Brienzwiler	555	3798	580	2135	15.5

3.1.2. Switzerland

Within an area of around 41,284 km^2, Switzerland exhibits a unique blend of topographic variation with a quarter of its land covered by glaciers, mountains, and lakes with elevation ranging from below 200 in the Ticino Canton to the summit of the Monte Rosa at 4634 m a.s.l in the Alps. The northern part includes the mid-range plateaus with higher elevation range towards the southern side. The Jura mountains line the western part of Switzerland. The Swiss Alps traverses through the country from the south-west towards the central region. The Alps includes the perennial snow/glacier area with approximately 120 glaciers according to the Swiss Glacier Monitoring Network. The topographical map of Switzerland is shown in figure 3.3.

Topography ranging from lowlands in the north and the presence of Alps in the south, clearly distinguishes the climatic pattern in the North and Southern regions of the country. The climate in Switzerland is strongly affected by the Atlantic westerlies allowing humid current in Switzerland, which in turn offers cooling effect in summer and a thermal envelope during winter. This also favors an annual precipitation of around 2200mm in the high mountainous region. In addition to this, the Alps also trigger different climatic patterns such as the inner Alpine valleys in the south east and south west which are in the rain shadow from both south and north, leading to drier conditions throughout the year. On an average, the annual precipitation ranges from 500mm - 700m in these valleys. However, the northern foothills of the Alps, the Alps and southern Switzerland receive around 2000mm in annual rainfall. The northern plateau experiences from 1000 - 1400mm of annual rain. The precipitation mostly occurs in the summer and is almost the double of winter precipitation (Meteoswiss). The mean temperature fluctuations in the Alps can reach a minimum

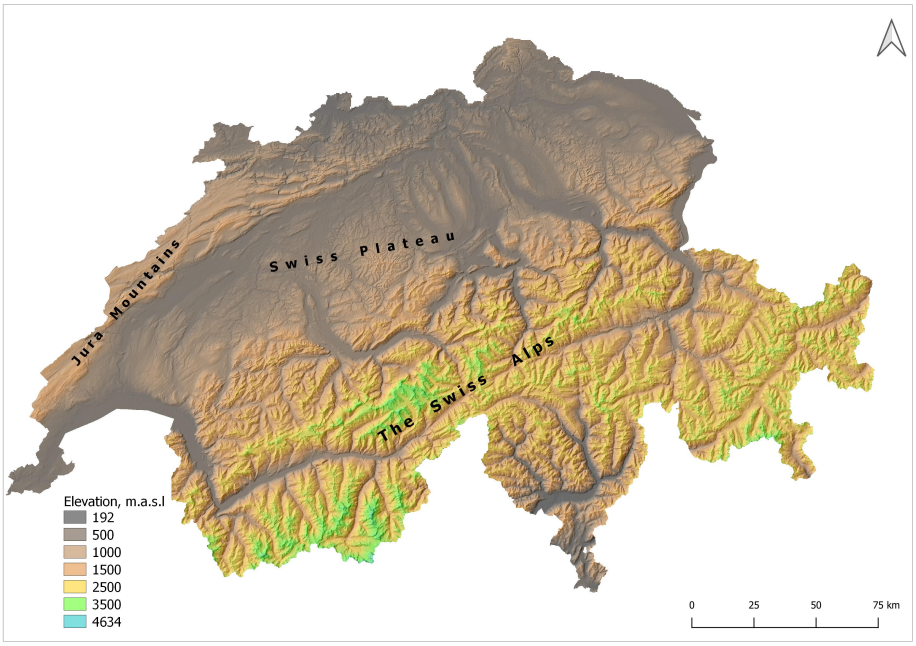

Figure 3.3.: Topographical map of Switzerland

of around -1°C in January to a maximum of 17°C in July. The mountainous regions are characterized by Alpine temperatures.

The average number of days with mean temperature less than 0°C is around 28 in the flatlands whereas for areas above 2500 m.a.s.l the average number of days in a year rises to 213. A more detailed picture can be inferred from table 3.3.

Table 3.3.: Elevation zone-wise characteristics in Switzerland

Zones, m.a.s.l	% of total area	Mean annual temperature,°C	Avg. no. of days, $T_{mean}<0°C$
< 0-500	17%	10.5	28
500-1000	29%	9.0	43
1000-1500	16%	6.3	76
1500-2500	27%	2.4	136
>2500	11%	-1.7	213

Above 1200 m.a.s.l, the winter precipitation predominantly falls as snow, with the snow pack lasting for weeks to months in the higher altitudes. The low-lying areas in the western and northern parts have transient snow characteristics, as the snow is very short-lived in these regions. The average snow season in Switzerland ranges from September to July. However, it is not uncommon to have the low lying areas completely devoid of snow and the higher elevation having snow all year round. For mid-elevation, the snow season starts in November and recedes completely by May. The summer discharge in Switzerland is highly influenced by the snow and glacier melts from the mountainous regions. Major European rivers such as the Rhine (375km) draining into the North sea, the Rhone (264 km) flowing

into the Mediterranean and the Inn (90km) draining into the Black sea originate in Switzerland. Due to the paramount importance of the snow-melt driven tributaries in Switzerland which feed these major rivers, the analysis of the performance of the methodology was designed to simulate the snow-cover distribution in partly longer duration snow conditions in this region.

For hydrological modeling, three catchments viz. Reuss at Seedorf, Aare at Brienzwiler and Thur at Andelfingen were considered. The Reuss and Aare catchments consist of 6.4% and 15.5% glaciated areas and experience a higher duration of snow cover. The mean annual flow in Reuss is about 42 cumecs with the peak flow month in June. Aare at Brienzwiler shows a mean annual discharge of about 37 cumecs with June/July as the peak flow month. Likewise for the Thur catchment at Andelfingen, the annual discharge is around 37 cumecs and the peak flow occurs in March/April. The further characteristics of these catchments are shown in table 3.2.

3.2. Data

3.2.1. Hydro-meteorological data

Both Germany and Switzerland have a well-distributed network of observation stations for meteorological variables. Switzerland, despite the mountainous terrain, boasts a reasonably denser network of precipitation and temperature monitoring stations, than other mountainous regimes around the world. Exploiting this data availability, daily station measured meteorological drivers, namely precipitation and minimum, maximum, and mean temperatures from 2010–2018 were acquired for the Swiss region from the Federal Office of Meteorology and Climatology (MeteoSwiss). Likewise for Germany as well, the same variables were acquired for 2010-2015 on a daily scale, from the Deutsche Wetterdienst (DWD). Similarly for the hydrological modeling part, daily discharge time series for the selected catchments were obtained from the Bundesanstalt für Gewässerkunde (BFG) for Germany and the Federal Office for the Environment (FOEN) for Switzerland for the same time period as the meteorological data.

3.2.2. Topography

To depict the topographical structure of the study regions, the Shuttle Radiation Topography Mission (SRTM) 90m resolution digital elevation model (DEM) [Jarvis et al., 2008] was used in this study. The DEM was upscaled to match the MODIS resolution of 500m, for consistency. Likewise, the aspect and the slope information were extracted from the resampled DEM.

3.2.3. MODIS snow-cover data

With the rapid advancement in RS technology, the global change monitoring, especially in the environmental field have been increasingly incorporating these RS products in different

aspects of environmental processes. The Moderate Resolution Imaging Spectroradiometer (MODIS) is one of these widely used platforms for earth and climate measurements. First launched as one of the sensors in the Terra satellite of the National Aero-Space Agency (NASA) Earth Observing System (EOS) in 1998 and later on board the Aqua satellite in 2002, MODIS has increasingly found its application in different fields of environmental monitoring, owing to it superior temporal resolution (daily) and comparable spatial resolution (upto 250m) on a global scale which allows the research community to track changes in the landscape over time globally. The further advantage of MODIS is that the passes of Aqua and Terra are envisioned in such a way that one passes the Equator from north to south in the morning and the other passes from south to north in the afternoon. This allows the space for accuracy enhancement by optimizing cloud-free remote sensing and minimising any other optical obscurities such as shadow or aerosols that are unique to morning or afternoon sunlight [Gafurov, 2010] for an intra-diurnal assessment of the global surface conditions such as the snow-cover, cloud cover, skin temperatures, etc. MODIS has a viewing swath width of 2,330 km monitoring the entire Earth surface in every 1-2 days. The orbital distance of the Terra and Aqua satellites is around 705km from the Earth. With sensors measuring 36 spectral bands ranging from 0.405 and 14.385 µm, MODIS acquires the surface information in 3 spatial resolutions, 250 meter in bands 1 and 2, 500 meter resolution in bands 3 to 7, and 1000 meter. MODIS inferred data include the global coverage distributed data pertaining to the land surface such as vegetation indices, surface albedo, land surface temperature, snow cover and surface reflectance. MODIS based products have been widely implemented in vegetation monitoring, long term land cover changes, global snow cover trends, water levels, and mapping wildfires, around the world.

In this study, the MODIS snow-cover products **MOD10A1** from Terra and **MYD10A1** from Aqua [Hall and Riggs., 2016] were acquired, processed and integrated in snow-melt modeling as a reference variable for calibration. These dataset are the version 6 products from MODIS and contain daily, gridded snow cover and albedo estimated using the radiance information measured by the MODIS on board both Terra and Aqua satellites. The snow cover information in these data is identified using the NDSI method (Eq. 2.1), mapping the global snow-cover at a resolution of 500m (at nadir) at a daily resolution. The NDSI measures the magnitude of the differences between the reflectance in visible and shortave infrared spectra. The snow cover information indicates the single best observation of the day for each pixel, and each observation depicts the best sensor view of surface in cell based on solar elevation, distance from nadir, and cell coverage. [Hall and Riggs., 2016].

The Aqua and Terra's sun-synchronous, near-polar circular orbit is timed in such a way that Aqua crosses the Equator from south to north at approximately 1:30 P.M. local time and Terra passes via the descending node, i.e. from north to south at around 10:30AM local time, thereby acquiring a global coverage in 1-2 days. These data are available from July 2002 for Aqua and February 2000 for Terra till date. In addition to the NDSI based snow cover data, the dataset also incorporates additional gridded information on the raw NDSI, information on the qualities of the NDSI snow cover and the NDSI algorithm, and snow albedo.

Among a wide pool of available satellite-based snow-cover products, MODIS snow-cover data was selected for this study mainly due to the high temporal resolution and mapping

accuracy relevant for modeling purposes, at a reasonably acceptable spatial detail. There have been many studies regarding the application of MODIS snow-cover data [Tong et al., 2009a; NSIDC] which have highlighted the accuracy of MODIS inferred snow-cover in terms of snow-cover change monitoring, and the assimilation in hydrologic and land surface models. Different studies have compared MODIS snow cover data with other satellite products and ground based snow depth measurements, and found accuracies between 90 - 95% in cloud-free conditions, however depending upon land cover, and the condition and depth of snow [Nester et al., 2012; Tong et al., 2009b; Parajka and Blöschl, 2012]. The MODIS snow cover products have found their applications ranging from SCA forcing for Snowmelt Runoff models [Immerzeel et al., 2009; Li and Williams, 2008; Tahir et al., 2011], for model evaluation [Shamir and Georgakakos, 2007; Bavera and De Michele, 2009], as an input to the models in data assimilation schemes [Zaitchik and Rodell, 2009], as integrated additional data in calibrating conceptual models [Parajka and Blöschl, 2008(b); Şorman et al., 2009; Franz and Karsten, 2013], for reconstructing the spatial distribution of SWE using distributed hydrologic models [Rittger et al., 2016; Molotch and Margulis, 2008], and for correcting basin-scale snowfall in mountainous basin [Shrestha et al., 2014].

Despite the wide-scale applicability of MODIS owing to its superior coverage and high spatio-temporal resolution, as indicated by numerous studies, the persistent cloud coverage, more often than not significantly limits MODIS application for snow cover mapping as well as integrating into the hydrological modeling context. However, as explained in Chapter 2, different spatio-temporal cloud filtering techniques have been devised recently. Here in this study, the MODSNOW algorithm [Gafurov and Bárdossy, 2009; Gafurov, 2010] was adopted for the cloud removal procedure in the study.

A gridded schema was extracted for both study regions assuming MODIS snow-cover data as a reference grid. This schema (464m $\times$ 464m) aws used as the reference gridded domain for the data interpolation and modeling. The schema resulted in 210566 cells in Switzerland and 167528 cells in BW.

4. Geostatistical Interpolation of meteorological inputs

4.1. Brief concept of kriging

The principle of Geostatistics mainly stems from the empirical works regarding interpolation techniques for mining purposes from a mining engineer Danie Gerhardus Krige from South Africa, later formalized by Georges Matheron, a French mathematician [Daya Sagar et al., 2018]. Since the inception of the approach , geostastical techniques have remained virtually synonymous to 'kriging' [Jieru, 2018] and have since then evolved from geological investigations in gold mining, to different fields inclduding interpolation of hydrological and hydro-geological variables in recent years.

Virdee and Kottegoda [1984] discuss that the economical aspects related to gold mining sector where kriging application found its roots benefitted from higher sampling density of observation owing to the value of gold. Regarding the hydrological investigations, with water being 'cheaper' than gold though equally valuable, the observational station density is limited. The variables such as precipitation, temperature, hydraulic transvissivity are generally limited to station observations at specific locations. Due to the spatial variability inherent in these hydrological variables, interpolation steps are required to regionalize these variables to unknown locations, thereby capturing the spatial distribution, for various practical implementation like distributed hydrological modeling [Lebrenz and Bárdossy, 2019]. However, the challenge lies in choosing the interpolation technqiues that best interpolates observed data [Caruso and Quarta, 1998]. Compared to other methods, kriging offers better suitability for data with inherent higher degrees of natural variability [Virdee and Kottegoda, 1984].

Kriging interpolation are based on the concept of statistical dependence or the spatial autocorrelation assuming the random variable values between a pair of points to be similar to a function of the distance between them. Kriging estimates the values of the variable at unknown locations or a spatial field by finding the weights (λs) of a linear estimator (Eq. 4.1) along with the uncertainty estimates related to each interpolated value. The linear estimator considers a linear relationship of the values in the neighbouring known samples x_i as:

$$\hat{Z}(x) = \sum_{i=1}^{n} \lambda_i Z(x_i) \tag{4.1}$$

where $\hat{Z}(x)$ is estimation of a random function $Z(x)$ with known values at n locations in the space $Z(x_i)$, where each value of $z(x)$ is the realization of $Z(x)$, λ_is are the weights which

are chosen a priori in such a way that the estimation is unbiased (Eq.4.2) and the estimation variance is minimized i.e. the condition of optimality (Eq.4.3) [Ahmed and Devi, 2008].

$$E[Z(x) - \hat{Z}(x)] = 0 \tag{4.2}$$

$$\sigma^2(x) = var[Z(x) - \hat{Z}(x)] \quad = -\sum_{j=1}^{n}\sum_{i=1}^{n} \lambda_j \lambda_i \gamma\left(x_i - x_j\right) + 2\sum_{i=1}^{n} \lambda_i \gamma\left(x_i - x\right) \rightarrow \text{minimum} \tag{4.3}$$

where $E[Z(x)]$ is the expected value of the random function $Z(x)$ and $\sigma^2(x)$ is estimation variance quantifying the uncertainty in the estimation of Z at an unknown location.

Matheron [1965] explained the intrinsic hypothesis of the ordinary kriging technique in two conditions: (i) the expected value of the random function $Z(x)$ remains constant throughout the domain under study (Eq. 4.2), i.e the first moment is stationary and (ii) the correlation between the two random variables or the variance of increment solely depends on the spatial distance between them (Eq. 4.5). By extension, Eq.4.2 then becomes Eq.4.4 as the mean is constant the the mean of the increment remains 0.

$$E[Z(x)] = m \tag{4.4}$$

$$\mathit{Var}\big[Z(x+h) - Z(x)\big] = 2\gamma(h) \tag{4.5}$$

where, m is the constant mean, h is the separation distance and $\gamma(h)$ is the semivariogram also called the variogram. This (semi) variogram is calculated for all $x, x+h \in$ domain D as:

$$\gamma(h) = \frac{1}{2} E[Z(x+h)] - Z(x)]^2 \tag{4.6}$$

Using the linear estimator Eq. 4.1 and the unbiasedness assumption in Eq.4.4, one can get Eq.4.7.

$$\sum_{i=1}^{n} \lambda_i = 1 \tag{4.7}$$

The estimation variance from Eq.4.3 can then be minimized to obtain the sets of weights for the best linear unbiased estimators. These weights reflect the 'structural' closeness of the known locations to the unknown ones. The optimization problem is solved by introducing a term Lagrange multiplies μ using linear equation system in Eq.4.8.

$$\sum_{j=1}^{n} \lambda_j \gamma(x_i - x_j) + \mu = \gamma(x_i - x) \quad \text{for } \; i = 1, \cdots, n \tag{4.8}$$

$$\sum_{j=1}^{n} \lambda_j = 1 \tag{4.9}$$

Substituting the kriging weights into Eq.4.8, the optimum minimum variance also termed as the kriging variance can be simplified as in Eq. 4.10. This equation has no theoretical significance but facilitates a simplistic estimation variance calculation.

$$\sigma_K^2(x) = \sum_{i=1}^{n} \lambda_i \gamma(x_i - x) + \mu \tag{4.10}$$

There are known limitations of the intrinsic hypothesis assumed in the ordinary kriging methodology as described in Lebrenz and Bárdossy [2019]:

(a) The stationarity assumption in the first condition of the intrinsic hypothesis (Eq. 4.4), forces an unbiased estimation error in the entire domain, as the variable is required to be stationary throughout the domain. This unbiased error imposes a systematic under-estimation in high observational magnitudes and over-estimation in locations with low values.

(b) The magnitude of observations have no influence on the magnitude of the estimation variance as it depends only on the observational spatial structure i.e on the a-priori variance of the observations and the selected variogram model [Jieru, 2018; Goovaerts, 2000]. However, the variograms are derived from the observations.

(c) The Gaussianity assumption for the marginal distribution of the observed data should be maintained for adequate performance, which is often not the ideal case with most of the observed variables [Journal and Alabert, 1989; Lebrenz and Bárdossy, 2019].

Different geostatistical methodologies have been devised to overcome these shortfalls in ordinary kriging. The External Drift Kriging (EDK) [Ahmed and De Marsily, 1987] allows the trend of the regionalized variable, which adds value to the non-stationarity requirement to avoid the aforementioned problem of unbiased estimation error. However, the other limitations remain the same with the EDK. However, EDK has found wide implementation in practical applications in different disciplines ranging from mining to hydrgeological and climatological studies [Bourennane et al., 2000] . Likewise, indicator kriging and probability kriging aim to address the inherent non-Gaussiantity of the marginal distributions of the environmental variables to fit the kriging assumptions [Carr and Mao, 1993; Carr, 1994].

This study uses EDK method for temperature interpolation and residual kriging for the interpolation of precipitation in the study domain. The employed techniques are further explained in the subsequent sections.

4.2. External drift kriging

EDK is the theoretical extension to ordinary kriging where one or more auxiliary variables are incorporated in the interpolation algorithm to estimate the variable of concern at unknown points. This allows the prediction of a variable Z using another deterministic variable(s) Y exhaustively known in the same domain [Bourennane et al., 2000] and is linearly

correlated to Z. This linear relationship has to be maintained in EDK approach. In case of a non-linear function describing the relation between the two variables exists, the auxiliary data should be first be transformed to a linear relationship and then transformed data can be then introduced as external drift [Bourennane et al., 2000]. The trend variable allows the expectation of Z to be non-stationary, thereby formulating the first condition of the intrinsic hypothesis as:

$$E[Z(x)] = a.Y(x) + b \tag{4.11}$$

where a and b are the coefficients of the linear relationship between Z and Y assumed to be constant throughout the domain. The linear estimator ($\hat{Z}(x)$) remains the same as Eq.4.1 and the unbiased estimation constant holds as Eq.4.2. The equality constraint can be further expanded from Eq.4.11 as:

$$a \cdot \left[\sum_{i=1}^{n} \lambda_i Y(x_i) - Y(x) \right] + b \cdot \left[\sum_{i=1}^{n} \lambda_i - 1 \right] = 0 \tag{4.12}$$

Similarly, the unbiased condition requires the following constraints Eqs.4.13 and 4.14 for constant and nonzero a and b. The optimization for the weights is done by minimizing the estimation variance through introduction of two Lagrange multipliers viz. μ_1 and μ_2 and the linear equation equation system can be expanded as Eq.4.15.

$$\sum_{i=1}^{n} \lambda_i = 1 \tag{4.13}$$

$$\sum_{i=1}^{n} \lambda_i Y(x_i) = Y(x) \tag{4.14}$$

$$\sum_{j=1}^{n} \lambda_j (x_i - x_j) + \mu_1 + \mu_2 Y(x_i) = \gamma(x_i - x) \quad \text{for } i = 1, \cdots, n \tag{4.15}$$

where, γ is the semi-variogram, $Y(x)$ is the trend variable that needs to be known throughout the domain in all known and unknown locations, where the estimations are to be made. The estimation uncertainty or the kriging variance is also modified to:

$$\sigma_K^2 = \sum_{i=1}^{n} \lambda_i (x_i - x) + \mu_1 + \mu_2 Y(x) \tag{4.16}$$

In theory, the theoretical variograms should be calculated using variable Z conditioned on the explanatory variable Y, i.e. using the regression residuals. However in practice, due to the computational simplicity, the estimation of variogram of residuals is usually skipped and calculated based on the variable Z only [Hengl et al., 2003; Ahmed and De Marsily, 1987])

4.3. Residual Kriging (RK)

The residual kriging approach [Phillips et al., 1992; Martínez-Cob, 1996] allows a linear regression (Eq.4.17) of the dependent variable Z_x at all points x_i on auxiliary variables Y_x and then ordinary kriging is done on the regression residuals, in contrast to the EDK where the kriging is done directly with the auxiliary variable. In general, the Ordinary Least Squares (OLS) method of regression is used. The residual r_x at for all the known locations are then calculated as in Eq.4.18 and is expected to follow the intrinsic hypothesis in kriging. However, as a result of the added information or the drift, a part of variability explained by the drift is lost, however the spatial variability is retained [Odeh et al., 1995; Prudhomme and Reed, 1999].

$$Z_y(x) = aY(x) + b \tag{4.17}$$

$$r(x_i) = Z(x_i) - Z_y(x_i) \tag{4.18}$$

For the unknown locations, the $\hat{Z}_y$ is calculated using the regression coefficients a and b from Eq.4.17 and the residual $\hat{r}(x)$ is obtained from the ordinary kriging of the residuals at known locations as in Eq.4.19.

$$\hat{Z}(x) = \hat{Z}_y(x) + \hat{r}(x) \tag{4.19}$$

As per the assumption of the OLS regression, the residuals are uncorrelated with the dependent variable Z_y, i.e. independently identically distributed irrespective of the location. In this case the regionalization fails and variogram does not exist. Techniques like Generalized Least Squares (GLS) method are available for the regression to tackle the contradiction, however, due to complexities in practical implementation, OLS (owing to the simplicity) has been preferred widely especially for the interpolation of environmental variables such as rainfall, temperature and evaporation [Prudhomme and Reed, 1999; Jieru, 2018; Martínez-Cob, 1996].

4.4. Evaluation of interpolation schemes

Leave-one-out cross validation (LOOCV) method was used in this study to validate or test the performance of RK in precipitation and EDK in temperature interpolation. LOOCV is generally used to evaluate different kriging techniques to identify the suitable approach for interpolation. However since kriging is not the main focus of the study, LOOCV was employed just to check if the adopted methods would have satisfactory performance in the region.

With LOOCV, stations are sequentially left out one by one and the Kriging is carried out for the left out station using the information from other available stations as training data.

The kriged estimates were then validated against original samples using different evaluation criteria. The error statistics used for the evaluation were Root Mean Square Error (RMSE) to measure the difference, Nash-Sutcliffe Efficiency (NSE), Pearson's correlation and Spearman's correlation for the whole season and winter season over different years in both Switzerland and BW.

4.5. Application of Kriging in this study

Due to the strong orographic effects in the mountains and the resulting spatial heterogeneity, rainfall interpolation is very complex [Bárdossy and Pegram, 2013] leading to anisotropy [Bacchi and Kottegoda, 1995]. This complexity coupled with data scarcity is hard to avoid even with the sophisticated kriging algorithms as the bias enforced by under-sampling at higher elevation still persists [Briggs and Cogley, 1996; Prudhomme and Reed, 1999]. The residual kriging offers the influence of other explanatory variables in explaining the precipitation dynamics thereby compensating for the lack of data in these regions [Odeh et al., 1995]. The RK was thus carried out in this study in conjunction with a Multiple Linear Regression (MLR) based approach using directionally smoothed elevation. Directional smoothing of elevation was done using half-space smoothing [Bárdossy and Pegram, 2013]. They found out that precipitation is influenced by the shadow effect due to the orographic impact on the first rising slope from valleys towards the uplifted terrain structure.

$$h_s(x) = \sum_{g=1}^{G} w(x - x_g) h(x_g) \tag{4.20}$$

where,

$$w(x - x_g) = \begin{cases} 0 & \text{if} \quad |x - x_g| > d \quad \text{or} \quad \langle v, (x - x_g) \rangle < 0 \\ \\ c_w \left(1 - \frac{|x - x_g|}{d}\right) & \text{otherwise} \end{cases} \tag{4.21}$$

where for a given location x, $h(x)$ is the local elevation, $h_s(x)$ is the shifted and smoothed elevation, G is the number of elevation grid points, v is the vector indicating advection direction, with a north and east component, and x_gs are the grid points of the DEM, c_w is the constant selected such that $\sum_{g=1}^{G} w(x - x_g) = 1$. The difference between x and x_g is a 2-D vector which provides the direction from x_g to x. $\langle , \rangle$ is the scalar product of the vectors.

Following Bárdossy and Pegram [2013], transformed elevation was considered instead of the local elevation. This transformation of terrain, i.e smoothing and shifting, was done to identify the directional advection for each day. Eight different directions with 45 degrees incremental angles, and 3 different smoothing distances (2, 3 and 5 kms) were used. For each time-step, a simple optimization was done to assess the correlation of the precipitation with the shifted DEMs, and the best direction and the smoothing radius for the timestep were identified. This shifted and smoothed elevation was then used along with X and Y coordinates of the stations in the MLR to obtain precipitation estimates for stations. The residuals were then calculated for each day, then intepolated using ordinary kriging to obtain the

kriged residuals. MLR estimated precipitation surfaces for each time step employing XY coordinates and the directionally transformed elevation for each grid point were summed with the kriged residual surfaces to obtain the final precipitation fields. 224 stations in BW and 449 stations in Switzerland were used to interpolate station based precipitation observations on to the schema grids.

Likewise, External Drift Kriging was opted for the study for temperature interpolation, with station elevation extracted from the DEM as a drift [Hudson and Wackernagel, 1994]. The station elevation correlation was checked with the temperature observations, and was found to be strongly correlated with monthly and seasonal temperatures. Daily minimum, maximum, and mean temperature observations from 85 stations in Baden-Württemberg and 365 stations for Switzerland were used for interpolation.

The summary of LOOCV for the interpolation are presented in table 4.1. It is well evident from the table that the overall mean kriging performance is satisfactory for both of the adopted interpolated methods. The winter performance was observed to be slightly decreased in both regions for temperature. However, winter precipitation was interpolated with higher accuracy. The kriging evaluation scores are similar for both regions.

A closer scrutiny at elevation zones, as shown in figure 4.1b with the case of RK interpolated precipitation in Switzerland, shows an overall decline in NSE performance in the winter season was observed with increasing elevation. NSE was selected here to evaluate how well the kriging process interpolated the large precipitation values during cross-validation, as these higher precipitation during the winter can in turn result in higher accumulation of snow. The idea was to not underestimate these events. This aforementioned loss in performance can be attributed to less density of stations in the higher elevation. Within a specific elevation zone, the elevation dependent decline was not observed. The NSEs range from 0.56 to 0.97 for the time period between 2010 and 2018. The station locations along with the corresponding NSE performance are shown in figure 4.1a. The NSE values of greater than 0.6 for all but one station indicate that the Kriging process works satisfactorily in the region. For temperature interpolation, however, no elevation specific trend was observed with EDK interpolation. The RMSE values were analysed in the case of temperature interpolation. The values ranged from 0.38 °C at elevation 432 m.a.s.l to 4.17 °C in one of the stations at around 2490 m.a.s.l. The values for the RMSEs for majority of the stations remained below 2.5°C. With an overall RMSE of about 1.28 °C for the winter period, the kriging methodologies were considered as well-validated in Switzerland.

The results for precipitation interpolation in Baden-Württemberg region (refer figure 4.3) also highlight the applicability of the kriging in the region. The lowest NSE was reported at a lower elevation of 252 masl. However, overall, the NSE performance shows a satisfactory performance of above 0.65 for all other stations. No elevation related trend was observed in this case. Similar results have been reported with the case of temperature interpolation with a mean winter RMSE of about 0.98°C. With these cross-validation results, the overall performance of winter for the whole as well as winter season was deemed adequate for further modeling purposes in the study.

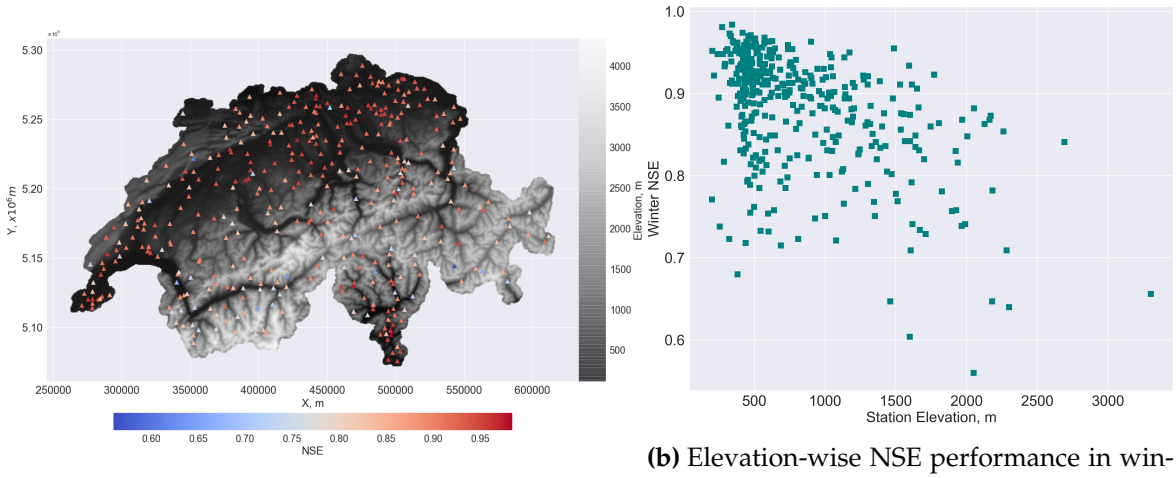

(a) Station-wise NSE performance in winter

(b) Elevation-wise NSE performance in winter

Figure 4.1.: Residual Kriging performance for precipitation in Switzerland

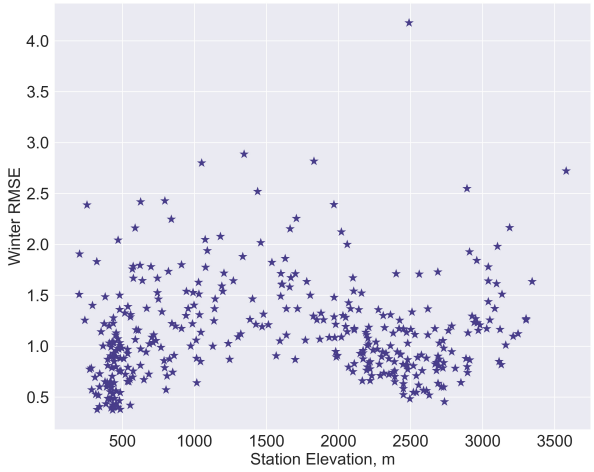

Figure 4.2.: Elevation-wise RMSE performance in winter for temperature interpolation in Switzerland

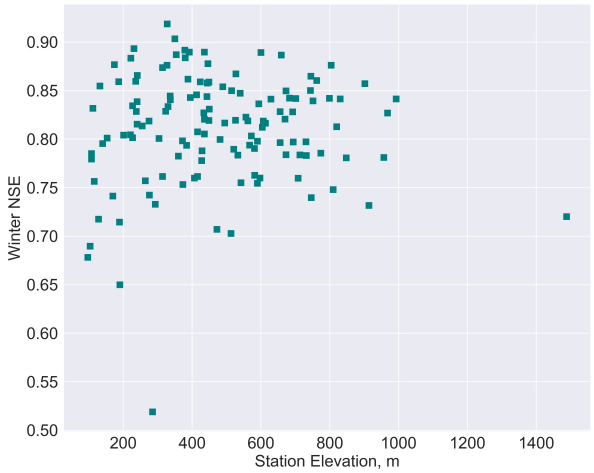

Figure 4.3.: Elevation-wise NSE performance in winter for precipitation interpolation in Baden-Württemberg

Table 4.1.: Leave-one-out cross validation statistics of RK for precipitation and EDK for temperature in BW and Switzerland

Region	Variables	Reference period	Pearson correlation	Rank correlation	RMSE	NSE	No. of stations
Switzerland	Mean temp.	Overall	0.990	0.990	1.130	0.971	365
		Winter	0.978	0.977	1.288	0.936	
	Precipitation	Overall	0.933	0.830	2.637	0.856	449
		Winter	0.950	0.823	2.166	0.883	
Baden-Württemberg	Mean temp.	Overall	0.992	0.992	0.938	0.978	85
		Winter	0.979	0.976	0.982	0.943	
	Precipitation	Overall	0.907	0.876	2.295	0.811	128
		Winter	0.960	0.912	1.479	0.901	

5. Snow-melt models and their extension

Snow is a crucial component of the water cycle that governs the annual variations in hydrology in the mountainous areas as well as in the mid- and high latitude regions around the globe. The accumulation in the snow pack provides a temporary reservoir of available water to be released at a favorable temperature for melt, which in turn recharges the hydrological discharge. The quantification of this accumulated snow water equivalent is highly imperative as the water coming from ablation governs water resources development trajectories such as hydropower, agriculture and navigation, as well as to balance the ecological environment [Girons Lopez et al., 2020; Hannah et al., 2007; Barnett et al., 2005]. Snow-related disasters such as avalanches and rapid onset of melt triggering floods also raises the need of accurately and reliably understanding the snow evolution and estimating the available water from snow as this need becomes starker given the evident impacts of rising temperatures and climate change.

As discussed in previous chapters, there have been advances in understanding and quantifying the underlying snow processes, ranging from expanded observational networks, experimental catchments for snow research [Pomeroy and Marks, 2020] to RS based snow monitoring. However, given the complexities of the snow-dominated terrain, the limitations of being non-representative with observational network and experimental sites, and limitations regarding standalone usage of RS data, still persist hindering the reliable estimation of underlying snow processes in a regional context. Snow-melt modeling remains the most widely used methods in practice to understand the accumulation, storage and ablation of snow and its resulting impact on the hydrology. Depending on the types, these models predict snow-related variables such as snow depth, SWE, snow density or resulting discharge which usually drive different operational applications [Avanzi et al., 2016]. However, based on the simulation strategy, these models are also restricted with data availability and the degree of detail required for simulation. The following section discusses the two major modeling techniques being used for snow-related studies.

5.1. Energy budget models

These models are physically based in nature and deemed to provide better representation of snow processes. These models consider the incoming solar radiation as the major control of the variability of the energy available for melting the snowpack [Girons Lopez et al., 2020] and are useful for distributed modeling context. Energy balance of the snow-pack is calculated at each time step and uses the basis as Eq. 5.1 [Todd Walter et al., 2005].

$$\lambda_F \rho_w \Delta M = S + L_a - L_t + H + LE + G + R - CC \tag{5.1}$$

where,

λ_F: latent heat of fusion, 335 $kJkg^{-1}$,

ρ_w : density of water, 1000 kg/m^3,

ΔM: Melt from the snow-pack (m),

L_a: atmospheric long wave radiation, kJm^{-2}

L_t: terrestrial long wave radiation, kJm^{-2}

LE: energy flux associated with the latent heats of vaporization and condensation at the surface, kJm^{-2}

G: ground heat conduction to the bottom of the snowpack, kJm^{-2}

R: heat added by precipitation, kJm^{-2}

CC: change of snowpack heat storage, kJm^{-2}

Owing to the physical basis, the simulation of snow-melt particularly in complex terrain as well as under vegetation cover, is realistic with these models. However, they require detailed information on elevation, wind speed and direction, cloud cover information, snow density and so on which are generally not available from conventional observational stations. Added to that is the limitation on methods to extrapolate of these 'rarer' inputs to the complex mountain terrain. Also the accurate spatial parameterization of model parameters often limit these models application on a regional context as the model complexities increase [Zhou et al., 2021].

Because of the data-intensive model requirements and in line with the research's objective to develop simplistic melt models with less data requirement, energy budget models are not considered in this study.

5.2. Temperature Index (TI) models

The temperature index models also known as the degree-day models are conceptual models which assume melt rate as a linear function of the air temperature [Martinec, 1960], if the temperature is above the freezing value, controlled by a proportionality constant commonly termed as the degree-day factor. The fundamental basis for these models is the assumption that the temporal variability in air temperature can be used as a proxy for the temporal variations in the incident solar radiation [Ohmura, 2001]. The simplest TI model basis is shown in Eq. 5.2.

$$M = DDF.(T_{air} - T_{crit}) \tag{5.2}$$

where, $M(mmday^{-1})$ is the snow-melt, DDF is the degree day factor $(mm^{\circ}C^{-1}day^{-1})$, T_{air} is the air temperature $(^{\circ}C)$ and T_{crit} is the threshold temperature above which snow starts to melt $(^{\circ}C)$ generally set to $0^{\circ}C$. The DDF parameter is often the parameter to be calibrated but also can be calculated based on measurements of snow density and through an empirical relationship [Zhou et al., 2021] as Eq. 5.3

$$DDF = 1.1 * \frac{\rho_s}{\rho_w} \tag{5.3}$$

where, ρ_s and ρ_w are the densities of snow and water respectively.

Simplistic formulation, computational efficiency and good performance in terms of snow-related simulations have allowed these models to be successfully applied in different contexts. The main attraction towards these models is the low and easily available data requirement which makes them a fit for data-scarce regions as well. However, the simplistic assumption of these models sometimes become the limitations as well. Representation of solar radiation by air temperature does not always hold true especially in high mountains where the temperature often stay within the freezing point [Gabbi et al., 2014; Pellicciotti et al., 2005] or wherever there is significant effect of sublimation of the snow water requirement on the snow processes [Girons Lopez et al., 2020]. To account for these drawbacks, there have been a lot of studies to extend the model formulation incorporating different variables such as radiation to create a hybrid model using energy balance and TI approaches [Hock, 1999]; or incorporating wind speed or relative humidity in TI models by Zuzel and Cox [1975]. Brubaker et al. [1996] proposed Eq.5.4 incorporating the net radiation into the basic degree day model.

$$M = m_Q R_d + a_r T_d \tag{5.4}$$

where, $M(mmday^{-1})$ is the snow-melt, m_Q is a physical constant that converts energy to water mass or depth $((mmday^{-1})(Wm^{-2})^{-1})$, a_r is the restricted degree-day factor $(mm^{\circ}C^{-1}day^{-1})$, and T_d is the degree- day index $(^{\circ}C)$, i.e T_{air} - T_{crit} whenever the T_{air} exceeds the T_{crit} value.

Some studies introduced the spatial heterogeneity of degree day factors in terms of basin characteristics such as forest covers [Kuusisto, 1980] and elevation zones in the snow-component of widely used hydrological models such as Snowmelt Runoff Model (SRM) [Martinec, 1975] and HBV (Bergström [1995]). Likewise, changing the model structure to a distributed approach to better capture the spatial heterogeneity with inputs distributed in space and time, has also been carried out in different studies at different spatio-temporal resolutions [Cazorzi and Dalla Fontana, 1996; Pellicciotti et al., 2005; Jost et al., 2012; Hock, 2003].

Girons Lopez et al. [2020] also evaluated various formulations of the temperature index approach to analyze their response via the HBV model in 54 mountainous European catchments. They found out that the rather simplistic snow routine in HBV was enough to reliably simulate snow processes and the resulting discharge. Specific modifications to the snow-module such as using an exponential melt function and incorporating a seasonally variable degree-day factors were found to be valuable additions among the modifications tested. Caicedo et al. [2012] also identified the best-performing variants of degree-day calculations for different regions in Colombia. They concluded that these specific targeted

alterations could improve the performance in terms of snow processes, however, not necessarily in all contexts. A careful scrutiny of these alterations to the model structure is highly pertinent as it relates to the application, availability of the data required to drive the mode as well as the purpose of study.

5.3. Snow-melt model variants

In line with the first research objective and with the degree-day approach as a basis, this research also extends Eq.5.2 to different variants incorporating different aspects governing snow hydrology such as precipitation-induced melt, radiation, and topographical characteristics. Due to inherent large-scale spatial variability in mountainous regions, distributed meteorological inputs were employed to drive the different variants of the extended degree-day snowmelt models on a daily timescale. The major parameters used in the models are defined below:

$P(t,x)$= precipitation amount at location x at time t, mm

$S(t,x)$= snow water equivalent amount at location x at time t, mm

$T_{av}(t,x)$= mean temperature at location x at time t, °C

$P_s(t,x)$ = water equivalent of precipitation falling as snow at location x at time t, mm

$M_s(t,x)$ = melt water amount at location x at time t, mm

T_T = threshold critical temperature defining snow or no snow, °C

D_s = dry degree day factor, $mm°C^{-1}$

$T_{mx}(t,x)$= maximum temperature at location x at time t, °C

$T_{mn}(t,x)$= minimum temperature at location x at time t, °C

scf= snow correction factor to account for the gauge undercatch of snow

The following model variants were used to estimate the Snow Water Equivalent (SWE) (mm) and the resulting snow-cover in each pixel. Different nomenclatures are given to the models for the ease of understanding. Each successive model represents a gradual parameter wise modification to the basic degree-day model.

5.3.1. Basic Degree-day Model (Model 1)

This model is the most basic of all model variants and was also used in the original HBV model. This model estimates the melt for each time-step as a linear function of the difference between daily mean temperatures and a threshold temperature value demarcating liquid precipitation and snow precipitation phases. A degree day factor controls the rate of melt. Equation 5.5 calculates the amount of SWE available in pixel 'x' at time 't'. Similarly the snow-precipitation and the resulting melt are calculated with Eq.5.6 as the model basis

for each pixel, 'x' in the study domain. A correction factor to account for the snowfall undercatch by the gauges and the vegetation interception scf is also used in this model and extended to all models in the study.

$$S\left(t,x\right) = \ S\left(t-1,x\right) + P_s\left(t,x\right) - \ M_s\left(t,x\right), \tag{5.5}$$

Where,

$$P_s\left(t,x\right) = \begin{cases} P(t,x)\cdot scf & \text{if} \quad T_{av}(t,x) < T_T \\ 0 & \text{if} \quad T_{av}(t,x) \geq T_T \end{cases} \tag{5.6a}$$

$$M_s\left(t,x\right) = \begin{cases} 0 & \text{if} \quad T_{av}(t,x) < T_T \\ min(S\left(t,x\right), \quad D_s \ \left(T_{av}\left(t,x\right) - T_T\right) & \text{if} \quad T_{av}(t,x) \geq T_T \end{cases} \tag{5.6b}$$

5.3.2. Wet Degree-day Model (Model 2)

This variant adds a precipitation melt factor which controls the melt rate based on air temperature and the precipitation amount falling on the pack. This factor was incorporated to account for the melt induced by rain at temperatures higher than the critical threshold temperature. From an energy point of view, this model does not find higher relevance as the heat transfer due to the liquid rain entering the snow pack is relatively small. However, this model was formulated to compare the effect of heat transfer from the air temperature to the snowpack and its effect on the snow melt, in wet versus dry winter conditions. Bárdossy et al. [2020] used a similar precipitation induced melt in their version of HBV. This melt factor, referred to as D_w increases the melt from Eq.5.6b on days with precipitation higher than a threshold value. For a given wet day i.e., $P(t,x) > P_T$, the melt is calculated as in Eq.5.7. For a dry day, melt is calculated as Eq.5.6b.

$$M_s\left(t,x\right) = \begin{cases} 0 & \text{if} \quad T_{av}(t,x) < T_T \\ min(S\left(t,x\right), \quad D(t,x) \ \left(T_{av}\left(t,x\right) - T_T\right) & \text{if} \quad T_{av}(t,x) \geq T_T \end{cases} \tag{5.7}$$

Where,

$D(t,x)$ = D_s + D_w($P(t,x)$ - P_T)

P_T = threshold precipitation depth beyond which the liquid precipitation contributes to melt, mm

D_w = the wet melt factor, $mm.mm^{\circ}C^{-1}$

$D(t,x)$ = combined melt factor on wet days, $mm^{\circ}C^{-1}$

5.3.3. Wet Degree-day Model with snowfall and snow-melt temperatures (Model 3)

The instantaneous forms of precipitation as snow and liquid gives a clear indication of two temperature thresholds which demarcate the solid and liquid state of precipitation [Schaefli

et al., 2005]. This model includes different snowfall and snow-melt temperatures in Model 2 for a more accurate representation of the liquid to snow phase partition and melt initiation. This has been previously discussed in [Debele et al., 2009; Girons Lopez et al., 2020]. For temperatures in between, snow is linearly interpolated for the day as a proportion of the precipitation. The formulation of the model are given by Eqs.5.8 and 5.9.

$$P_s\left(t,x\right)=\begin{cases} P\left(t,x\right) & \text{if } \; T_{av}(t,x)<T_S \\ P\left(t,x\right)\cdot\left(\frac{T_{av}(t,x)-T_M}{T_S-T_M}\right. & \text{if } \; T_S\leq T_{av}(t,x)\leq T_M \\ 0 & \text{if } \; T_{av}(t,x)>\; T_M \end{cases} \tag{5.8}$$

$$M_s\left(t,x\right)=\begin{cases} 0 & \text{if } \; T_{av}(t,x)<T_M \\ min(S\left(t,x\right), \quad D(t,x)\;\left(T_{av}\left(t,x\right)-T_M\right)) & \text{if } \; T_{av}(t,x)\geq T_M \end{cases} \tag{5.9}$$

Where,

T_S and T_M are the snowfall and snow-melt temperatures respectively.

5.3.4. Aspect distributed snowfall temperatures (Model 4)

This model was envisioned with an assumption that topographical aspect plays a major part in the spatial distribution of snow-fall and snow-melt temperatures. In general, south facing slopes are warmer in the Northern hemisphere resulting in a faster melt of snow compared to the north facing slopes. Based on this assumption, this variant distributes the snowfall temperature in Model 3, according to the topographical aspect. The snowfall temperature distribution is done by Eq.5.10 below:

$$T_{S,x}\;=\;T_{Smin}+\left(T_{Smax}-\;T_{Smin}\right)*\left[0.5*\cos\left(aspect_x\right)+1\right]^{PF} \tag{5.10}$$

Where,

T_{Smin} = lower bound of the snowfall temperature, (°C)

T_{Smax} = upper bound of the snowfall temperature, (°C)

$aspect_x$ = topographical aspect of grid 'x', (radians)

PF = power factor to distribute the aspect

5.3.5. Aspect distributed snow-melt temperatures (Model 5)

This model distributes the snow-melt temperature in Model 3 within a range defined by minimum and maximum snowfall temperature, according to the topographical aspect. The snow-melt distribution is represented by Eq.5.11 below:

$$T_{M,x}\;=\;T_{Mmin}+\left(T_{Mmax}-\;T_{Mmin}\right)*\left[0.5*\cos\left(aspect_x\right)+1\right]^{PF} \tag{5.11}$$

Where,

T_{Mmin} = lower bound of the snow-melt temperature (°C)

T_{Mmax} = upper bound of the snow-melt temperature (°C)

5.3.6. Radiation Induced melt Model (Model 6)

The integration of radiation information in degree-day models can lead to better estimation of snow-melt [Hock, 2003]. This model was formulated to accommodate the radiation data in addition to the aspect-based temperature distribution. The radiation induced melt was added to Model 5 by incorporating the diffused incident radiation on the snow pixel on a cloud-free day. The incident global radiation is calculated using a viewshed based algorithm 'r.sun' [Hofierka and Suri, 2002; Neteler and Mitasova, 2002] and has an added advantage of radiation distribution in the valleys. Daily temperature difference $(tmax - tmin)$ for each grids was also calculated using interpolated daily minimum and maximum temperatures and was used as a cloud cover proxy. For this study, pixels with a daily temperature difference above a certain threshold were assumed to be cloud free and this is where radiation induced melt became active. Likewise, temperature differences lesser than the threshold render the pixels cloudy. The diffusion factor ranging from 0.2 for clear sky conditions to 0.8 for overcast conditions diffuses the incoming radiation. The radiation induced melt is added to the melt outputs from the preceding models on cloud-free pixels and is calculated using Eq.(5.12). Figure 5.1 below shows an example of diffused radiation calculated for a cloud free day in Baden-Württemberg.

$$M_{s-R}(t,x) = \begin{cases} (1-alb)\cdot r_{ind}\cdot R_D(t,x) & \text{if } T_{mx}(t,x) - T_{mn}(t,x) \geq 5°\text{C} \\ 0 & \text{if } T_{mx}(t,x) - T_{mn}(t,x) < 5°\text{C} \end{cases} \tag{5.12}$$

Where,

$M_{s-R}(t,x)$ = Radiation induced melt at grid x at time t, mm

$R_D(t,x)$ = Diffused radiation at gird x at time t, $Wh \cdot m^{-2} day^{-1}$

alb = Albedo of snow

r_{ind} = Radiation melt factor, $mm \cdot (Wh.m^{-2} day^{-1})$

$(T_{mx}(t,x) - T_{mn}(t,x))$ = temperature difference at time t, as a cloud proxy to define clear-sky and overcast conditions

5.3.7. Data requirement of the models

The main objective of this study was to develop simplistic model variants with less input data requirement and propose a calibration methodology driven by freely available data. The idea was to drive these variants with reasonably accurate input data, to facilitate the extent to different mountainous contexts. Table 5.1 summarizes the input data requirement for each model. The major inputs are the elevation data (DEM), and daily interpolated precipitation and temperature. The other variables are the derivatives from these major

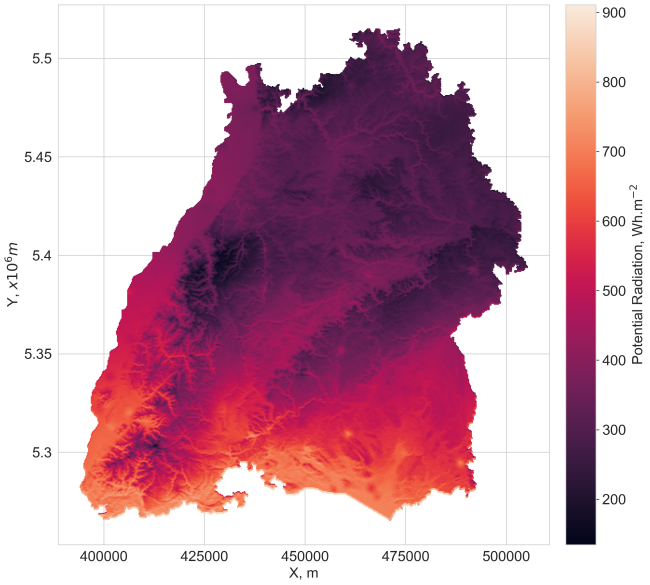

Figure 5.1.: Illustration of potential radiation calculated using r.sun.daily algorithm for Baden-Württemberg on 2015-03-12

inputs. For instance, daily temperature difference was considered as a proxy for the cloud information. The aspect information and daily global radiation are derived from the DEM. In addition to the data presented in the table, the daily MODIS snow-cover distribution is also required for model calibration and evaluation. Freely available inputs such as the DEM and the MODIS images provide a crucial flexibility with minimum data requirement to drive the snow-melt models. Likewise, daily observed stream-flows are also used for calibration and validation of the HBV model.

This study presents a distributed modeling approach with model computations done at pixel level of a gridded domain. A gridded 464m x 464m schema was extracted for both regions using the MODIS snow-cover data as a reference. This schema was considered as the reference gridded domain for the data interpolation and model run. For this, the input data were pre-processed and interpolated onto the aforementioned grid cells. Though gridded precipitation and temperature data are availble from both DWD and Meteoswiss for Germany and Switzerland, the interpolation was opted for to maintain the uniformity with MODIS snow-cover data.

A general methodological snow-melt modeling approach considered in this study is shown in figure 5.2 and is further discussed in subsequent sections.

5.4. HBV Model

In this study, to assess the performance of the standalone calibration approach employed on the snow-melt models on discharge response, a widely used conceptual model Hydrologiska Byråns Vattenbalansavdelning (HBV) [Bergström, 1995] was also used at catchment

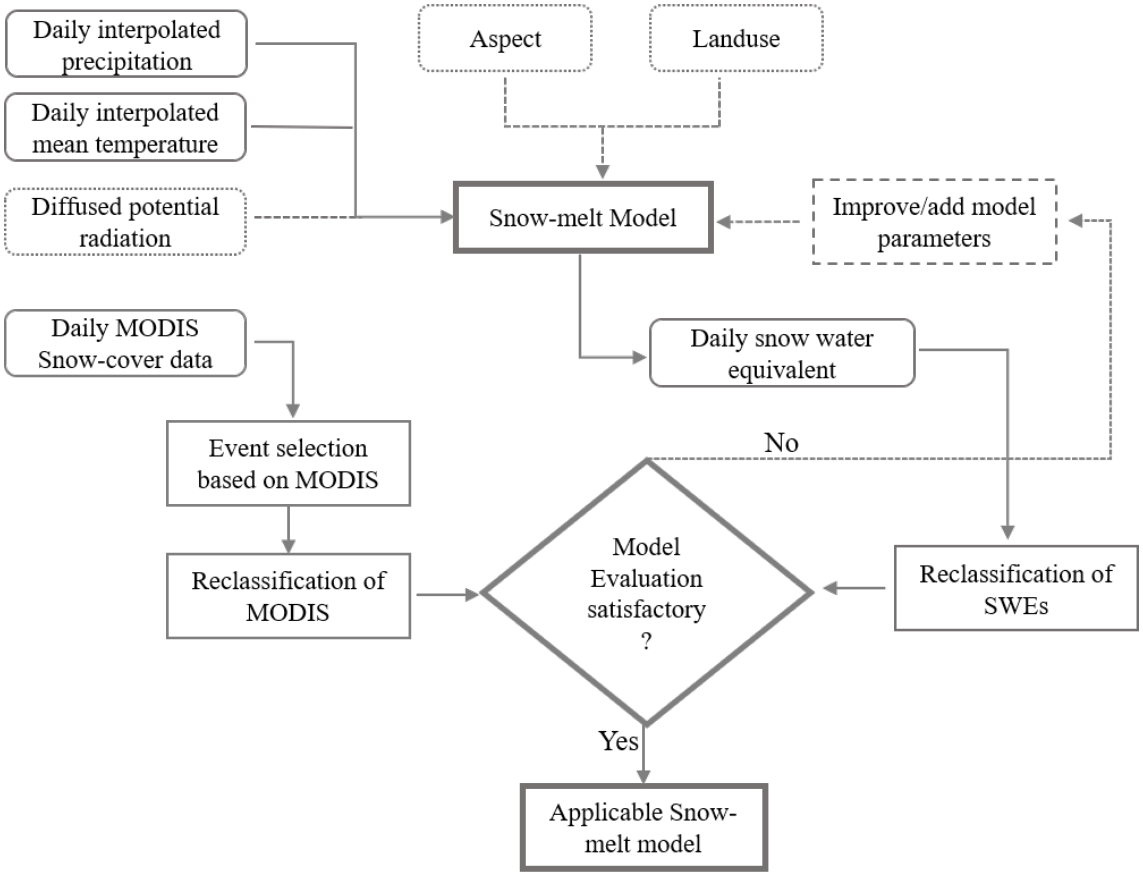

Figure 5.2.: Methodological approach for the study

level. A basic introduction to the standard HBV model is given in the following section and the details can be read from Bergström [1995].

The HBV model is a conceptual model which has been widely used around the world due to the simplistic representations of the hydrological processes [Das et al., 2008; Götzinger and Bárdossy, 2007]. The main drivers of the HBV are precipitation, temperature and estimates of potential evapotranspiration [Seibert, 1996]. Primarily developed as a semi-distributed model, the model has been used in distributed configuration over the years. The model has three distinct subroutines, the snow accounting routine, soil moisture accounting routine, and the runoff response routine, explained in brief below:

5.4.1. Snow accumulation and melt

The phase partion between snow and liquid precipitation is done based on a critical temperature T_{crit} and is calculated as in Eq.5.6(a). Similarly, the melt is calculated as Eq.5.6(b). In addition, the HBV model introduces a refreezing component in the snow routine. The melt waters and incident rainfall are retained within the snowpack with the outflow determined by the exceedance of a certain fraction of the SWE. Likewise, the liquid water within the snow pack is refrozen by a refreezing coefficient, CFR [Seibert, 1996].

Table 5.1.: Inputs required for the different model variants

Models	Spatial inputs	Spatio-temporal inputs (daily)		
	DEM	Precipitation, mm	Mean Temp.,°C	Max. / Min Temp, °C
Model 1	*yes*	*yes*	*yes*	-
Model 2	*yes*	*yes*	*yes*	-
Model 3	*yes*	*yes*	*yes*	-
Model 4	*yes*	*yes*	*yes*	-
Model 5	*yes*	*yes*	*yes*	-
Model 6	*yes*	*yes*	*yes*	*yes*

$$refreeze = CFR \cdot D_s \left(T_{crit} - T\left(t,x\right)\right) \tag{5.13}$$

The accumulated SWE of the snow pack is calculated by Eq.5.14.

$$S\left(t,x\right) = \begin{cases} S\left(t-1,x\right) + P\left(t,x\right) & \text{if } T\left(t,x\right) <= T_{crit}, \\ S\left(t-1,x\right) - M\left(t-1,x\right) & \text{else.} \end{cases} \tag{5.14}$$

$$LP\left(t,x\right) = \begin{cases} 0.0 & \text{if } T\left(t,x\right) <= T_{crit}, \\ P\left(t,x\right) + min(S\left(t-1,x\right), M\left(t,x\right)) & \text{else.} \end{cases} \tag{5.15}$$

where $S\left(t,x\right)$ is the water equivalent of the snowpack in pixel x at t, $P\left(t,x\right)$ is the precipitation falling on the snowpack in pixel x, $M\left(t,x\right)$ is the melt water exiting the regime and $LP\left(t,x\right)$ is the liquid water content that can come from melt or precipitation or both. All units are in mm.

5.4.2. Evapotranspiration and soil moisture

The field capacity, FC (mm) of the soil pack and the soil moisture content SM (mm) control the amount of water divided into soil moisture recharge and the ground water recharge. The available moisture AM (mm) at a given time t in pixel i is given by:

$$AM\left(t,x\right) = SM\left(t-1,x\right) + \left(LP\left(t,x\right) \cdot \left(1 - \left(\frac{SM\left(t-1,x\right)}{FC}\right)^{\beta}\right)\right) \tag{5.16}$$

Actual evaporation from the soil profile is then calculated based on the antecedent soil moisture ($SM_{t-1,x}$, mm) and the permanent wilting point (PWP, mm) as follows:

$$AE\left(t,x\right) = \begin{cases} min(AM\left(t,x\right), PE\left(t,x\right)) & \text{if } SM\left(t-1,x\right) > PWP, \\ min(AM\left(t,x\right), \left(SM\left(t-1,x\right)/FC\right) \cdot PE\left(t,x\right)) & \text{else.} \end{cases} \tag{5.17}$$

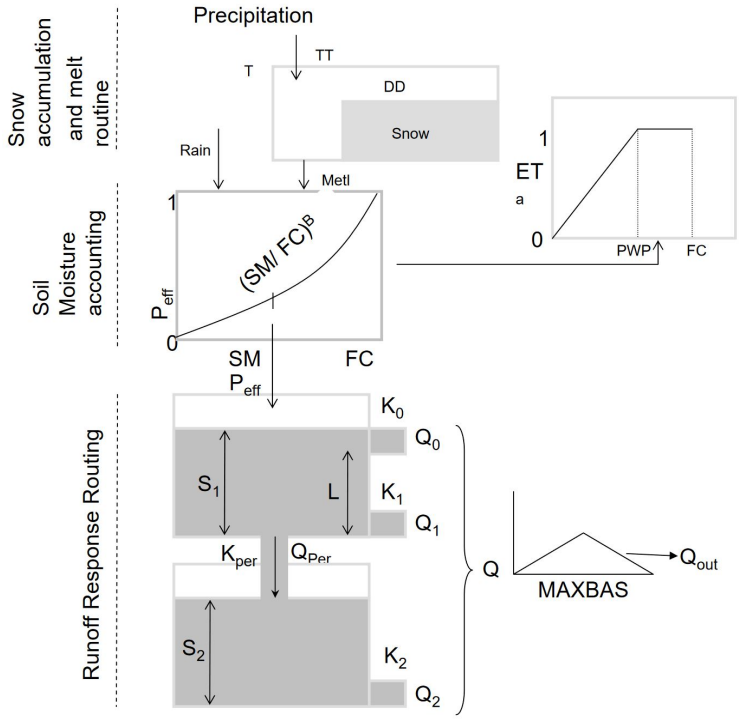

Figure 5.3.: The HBV model schematics, [Singh, 2010]

where, β is a unitless constant related to the soil profile's ability to retain moisture, $PE\,(t,x)$ is the potential evapotranspiration in mm and $ET\,(t,x)$ is the actual evapotranspiration in mm. The soil moisture SM at time t in pixel x is then calculated as in Eq.5.18.

$$SM\,(t,x) = max(0.0, AM\,(t,x) - ET\,(t,x)) \tag{5.18}$$

5.4.3. Runoff reservoir routing

This routine follows the tank model approach. Two reservoirs are available to simulate the runoff response as either direct runoff or as percolation. The runoff from the upper reservoir $R_N\,(t,x)$ (mm) is the amount of water that is not retained by the soil and is available for routing through the model reservoirs and is calculated as in Eq.5.19. Likewise, once the upper reservoir storage $U_{R-ST}\,(t,x)$ (mm) exceeds a threshold of UT, the direct runoff $U_{R-UO}\,(t,x)$ is allowed from the upper outlet of the reservoir (Eq.5.20). This is controlled by a coefficient K_{u-U}. Similarly the lower outlet allows the delayed runoff $U_{R-LO}\,(t,x)$ as given by Eq.5.21 and is controlled by another coefficient K_{u-L} . Likewise, the amount of water percolating downwards to the lower reservoir $UR_{LR}\,(t,x)$ recharging the groundwater storage is controlled by a percolation coefficient K_d and is calculated as Eq.5.22.

$$RN\,(t,x) = LP\,(t,x) \cdot \left(\frac{SM\,(t-1,x)}{FC}\right)^{\beta} \tag{5.19}$$

$$U_{R-UO}(t,x) = max(0.0, (U_{R-ST}(t-1,x) - UT) \cdot K_{u-U}) \tag{5.20}$$

$$U_{R-LO}(t,x) = max(0.0, (U_{R-ST}(t-1,x) - U_{R-UO}(t,x)) \cdot K_{u-L}) \tag{5.21}$$

$$UR_{LR}(t,x) = max(0.0, (U_{R-ST}(t-1,x) - U_{R-UO}(t,x) - U_{R-LO}(t,x)) \cdot K_d) \tag{5.22}$$

$$U_{R-ST}(t,x) = max(0.0, (U_{R-ST}(t-1,x) - U_{R-UO}(t,x) - U_{R-LO}(t,x) - UR_{LR}(t,x) + RN(t,x))) \tag{5.23}$$

Likewise, for the lower reservoir routing, the groundwater recharge is then calculated as Eq.5.24 and the lower reservoir storage L_{R-ST} controlled by a lower reservoir runoff coefficient K_{L-L} is given by Eq.5.25.

$$L_{R-O}(t,x) = max(0.0, (L_{R-ST}(t-1,x) \cdot K_{L-L})) \tag{5.24}$$

$$L_{R-ST}(t,x) = max(0.0, (L_{R-ST}(t-1,x) + UR_{LR}(t,x) - L_{R-O}(t,x))) \tag{5.25}$$

The simulated discharge is then calculated for each pixel x at time t as:

$$Q_s(t,x) = (U_{R-UO}(t,x) + U_{R-LO}(t,x) + L_{R-O}(t,x)) \cdot CC \tag{5.26}$$

where CC is a conversion constant that converts mm/day to m^3/sec in this case, Q_s is the simulated discharge in m^3/sec.

6. MODIS based calibration

The previous chapters on interpolation and cloud removal of MODIS products explained the preparation of the driving input variables required for the proposed snow-melt modeling approach. This chapter describes the calibration methodology in detail along with different validation techniques employed to evaluate the models' performance in different layers of scrutiny.

6.1. Calibration of snow routine

The choice of calibration methodology is one of the governing factors that defines the model's ability to understand and simulate the underlying processes, especially in the snow-dominated regimes where compensation can occur between the snow processes and runoff generation [Ismail et al., 2020]. As already discussed, the model complexities and the data availability limit the spatial understanding of the snow processes in the mountains. Due to this, the traditional calibration approaches are limited to either calibrating on discharge only which can cause parameter compensation with the snow routine, or calibration with localized snow-depth information and SWE measurements. Owing to the non-representative case with the widely used point-based snow depth and snow water equivalent measurements, the calibration and simulation is very uncertain due to the high variability of snow accumulation. Also due to the compensation and because of the conceptual basis, the simplistic representations driven by non-representative data can pose a very critical challenge of uncertain and unreliable estimation of water flowing out of the snow regime often leading to the "right for the wrong reasons" conclusion, even if the calibrated discharge is deemed accurate enough. [Kirchner, 2006; Seibert, 2000]. The studies done by Parajka and Blöschl [2008(b)] and Duethmann et al. [2014] concluded that solely discharge based simulations can not reproduce the snow-cover distribution adequately. Similar results were found out by Finger et al. [2015] where erroneous glacier mass balance was observed even with a higher accuracy of runoff simulation by the model.

This highlights the crucial need to identify and reliably simulate these internal processes, which have not undergone validation against observations [Seibert, 2000]. The addition of internal catchment variables can help improve internal process identification and model parameter identifiability to avoid the parameter compensation and maintain model-internal consistency [He et al., 2018; Parajka et al., 2009; Seibert, 2000]. For this, multi-objective calibration techniques are being employed in snow melt modeling in many snow-related research such as incorporating measured snow depths [Parajka et al., 2007], with satellite snow cover images [Parajka and Blöschl, 2008(b); Duethmann et al., 2014], and using glacier mass balance [Stahl et al., 2008; Schaefli and Huss, 2011]. These studies highlight the value

of the additional variable in a more reliable understanding and simulation of the underlying processes.

However, despite of this well-researched fact of added reliability, increased robustness of parameter estimation and decreased uncertainty [Konz and Seibert, 2010] with incorporation of additional observation, the data limitations in the mountains often restrict the desired implementation of this approach. The limited or under-representative input data can compromise model accuracy, due to the equifinality problem with estimated parameters as well. This become more pronounced when the results are extrapolated to ungauged settings or projections under climate change [de Niet et al., 2020]. To overcome the data limitation in the mountainous regimes, the RS imageries pertaining to snow (MODIS, Landsat, AVHRR and so on) have been increasingly used in the recent years in conjunction with snow-melt models and hydrological models for calibration purposes [Nourani et al., 2021] as an additional variable. The added value for this is that the data is the free and global availability and acceptable results in many studies. Conceptual models like SRM [Martinec, 1975] make use of the snow covered area information from the earth observation satellites in constraining the model objective function. While the RS snow-cover information like MODIS do not contain the snow depth or the SWE information, the spatial distribution they offer at a reasonable spatio-temporal resolution offers a very pertinent basis for the formulation and evaluation of distributed models. These data can add value to the dishcarge time-series as well, which are spatially integrated but provide a quantitative proxy information on the water balance particularly in the mountains [Duethmann et al., 2014; Finger et al., 2011]).

Parajka and Blöschl [2008(b)] employed a weighted sum based multi-criteria objective function to calibrate a hydrological model using satellite-based SCA and discharge calibration in an extensive study in over 148 Austrian catchments and concluded that the inclusion of MODIS snow cover during model calibration led to better SCA simulation and similar or better runoff simulations during the validation period. Likewise, a study from Finger et al. [2011] suggested better performance of a Monte-Carlo based calibration of a hydrological model combining discharge and snow cover data showed the best results among calibration against discharge, satellite snow cover, and glacier mass balance. Shrestha et al. [2014] also used a multi-objective calibration of a distributed model based on MODIS snow-cover and discharge to optimize a snow-fall correction factor for a snow-dominated basin in Japan with the result suggesting improved correlations in SCA and discharge after the optimized correction factor was used. Apart from the multi-calibration approaches, Széles et al. [2020] calibrated a hydrological model by implementing a step-based technique to calibrate the individual modules of a hydrological model including snow, soil moisture and runoff generation processes, which they concluded to be a well-informed runoff simulation. MODIS snow-cover data was used in the implementation as a gap-filling information for the missing observed time-lapse photos of snow-cover. Franz and Karsten [2013] implemented a MODIS Fractional Snow Cover Area (fSCA)-based calibration of a distributed hydrological model, SNOW17, with an areal snow depletion concept in which they concluded that calibrating only on MODIS SCA did not bring any improvement in the hydrological predictions. Corbari et al. [2009] using a AVHRR based pixel wise elevation based procedure to correct snow coverage retrieved from National Oceanic and Atmospheric Administration (NOAA) AVHRR satellite image using a SCA based calibration approach. They also concluded that

the calibration of the distributed hydrological model solely on SCA brought a better performance in terms of discharge simulation. All these recent and ongoing studies highlight the added value of freely available data like MODIS in calibrating snow routines in conjunction with other variables leading to improved representation of the underlying processes and in some cases the hydrological predictions.

6.2. Novelty of the study

This research is motivated from the aforementioned studies to improve the simulation of snow accumulation and ablation in data-scarce mountainous regions, exploiting the vital snow-cover distribution from freely available data like MODIS snow-cover products. A standalone calibration of snowmelt modules based solely on pixel-wise MODIS snow-cover information was not found to be widely implemented despite being already identified as a crucial hydrological information. The need to further explore the gap in incorporating the spatial distribution information of snow, which MODIS snow-cover data can provide on a daily basis and with a reasonable spatial detail was thus identified. The standalone approach was considered because estimation of the parameters solely from any RS based snow-cover information would then eliminate the reliance on a single calibration variable such as SWEs or discharge which are not readily available in the higher altitudes, and when available only at point locations, thereby preserving the spatial heterogeneity as well. Likewise, calibrating the simplistic and computationally efficient parsimonious snow routines against the snow-cover images allows seamless and independent evaluation of the snow processes thereby eliminating the need to pass the snow simulation through a more complex hydrological model.

The presented approach using MODIS snow-cover images for calibration against the satellite-based spatial binary (“snow”, “no-snow”) observations estimates model parameters from individual or sets of MODIS images. This allows independent evaluation snow accumulation and melt just relying on snow-cover information, offers a wide range of applicability across a wide geographical context, allows immediate verification with point measurements, and holds a high relevance in data-scarce regions, particularly in identifying time-continuous snow extents (with depth information) free from highly localized influences. One can calibrate relatively complex snowmelt modules with reasonably accurate precipitation and temperature data without over-calibration, mainly owing to the robust binary data selected for calibration and the spatial extent of the satellite images. This also facilitates the formulation of a flexible snowmelt module useful for distributed hydrologic modeling around the world.

6.3. The Calibration Methodology

The interpolated precipitation, temperature and the calculated solar radiation data were used to drive the snow-melt model variants and the cloud-reduced MODIS snow-cover

images were used to calibrate these models both Switzerland and Baden-Württemberg regions. All the model variants were run to obtain the SWE estimates at each pixel using the distributed input variables. The model outputs were calibrated on a pixel-by-pixel basis against binary ('0' for no snow and '1' for snow) information coming in from a set of cloud-reduced MODIS composite images for the snow season of 2012-13 for both regions. The snow season was selected as October–May for Baden-Württemberg and September–June for Switzerland, assuming a possible snow cover being present for the time period. The calibration was initially done for both regions on daily snow-cover images with more than 60% valid pixels (< 40% cloud cover) for the snow season in different years. These thresholds of cloud cover were also explored with a sensitivity analysis. Similarly, the calibration methodology was also tested using snow-cover images in different periods during the snow seasons to identify which duration in each region gives the better performance.

6.3.1. Reclassification of the model outputs

The first step for the calibration was the reclassification of the modeled SWE outputs to binary information, i.e. the snow cover. A pixel was classified as snow-covered if the simulated SWE exceeded 0.5 mm of water which corresponds to a snow depth of approximately 2.5 mm. This assumption was later tested with different thresholds to demarcate 'snow' and 'no snow' pixels to identify the actual basis for SWE to snow-cover reclassification.

$$SC\left(t,x\right)=\begin{cases}0 & \text{if} \quad S\left(t,x\right)<0.5\text{mm}\\ 1 & \text{if} \quad S\left(t,x\right)>=0.5\text{mm}\end{cases} \tag{6.1}$$

where,

$SC\left(t,x\right)$ is the binary snow-cover information at time t for a pixel x

$S\left(t,x\right)$ is the SWE simualted by the models time t for a pixel x.

6.3.2. Objective function

The evaluation of the proposed calibration is based on a simple Brier Score (BS) (Eq.6.2). The BS is a score function, proposed by Glenn W. Brier, that measures the accuracy of probabilistic predictions of mutually exclusive discrete outcomes or classes [Brier, 1950]. In this study, the BS shows the mean squared error between observed binary values of snow and no snow occurrences between MODIS and those simulated by the extended degree-day models. The values of BS vary from 0 to 1 with the values tending to ‚0' showing better agreement between the model outputs and the MODIS.

$$BS(t)=\frac{1}{N}\sum_{t=1}^{N}\left(f_i(t)-O_i(t)\right)^2 \tag{6.2}$$

Where,

$f_i(t)$ = simulated snow-cover (0/1) on day t and pixel i, $o_i(t)$ = observed snow-cover (0/1) on day t and pixel i

The calibration is done by minimizing the objective function in Eq.6.3 which is expressed as the sum of the BS values over the days with observed MODIS snow-cover:

$$OF = \sum_{k=1}^{K} BS(t_k) \tag{6.3}$$

Where,

t_k are the days with observed MODIS snow-cover.

The snow model parameters were estimated by minimizing objective function Eq.6.3. In order to reflect the equifinality of the model, the Robust Parameter Estimation (ROPE) [Bárdossy and Singh, 2008] methodology was applied for the model parameter optimization. A brief concept of ROPE is given in next section.

6.3.3. Robust Parameter Estimation (ROPE)

ROPE uses the concept of data depths to identify best-performing robust parameter sets and their properties for different calibration periods in different catchments, with an underlying assumption that it identifies parameters sets without overemphasizing the processes defined by the parameters. Data depths provide a quantitative estimate of the central tendency compared to a dataset or a distribution [Bárdossy and Singh, 2008]. Tukey [1975] first used the concept of depth functions to analyse multivariate dataset followed by the different generalizations in [Rousseeuw and Struyf, 1998; Liu et al., 1999; Zuo and Serfling, 2000]. The data depth concept is based on the computational geometry and gives the information if a point is at or near the center of a point cloud corresponding to higher data depth values or at the periphery (lower data depth values). In hydrological models, there exists a deep-lying problem of equally performing parameter vectors which renders the decision to select one of the sets for prediction, difficult. Bárdossy and Singh [2008] investigated the properties of the set of best performing parameter sets using the data depth concept. This study analyzes models with more than 5 parameters.

Different applications of the concept of data depths in hydrology can be found in [Chebana and Ouarda, 2011] to identify weights of a non-linear regression models for flood estimation, [Singh and Bárdossy, 2012] for ICE algorithm, [Bárdossy and Singh, 2011] for regionalization of hydrological model parameters, and [Singh et al., 2013] to define predictive uncertainty. The fundamental concept of depths of data applied in hydrology is provided in [Singh, 2010]. The half space depth of a point p for a d dimension dataset can be defined as the minimum number of points that lie on either side of the hyperplane through p calculated over the infinite number of hyper-planes slicing through the point cloud. The half space depth of the point p in reference to a set X in a D-dimensional space as can be expressed as :

$$D_X(p) = \min_{n_h} \left(\min \left(|\{x \in X \langle n_h, x - p \rangle > 0\}| \right), \left(|\{x \in X \langle n_h, x - p \rangle < 0\}| \right) \right) \tag{6.4}$$

The ROPE methodology followed the following sequential steps for this study:

1. The bounds for the model parameters were set.

2. 'N' random parameter sets (X_N) were generated in the 'd' dimensions space limited by the bounds set in Step 1.
3. The models were run for each parameter sets and the corresponding objective functions were calculated.
4. Based on the model performance, a pre-defined subset of the best performing parameter sets $X_N^{'}$ were drawn.
5. 2*N random parameter sets were again generated within the bounds of the best performing sets from Step 3.
6. A set of Y_M parameters were identified where for each vector $\theta \in Y_M$, the depth calculated with respect to the subset $X_N^{'}$ is greater than 0, i.e $D(\theta) > 0$.
7. Within the bounds defined by the 'deep' parameter sets in Step 6, further 'N' parameter sets were generated so that $X_N = Y_M$.
8. Steps 3-6 were repeated for various iterations assuming that the performance corresponding to Y_M does not differ more than what one would expect from the observation errors.

With the ROPE methodology, a set of 1000 heterogeneous parameter vectors with similar model performance were obtained. These sets of 'good' points can be defined as the parameter sets that are less-sensitive and transferable, thereby providing a 'compromised' solution. These parameter vectors were estimated for each region assuming spatio-temporally constant/variable (wherever possible) parameter distribution and were estimated within a plausible range as described in different snow modeling studies. For the ease of result interpretation, the modeling results are shown based on the parameter vector with the best objective function value.

6.4. Calibration Results

6.4.1. Switzerland

To evaluate the methodology in a longer duration snow context, a set of MODIS images for the whole snow season of 2012-09-01 till 2013-06-30 was considered as the reference snow-cover distribution in Switzerland to calibrate the extensions of the snow-melt models . All the models were calibrated with the same objective function and the calibration performance of each variants were evaluated in terms of the Brier scores. The results are analyzed on the basis of confusion matrices showing the proportion of true and false identifications of snow and no-snow pixels. The Brier score is the overall error imparted by the model, i.e. the sum of falsely identified instances of snow and no-snow pixels.

Table 6.1 summarizes the performances of all six variants after the ROPE calibration. The results in the table depict the normalized confusion statistics calculated for the reference

time period for Switzerland with the columns indicating the proportions of true negatives (both 'no snow'), false positives (MODIS: 'no snow', simulated: 'snow'), true positives (both 'snow') and false negatives (MODIS: 'snow', simulated: 'no snow'). All model variants reported very good simulation of the snow-cover distribution with the BS ranging from 0.084 to 0.095. The results indicate a very close performance in Switzerland, when calibrated using the images for the whole season. However, in comparison among all, the Model 6 with the radiation component performed the best in terms of overall BS as well as the reduction in the false recognition of snow, although slight overestimation of snow was observed with the simulation from Model 6.

Table 6.1.: Normalized confusion matrices for the calibration period of 2012-09-01 till 2013-06-30 for Switzerland

	True positive	False positive	True negative	False negative	BS
Model 1	0.625	0.036	0.280	0.059	0.095
Model 2	0.621	0.039	0.289	0.050	0.089
Model 3	0.626	0.035	0.289	0.051	0.086
Model 4	0.625	0.035	0.289	0.050	0.085
Model 5	0.622	0.039	0.293	0.047	0.086
Model 6	0.610	0.050	0.306	0.034	0.084

To further scrutinize the performance of the model variants at different elevation zones, the region of Switzerland was divided into five elevation zones, i.e. <500 masl, 500-1000 masl, 1000-1500 masl, 1500-2500 masl and >2500 masl. The areal proportion of these zones can be observed from table 3.3. The total errors, over-estimation errors and under-estimation errors were calculated for each elevation zones for all the models. The under-estimation error refers to the average normalized false negative instances, over-estimation error shows the average normalized false positive instances and total error refers to the mean values of BS for each elevation zones. Figure 6.4 shows the results of this elevation based evaluation. It is evident from the figure that a clear reduction in over-estimation error is observed in all the elevation zones with Model 6. The model however, underestimates the snow for lower elevation zones. The Brier scores remain the lowest for <500 masl (17% of the total area) and >2500 masl (11% of the total area), i.e. the low and the high snow-dominated zones are best represented by this model. For the mid-elevation zones, the model errors are comparable to other variants and with the lowest mean error, i.e the Brier score, this was the best performing variant in Switzerland. Model 1, the simplest of the models, overestimates snow throughout the elevation zones and the overall error also remains the highest. Models 3, 4 and 5 show similar attributes in terms of over and under-estimating the snow detection. Owing to the comparatively superior performance among the models, Model 6 with the radiation induced melt was selected as the reference model for further analysis in Switzerland. This has also been pointed out by [Hock, 1999] that including inclusion the effect of solar radiation on melt provides a more realistic spatial distribution of snow accumulation and melt.

The results were validated in different cloud-free days at the start, mid and late winter in different years. The validation time-series of Brier scores are shown in Annex A.1. It is to be noted that red highlights in the figure show the best performance for the day. The results suggest that the simulated snow-distribution is adequately represented by the model variants with models 5 and 6 exhibiting better agreement in most of the days. Figure 6.1 shows an example of the validation of the radiation-based model on the snow-cover image for a relatively cloud-free day of 2013-01-08. The illustration shows that the model calibrated on the images for the whole season very well simulates the MODIS snow-cover distribution for the day with a very good BS of 0.077.

Calibration on a single day image

In addition, the calibration was also tested on a relatively cloud-free single image for 2012-01-18 in Switzerland. The normalized confusion matrices are shown in Annex A.3. The figures suggest gradual improvement in the model performance with additional parameters, with the BS ranging from 0.044 to 0.0365. Model 6 including the radiation induced snow-melt shows the best performance among the models, with a BS value of 0.0365. Model 5 has the next closest match. The models 5 and 6 both improve the true negatives and true positives with Model 6 exhibiting lesser false recognition of snow. The simulation of the snow-cover by Model 6 for this day is shown in figure 6.3. The single day calibrated parameters were used to run the radiation variant using all the images available for the period of 2011-01-01 till 2018-12-31. The normalized confusion matrix of MODIS snow-cover and snow-cover simulated by the model in figure 6.2 reflects very good capability of the model to identify and predict snow ('1') with 0.947 and no-snow pixels ('0') with 0.932 as a proportion of all the valid pixels. The false negatives and true negatives amount to less than 10 % of the total pixels.

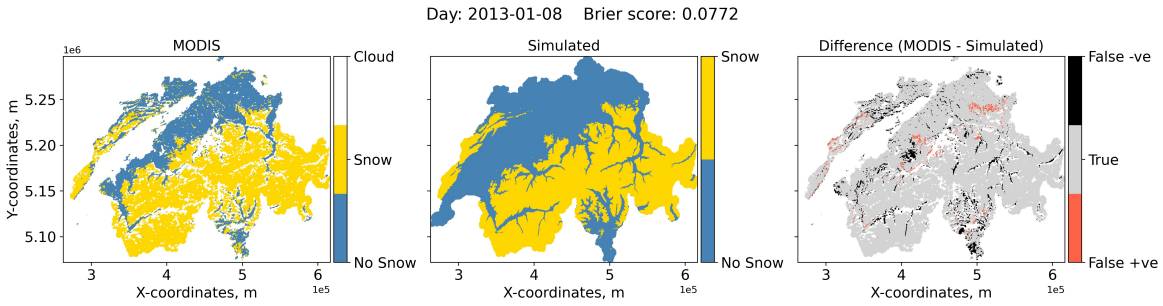

Figure 6.1.: MODIS inferred (left) vs Model 6 simulated snow distribution (centre) and differences between MODIS and simulated image (right) for Switzerland

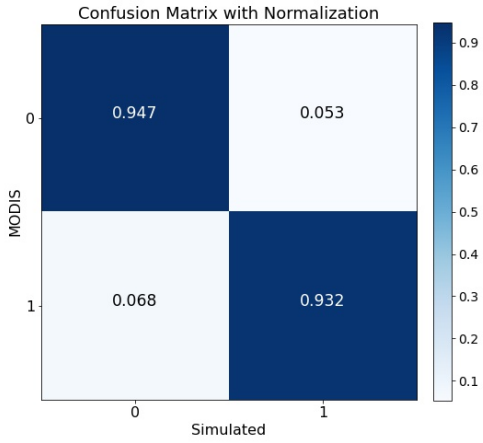

Figure 6.2.: Normalized confusion matrix for the simulation of 2011-01-01 till 2018-12-31 for Switzerland

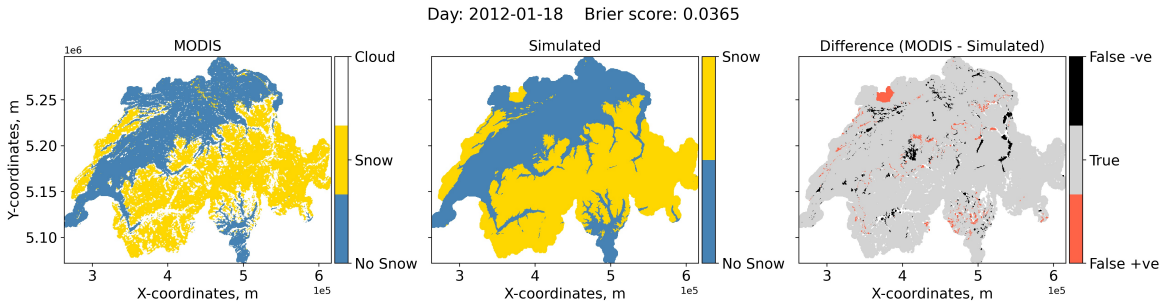

Figure 6.3.: Single day (2012-01-18) calibration result of Model 6 for Switzerland

Both the seasonal calibration and the single day calibration suggest that this approach of calibrating against MODIS on a pixel level is very flexible in the sense that selective images can be selected to tune the snow-melt model parameters thereby identifying the spatial extent of snow-cover without much loss in model performance.

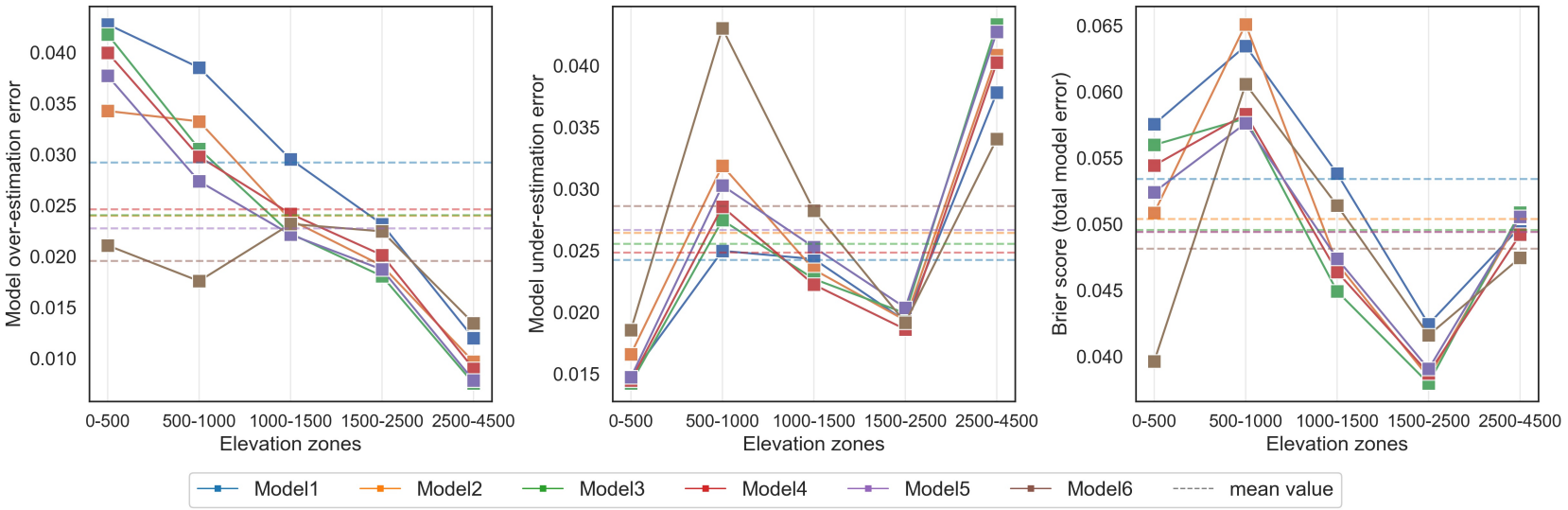

Figure 6.4.: Model performances in different elevation zones (left: over-estimation error, middle: under-estimation error, right: total error (BS), dashed: mean error for all elevation zones) in Switzerland

6.4.2. Baden-Württemberg

Likewise, the entire approach was replicated in the southern German region of BW to test the efficacy of the approach in a lesser duration snow context. For this, a set of images corresponding to the winter season of 2012-13 i.e 2012-10-01 till 2013-05-31 were used for calibration. The results were similar to the Swiss calibration, as all the models adequately simulated the snow-distribution pattern for the reference season. Table 6.2 shows the result of the calibrations in terms of Brier scores, and true and false identification scores of snow. Here as well, the Model 6 was the best performing variant among all based on the proportions of the true and false instances. A gradual improvement in model performance with additional parameterization was observed in BW. Though the results are comparable to the Swiss context, the BS values exhibit a starker Model 6 performance when compared to other models. With better representation of truly identified instances and a subsequent reduction in false identification as shown by Model 6 performance reflects the importance of radiation component in melting the snow in diverse regions. All other models show similar performances in the region. An illustration of the validation of Model 6 on a cloud free day of 2013-03-04 is shown in figure 6.6. The simulation shows a very close match with MODIS image for the day with about 93% accuracy when calibrated on seasonal images.

Table 6.2.: Normalized confusion matrices for the calibration period of for 2012-10-01 till 2013-05-31 for Baden-Wu̇rttemberg

	True positive	False positive	True negative	False negative	BS
Model 1	0.758	0.031	0.169	0.042	0.073
Model 2	0.759	0.032	0.168	0.041	0.073
Model 3	0.760	0.034	0.167	0.040	0.074
Model 4	0.758	0.032	0.168	0.041	0.073
Model 5	0.756	0.030	0.171	0.043	0.073
Model 6	0.762	0.027	0.173	0.037	0.064

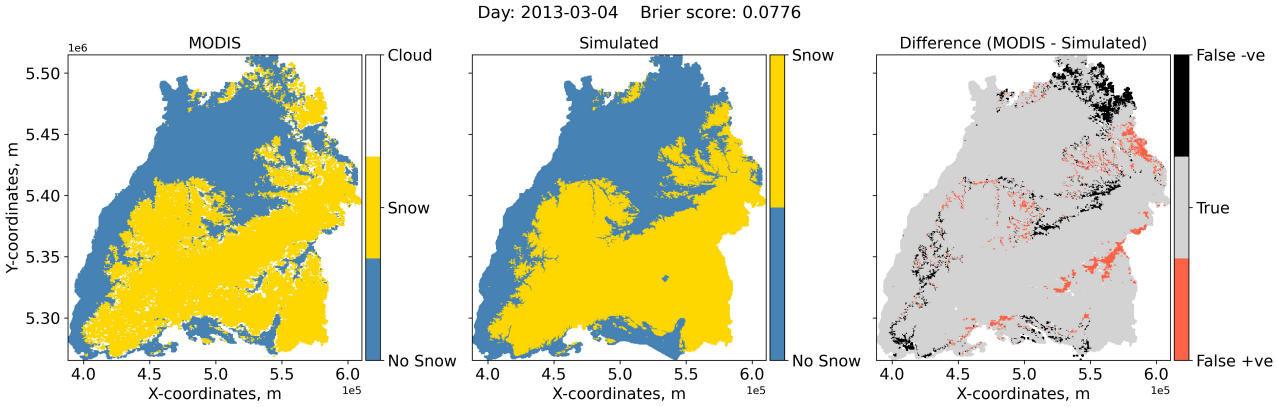

Figure 6.5.: MODIS inferred (left) vs Model 6 simulated snow distribution (centre) and differences between MODIS and simulated image (right) for BW

The calibration for all the models were further analyzed in different elevation zones in BW. The region was divided into four elevation classes, namely <300 masl, 300-600 masl, 600-900 masl, >900 masl, for which the proportion of the area covered within are shown in table 3.1. The results shown in figure 6.8 suggest Model 1 and Model 6 show the lowest under-estimation error. This error is seen to be increasing with increasing elevation zones. The over-estimation error decreases with increasing elevation for all models except Model 1 which shows a different trend of highest over-estimation in the snow-dominated part of the region with a corresponding reduced under-estimation error. The simplistic approach is Model 1 tends to falsely identify snow pixels in the upper zones. Rest of the models show similar behaviour across the elevation zones. As indicated by the rightmost plot, the overall error is reduced with Model 6 throughout all elevation zones.

Calibration on a single day image

Similar to the case in Switzerland, the single day image calibration was done here as well with a relatively cloud-free MODIS image for the day 2010-02-27 selected as the reference image. As in Switzerland, all models were able to mimic the snow-distribution pattern for the reference day reasonably well where Model 6 performed the best in terms of the BS and is shown in figure 6.6. The models were further validated for different cloud free days in different years as well and can be inferred from Annex A.2. The simulations were able to capture the snow-distribution reasonably well in BW, albeit not as good as in Switzerland as reflected by the Brier scores for single day calibration. Short duration snow or lesser snow availability can be attributed to this drop in model performance, as it imparts added uncertainty in model prediction. Figure 6.7 shows the normalized confusion matrix based on Model 6 simulation from 2011-01-01 till 2015-12-31 using the images during the time-period. It is evident from the figure that the model is able to simulate the snow-distribution well enough with 83% of correctly identified 'snow' pixels. This performance, however, shows that the model still has room for improvement especially in regions like BW, where snow-melt has a major implication on water availability.

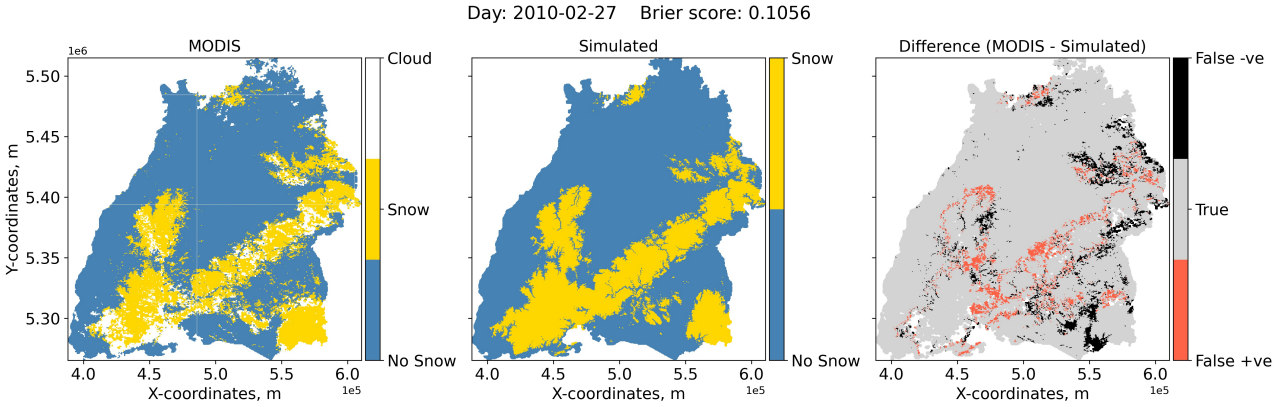

Figure 6.6.: Single day (2010-02-27) calibration result of Model 6 for BW

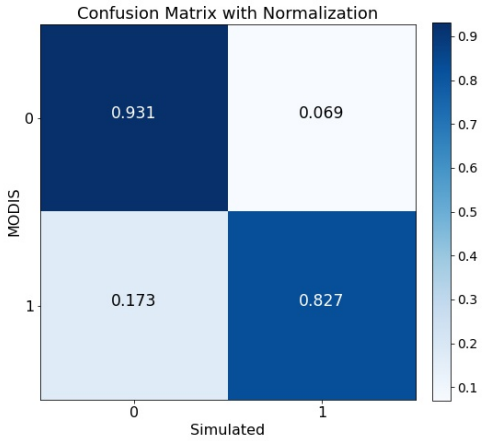

Figure 6.7.: Normalized confusion matrix for the simulation of 2011-01-01 till 2015-12-31 for BW

The calibration and validation statistics suggest that all models perform reliably in terms of identifying MODIS snow-cover distribution in the overall scenario. However, based on the validation, and model performance throughout the elevation zones, Model 6 was selected for both Switzerland and Baden-Württemberg as reflected by the lowest overall error and from hereon used as the reference model for further analysis.

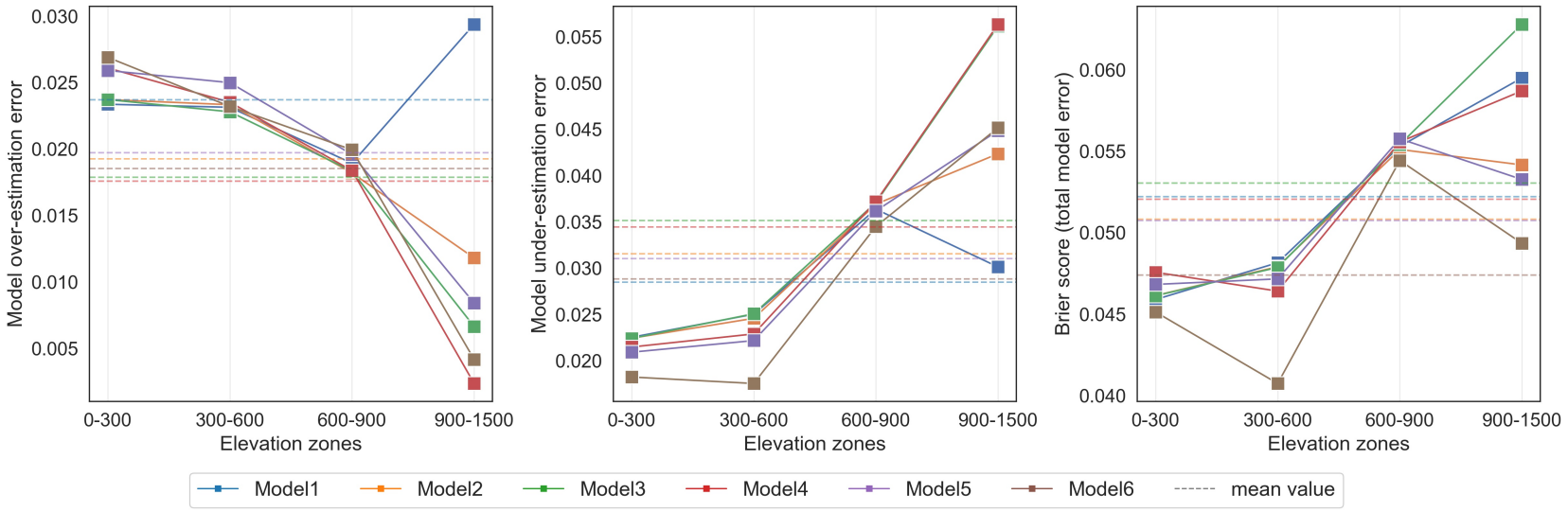

Figure 6.8.: Model performances in different elevation zones (left: over-estimation error, middle: under-estimation error, right: total error (BS), dashed: mean error for all elevation zones) in BW

6.4.3. Reference model parameters

The calibration of the reference model i.e. Model 6 using ROPE for the reference period i.e. 2012-13 winter season for each region, yielded 1000 good parameter vectors. Figure 6.9 shows the box-plots of the set of these best calibrated reference model parameter vectors. The parameter values are normalized in the figure based on the parameter bounds set for calibration which are further shown in table 6.3 along with the parameter vector with the best Brier score value for the calibration period. The box-plots suggest that, the temperature related parameters and the radiation more sensitive, and more so with melt temperatures T_{Mmin} and T_{Mmax}, and the radiation melt factor R_{ind} that directly govern the snow-melt. The median values of the D_s parameter is around 1.9 $mm.^{\circ}C^{-1}$ whereas for BW it is around 2.2 $mm.^{\circ}C^{-1}$, which are within accepted range for this parameter. Likewise, the median values for T_s is similar for both regions (-1.8°C for Switzerland and -1.6°C for BW). The median melt temperature T_M was found to be slightly higher for Switzerland than BW, indicating a faster snow-melt in BW. Similarly, the median calibrated albedo value was around 0.66 for both regions, a plausible value for snow. The median under-catch correction factor scf value for both regions were around 1.3, meaning 30% of missed precipitation as snow, which is again an acceptable figure. The calibrated parameters thus can be considered as being within a plausible range. The precipitation threshold P_T, wet degree-day factor D_w and power factor PF are the least sensitive ones in reference to the objective function.

Table 6.3.: Best performing reference model parameter sets with respective calibration bounds

Parameters	Calibration bounds		Best performing vectors	
	Upper	Lower	Switzerland	BW
D_s	3	1.5	1.77	1.60
P_T	10	0	2.52	6.98
D_w	1	0	0.53	0.73
T_s	3	-3	-2.53	-1.40
T_{Mmin}	3	-3	0.74	-0.43
T_{Mmax}	3	-3	1.11	-0.23
PF	10	0	4.83	9.57
r_{ind}	1	0	0.07	0.01
alb	0.9	0	0.80	0.28
scf	1.5	1.01	1.40	1.47

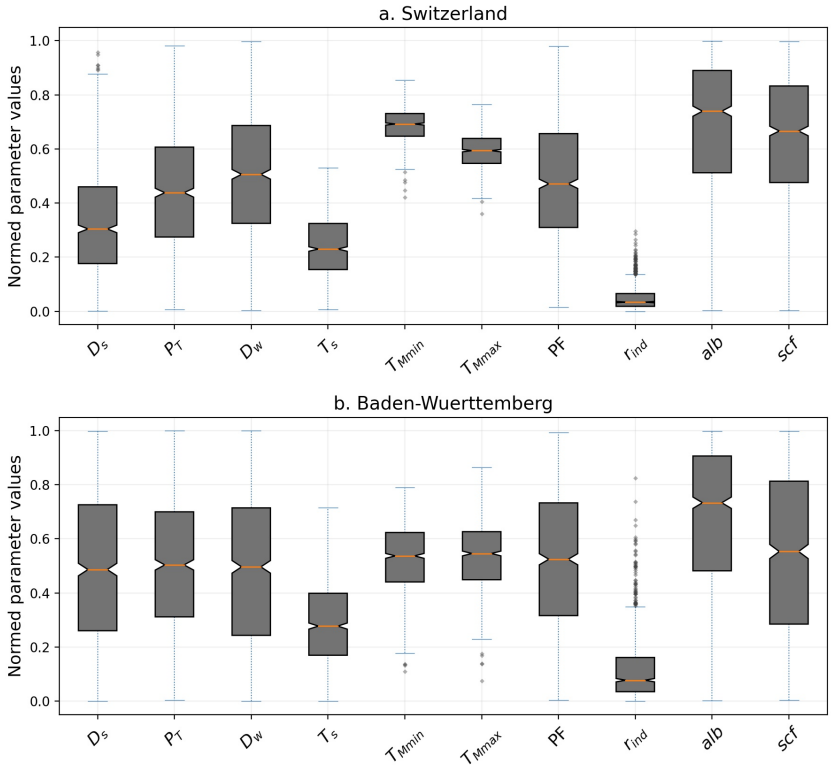

Figure 6.9.: Boxplot of 1000 best reference model parameters estimated with ROPE

6.5. Transferability of calibrated parameters

To test for the transferability of the model parameters through different seasons, the calibrated model parameters were also validated on the set of available snow cover images for the average onset and average melting seasons of different years. The goal here, was to investigate a relatively stable parameter-set across the time domain that can depict comparable model performance for different seasons. A calibrated well-performing parameter vector was used to compare the results in different seasons. The best model (Model 6) is used as the reference model in this analysis. Peak snow onset periods (October - December for Switzerland and November - December for BW) and peak melting periods (January - April for Switzerland and January - March for BW) for 2010 - 2015 were selected as the calibration and validation periods. The models were calibrated for onset periods for each year and then run to predict the snow distribution in the corresponding melting season as well as to hindcast the snow distribution in the onset and melting seasons of preceding year. Tables 6.4 and 6.5 summarize the model performance (BS) for different simulation periods for Switzerland and BW, respectively. The '*', '**' and '***' highlights depict hindcast, calibration and prediction for each year.

For the ease of understanding, the case of model calibrated for 2011 October - December

period for Switzerland is taken here for discussion. The best calibrated parameter vector from the Swiss model run was used to hindcast the snow cover distribution in the preceding onset (2010 October - December) and melt (2011 January - April) seasons, and predict for the corresponding melting season (2012 January - April). The 2011 model performance was then compared with the hindcast of the succeeding calibration and the prediction of the previous calibration. Here in this example the hindcast performance (**0.068** for Oct-Dec 2010 and **0.0661** for Jan-Apr 2011) is very close to the ones simulated by the 2010 model (**0.0675** for calibration period and **0.061** for forecast period). The other results are also comparable throughout the years. These results are again compared with the model calibrated on a single day image in the last column (2012-01-18) as described in earlier sections. Here as well, the model calibrated on a single image is able to adeptly track the distribution in different snow-onset and melt seasons in different years, without much loss in performance.

Likewise in the BW region as well, the transferability of the parameter sets was tested. Based on the results shown in table 6.5, the calibration performance and the performance during validation of hindcast and forecast remain fairly close, albeit not as good as in Switzerland. Due to a more uncertain distribution of snow, the onset season in BW is more strong and defined, with a more uncertain melting rates. This can be observed with the hindcast performance based on the calibration during onset season of the succeeding year, which gets worse as compared to the performance of the forecast for the same period. However, the drop in Brier scores is not that significant and the results are considered to be acceptable.

As an illustration, a set of good parameter vector for the aforementioned seasons and the reference day are shown below in figures 6.10(a) and 6.10(b). The P_T and D_w parameters are less sensitive and the fluctuations in these parameters do not have major implications on the model performance. Apart from these parameters, it is apparent that the individual parameter values do not fluctuate a lot and are more or less stable in Switzerland. The calibrated parameters from the single day calibration, understandably shows quicker melt with low values of snow-melt temperatures, apart from which the parameter sets can be inferred as temporally stable for the said periods for this region. However, individual parameter values here have a wider spread in BW for the same periods in comparison with Switzerland. As discussed above, this can be attributed more to the lesser and more uncertain availability snow in different seasons. This shows that with continuous updating of the approach for each season, the approach has the potential to forecast the snow-availability.

	D_s	P_T	D_w	T_s	T_{Mmin}	T_{Mmax}	PF	r_{ind}	alb
2010	1.6412	6.677	0.2098	-1.787	0.673	1.228	1.0246	0.0021	0.77
2011	1.7396	7.8749	0.1358	-2.7674	1.325	1.8507	3.6165	0.0027	0.6242
2012	1.5386	0.5994	0.3021	-2.8419	1.4176	2.085	3.6551	0.006	0.8971
2013	1.5463	8.5786	0.6704	-2.5345	0.4018	0.6695	0.0899	0.006	0.8966
2014	1.5135	3.7622	0.0235	-2.9109	1.7374	2.2875	2.5869	0.0071	0.6862
2015	1.514	6.055	0.0493	-2.77	0.563	2.207	2.219	0.0035	0.8203
18-Jan-12	1.5935	8.1543	0.0002	-2.9109	-0.0867	0.2738	0.1177	0.004	0.78

(a) Switzerland

	D_s	P_T	D_w	T_s	T_{Mmin}	T_{Mmax}	PF	r_{ind}	alb
2010	1.893	7.231	0.052	-2.853	1.032	1.108	4.5	0.009	0.817
2011	1.949	2.32	0.072	1.342	1.854	2.444	0.18	0.38	0.713
2012	2.64	6.204	0.066	1.214	1.992	2.148	1.366	0.2	0.8
2013	1.673	7.903	0.085	0.574	0.623	0.743	6.691	0.013	0.687
2014	2.664	9.01	0.466	-0.286	1.526	2.957	0.015	0.109	0.249
2015	1.587	3.074	0.003	-0.323	1.493	2.109	5.975	0.001	0.401
27-Feb-10	1.505	9.596	0.085	-2.891	0.239	0.359	0.731	0.01	0.788

(b) Baden-Württemberg

Figure 6.10.: Calibrated parameter sets for onset periods in different years

Table 6.4.: Model calibration, hindcast and forecast performance in terms of Brier scores in different seasons for Switzerland

Validation Periods	Calibration Periods						
	2010/ Oct-Dec	**2011/ Oct-Dec**	**2012/ Oct-Dec**	**2013/ Oct-Dec**	**2014/ Oct-Dec**	**2015/ Oct-Dec**	**Jan 18 2012**
2010/ Jan-Apr	0.0683*						
2010/ Oct-Dec	0.0676**	0.0685*					0.0734*
2011/ Jan-Apr	0.0607***	0.0661*					
2011/ Oct-Dec		0.0853**	0.0862*				0.0906*
2012/ Jan-Apr		0.0512***	0.0597*				
2012/ Oct-Dec			0.0803**	0.0855*			0.0886**
2013/ Jan-Apr			0.0665***	0.0567*			
2013/ Oct-Dec				0.1005**	0.1244*		0.1064***
2014/ Jan-Apr				0.0510***	0.0631*		
2014/ Oct-Dec					0.0728**	0.0748*	0.0894***
2015/ Jan-Apr					0.0999***	0.0827*	
2015/ Oct-Dec						0.0910**	0.0975***
2016/ Jan-Apr						0.0937***	

* Hindcast ** Calibration *** Forecast

Table 6.5.: Model calibration, hindcast and forecast performance in terms of Brier scores in different seasons for BW

Validation Periods	Calibration Periods							Swiss 01.12.2018
	2010/ Nov-Dec	2011/ Nov-Dec	2012/ Nov-Dec	2013/ Nov-Dec	2014/ Nov-Dec	2015/ Nov-Dec	Feb27 2010	
2010/ Jan-Mar	0.119*						0.115**	
2010/ Nov-Dec	0.078**	0.085*					0.085***	**0.083***
2011/ Jan-Mar	0.179***	0.231*						
2011/ Nov-Dec		0.240**	0.238*				0.255***	**0.255***
2012/ Jan-Mar		0.298***	0.281*					
2012/ Nov-Dec			0.234**	0.237*			0.241***	**0.24****
2013/ Jan-Mar			0.215***	0.179*				
2013/ Nov-Dec				0.296**	0.373*		0.324***	**0.324*****
2014/ Jan-Mar				0.218***	0.306*			
2014/ Nov-Dec					0.228**	0.234*	0.236***	**0.236*****
2015/ Jan-Mar					0.245***	0.251*		
2015/ Nov-Dec						0.205**	0.209***	

* Hindcast ** Calibration *** Forecast

6.6. Simulated snow-cover characteristics

To analyze the characteristics of simulated snow-cover, several diagnostics were compared with MODIS as an evaluation of the calibration methodology. The average simulated and MODIS derived fractional areal extents of SCA different validation days are shown below in for selected validation (cloudfree) days are also presented below in figure 6.11. It can be inferred that the model can adequately track the seasonal evolution of the snow covered area in Switzerland.

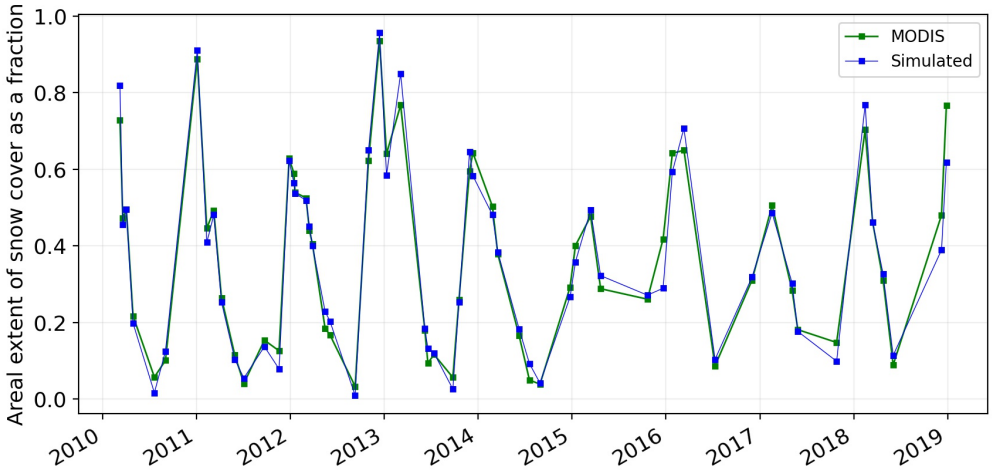

Figure 6.11.: Mean Areal Extent of snow cover for different validation days in different years

For the further analysis of spatio-temporal snow characteristics, cumulative SCAs below different elevation levels, Snow Cover Duration (SCD), Snow Cover Onset Date (SCOD), and Snow Cover Melt Date (SCMD) for hydrological years (09-01 to 08-31) from 2010 to 2018 were analyzed using the MODIS and simulated snow distribution. Due to persistent cloudy pixels even after cloud filtering in daily MODIS images, the SCDs for MODIS 8 day products containing the maximum occurrence of snow/no snow within an 8-day period were compared with the 8-day aggregated simulated values. Figure 6.12 below shows the cumulative SCA for the reference day (2012-01-18). The plot shows a very good agreement of the simulated hypsographic curves with the MODIS inferred elevation discretized cumulative SCAs. These plots are analyzed for different validation days and are presented in the Annex A.4 section.

For the snow-cover duration, an average percentage of days with snow, throughout the hydrological years of 2010/11 till 2017/18 were considered. This was anlayzed using an 'agreement' index, given by Eq.6.5 below.

$$Agreement = \left(1 - \frac{|SCD_{sim} - SCD_{MODIS}|}{SCD_{MODIS}}\right) * 100 \tag{6.5}$$

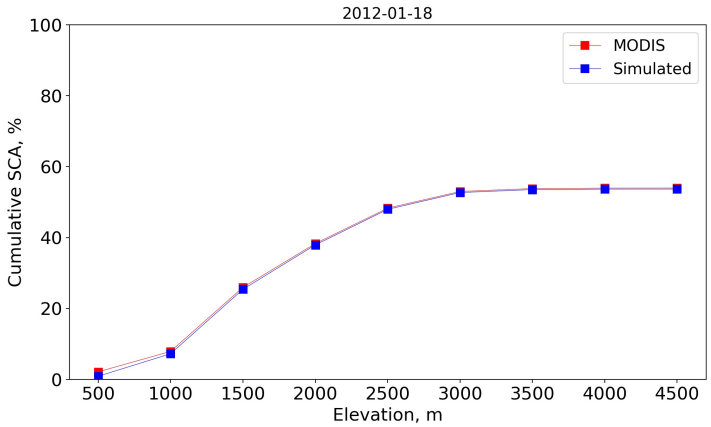

Figure 6.12.: Cumulative simulated and MODIS SCAs at different elevation zones

where, SCD_{MODIS} is the proportion of snow-covered days aggregated from MODIS and SCD_{sim} is the simulated proportion of the snow-covered days.

The average SCDs of the hydrological years for MODIS-8day and modeled outputs is shown below in Figure 6.13. The graph represents a consistent agreement of mean snow-covered days except for pixels with elevation less than 600m. A slight over-estimation can be observed in the pixels from 2800 – 3600m range. Year wise comparison of the SCDs is provided in Annex A.5. Apart from the pixels below 200m elevation, the simulated SCDs replicate the MODIS SCDs, albeit with slight underestimation in most of the years. However, it should be pointed out that the MODIS 8-day products are also not completely free from cloudy pixels. Likewise the spatial comparison of mean snow cover days shown in figures 6.14a and 6.14b suggest that the higher and mid elevation show good agreement with more erroneous predictions in the lower elevation zones. These low lying areas are usually characterized by transitional snowfall events which is not captured adequately with the model simulation. However, with majority of the pixels showing agreement above 50%, it was considered a reliable simulation in this study.

6.6.1. Comparison with station observed snow depths

The snow depths measurements from 30 available stations with complete set of daily data for water years (2010/11 – 2017/18) in Switzerland were used to further assess the model results. A snow depth threshold of 2.5mm was considered as a threshold to omit the transient snow fall events. Values higher than this threshold snow depth were considered as '1' and the lower ones as ‚0'. For comparison with the station data, the pixel bounding the station was considered. The mean SCDs for hydrological years 2010-11 to 2017-18 were also calculated, summing the days of snow. The figure 6.15 shows the mean SCDs for the aforementioned years. It can be observed from the figure that the SCDs are well simulated by the models except for the stations within 500 -1000m elevation.

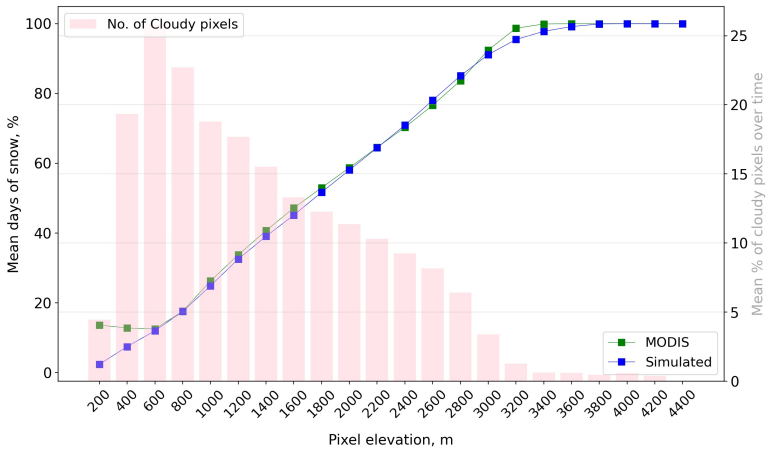

Figure 6.13.: MODIS derived and simulated mean days of snow (expressed as % days in a year)

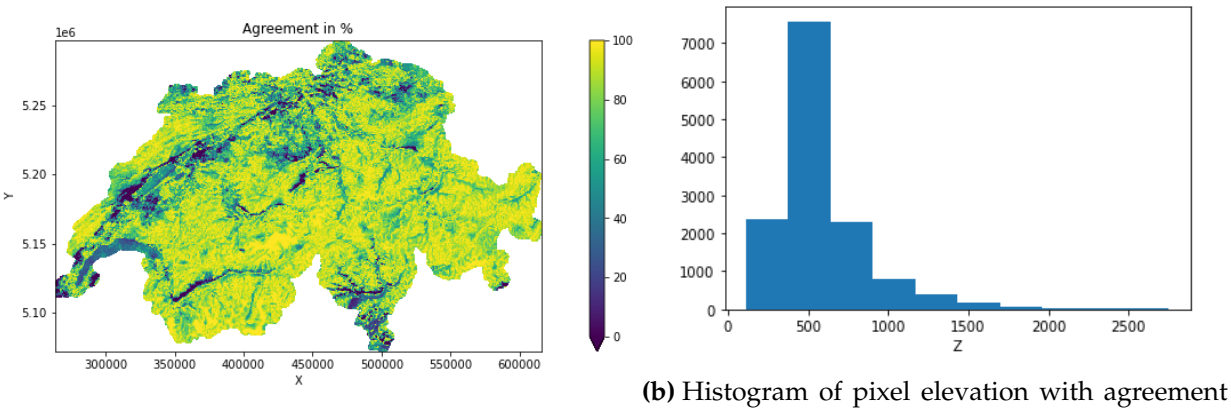

(a) Mean agreement

(b) Histogram of pixel elevation with agreement less than 50%

Figure 6.14.: Mean agreement between MODIS and simulated snow-cover duration across the water years of 2010/11 - 2017/18

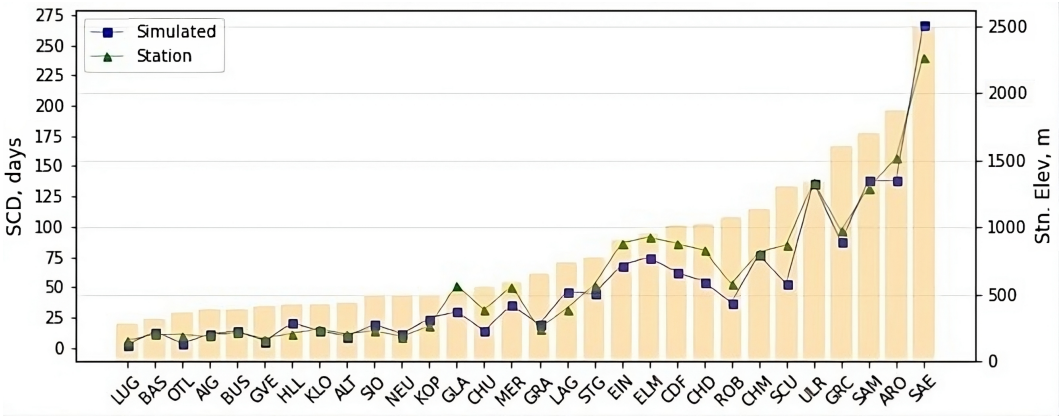

Figure 6.15.: Simulated mean SCDs vs mean SCDs calculated from the snow stations

Snow Cover Onset Date (SCOD) and Snow Cover Melt Date (SCMD)

In order to track the snow-cover onset and melt dates, an approach adopted in Wang and Xie [2009], was used in the study. To calculate the snow onset day, the snow cover duration (SCD') during the onset phase (September 1 onwards) is calculated by summing up the values of a pixel with '1' i.e. snow till a fixed date after which it is assumed to have more or less a constant snow cover in the region. The snow cover onset date was then calculated by Eq.6.6.

$$SCOD = FD_1 - SCD' \tag{6.6}$$

where, FD_1 is the fixed date after which constant snow cover is present. The choice of the fixed date depends on the climate and topography of the region of interest [Wang and Xie, 2009]. The assumption made in this approach is a continuous snow-cover present in a pixel such that the fallen snow remains in the pixel and doesn't deplete till the melting onset, thereby excluding the transient snow-fall events. These transient snow events are still noticed by MODIS as snow pixels and can cause earlier detection of snow as compared to the station data. However, a general idea of snow cover onset and melt can be reliably garnered in higher elevations with this assumption. Since the simulated data comes from the calibration against MODIS, the simulation result was assumed to be the truth and was validated against the station data. Dec 22 (Julian day: 355) was assumed as the fixed date FD_1 for Switzerland with SCD' as the snow covered days from September 1 till December 22.

Likewise, the snow cover melt date (SCMD) is the date when the snow starts to melt in the pixels. The SCMD is calculated as:

$$SCMD = FD_2 + SCD' \tag{6.7}$$

where, FD_2 is the fixed date after which snow starts to melt. SCD' is the duration during the melt period till the snow is completely melted in the pixel. Here as well, the assumption is that after the fixed date, the transient snow events are not counted within the pixel, i.e. the pixel remains snow-free till the next snow season. This can again lead to a delayed melt as MODIS pixels still observe the pixel as snow. For this, the FD_2 was assumed to be at a fixed date of 32 (February 1).

Figures 6.16a and 6.16b compare the observed and simulated snow onset days and snow melt dates in the availble 30 stations. Mean agreement for SCOD was 99% whereas for SCMD was around 91%. It can be inferred that the drop in performance in simulating the SCMDs in the stations between 500-1000 masl is due to an early melt in the simulated pixel. A fixed date assumption for all elevation zones might not work, especially in the mid-elevations where the snow availability is harder to assess. The lower elevation are more or less snow-free by the onset of melt whereas at higher elevations, the snow remains in the pixel for a longer time. This can be one of the future direction of the research. However, the combined agreement of of greater than 90% suggests that the model does well in simulating the Mean SCOD and SCMD for the station data.

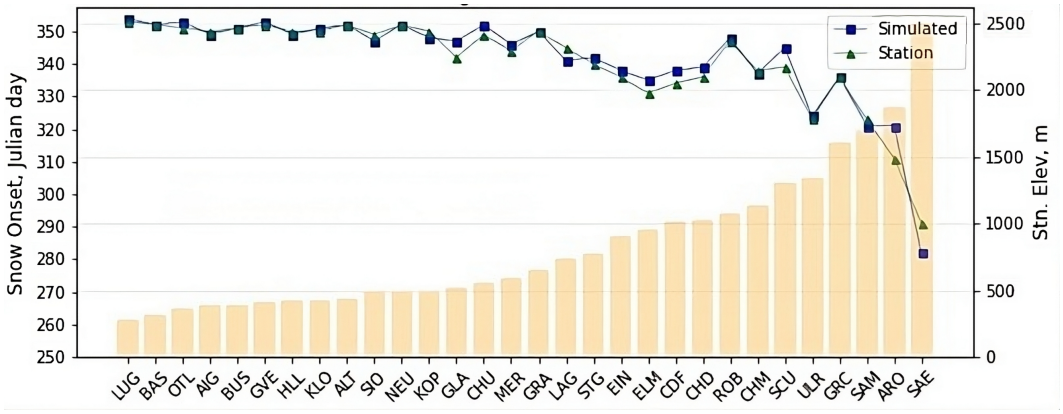

(a) Snow cover onset dates

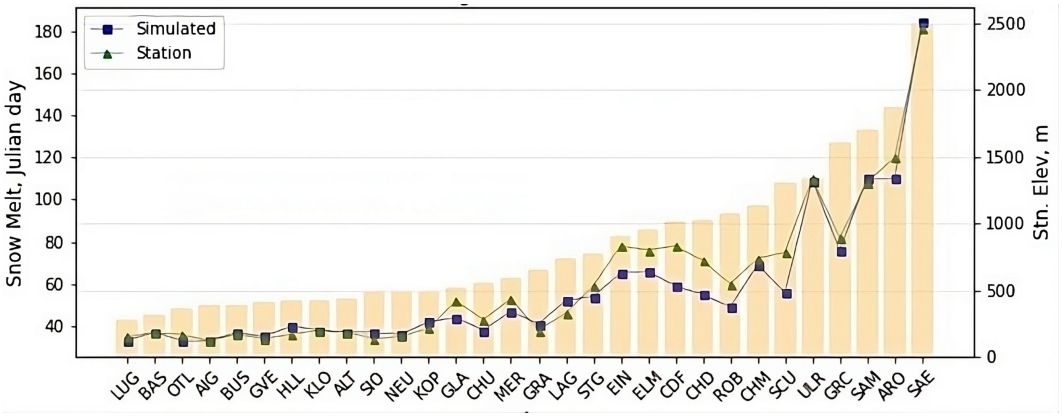

(b) Snow cover melt dates

Figure 6.16.: Comparison of simulated and station observed mean SCODs and mean SCMDs for Switzerland (WY 2010/11 - 2017/18)

6.6.2. Snow onset and disappearance timings

To analyze the snow onset and disappearance timings, four stations at different elevation zones were selected, namely MER (588 masl), CHM (1136 masl), ARO (1878 masl) and SAE (2502 masl). The figure shows the comparison of the simulated and observed snow appearance and disappearance timings. The snow hydrographs (in green) are the actual daily snow depths observed at the stations whereas the blue boxes indicate the period of snow persistence before it disappears from the station pixel.

It is clear that the blue boxes well bound the daily snow hydrographs in the higher elevations (stations ARO and SAE) with the exception of events in 2014. The patterns also match in the mid elevation station CHM and the lowest elevation station selected MER. The transient events towards the melt period are not captured well in the station MER which led to the earlier melt. The results suggest that the timings along with the distribution of snow as discussed in the earlier plots are well matched by the calibrated model and can be deemed applicable for further analysis.

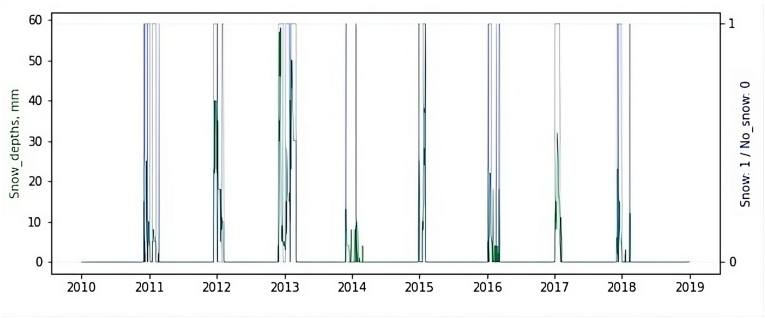

(a) Station MER (588m)

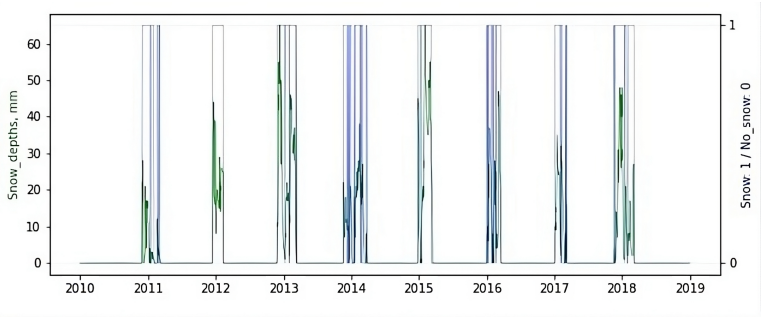

(b) Station CHM (1136m)

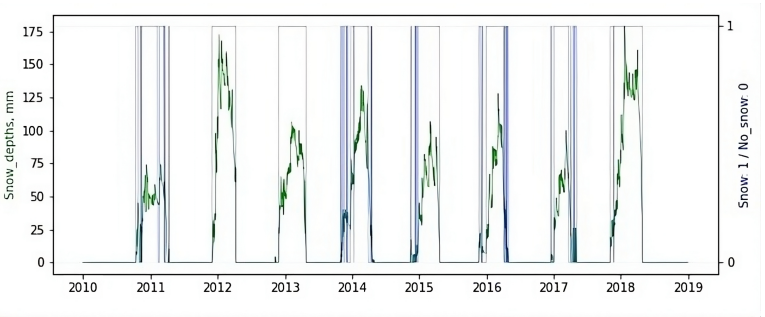

(c) Station ARO (1878m)

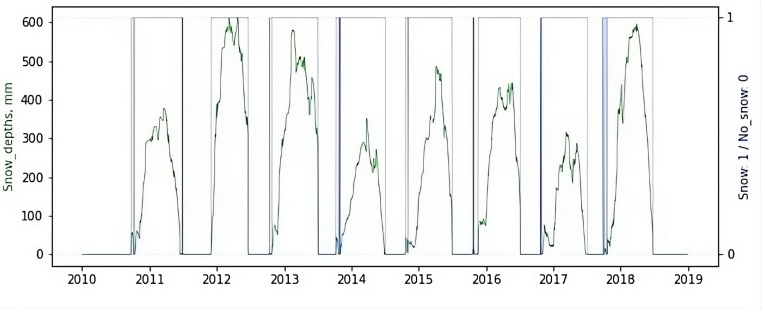

(d) Station SAE (2502m)

Figure 6.17.: Comparison of snow appearance and disappearance timing between simulated and station data

7. Sensitivity analysis and validation of the methodology

The preceding chapter discussed the parameter estimation approach and the results associated with it. This section deals with the sensitivity tests on different assumptions made and the validation of the methodology at catchment levels and in hydrological modeling. As identified in the earlier chapter, Model 6, i.e the model with the radiation component is used as the 'reference model'.

7.1. Sensitivity analysis based on thresholds

Assumptions on different thresholds and periods were made during the calibration in the study, broadly categorized as thresholds for snow/no-snow differentiation on a pixel level, and set of images used for calibration. These assumptions raise a question on what are the best possible minimum thresholds for these key factors, given the uncertainties in MODIS as well as interpolated meteorological drivers, and which set of images to select for calibration. Since the parameter estimation approach is governed by these assumptions, the entire calibration routine was tested via a sensitivity analysis, which is further explained in subsequent sections.

7.1.1. Thresholds for 'snow/no snow' differentiation

As this methodology relies on binary 'snow' or 'no snow' calibration, it is very pertinent to have a plausible and reliable choice of threshold value to define as pixel as snow-covered or not. Three specific thresholds were assumed in this category:

1. **The cloud threshold** as a percentage of valid pixels was assumed to demarcate the number of daily images to be used as a reference series to calibrate against. This threshold governs the number of images (i.e. days) selected for calibration. As discussed earlier, the cloud obscurities severely limit the integration of RS into snow-melt and hydrological modeling context. For the earlier runs, a baseline cloud threshold was assumed as 40% so that only the images with more than 60% valid pixels within the whole or a certain period of the snow-season. The resulting simulated snow-cover distribution as shown by the results were very well simulated. However, the sensitivity analysis was carried out to assess how sensitive the entire approach is to the selection

of images based on clouds and to find what minimum percentage of clouds is permissible to achieve a similar or even better model performance. Since this approach works on a pixel-by-pixel basis, the initial hypothesis is that the cloud obscurities do not have a significant impact on the calibration and can be even done on patches of pixels rather than a whole cloud free image without much loss in performance. Thresholds ranging from 10% to 90% were used for the sensitivity runs.

2. **NDSI** thresholds to demarcate the snow and no snow pixels in the reference MODIS images was also assumed as 0.1 (values ranging from 0-100) for baseline runs. A pixel with a NDSI value greater than 0 is assumed to have some snow present and that with <=0 is snow free. The commonly used threshold of NDSI is 0.4 [Hall and Riggs, 2007; Dozier, 1989]. For this analysis, thresholds ranging from 0.01 - 0.95 were used for the analysis.

3. **SWE thresholds** are assumed in the study to transform the simulated SWEs to binary information. It basically can be defined as the minimum required simulated SWE in a pixel to classify it as a snow pixel. Different thresholds ranging from 0 to 5mm have been assumed in different studies. SWE thresholds are interchangeably used as detection threshold in this thesis.

Sensitivity analysis was carried out for different thresholds using the reference model for both Baden-Württemberg and Switzerland to identify the best snow/no snow differentiation. The time period used for the calibration was from 2013-2015 for uniformity and the entire winter season images were considered for both regions to meet the cloud criteria. Figures 7.1a and 7.1b show the synopsis of the sensitivity analysis for cloud thresholds upto 50% and NDSI threshold upto 0.7. A more detailed presentation is available in Annex B.1 and B.2. The figures present NDSIs as multiples of 10, i.e actual NDSI multiplied by 100.

From the figures, it can be clearly inferred that the best performance can be achieved with a NDSI threshold of 0.3, cloud threshold of 10% and a SWE threshold above 0.5 mm in terms of Brier scores in Switzerland. Likewise, for BW, the results show that, a SWE detection threshold of 2.0 mm or above, along with the NDSI threshold of 0.3 and a cloud threshold of 10% simulates the snow cover distribution best. The similarity in terms of best performing thresholds highlights the applicability of the adopted methodology in different snow regimes.

Further scrutinizing the results as illustrated in the Annex figures, it is clear that for Baden-Württemberg, the NDSI thresholds of 0.3 and 0.4 show similar performance with SWE threshold higher than 2.0mm during model calibration when the MODIS images fitting cloud threshold criteria of 10% is implemented. For Switzerland, a NDSI threshold of 0.3 along with SWE thresholds higher than 0.5 mm gives the best result. In Switzerland, the model simulation is more sensitive to the selection of NDSI thresholds as the model performance severely drops after NDSI of 0.6. In contrast, in BW, the model performance drop is not so drastic as in Switzerland, as the NDSI values upto 0.7 give comparable results. Detection thresholds of 2mm and above show a good simulation, with NDSI thresholds of 0.3 and 0.4 giving similar results when the SWE threshold of higher than 2.0mm is used with 10% cloud thresholds.

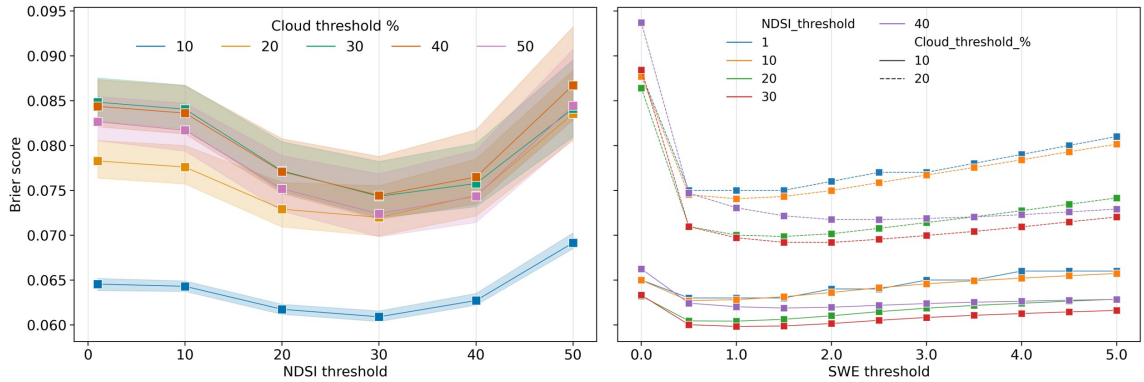

(a) Switzerland

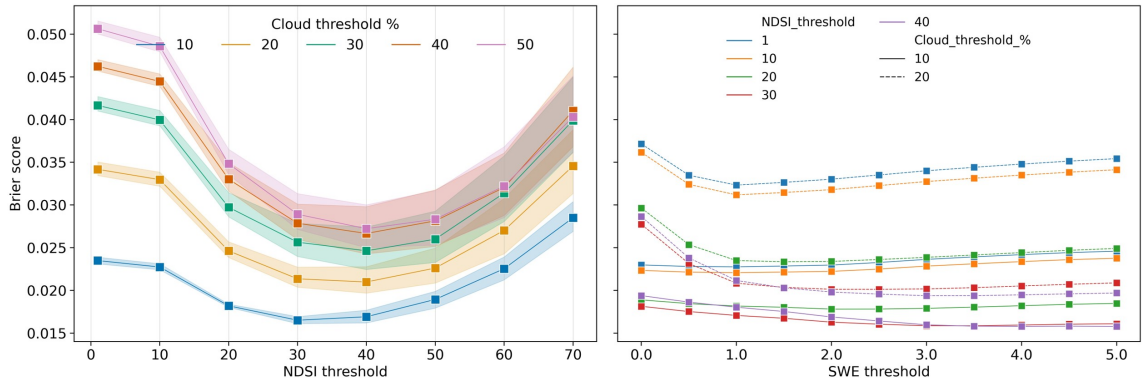

(b) Baden-Württemberg

Figure 7.1.: Model performance for different thresholds; left plot: The shaded part shows the performance for different SWE thresholds. right plot: Dashed and solid lines respectively show performance for 10% and 20% cloud thresholds. Detection threshold in the X-axis level refers to the SWE threholds. NDSIs are presented as actual NDSI multiplied by 100.

There have been different studies to analyse the threshold defining snow or no-snow conditions such as Härer et al. [2018] who used seasonally and locally optimized NDSI thresholds ranging from 0.15 to 0.74 to reliably estimate the SCA in local context. They conclude that for 500m resolution, a NDSI threshold of 0.40 remains valid. Tong et al. [2020] investigated the sensitivity and the related accuracy of different NDSI thresholds to evaluate the spatial seasonal patterns of the thresholds in Austria. They compared the snow cover mapping based on different thresholds with the established NDSI threshold of 0.4 and concluded that they are very sensitive to the snow depth threshold demarcating snow cover at the ground. They found out that the NDSI threholds have a distinct spatial and seasonal pattern, i.e strong variability during seasons, decreasing trends with increasing elevation and generally lower in the forested areas than on open land. Zhang et al. [2019] tested different criteria to select NDSI threshold for MODIS products based on the locally optimal NDSI threshold, a threshold of 0.1 and the globally accepted NDSI threshold of 0.4. They found out that for China, 0.1 NDSI threshold had the best results in snow cover mapping than the widely used 0.4 threshold. The results from this analysis also fits well among the results from these studies in terms of NDSI. However, in this study, MODIS was employed as the observed snow cover distribution whereas in reality, the spatial detail of MODIS and the associated uncertainty [Tong et al., 2020] makes it harder to reliably detect where the snow actually is. Added to that the uncertainty with the interpolated precipitation data in the higher elevations, make a very hard case for a clear recommendation of a definite threshold for future applications. We can however, safely conclude that a NDSI threshold of 0.2 -0.5 can be used to classify snow and no-snow pixels for snow-melt modeling employing MODIS information as a calibration reference. Likewise, in conjunction to this, SWE thresholds of 0.5 - 5mm for longer duration snow conditions and 2 - 5mm for shorter duration snow locations can be used without a major loss in performance. Nester et al. [2012] also identified a SWE threhold of 2.5mm as an optimum threshold for error analysis with MODIS SCA. A snow depth threshold of 20mm was implemented by Tong et al. [2009a] in their study in Canada for cloud cover reduction in MODIS. These SWE thresholds are in general more sensitive to the type and the density of vegetation [Roy et al., 2010] for studies pertaining to higher resolution simulation. Parajka and Blöschl [2008(b)] and Zhang et al. [2019] employed a 10mm snow depth (2mm of SWE considering 20% snow pack density) to demarcate the snow depth to binary snow information. The snow depth less than 1cm can be considered as traces and usually introduce more uncertainties [Zhang et al., 2019]. The results presented here are in line with these studies, though numerous other adopted values are found in different literature and are more site specific. For a 500m resolution study using MODIS, the recommended range is plausible.

Different studies have identified the cloud threshold to be one of the critical factor for evaluating the model errors in terms of SCA or resulting discharge [Parajka and Blöschl, 2008(b); Nester et al., 2012; Şorman et al., 2009; Udnæs et al., 2007]. Şorman et al. [2009] adopted a cloud threshold of 20% in hydrological modeling context for a multi-variable constrained calibration. Parajka and Blöschl [2008(b)] recommended a 60% cloud threshold as a reasonable compromise between snow data availability and SCA robustness. Udnæs et al. [2007] incorporated the snow cover data in a hydrological model with images showing cloud obscurity less than 30% of the catchment. Rodell and Houser [2004] in their study of updating snow-water storage in a land surface model using MODIS, assumed a minimum of 6% vis-

ibility (94% cloud threshold) for MODIS to be useful. Nester et al. [2012] suggested a cloud threshold of 80% as no significant differences were observed in model errors for <50% and 50-80% cloud cover in their study. In this study, A cloud threshold of 10% (i.e images with more than 90% of valid data) was found to be the ideal threshold for the selection of MODIS images for calibration. However, the results suggest that the methodology is not very sensitive in terms of cloud coverage. This highlights the fact that the calibration on binary pixel information is adept in simulating only based on on patches of snow-covered pixels free from clouds, which further showcases the flexibility of this calibration.

7.2. Sensitivity analysis on the selection of calibration periods

The selection of images for calibration is an important criteria for successful calibration and resulting impact on parameter transferability. The snow season has a onset phase, which governs the availability of water stored in the snow-pack in the mountainous and mid-latitude regions, and the melt phase which determines the timing of availability of water. It is thus, very pertinent to know which minimal set of images are enough for calibrating the snow-melt models. The MODIS images for whole season fitting a certain cloud criteria were selected for baseline simulations. However, to assess the performance of the selection of calibration images, whole or different periods within the snow season of 2012-13 was carried out to analyse the resulting temporal transferability within the different periods in the season. For this, the reference model was calibrated against sets of MODIS images representative of different phases of the snow-season, i.e whole season (September-June for Switzerland and October – May for BW); snow accumulation period (September – February for Switzerland and October - February for BW); ablation period (March – June for Switzerland and March – May for BW), peak snow month (February for both) and the cloud-free day with peak amount of snow (February 18 for Switzerland and February 12 for BW). The thresholds were then considered as defined in the sensitivity analysis in the earlier section as NDSI threshold: 0.3, cloud threshold%: 10%, SWE threshold: 2.5mm for BW and NDSI threshold: 0.3, cloud threshold %: 10%, SWE threshold: 0.5 mm for Switzerland). The model was calibrated with ROPE and 1000 best performing parameter vectors were estimated for each season for both regions.

These calibrated parameter vectors for each of the calibration periods were then iteratively compared with the parameters from other periods ('validation parameters') based on the concept of convex hull and data depths. The depth of each set of calibrated parameter vectors were iteratively estimated in reference to the convex hull defined by the validation parameters. The analysis was done to check to what degree, the calibrated set of parameters were contained by the convex hull. Higher values of the half space depth indicate a deeper residence of the reference values inside the hull defined by the validation vectors. All the parameter vectors whose depths are greater than '0' were then divided by the total number of parameter vectors i.e, 1000 to obtain the proportion of parameter sets contained by the convex hull. This containment proportion gives a measure of the transferability of the parameters with higher proportion meaning the calibrated parameters have similar per-

formance in the validation period as well. The calibrated parameters were validated for each season to analyze the temporal transferability of the parameter vectors and identify the calibration period with a 'good' performance in all the seasons/periods.

Figure 7.2a and 7.2b show the transferablity of the calibrated parameter vectors in different seasons in terms of the percentage of reference parameter vectors for each period within the snow season contained by the hull of the validation parameter vectors for BW and Switzerland respectively. This transferability of parameters was used to evaluate which period is suitable for calibration in different snow regimes.

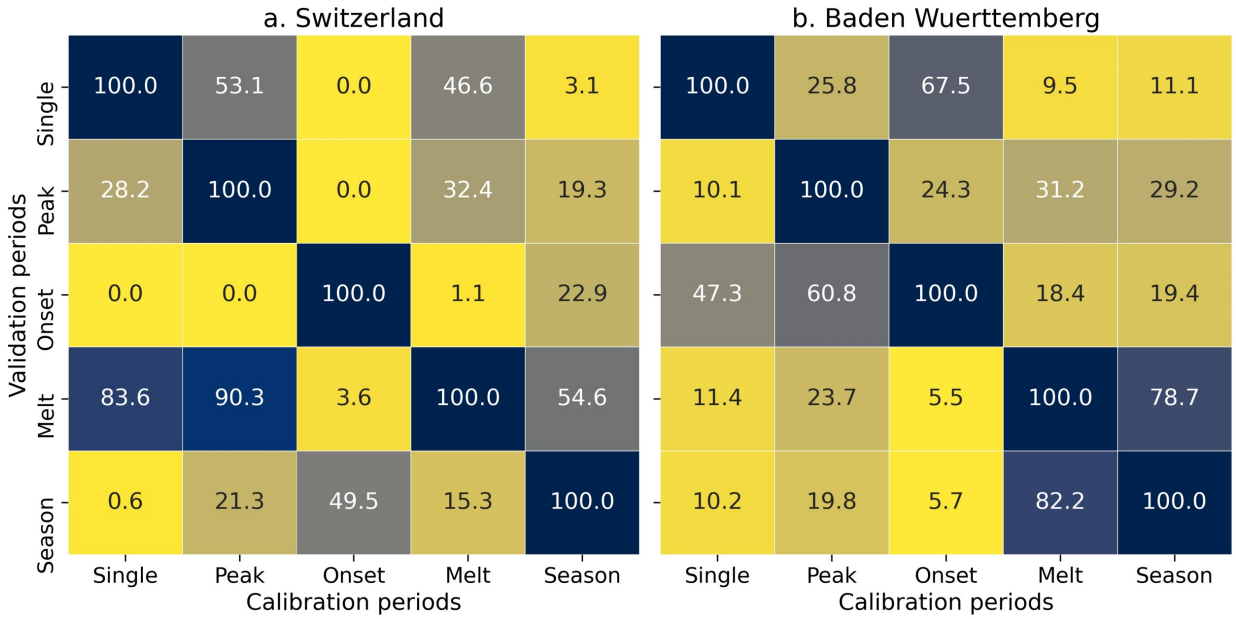

Figure 7.2.: Percentage of calibrated parameter sets contained by the convex hull of the validation parameter vectors

It is evident from the figures that the parameters estimated using the whole season images impart better validation in both regions, as reflected by the higher containment of the calibration parameters in reference to the validation periods. This is understandably so, because the whole season images capture the dynamics of snow accumulation and ablation. However, BW and Switzerland exhibit different results when it comes to period based calibration. In Switzerland, the melt season calibration offered better temporal transferability as higher proportion of the parameter vectors estimated with ablation period images were contained in the convex hull from different reference periods. In contrast, BW exhibits higher transferability with onset period calibration as the percentage of contained vectors is relatively higher compared to other calibrated sets. This is further clarified by figures 7.3a and 7.3b which shows the dispersion of Brier score values in different calibration and validation periods. These figures clearly show that in BW, the onset season calibrated parameters are well validated for the peak snow season and the single day event. The parameters estimated with the melt phase calibration can also be deemed reasonably comparable to onset season performance. The whole season calibration show better validation in the onset and melt seasons but the spread of the box plot suggests higher uncertainty towards with peak snow

month and peak snow day images. In Switzerland, melt season estimated parameters show a very good validation throughout the seasons or periods considered. The whole season calibration also performs reasonably well during the validation with comparable results for almost all the seasons. It can thus be concluded that, based on these results, a more robust set of parameters were estimated when calibrating the model using the onset period images for BW and the melt period images for Switzerland. This indicates that for a shorter duration snow regime like BW, the images available during the accumulation/onset period can be effectively used for more robust calibration as these regimes exhibit a strong onset of snow but a more uncertain melt season with lesser availability of snow due to quicker melt. However, for longer duration of available snow as in Switzerland, the melt season is well-defined due to which the images towards the end of the season are adequate enough to simulate the snow accumulation and ablation in the region with higher accuracy and these calibrated parameters were found to be robust as shown by the spread of Brier-scores in the validation periods. This calibration approach is thus, flexible enough to utilize the image available for a certain period of time within the snow season to simulate the snow-cover distribution with a reliable detail. This indicates that the set of images available towards the end of the season can simulate the whole snow season very well.

7.3. Validation of the parameter estimation

The validation of the snow-melt model and the calibration, in this study, was carried out distinctly as regional validation, i.e for Switzerland and BW regions, and validation at the catchment level. Validation of estimated parameters and the resulting snow-cover distribution on a regional basis, have already been discussed in the earlier chapter where the calibrated parameters were used to validate the simulated snow-patterns for different seasons using the sets of MODIS images representative of the season as well as on individual images representing unique isolated events, for both BW and Switzerland. Based on the performance of the model variants in terms of overall Brier scores and in different elevation bands, the best performing model variant was used for this analysis. This section deals with the validation approach at catchment level.

7.3.1. Validation in hydrological modeling

To evaluate the performance of the snow models at a catchment level and subsequently for the discharge evaluation, five catchments viz. Neckar-Horb and Neckar-Rottweil in BW, and Reuss-Seedorf, Thur-Andelfingen and Aare-Brienzwiler in Switzerland, were selected. In addition to the simulated SWEs, the melt models also calculate the distributed melt-water outputs. Once the snow-melt model performance was adequately validated for each catchments and the parameters were deemed 'applicable', the models were run again to obtain the gridded melt outputs, assuming the model predicted both the snow distribution as well as the water content adequately. To evaluate and validate the snow-melt exiting the regime and its resulting impact on the discharge, a hydrological modeling based validation was

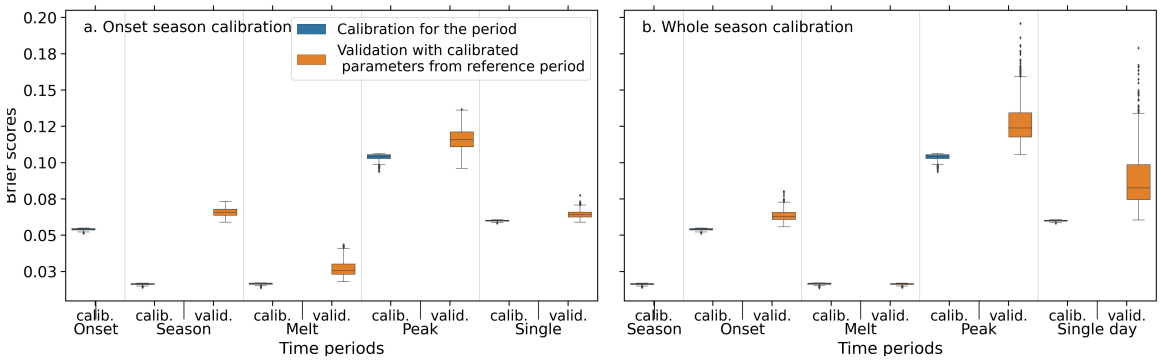

(a) BW

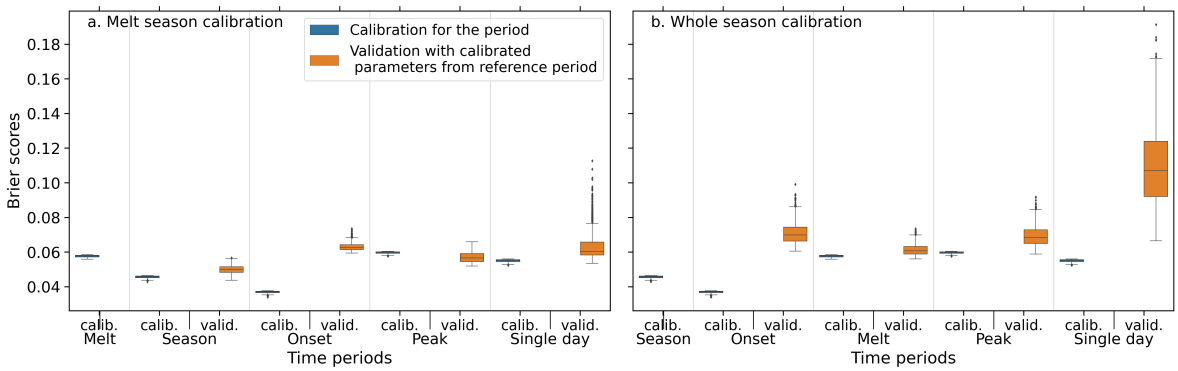

(b) Switzerland

Figure 7.3.: Model performance in different validation periods (a) Switzerland (left plot: validation results for melt season calibrated parameters, right plot: validation results for whole season calibrated parameters) (b) Baden-Württemberg (left plot: validation results for onset season calibrated parameters, right plot: validation results for whole season calibrated parameters); X-axis labels 'calib.': calibration performance for the same season, 'valid.': validation performance using the reference season parameters

carried out on a catchment scale using two hydrolgical models, namely the widely used hydrological model HBV [Bergström, 1995], henceforth termed as 'standard HBV' and a modified HBV model which accommodates the the distributed melt outputs from the best performing snow-routine variant as standalone inputs (from hereon termed as the 'modified HBV').

7.3.1.1. Comparison of snow simulation

For the catchment based evaluation, the first stage was to compare the efficacy of the standalone calibration on MODIS images with the snow-routine of the standard HBV calibrated on discharge. The reference snow-melt model (Model 6) was calibrated for all five catchments on snow-cover distribution for the winter season through 2010-2015 for BW and 2010-2018 for Switzerland. ROPE was used to calibrate the catchment models and subsequently 1000 sets of best performing parameter vectors for each catchment were estimated, based on the overall Brier-scores. Figure 7.4 shows the boxplots of 1000 best parameters for all catchments. The Y-axis has the normalized parameter values based on their min-max range set for optimization. The parameter ranges were found to be plausible. It is indicative from the figure that all parameters are relatively stable and less sensitive to the model performance, except the radiation melt factor r_{ind}, T_{Mmax}, T_{Mmin} and to some extent T_S. Since these parameters directly govern the snow accumulation and melt, they are understandably more sensitive and prone to be constrained by the objective function.

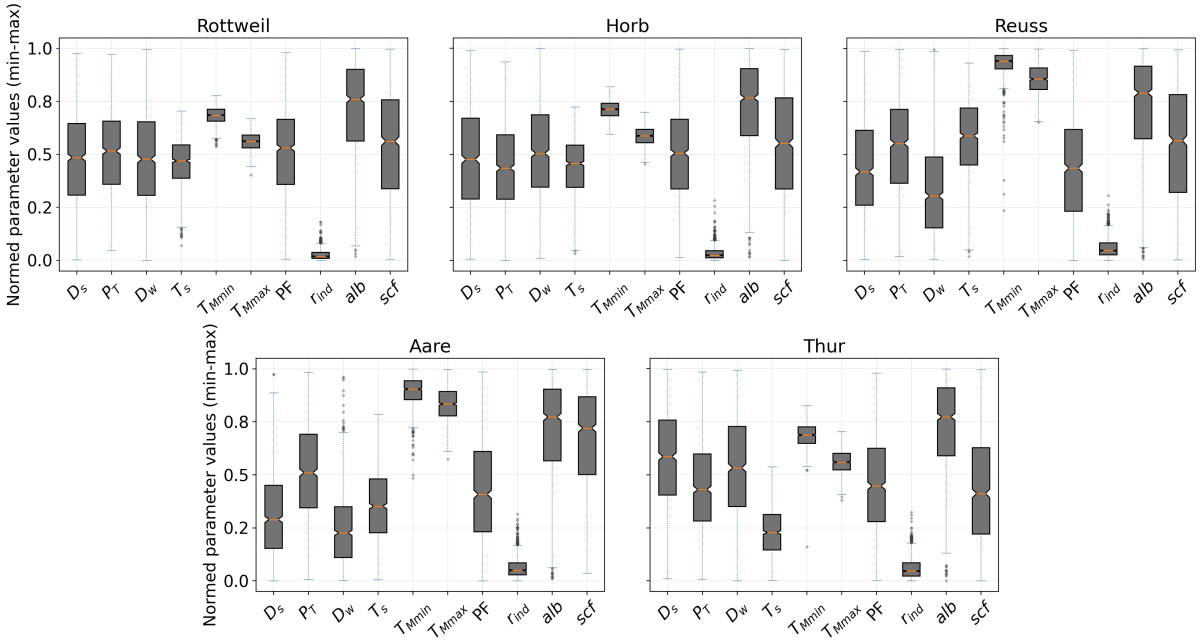

Figure 7.4.: Model 6 parameter dispersion for different catchments

The simulated snow-cover distribution was then compared with snow-cover distribution

simulated by the standard HBV's snow sub-routine as an evaluation of the representation of the snow snow accumulation and melt processes within. The objective here was to compare the calibrated snow routine parameters based on images and that from the ones calibrated on discharge, and to further investigate the possible parameter compensation in the model. For this, the standard HBV was first calibrated with ROPE and the 1000 best parameter sets were obtained. From these vectors, a subset of 1000 HBV snow parameter sets was drawn and then the snow-routine of HBV was run with these parameters and the respective Brier-scores were obtained. The comparison was done based on the performance of snow-cover simulation using these two distinct calibrated parameters, in terms of Brier scores.

The violin plots from the figure 7.5 clearly show that the snow-melt model calibrated on images simulates the snow-cover distribution with better reliability and performance than the HBV's snow routine in all catchments, with the median Brier-score values for the snow-melt models in all catchments significantly lesser than their counterparts. Moreover, the shape of the violin plots indicate that the Brier-score values for the snow-melt models depict a very narrow spread in contrast to a much wider spread from the standard HBV snow routine. This highlights the higher uncertainty pertaining to the simulation of snow accumulation and melt processes. This further hints that the snow-routine parameters suffer from compensation with other parameters when the standard HBV is calibrated on discharge only. This parameter compensation has been highlighted in different snow related studies [Ismail et al., 2020; Parajka and Blöschl, 2008(b); Duethmann et al., 2014; Finger et al., 2015]. This compensation often leads to unreliable estimation of melt-waters exiting the snow regime, drawing "right for the wrong reasons" conclusion, even if the calibrated discharge seems well simulated [Seibert, 2000].

It is to be noted from the figure that the spread of the Brier scores is more pronounced in the shorter duration snow regimes, viz. Horb and Rottweil for the HBV simulations. The HBV calibrated on discharge is not able to capture the snow processes well in these BW catchments, albeit the performance is slightly better in the Swiss catchments which boast a longer duration of snow. Standalone calibration based on images thus adds value to these regions in estimating the snow cover distribution and the available melt, as these catchments have a strong dependence on the melt waters.

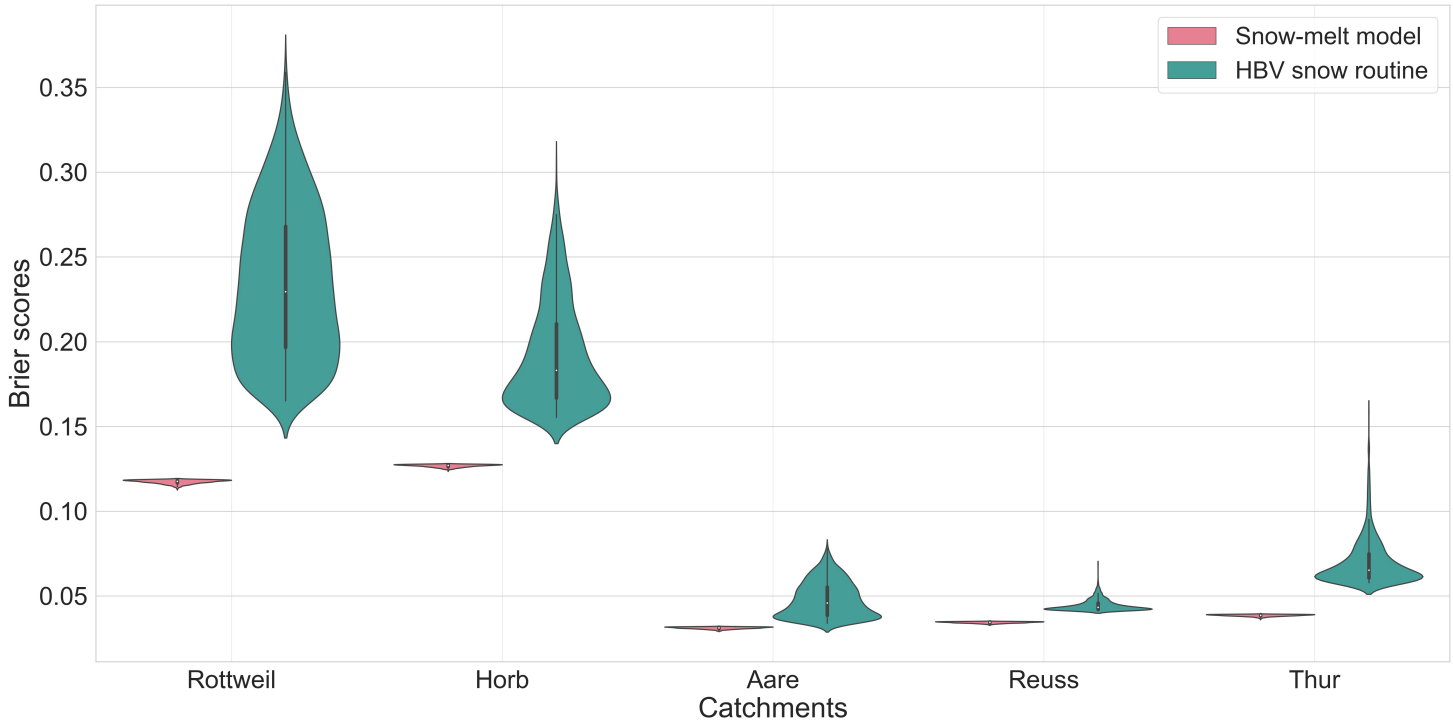

Figure 7.5.: Comparison of the performance of reference snow-melt model and standard HBV's snow routine in different catchments in terms of Brier-scores; The height of the violin plots shows the range of Brier-scores whereas the shape of the curve depicts their density.

7.3.1.2. Comparison of discharge simulation

After the comparison of the snow routines based on snow-cover distribution simulation, the melt output from the snow-melt models were also evaluated to analyse if the standalone calibrated melt brings about improvement in discharge simulations, to look for a snow-processes informed discharge estimation. For this, the best performing parameter vector from the snow-melt models for each catchment was used to simulate the distributed melt outputs exiting the snow-regime, which was in turn, used as an standalone input in the modified HBV model. Both hydrological models were calibrated on a catchment scale daily discharge for the period of 2011-2015 for BW and 2011-2018, with 2010 as the warm-up year. Nash-Sutcliffe Efficiency (Eq.7.1) was used to evaluate the performance of discharge simulations, where the simulated and observed variables refer to modelled and observed discharge at time t.

$$NSE = 1 - \frac{\sum_{t=1}^{T} \left(Y_o^t - Y_m^t \right)^2}{\sum_{t=1}^{T} \left(Y_o^t - \bar{Y}_o^T \right)^2} \tag{7.1}$$

Where,
Y_m^t = Simulated variable at time t,
Y_o^t = Observed variable at time t,
$\bar{Y}_o^T$ = mean of observed variable for the time period T,
T = length of time series,

The melt outputs were evaluated as a comparison of two different simulated discharge series for the winter periods based on their NSE values. 1000 best NSEs were obtained with ROPE calibration. Due to the reduced number of parameters required for calibration for the modified variant of HBV, the calibration was done in three ROPE iterations whereas the calibration of the standard HBV was done with five iterations of ROPE. The results of the calibration are shown in table 7.1 and figure 7.7.

Table 7.1.: Comparison of HBV and Modified HBV NSE performance

	HBV NSEs			Modified HBV NSEs		
	Min	Max	Median	Min	Max	Median
Rottweil	0.595	0.672	0.609	0.663	0.724	0.676
Horb	0.653	0.700	0.663	0.738	0.821	0.755
Aare	0.395	0.566	0.424	0.658	0.678	0.663
Reuss	0.635	0.779	0.656	0.781	0.796	0.785
Thur	0.702	0.768	0.712	0.731	0.776	0.739

The results clearly suggest that the modified HBV well outperforms the standard HBV simulations. The addition of melt significantly improves the hydrological model performance in each of the catchments, notably the most in the snow dominated ones in Reuss and Aare. The median NSEs are improved throughout the catchments in the study domain. The spread

of NSEs as indicated by the violin plots is also smaller with the modified HBV. Due to the reduced parameter space in the case of the modified variant, the hull containing the equifinal parameter vectors is smaller as compared to the ones representing the calibrated standard HBV parameters. This attributes to the uncertainty reduction in the simulation as depicted by the narrower spread of the NSEs. The results thus indicate towards a well-informed discharge simulation with the improvement in model performance coming with a better computational efficiency and a better simulation of the snow accumulation and melt. As an illustration of the winter flow simulation, figures 7.6a and 7.6b show the case of an isolated hydrological simulation in Horb catchment for the winter of 2012-13. The figures show that the melt input adds value to the discharge simulation during the season quite efficiently as compared to its HBV counterpart. The 1000 best hydrographs envelope the observed discharge better than the HBV model indicating a better representation of the snow-melt process.

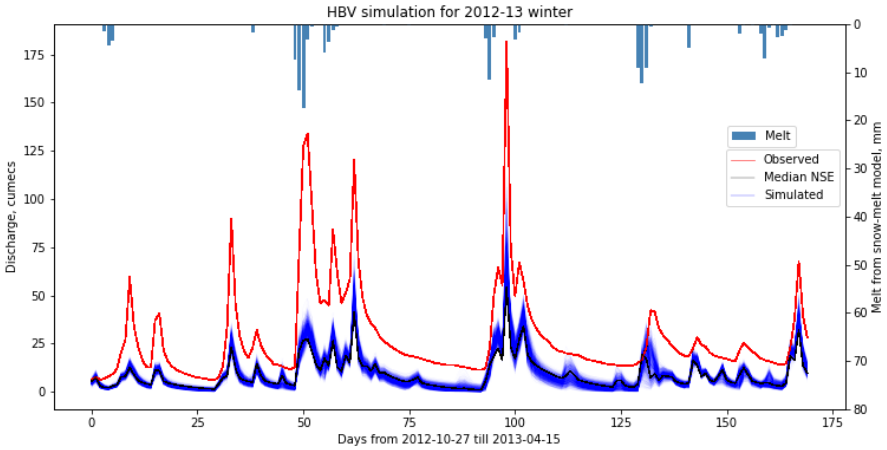

(a) Standard HBV simulation

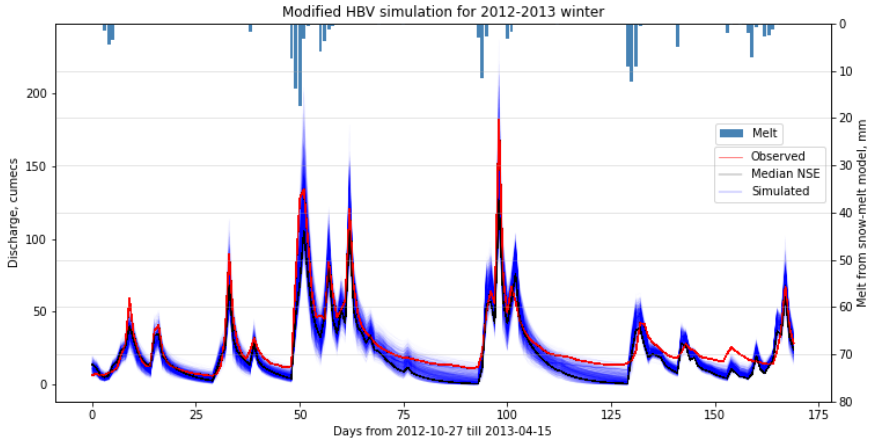

(b) Modified HBV simulation

Figure 7.6.: Simulated hydrographs for the 2012-13 winter in Horb

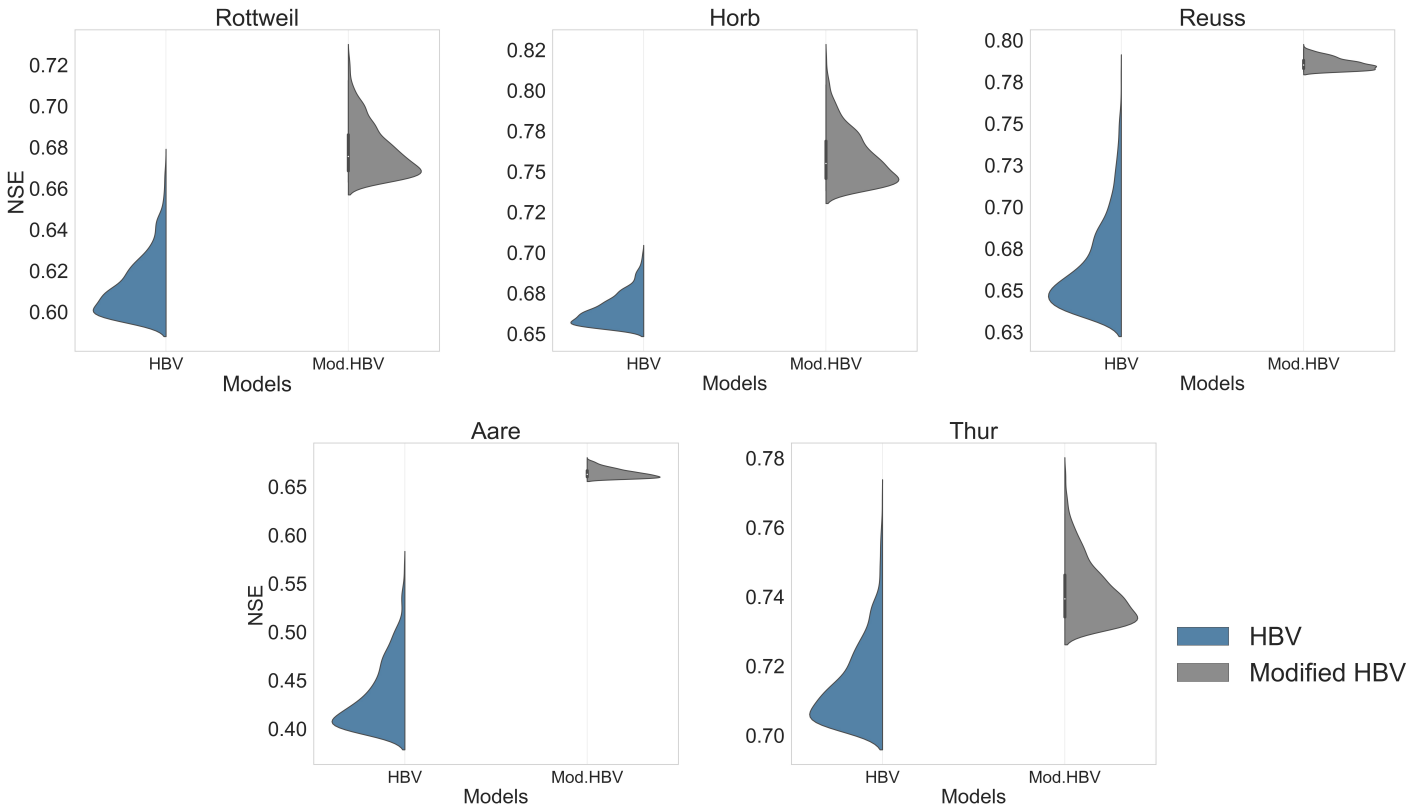

Figure 7.7.: Comparison of NSE performance for the standard and the modified HBV models in different catchments. The shape of the violin plots indicate the density plots for the 1000 best NSEs for each mode

It is to be clarified that this study's objective is not to assess the model performance of HBV and its predictions but rather to evaluate the performance of the melt outputs of snow-melt models calibrated on snow-cover distribution in a basic hydrological model. Also, it is important to note that though Aare and Reuss catchments are glaciated, the glacial-melt was not taken into account. This was intentionally not included in the simulation because of the MODIS' limitation to identify the glaciers [Muhammad and Thapa, 2020] and to avoid further parameterization of the hydrological model by including glacier component. Since, the objective was to evaluate the snow-melt model calibration and the implication of standalone melt inputs, both hydrological models were calibrated on equal terms with similar approach with results comparable to each other. With the standalone melt, the NSE performance of the hydrological models were improved. The value of adding snow cover in hydrological context has been highlighted by different studies. Parajka and Blöschl [2008(b)] pointed out that the median runoff model efficiency was improved with MODIS data incorporated in a multi-variable weighted calibration in comaparison to discharge based calibration. Bennett et al. [2019] also found that in their study, the inclusion of MODIS fSCA improved the internal snow timings and the hydrological simulations. Finger et al. [2011] also concluded that the models combining discharge and snow cover data showed the better discharge performance in comparison to other combinations used. Similar finding was put forward by Corbari et al. [2009] in which they concluded that the calibration of a hydrological model solely based on SCA showed a better performance in terms of discharge simulation. The results in this thesis are in line with these studies, thereby adding value to the importance of MODIS data in snow and hydrological modeling context.

7.3.2. Discussion on model uncertainty

One of the well known problems in hydrological modeling is the model complexity and the accuracy of the estimated parameters of the models. The complex models go into the details of sub-processes thereby demanding an intensive set of data to drive them. As snow is one of the major components of the hydrological cycle, it is imperative to have an extensive set of data to run the complex hydrological models. The rugged topography and the high spatial variability of the factors associated with snow processes such as the land cover, radiation, aspect, etc add more complexity to the snow simulation as they impart a high spatial and temporal variability in both accumulation and ablation processes. This poses a big question over the representativeness and accuracy of the in-situ observations [Clark et al., 2011]. Coupled with this, conceptual models which are the simplistic representations of the complex processes and their drivers are under constant scrutiny over the accuracy of the parameters estimated during calibration. Wagner et al. [2009] argues that due to the limited number of observations driving the models, different model structures and the estimated parameter sets may explain the observations equally well. Due to this well known problem of equifinality [Beven, 2001], only a set of acceptable model parameters can be assessed. A targeted inclusion of a specific additional information in the models can then lead to a reduction in the acceptable model parameter space, which in turn will lead to the reduction in uncertainty.

In the case of simulation of snow processes, the parameters associated with a hydrological

model can then be split into two distinct sets of parameters, namely the parameters driving the snow accumulation and ablation processes θ_s and the parameter governing other processes (θ_m). With an independent calibration of the snow related parameters $theta_s$ irrespective of the parameters θ_m, then a parameter set of M_s can be obtained. However, the equifinality can occur here as well with the snow-model calibration, albeit the equifinal parameter space becomes smaller. Then for each parameter vector $\theta_s \in M_s$, the hydrological model parameters θ_m can be calibrated leading to a set of other parameters, say M_m. With this we can obtain a well performing parameter set $M_{sm} = M_s \times M_m$. However, if the parameters of the model θ_m are estimated such that the model quality is the same as for calibrating the parameters (θ_s, θ_m) jointly (without using snow observations) obtaining the parameter set M, then the parameter set $M_{sm} = M_s \times M_m \subset M$. This is because all parameter combinations in M_{sm} could also be obtained from the traditional discharge based model calibration. However the important thing to consider here is that the set M might succumb to parameter compensations, that can lead to unreasonable snow parameters θ_s which are not acceptable for the snow model evaluation. Due to this, the standalone model calibration of the conceptual model may not lead to a better model performance, but instead can reduce uncertainty. On the other hand, the separate calibration of the hydrological and the snow-melt models allows the user to include more relevant parameters into the snow model, as it won't add complexity to the entire hydrological model. If the snow routine is calibrated together with the hydrological model, the increase in parameter space would then lead to a much more complex and uncertain calibration procedure with possible parameter compensation which have been well highlighted by the results.

For the evaluation of the uncertainties in simulation of snow accumulation and melt processes, the simulated snow-cover distribution based on snow-melt models calibrated on MODIS snow-cover and the snow-cover distribution simulated by the snow-routine of the standard HBV calibrated on discharge, were compared. The results show that independently calibrated snow parameter set θ_s provide a more reliable simulation of the snow-processes. As observed with the reduced spread of the violin plots in figure 7.5, the uncertainty related to snow processes simulation is greatly reduced with the snow-cover based calibration. A subsequent reduction in model uncertainties in terms of hydrological discharge prediction was also observed with the inclusion of melt inputs as shown by the results. The parameter set θ_m reduces to $\theta_m\prime$ when the truncated hydrological model with standalone melt inputs are used. This reduced parameter space, in addition to the snow-processes informed input, also allows a subsequent reduction in modeling uncertainties as the equifinal set of calibrated parameters becomes smaller. This comes with better computational efficiency as it takes lesser time to calibrate a model with reduced parameterization. This improvement in model performance can be attributed to 'a right reason' with a better representation of the underlying snow processes. Finger et al. [2015] have also discussed that additional calibration data add more value to the modeling than more complex and sophisticated parameterization of the processes. Due to the standalone nature of the calibration, incorporation of additional parameters in the independent snow-melt models to better represent the snow dynamics is possible which in contrast would have added further uncertainty during the calibration of the hydrological model with additional parameters. Di Marco et al. [2021] also concluded that a combination of MODIS fractional snow-cover area

and streamflow data led to a reduction of predictive uncertainty of a hydrological model thereby leading to sharper and reliable flow simulations. The approach of calibration at pixel level based on binary information allows relatively complex snowmelt modules to be calibrated with more robustness, as the uncertainty associated with calibration data is significantly reduced. This is often the case with calibration based on snow depth or snow water equivalent, as these data are prone to inaccuracies and to be severely under-representative in most of the mountainous areas around the world. In addition, calibrating on '1' and '0', instead of a continuous values, allows the snow-melt model calibration to converge faster thereby gaining computational efficiency. A dedicated snow-melt model thus allows this, as it is relatively quicker to calibrate on the images and the resulting melt can be used in the hydrological models for efficient calibration with reduced uncertainties. The calibrated discharge, even if it is similar to that calibrated by the a hydrological model, is considered to be good as it simulates the snow processes reliably and is for a right reason.

With these results, it can be concluded that the presented approach of estimating the snow model parameters using readily available MODIS images, offers adequate flexibility, albeit the simplicity, to calibrate snow cover distribution in different snow regimes with reasonably accurate precipitation and temperature data. The use of a standalone snow-melt model was observed to provide a relatively more stable and reliable simulation of the snow-cover distribution and the subsequent melt volumes. Furthermore, this independent calibration can prove crucial for episodic snow days in the winter season in areas with lesser snow while calibrating a hydrological model, as the snow routine can be efficiently calibrated with MODIS information, without having to calibrate the whole hydrological model. This can save computational time as this independent calibration permits flexibility on these episodic days and the results can be passed through the hydrological model as standalone inputs.

8. Practical extension of the approach

The earlier chapters established the validity of the calibration methodology adopted in this study. Based on this, the practical implementation of the snow-cover based calibration was further explored. This chapter deals with two case studies, (i) extension of this approach in a data scarce scenario, and (ii) an implementation of MODIS based model inversion to calculate the seasonal snow accumulation.

8.1. Application in a data scarce scenario

To test the extension of the study hypothesis to a data scarce scenario, a case study was done in the Bavaria region of south-east Germany. The Bavaria region, with an area of around 70,548 km^2 is the largest German state with elevations ranging from 106 to 2962 m.a.s.l. The Bavarian region is constituted by the high plateaus and mid-sized mountains with the German part of the Alps lining the southern border with Austria. The Bavarian Alps are lower than the regional climatic snow line or 3200 m.a.s.l reaching the highest elevation of 2962 m.a.s.l at Zugspitze. Figure 8.1 shows the map of Bavaria with the topography of the region. The region is drained by Main River in the north and Danube river through the center.

The entire region of Bavaria was used for simulating the snow-cover data incorporating both the relatively longer duration snow conditions in the Alps in the south and short duration snow conditions for the rest of the study area. Likewise, for the validation of the snow-cover simulation in hydrological model, two catchments namely, Isar at Plattling and Amper at Stegen were chosen.

8.2. Data used

The following driving datasets were used in this component of the study:

8.2.1. Meteorological inputs

Though the Bavarian region of Germany has a well-distributed network of observational stations, the observation data was not used in the study in order to mimic a data scarce scenario. Furthermore, it was deemed a pertinent part of the research, to evaluate the methodological approach with a 'reasonably' accurate meteorological data. For this, the interpolated daily gridded climate dataset, called the European Observations (E-OBS) was

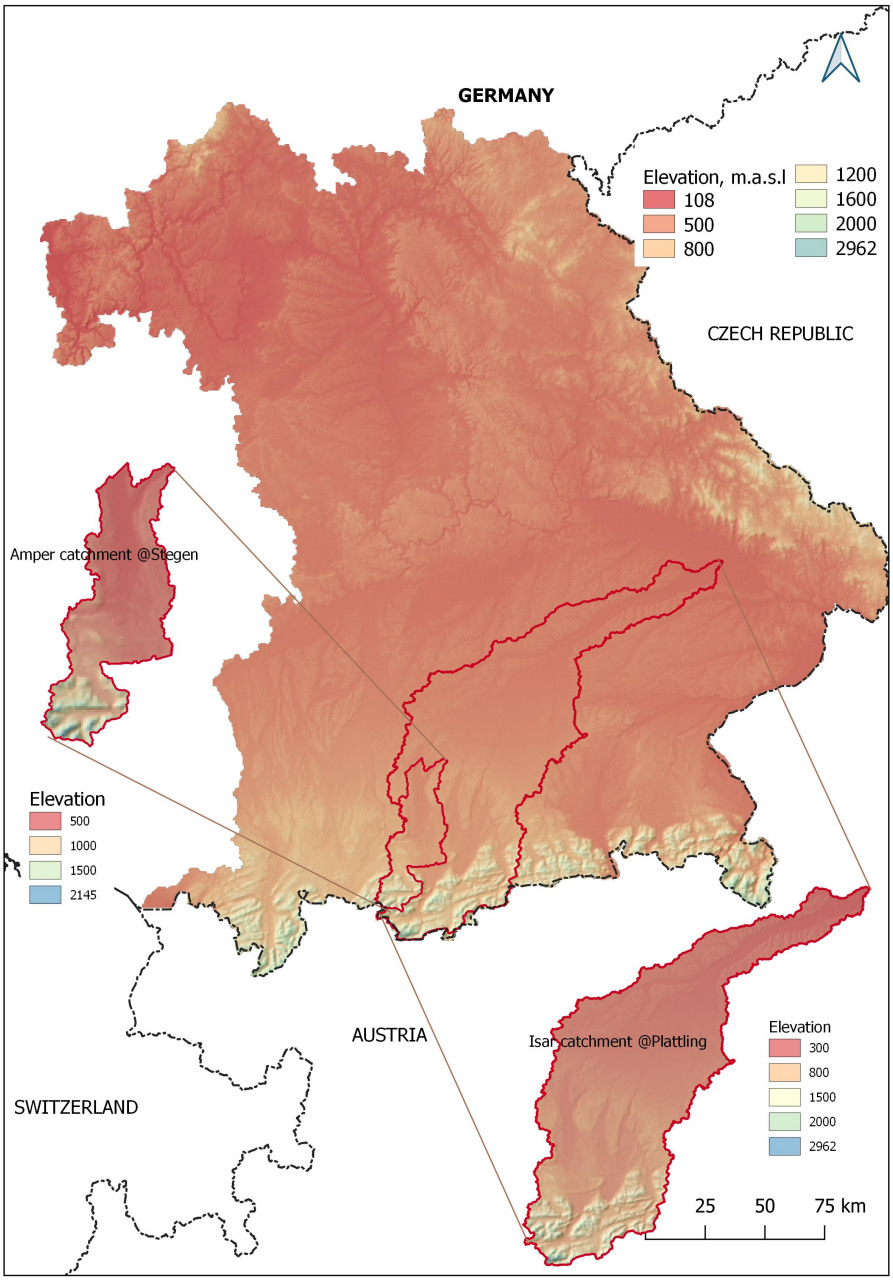

Figure 8.1.: Bavaria region as the study domain in south eastern Germany with selected catchments

considered in this study. The data is a product of the interpolation of 7852 weather stations from the European Climate Assessment and Dataset (ECA&D) project [Haylock et al., 2008]. The used data is on a 0.25° resolution which roughly translates to a spatial resolution of 30×30 km and is available on a daily scale. The variables obtained for the E-OBS data were daily precipitation, and min., max. and mean temperature data for a period of 2011 till 2019.

In addition to these data, the WorldClim (WClim) climate surfaces were also used for downscaling the coarser E-OBS data into a more MODIS friendly resolution. WorldClim [Hijmans et al., 2005] provides a set of climate surfaces as the long-term average of different climatic variables such as minimum and maximum temperature, precipitation, and 19 derived bioclimatic variables at a global scale. The spatial resolution of these data is 0.0083° (roughly around 1000x1000m). For each variable, each pixel consists of 12 monthly values. In this study only the precipitation surfaces and min., max., and mean temperatures were employed. The WorldClim data is developed with a thin-plate smoothing spline method from Hutchinson [1995], and is calculated based on data from 47554 weather stations around the world. For the interpolation, the DEMs from SRTM and GTOPO30 from the United States Geological Survey (USGS) [Moreno and Hasenauer, 2016] are used in the WClim methodology.

8.2.2. Spatial downscaling of E-OBS data

A downscaling methodology was carried out to bring the coarse resolution E-OBS data to a finer 1000×1000m resolution using the WClim surfaces to estimate the required daily precipitation and temperature data. The spatial downscaling was adopted and slightly modified from Moreno and Hasenauer [2016]. The spatial delta method was combined with a Ordinary Kriging of the anomalies. Moreno and Hasenauer [2016] used the monotone cubic interpolation to interpolate the residuals. The general methodology of the downscaling is shown in figure 8.2. Following steps were carried out for the downscaling procedure:

Step 1: The first step upscales the WClim monthly data to the E-OBS resolution of 30x30km by averaging the 1x1km WClim pixels contained within the E-OBS pixels.

Step 2: The anomalies were calucated between the upscaled monthly WClim pixels and the daily E-OBS pixels for both temperature and precipitation, to obtain daily anomalies based on monthly long-term means. To temperature anomalies were calculated as the differences between the cell values of upscaled WClim and E-OBS temperature data (Eq.8.1).

$$dT = WC_{30} - E_{OBS} \tag{8.1}$$

To avoid the negative precipitation values, for precipitation a ratio of E-OBS data to WClim monthly upscaled estimates was considered as an anomaly.

$$dP = \frac{E_{OBS}}{WC_{30}} \tag{8.2}$$

where, E_{OBS} and WC_{30} are the 30x30 km daily E-OBS and upscaled WClim data, and dT and dP respectively are the temperature and precipitation anomalies.

Step 3: This step calculates the daily variograms of the anomalies. Ordinary kriging was

then applied using these variograms to interpolate the anomalies to a finer 1 x 1km pixel. For this, 4 immediate neighbors from the 30x30km resolution surrounding the 1 x 1km resolution pixel were selected.

Step 4: The final step then calculates the downscaled value at each finer pixel using the original WClim data and the interpolated anomalies. The final downscaled values were calculated as

$$T_{1km} = WC_T - dT_{anom} \tag{8.3}$$

$$P_{1km} = WC_P \times dP_{anom} \tag{8.4}$$

where, T_{1km} and P_{1km} are the downscaled temperature and precipitation; dT_{anom} and dP_{anom} are the interpolated temperature and precipitation anomalies from step 3; and WC_T and WC_P are the original WClim temperature and precipitation data.

8.2.3. Results and discussion

Downscaling results

The downscaled precipitation and temperature data were compared and analyzed against the interpolated surfaces of station-based precipitation and temperature data estimated by kriging, assuming the interpolated data as the reference observed baseline. Figures 8.3 (a) and (b) show the winter RMSEs for temperature and precipitation respectively, calculated against the observed kriged data.

The results show that based on the winter RMSEs, the downscaling results are acceptable, given the coarse resolution global dataset considered for this analysis. Very few pixels report RMSE values greater than 2°C for temperature, with a mean value of 0.46 °C. Elevation-based scrutiny shows that the elevation zones around 1000 m.a.s.l show higher RMSEs for both temperature and precipitation. RMSEs less than 5mm were predominantly observed with the downscaling approach which was assumed to be reasonably accurate enough for snow-cover simulation. The mean RMSE for winter precipitation was found to be 2.64mm.

Likewise, figures 8.4 (a) abnd (b) respectively show the spatial distribution of mean daily temperature differences and differences in mean winter precipitation sums for the time period considered in the study. The results indicate that the temperature downscaling works adequately except for some pixels in the southern high elevation region. The maximum pixel by pixel basis difference is around 5.5 °C and the minimum is around -2.4 °C.However, for precipitation, the winter precipitation sums in the mountains is underestimated by around 200mm and in few pixels by 400-500 mm. The north-eastern part shows an overestimation by around 200mm after downscaling. The spatially averaged mean error remains at around 30mm for the entire region. This highlights the need to further explore and refine downscaling techniques other than the simplistic spatial delta methodology in the future research but given the resolution of the E-OBS data and the WClim climate surfaces used as the predictor variable, the results were considered to be reasonably adequate enough to mimic a data scarce scenario.

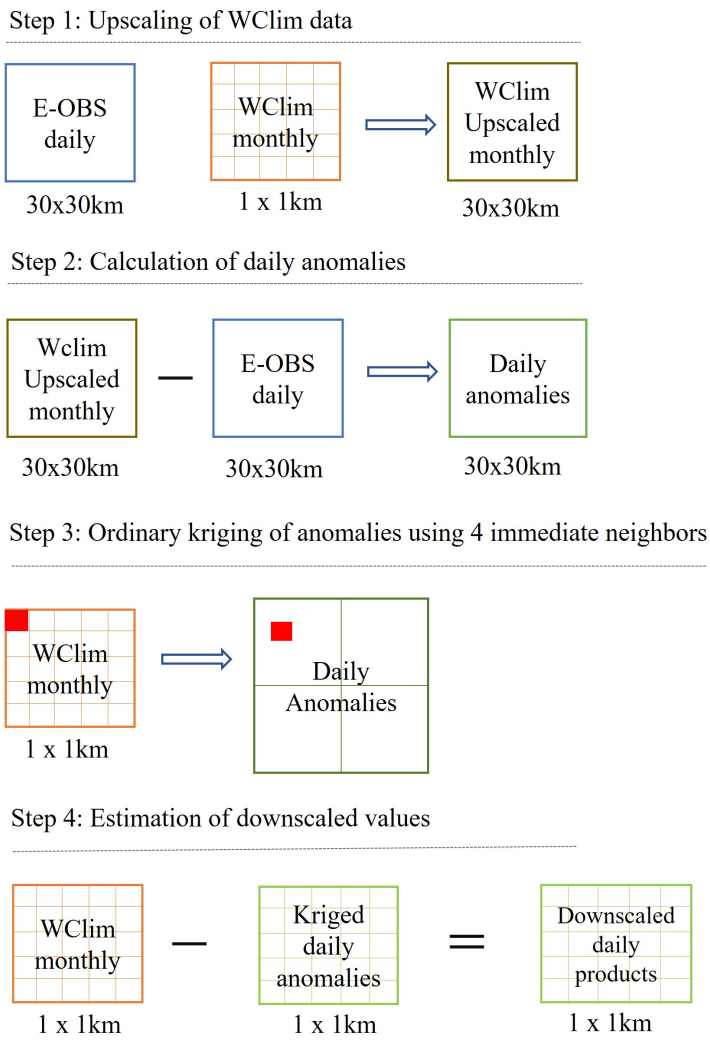

Figure 8.2.: Spatial downscaling of meteorological data (modified from Moreno and Hasenauer [2016])

Snow-melt model results

With **Model 5** as the reference model to avoid additional parameterization with radiation data, the inputs were prepared on a 1x1km resolution. The SRTM derived elevation information as well as the MODIS snow-cover data were also resampled to 1000m resolution by averaging the elevation and the NDSI values. The snow-cover data was then classified into snow or no-snow covered values using a NDSI threshold of 0.4. Once the model inputs were setup, the reference model was run for the winter periods of 2016-2018. The best overall Brier score value for the calibration period was observed to be 0.0136 for Isar and 0.0286 for Amper among the 1000 best values obtained from ROPE calibration. The Brier score values as well as their dispersion are very low as depicted by the ranges in table 8.1. This shows a very reliable simulation of the MODIS snow-cover distribution even when using a simplistically downscaled global dataset. Likewise the parameter dispersion in figure 8.5

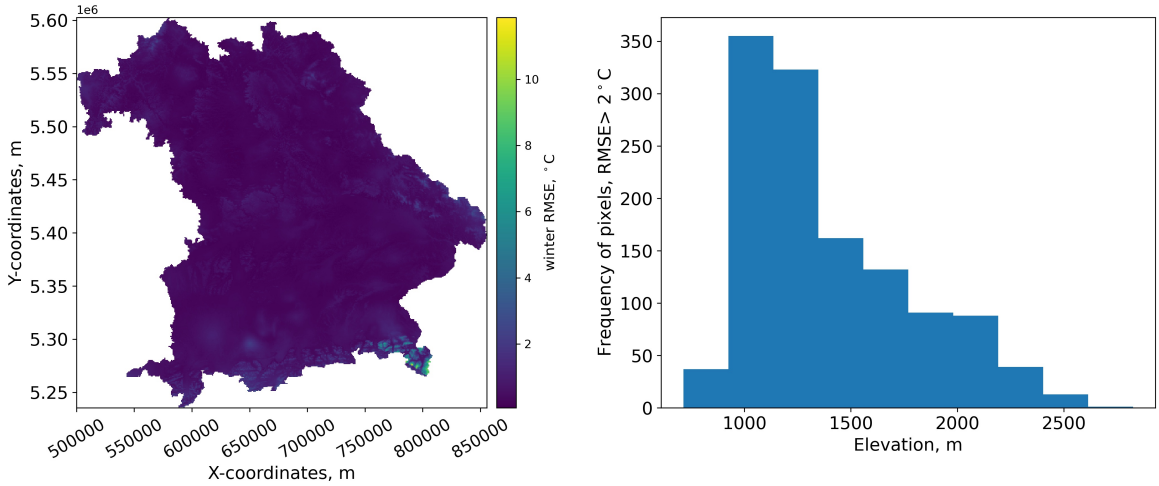

(a) Mean temperature

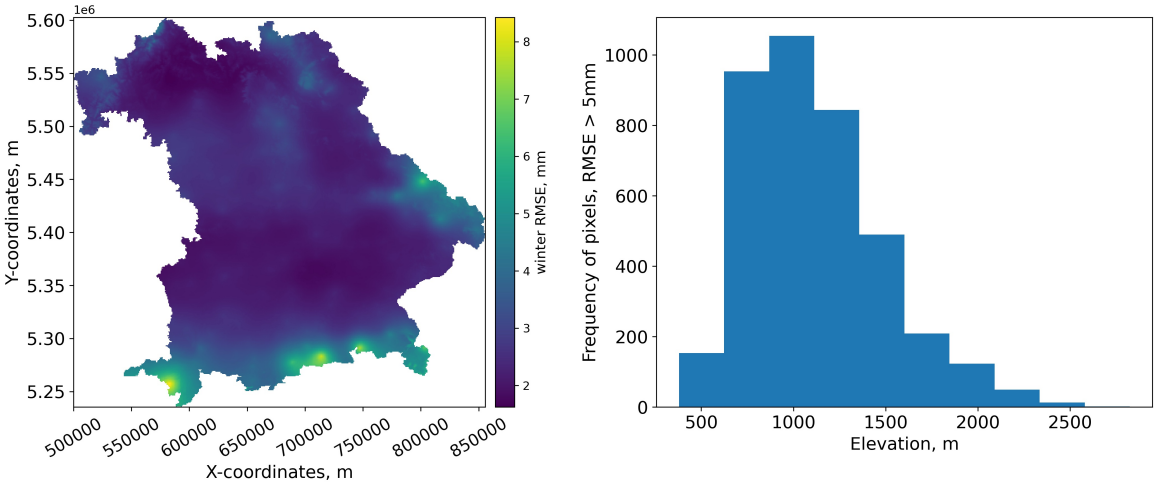

(b) Precipitation

Figure 8.3.: Winter RMSEs estimated for downscaled variable with respect to the interpolated observed data; left panel: spatial distribution of winter RMSEs, right panel: histogram showing frequency of pixels and elevation with RMSEs >2°C for temperature and RMSEs >5mm for precipitation

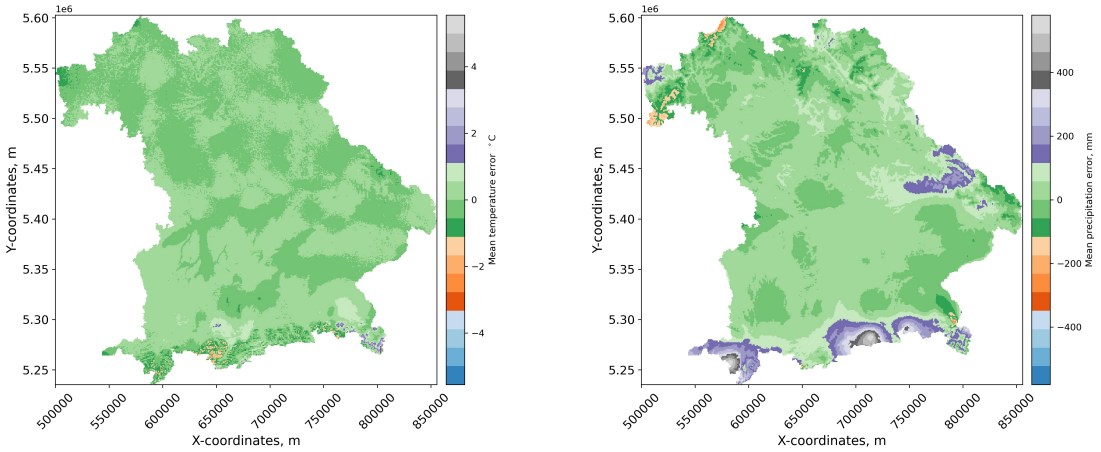

(a) Mean temperature differences for winter

(b) Differences in winter precipitation sums

Figure 8.4.: Mean differences for winter season calculated at pixel level for the period of 2015-2018

suggests that the parameters are within plausible ranges and are more or less stable, without much outliers. As in the case with Isar catchment (not shown here), the precipitation threshold triggering the rain on snow melt (Pcp_{th}) and the power factor governing the distribution of the snow-melt temperature (PF) are more or less insensitive and are prone to more fluctuations during calibration. Rest of the parameters exhibit relative stability.

Table 8.1.: Snow-melt model performance (Brier scores) in Amper and Isar

	Min.	Max.	Median
Amper	0.0286	0.029	0.0289
Isar	0.0136	0.0138	0.137

Hydrological modeling results

Likewise, the best parameter vector for each catchment was then used for a period of 2016-2018 to estimate the melt output from the calibrated model. The melt output was used as standalone input to the modified HBV model. The standard HBV model was also calibrated on discharge for both catchments for a period of 2015-2018 with 2015 as the warmp up year. The corresponding best performing NSEs were estimated by calibration and compared as shown in table 8.2.

It can be inferred from the figures, that the calibration on snow-cover distribution and the resulting melt improved the hydrological simulations to some extent in both overall and winter periods (October to April) in both catchments. The results suggest that as long as the models are run and calibrated on equal grounds, here the downscaled precipitation and temperature, the calibration on snow-cover distribution can bring about improved hydrological

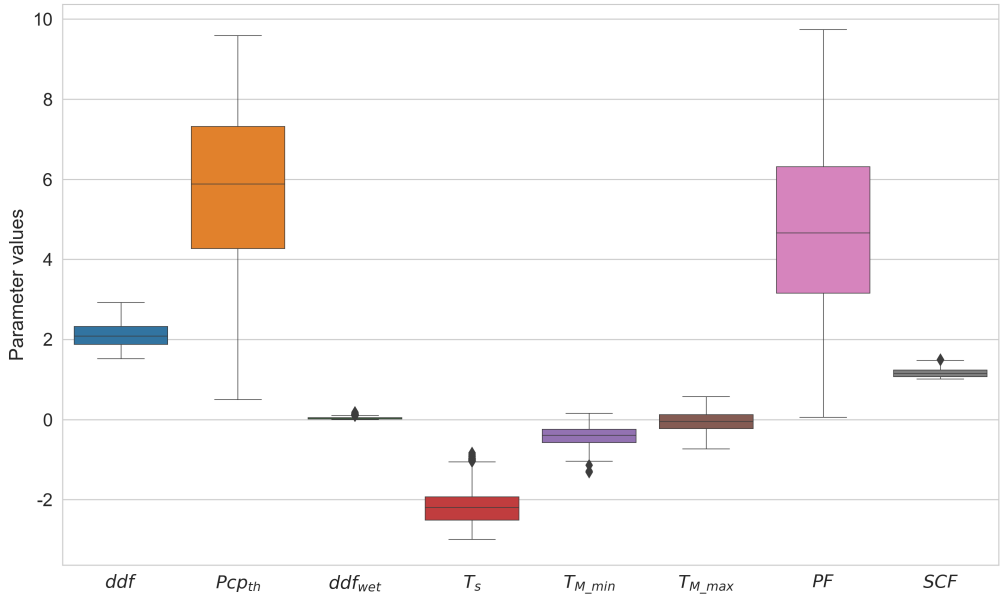

Figure 8.5.: Simulated parameter ranges for Amper catchment (based on 1000 best parameter vectors from ROPE

Table 8.2.: NSE performance for HBV and modified HBV in different periods; the bolded text shows the better performance of the model.

Catchments	Period	HBV	Modified HBV
Amper	Winter	**0.72**	**0.722**
	Overall	0.566	**0.579**
Isar	Winter	0.733	**0.754**
	Overall	0.593	**0.627**

predictions in the catchments. Despite a modest increase in the NSE values, the improvement can be again deemed for a right reason and with a reduced uncertainty pertaining to the snow processes simulation. This extension to data scarce region was envisaged to assess whether a reasonably accurate model forcing could drive the calibration methodology and in turn impart improved hydrological predictions. This can be a very valuable tool in the data scarce mountainous catchments where using MODIS and freely available global datasets with established regionalized parameters can allow decision makers to estimate the availability of snow and the resulting melt waters in the regime. However, the regionalization of parameters must be studied in more detail in future studies so that this methodology can be extended to different areas.

8.3. Model inversion

The snow cover is one of the key components of the hydrology in snow-dominated regimes, where the evolution of snow cover governs the amounts and timings of the water available for the downstream areas. The mountainous areas have a very significant dependence on the spatio-temporal availability of the runoffs triggered by the snow ablation process. This available water is not only the source for water supply and ecosystem, but also a very important variable governing the water resources trajectories in the regions such as hydropower systems as well as the occurrences of natural hazards such as floods and avalanches [Viviroli et al., 2011; Largeron et al., 2020]. Monitoring and forecasting the evolution of snow-cover is thus very important and is challenging at the same time owing to the strong variability in snow characteristics and the subsequent less observational network. Remote sensing based snow cover monitoring approaches to some extent provide some overview on the seasonal snow evolution. The importance and applicability of the snow-cover products such as the MODIS have been already established and discussed in detail in this study. However, in addition to the distribution of snow, the depletion pattern of the snow-cover also hold a crucial proxy information on the available accumulated SWE in the mountainous regimes. This accumulated SWE can be translated to total discharge volume during the snowmelt season [Rango and Itten, 1976]. The accurate estimates of the SWE have been one of the unsolved problems in mountain hydrology. Operational models often lack the accuracy in estimating the water coming in from snowmelt due to high uncertainties [Bair et al., 2013]. The scarce and sparse observational networks also render it practically impossible to determine the areal distribution of available water stored in the snow cover [Martinec and Rango, 1981]. With the snow-cover depletion information coming in from the snow-cover images, it is however, possible to retroactively estimate the SWE values at a reasonable spatial detail by incorporating the SCA and a snow-melt model. This reconstruction has been used by Molotch [2009] in the Rocky mountains and in Sierra Nevada by Rittger et al. [2016]. This approach has crucial advantage in the mountainous areas, where the extensive observations are not available. Raleigh and Lundquist [2012] have highlighted the importance of this reconstrution of SWEs with model inversion as the better approach compared to forward based modeling for SWE estimation in areas with highly uncertain precipitation. The amount of snow melted at a reference point when the snow fully disappears can be estimated with a reliable spatial temperature interpolation and the estimation of melting degree-days. This inversion approach can be used to improve the areal SWE estimates during the ablation period, correct the winter precipitation as well as can be utilized to forecast the spring discharge [Martinec and Rango, 1981]. With this backdrop, in this study, a MODIS snow-cover based inversion was tested based on the Model 6 with radiation component as the basis, utilizing minimal meteorological inputs, i.e. only temperature and radiation data were used as the drivers. Switzerland was selected as the study area mainly because of the diverse distribution of topography and a dense network of temperature measurements which allows a more reliable interpolation.

8.3.1. The concept

This technique, first implemented by Martinec and Rango [1981], utilizes the satellite-derived snow-cover depletion as an information on melt rates to retroactively estimate the availability of snow at different spatial scales. For this inversion (widely known as reconstruction of SWE), the SWE $S_{(N,x)}$ at a point x at day N is calculated as:

$$S_{(N,x)} = S_{(0,x)} - \sum_{j=1}^{N} M_{(j,x)} \tag{8.5}$$

where, $S_{(0,x)}$ is the maximum snow water equivalent before the melt initiation and $M_{(j,x)}$ is the melt at any time j. N is the number of days during the melt. $M_{(j,x)}$ continues through j till N and is calculated as:

$$M_{(j,x)} = M_{P(j,x)} \times fsca_{(j,x)} \tag{8.6}$$

where $M_{P(j,x)}$ is the maximum potential melt induced by temperature and radiation, and widely adopted from the restricted degree day model of Kustas et al. [1994] which is shown below in Eq.8.7.

$$M_{P(j,x)} = m_q \cdot R_d + B_r \cdot T_d \tag{8.7}$$

where, m_q is the factor controlling the radiation induced melt, R_d is the mean daily net radiation, B_r is the degree day melt factor and T_d is the average daily air temperatures greater than 0°C. Usually, T_d is considered to be 0 if the air temperature is below 0. This is the underlying assumption in the reconstruction approach that once the snow-cover depletion starts, all the accumulation occurring during the ablation period are considered traces without accumulating to the snowpack and thereby neglected. Furthermore, the evaporation from and condensation on the snowpack are also neglected in the mountainous basins.

8.3.2. Methodology and Data

The motivation for this case study was to evaluate the estimation of accumulated snow precipitation in Switzerland using the minimal and freely available RS data inputs to allow for the extension to different ungauged mountainous basins around the world. Earlier reconstruction approaches are carried out in elevation zones without taking the forest canopy effect into consideration. However, in mountainous terrain, the effect of canopy cover is a very critical aspect as the forest cover can impart significant differences in the accumulated SWEs than from the open areas, mainly attributed to (a) the canopy interception of snow reduces the snow accumulation on ground, and (b) the canopy also limits the incident solar radiation [Jenicek et al., 2018]. The latter part is more important during the melt season which delays the melt in the forested areas. To incorporate this uneven distribution of snow, this study utilized a semi-distributed approach in which the whole region of Switzerland was divided into Hydrologic Response Unit (HRU) which are spatial units depicting unique combinations of elevation zones and land cover types, as shown in table 8.3. Each pixel in the study domain was classified based on landcover classes and elevation zones and later

combined to establish 27 HRUs in Switzerland. Figure 8.6 shows the spatial distribution of the HRUs in Switzerland. The MODIS landcover data was utilized to classify the landcover classes along with elevation data to demarcate the HRUs in the study.

The major input for this inversion approach was only the interpolated daily mean temperatures. Daily potential radiation was calculated from DEMs as explained in the earlier sections. In addition to this, MODIS snow cover images were also incorporated to define the snow cover depletion curves at hydrologic response unit (HRU) levels. The MODIS cloud-Gap filled snow-cover product MOD10A1F (Terra) was opted for in this case as the they are considered to be more accurate than other MODIS snow-cover products [Hall et al., 2019]. Furthermore, the Terra and Aqua combined MODIS Land Cover Type (MCD12Q1) Version 6 [Friedl and Sulla-Menashe, 2015] was considered for the year of 2017-18 for the categorization of the study area into different HRUs. The classification system selected for the landcover data was Food and Agriculture Organization - Land Cover Classification System (FAO-LCCS 2). The elevation data was as before from resampled SRTM data. Moreover, the MOD44B MODIS/Terra Vegetation Continuous Fields which includes pixel wise forest cover fraction, and vegetation and non-vegetation cover fractions [DiMiceli et al., 2022], was also incorporated in the study for the evaluation of the effect of tree cover, in the study. All the inputs including temperature, solar radiation, MODIS snow-cover and forest cover proportions were then lumped to each HRU based on their averages.

8.3.2.1. MODIS based snow cover depletion curves

For the identification of the snow depletion curves, MODIS NDSI data was preprocessed to obtain the fractional SCA for each pixel. A NDSI threshold based approach was employed for the data preprocessing. The threshold was assumed to be 0.4, as established by earlier results, and was used to demarcate the snow contained in each pixel. The unforested pixels with NDSI values less than the threshold were assumed to be snow-free and the values higher than 0.4 were classified as snow pixels. For the forested pixels, a threshold of 0.1 for pixels with forest cover more than 25% was used assuming the underestimation of snow under forest canopy by MODIS. The average NDSI values at each HRU was assumed to be the fractional snow-covered area (fSCA) as the NDSI pixel values higher than the assumed thresholds are often comparable to the fraction of snow available at the pixel level [Hall et al.,

Table 8.3.: Classification of elevation and land cover units in Switzerland

Elevation zones	Z_class	Landcover	LC_class
<500	Z_1	Barren land	LC_1
500 - 1000	Z_2	Water/Ice	LC_2
1000 - 1500	Z_3	Forest	LC_3
1500 - 2500	Z_4	Cropland/Shrubland	LC_4
2500 - 3500	Z_5	Urban	LC_5
<3500	Z_6		

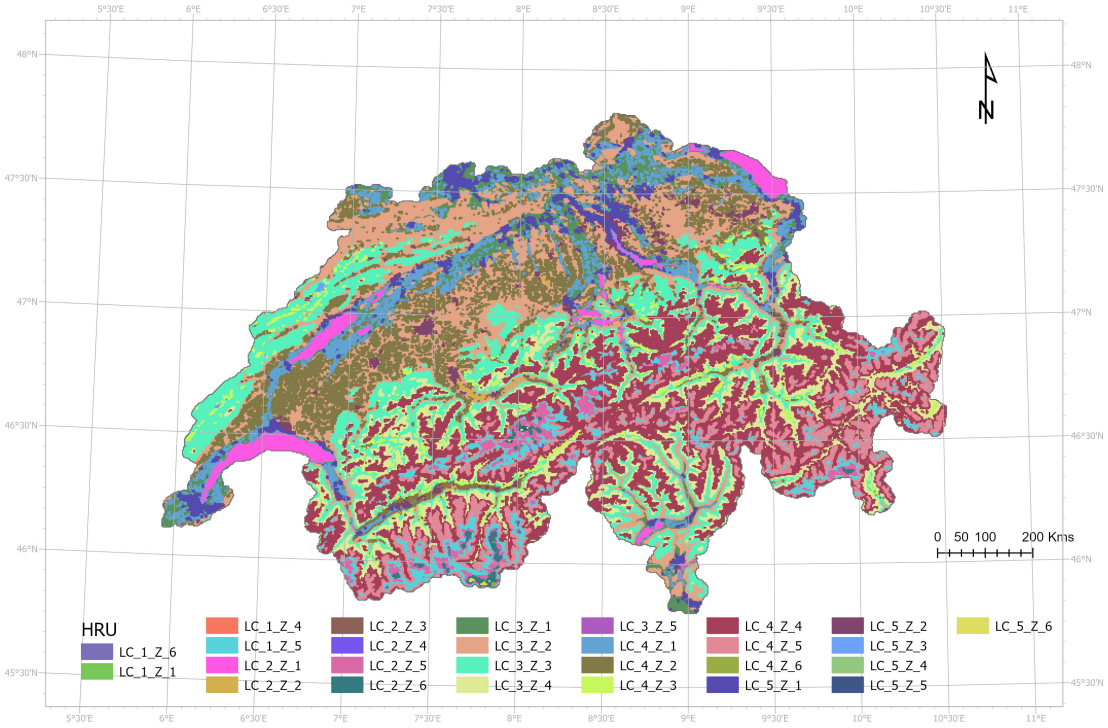

Figure 8.6.: Spatial distribution of HRUs in Switzerland; LC refers to the land cover class and Z refers to the elevation zones

2019]. Based on this, the snow-depletion curves were identified for each HRU. The HRU $LC5 - Z6$, i.e urban area in elevation zone $Z6$ was not included in this study because the variation of snow, judging by the SCA curves, is nominal owing to the alpine characteristics and also due to very low areal coverage.

The most critical information for the inversion approach is the identification of the melt onset and snow disappearance dates. The model retrospectively calculates the melt from the day of snow disappearance, going backwards till the maximum accumulation point in time, when the melt onset starts. For this, the snow depletion curve for each HRU was manually inspected to identify the onset and melt dates. Figure 8.7 shows the illustration of the snow depletion curves for the elevation zone 4 for different HRUs.

8.3.2.2. Maximum potential melt

With the semi-distributed basis, this methodology modifies the maximum potential melt from Eq.8.7 based on vegetation cover fraction to incorporate the impact of forest canopy cover. The maximum potential melt, $M_{P(j,x)}$ was modified for a HRU, x as shown in Eq.8.8.

$$M_{P(j,x)} = \begin{cases} \left(mf_x + (1-alb)\cdot r_{ind}\cdot R_{D(j,x)}\right)\cdot\left(T_{av(j,x)} - T_{(M,x)}\right) & \text{if } T_{av(j,x)} \geq T_{(M,x)} \\ \left(mf_x + (1-alb)\cdot r_{ind}\cdot R_{D(j,x)}\right)\cdot\left(T_{av(j,x)} - T_{(S,x)}\right) & \text{if } T_{(S,x)} \leq T_{av(j,x)} < T_{(M,x)} \\ -refr_x\cdot\left(T_{av}\left(j,x\right) - T_{(S,x)}\right) & \text{if } T_{av(j,x)} < T_{(S,x)} \end{cases} \tag{8.8}$$

where,

mf_x is the melt factor for an HRU x that governs the melt and is differentiated based on forest cover fraction as shown in Eq.8.9.

$$mf_x = \begin{cases} af_x\cdot(1-tree_{frac,x}) + bf_x\cdot tree_{frac,x} & \text{if } LC = 3 \text{ and } tree_{frac,x} \geq 0.25 \\ af_x\cdot(1-tree_{frac,x}) + bf_x\cdot tree_{frac,x} & \text{if } LC \neq 3 \text{ and } tree_{frac,x} \geq 0.4 \\ af_x\cdot(1+c_{fac,x}) & \text{else} \end{cases} \tag{8.9}$$

af_x and bf_x are the melt factors for non-tree and tree cover in the HRU x,

$tree_{frac,x}$ is the proportion of tree cover in the HRU x,

LC is the land cover class. $LC = 3$ refers to an HRU x marked as forest cover,

$c_{fac,x}$ is a factor for non-forested HRU x.

$refr$ is the refreeze coefficient if the air temperature was below the snowfall temperature which allows the SWE to be refrozen into the pack.

The assumed actual melt for the time-step j, $M_{(j,x)}$ is calculated as in Eq.8.10 and the corresponding SWE, $S_{(j,x)}$ is estimated from Eq.8.11.

$$M_{(j,x)} = \min\left(S_{j-1,x}, M_{P(j,x)}\times fsca_{(j,x)}\right) \tag{8.10}$$

$$S_{(j,x)} = \max\left(0, S_{(j-1,x)} - M_{(j,x)}\right) \tag{8.11}$$

where, $S_{(j-1,x)}$ is the availble SWE from the earlier time-step and $fsca_{(j,x)}$ is the fractional snow covered area at x in time j.

8.3.2.3. Calibration

The calibration was done with ROPE for each HRU, to optimize the initial SWE till the SWE depletion matches the snow curve depletion pattern at the end of the season when snow fully disappears. The parameters to be calibrated were the initial snow water content, the melt factors a_f and b_f, the refreezing coefficient $refr$, threshold temperatures for snowfall

and snowmelt T_S and T_M respectively, and the radiation factors r_{ind} and albedo alb. The objective function used for the calibration was the Pearson correlation calculated as in Eq.8.12. It allows the comparison of patterns between two variables.

$$r = \frac{\sum \left(X - \bar{X}\right) \cdot \left(Y - \bar{Y}\right)}{\sqrt{\left[\sum \left(X - \bar{X}\right)^2 \cdot \sum \left(Y - \bar{Y}\right)^2\right]}} \tag{8.12}$$

where, X and Y are the fractional snow covered area and the simulated SWE timeseries for the ablation limb in this case, and $\bar{X}$ and $\bar{Y}$ are the mean values for X and Y.

8.3.3. Results

The snow-melt model was setup for the winter season of 2017-18. The Snow Depletion Curve (SDC)s were identified for each HRU class. As an illustration, the SDCs for different HRUs in elevation zone $Z4$ are shown in figure 8.7. It is evident from the figure that the snow-cover remains in the HRUs related to snow/water landcover class ($LC = 2$) and barren land ($LC = 1$) for a longer duration. The urban HRUs ($LC = 1$) depict the quicker depletion within a month from the onset of melt in April. The urban areas are known to be acting as a heat sink that triggers a faster melting. The HRUs with forest cover ($LC = 3$) also show lesser duration of snow-cover with a delayed depletion than the urban class. However, this could relate to the limitation of the RS approach in identifying the snow present under the canopy. Due to this, the forest related HRUs were further scrutinized with additional parameterization using tree proportion in the study. Any snow-precipitation after the onset of melt was considered transient and thus neglected.

Once the SDCs were identified and the inputs were lumped to the HRU level, the snow-melt model was run to retrospectively calculate the accumulated snow precipitation prior to the onset of melt. Figure 8.8 shows the estimated snow-precipitation in the season in different HRUs against the observed solid precipitation, prior to the onset of melt. It can be inferred from the figure that the median values in the box plot are very close to the observed accumulation (denoted by '$*$') and are contained by the box-plot of 1000 best parameter estimates from ROPE, except in few HRUs. The results show reasonable accuracy given that the input was just the mean temperature and the SDCs.

Furthermore, the simulated depletion of SWE (with best objective function values) compared against the SDCs for selected HRUs for higher elevation zones is shown in figure 8.9. The figures suggest that the simulation does well in mimicking the snow-cover depletion in most of the HRUs. Large discrepancies were observed in few HRUs such as the $LC1\_Z5$, $LC2\_Z4$, $LC4\_Z5$ and $LC4\_Z4$. No clear trend of simulation errors was observed with these anomalous results, though elevation zone 4 showed similar discrepancies in the barren land and water/ice landcover classes, with a rapid onset of melt simulated in these areas. In the forested HRUs, the SWE depletion and the SCF depletion follow similar trends in the higher elevation areas. Erroneous predictions are observed with the cultivated/shrubland HRUs where the model does not capture the depletion trends with good accuracy.

Given the uncertainties in the precipitation observations from under-catch in the higher elevations owing to wind displacement, canopy interception and the inadequate accuracy of

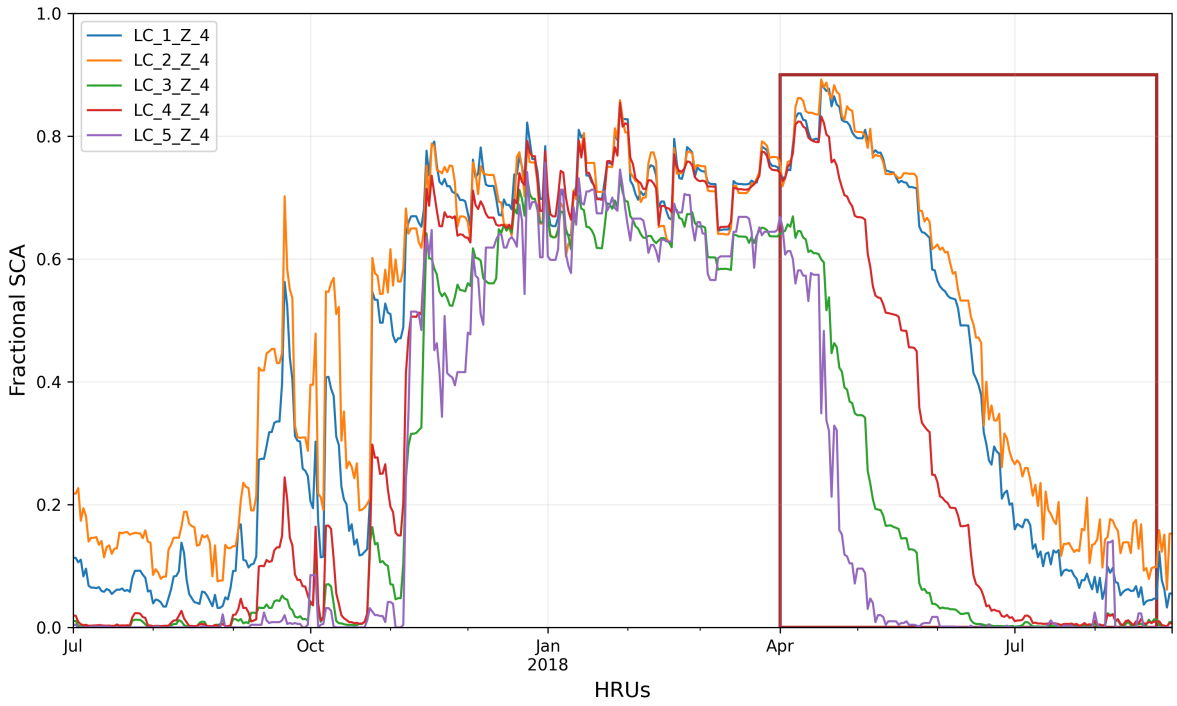

Figure 8.7.: Snow-cover evolution for the winter season of 2017-18 for different HRUs; the red bounding box shows the depletion curves considered in the study

temperature interpolation, the results were considered to be satisfactory as it can add a crucial value to mountainous regions with the maximum snow-accumulation approximated using freely available MODIS data and temperature inputs. However, as a future outlook, this presented methodology though promising, requires further polishing and more research in identifying pixel wise maximum accumulation and the resulting contribution to spring discharge which is a very pertinent information to water resources projects, especially for hydropower generation purposes.

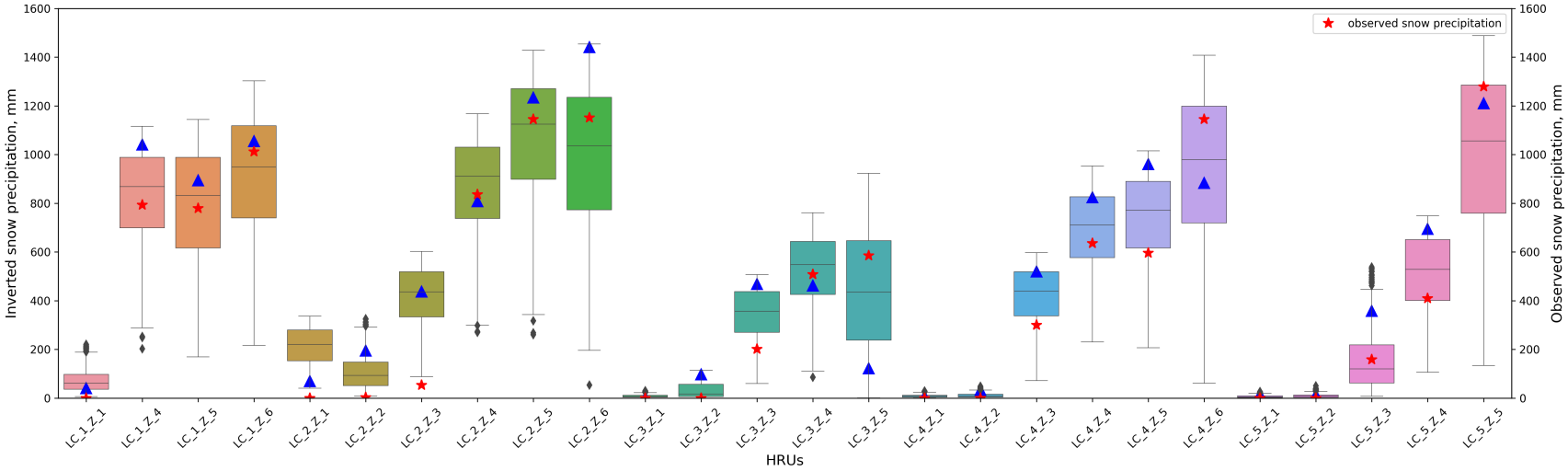

Figure 8.8.: Simulated vs observed accumulated snow precipitation in different HRUs; **red asterisk** represents the observed accumulated values, **blue triangle** represents the best calibrated values

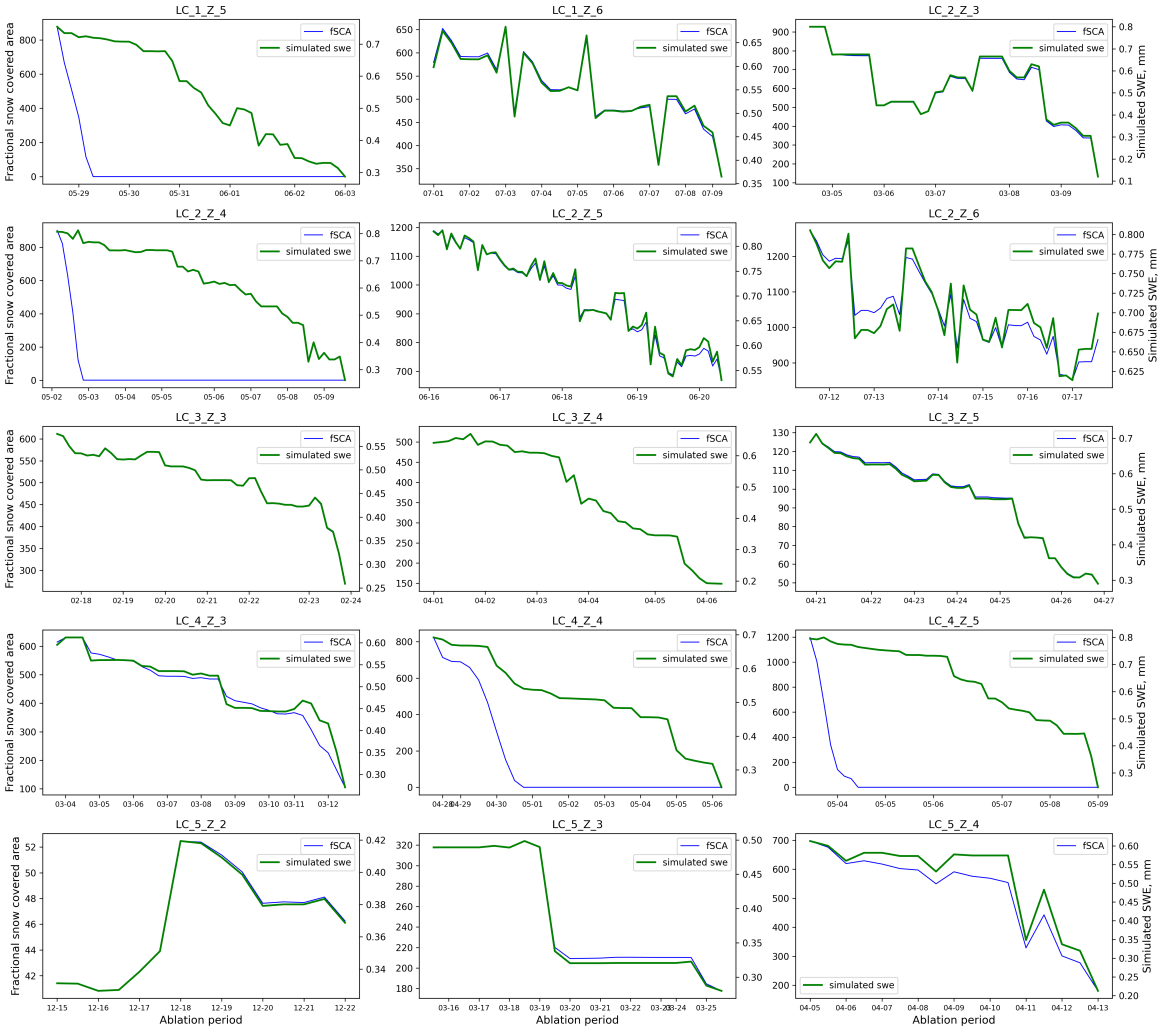

Figure 8.9.: Depletion curves for simulated SWE and MODIS based SCA for selected HRUs

8.3.4. Extension using RS based Land Surface Temperature (LST)

Due to very sparse network of meteorological stations in most of the mountainous regions around the world, it is very imperative to find the alternatives to station measurement to estimate the snow-cover with a reasonable accuracy. The presented approach of reconstruction requires temperature data at minimum, to allow the calculation of the melting degree days even with the simplest of the models being employed. With the advancement of the satellite based products, there have been a global coverage of critical land surface parameters such as surface temperature and vegetation indices, etc. Owing to this reason, this study further attempted to implement the skin temperatures, also known as Land Surface Temperature (LST), in snow-melt modeling to evaluate the efficacy of these data for modeling purpose. The LST measures the thermal radiance emission from the land surface and offers a unique perspective on land surface energy balances as it can be considered a very pertinent proxy for the energy partitioning at the land surface and atmosphere boundary

[Hulley et al., 2019] and are retrieved from space-based Thermal Infrared (TIR) data. However, the vegetation cover and spatially changing surface conditions render this variable sensitive in terms of temperature distribution. The LST have a very wide applicability in terms of assessing the temperatures of the surface cover such as canopy temperatures, soil top layer temperatures, snow-cover temperatures and so on in spatial resolution ranging from leaf to landscape level. This environmental variable gives crucial information about the redistribution of the energy into latent and sensible heat fluxes and is a very prominent actor in processes related to surface energy distribution and water balances [Li et al., 2013] measuring the thermal heterogeneity of the earth surface [Jin and Dickinson, 2010]. Increasing number of studies have highlighted the importance of LSTs in ecological context such as land cover classification in combination with vegetation indices [Lambin and Ehrlich, 1995; Nemani and Running, 1989], land cover dynamics monitoring [Julien and Sobrino, 2009], as a indicator for soil moisture for monitoring droughts [Anderson et al., 2007; Wan et al., 2004], and so on.

Due to the redistribution properties in the form of heat fluxes, the LST is considered one of the most important variables describing the diurnal variation of air temperatures. The relationship between air temperature and LSTs has been explored in numerous studies.Fu et al. [2011] estimated the daily minimum air temperature with reasonable accuracies (1.78 - 2.77 °C RMSE) in an alpine meadow on the northern Tibetan Plateau using a linear relationship between MODIS LST and maximum observed temperature. Hengl et al. [2012] simulated the air temperature as a function of latitude, longitude, distance from the sea, elevation, time, insolation, and the MODIS LST images using a regression kriging method with an accuracy of around $\pm$2.7°C. The popular Temperature Vegetation Index (TVX) method, proposed by Nemani and Running [1989] and Goward et al. [1994] also used LSTs to estimate the air temperature based on the assumption that a strong negative correlation exists between LST and vegetation index. It further assumes that the temperature of a fully vegetated canopy is the same as the temperature within it. Zhu et al. [2013] used this method to estimate daily maximum and minimum air temperature using the NDVI and the LST data with reasonable accuracy. There are many studies, that have been carried out incorporating the LST in simple snow-melt modeling to tackle the problem of data scarcity. Mostovoy et al. [2006] studied the sensitivity of different factors such as the pixel resolution, satellite overpass time, season, land cover type, and the vegetation fraction on the estimation of daily maximum and minimum temperatures and the resulting correlation coefficient. Colombi et al. [2007] employed a linear regression technique to estimate daily mean air temperature from instantaneous values of station based temperature and LST data, with a good accuracy of about 1.89°C. Shen and Leptoukh [2011] also estimated the air temperature from MODIS LST data over central and eastern Eurasia with a reasonable estimation performance of about 3°C as the mean absolute error. Yang et al. [2014] implemented a simple linear regression based approach to estimate the daily air temperatures from MODIS LST images to improve the temperature index snow-melt routine in a hydrological model. They suggest that the estimated temperature can be a valuable source of information in extending the input data in data sparse conditions.

As a practical implementation of the MODIS snow-cover related reconstruction approach in this study, an attempt was made to estimate the daily mean air temperatures based on

MODIS LST data to assess its applicability in data scarce regions. For this the MODIS LST products MOD11A1 (on board Terra satellite)[Wan et al., 2021] and MYD11A1 (on board Aqua satellite) were considered in this study. As explained above, MODIS LST products have been widely used for different studies including the estimation of daily air temperatures, especially owing to free global availability with a reasonable accuracy of about 1°K at a daily temporal resolution. The sun-synchronous nature of Aqua and Terra satellites offers a relatively close temporal proximity of about 3 hours between the overpasses from these two satellites [Crosson et al., 2012]. Both the Aqua (1:30 AM/PM) and Terra satellites (10:30 AM/PM) make two overpasses in a day, bringing up a total of four overpasses in a day. The 10:30 AM Terra overpass senses a cooler surface temperature than Aqua at 1:30 PM overpass and in contrast, a warmer surface is sensed by Terra at 10:30 PM than Aqua's overpass at 1:30AM.

8.3.4.1. Linear regression approach

Many studies have highlighted the linear relationship between air temperature and the LSTs. Several explanatory variables such as elevation, vegetation indices, land cover, distance from the seas, latitude etc have been incorporated in determining the optimal relationship between air temperature and LSTs. The main goal of this practical extension was also to find a relationship between air temperature and LST via a regression technique, which could in turn be used in snow-melt modeling context in different data scarce mountainous regimes across the world. In this study, the four LST datasets within a day, i.e. day and night passes of Aqua and Terra were used. The LSTs were extracted to the Swiss temperature station locations assuming the LST of the cell bounding the station to be representative of the station. Aqua-day, Aqua-night, Terra-day and Terra-night were used as the explanatory variables to derive mean air temperature in a simple linear regression technique employed to derive the relationship.

An example of the regression implementation in Bavaria is shown in this section. Figure 8.10 shows that the LSTs have the potential to predict the mean air temperature with high levels of accuracy. For the winter season of October to April, the overall RMSE is around 1.25°C which is a very good prediction as figure 8.10(a) shows a very dense scatter in the central part with few outliers around it. The very low and very high tails are also tapered, meaning good prediction accuracy for the tail values. However, for snow-melt modeling, the relevant temperature range is from -3°C below which there is always accumulation till +3 °C, above which snow melts. The goal of this section was to estimate this range of temperature with adequate accuracy. However, as figure 8.10(b) shows, there is a high level of uncertainty in the prediction of mean air temperature especially for the -3 till +3 °C zone. The estimated values at the lower end range from -4°C to +1°C, whereas in the higher tail, the estimated values range from -3°C to +4 °C for an observed temperature of +3 °C. The observed and estimated rank scatter plot (figure 8.10 (c)) also depicts a dense cluster at the tails which shows that LSTs explain the mean air temperature to some extent. However, a slight asymmetric structure can be observed from the figure as the cluster of data points towards the bottom right of the plot indicates that higher observed values are under-predicted. The low observed values are reasonably simulated well compared to the higher counterparts, as

shown by the less density of points in the top-left corner.

It is very important to get the prediction of this temperature range right for snow-melt studies. Due to time limitation, this topic was unfortunately not explored further. Different variables were tested for the study regions such as the NDSI and NDVI values, landcover and elevation classes, distance from the coastline, and so on. However, the results were similar for this range. This was also not found well studied upon in different literature as most of them have quoted overall or seasonal accuracies in terms of RMSEs. Tang et al. [2010] in their work have argued that the LSTs as a proxy for air temperature should be used only in applications where the sensitivity of algorithm to temperature is very small. Snow-melt modeling is highly temperature sensitive, thus can lead to rapid onset and disappearance of snow, as opposed to the reality, rendering the whole simulation completely unusable. Due to this reason, this estimated temperature was not used further. However, a clear correlation between LST and air temperature was observed. It is thus to be highlighted that this relationship can be exploited in the future works as an extension of this thesis by deeply understanding the various factors influencing air temperature and the associated errors in prediction, i.e. random or systematic. Furthermore, the improved estimates of air temperature from LSTs can be employed to drive the reconstruction approach in data scarce mountainous regimes to estimate the peak snow accumulation and the resulting melt volume, which is as discussed, a crucial and well-informed information in the mountainous regimes.

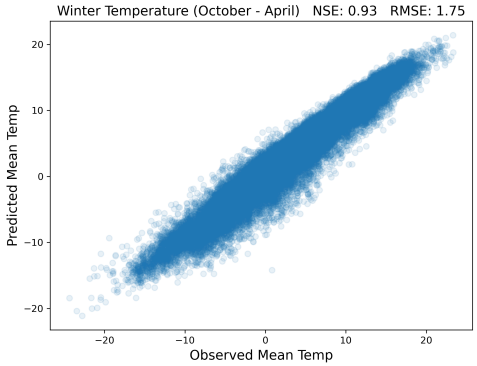

(a) Overall

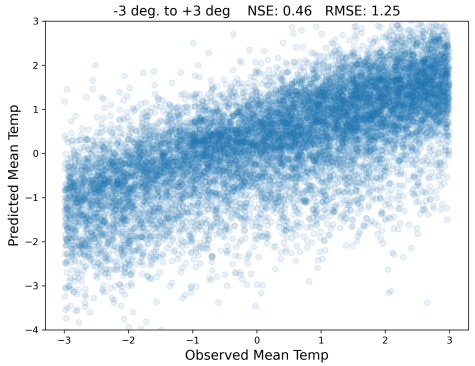

(b) -3°C to +3°C

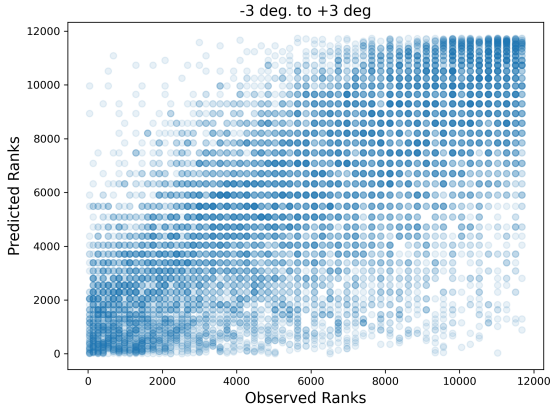

(c) Rank comparison

Figure 8.10.: Observed vs estimated mean air temperature from MODIS LSTs

9. Conclusion

It has been well established that accurate and reliable estimation of snow-cover distribution is highly crucial in the snow-dominated regions around the world, to predict the river discharge with higher certainty and reliability. This thesis aimed at addressing the problem of unreliable estimation of snow-cover distribution owing to sparse unrepresentative observations. The study was carried out in two different mountainous regimes in Europe, with an overarching goal to assess the capability of freely available with global coverage RS images in reliable identification of snow-cover distribution through parsimonious snow-routines. Specifically, the study extended the TI-based snow-melt modeling approach to different variants and evaluated a novel pixel-wise snow-cover calibration scheme for estimating the parameters of the models for Switzerland and Baden-Württemberg in Germany, solely based on MODIS snow-cover images. This chapter discusses the outcomes of this research against the set core objectives in terms of following aspects:

Extension of snow-melt models and simulation of snow-cover distribution

Different model modifications incorporating factors governing the different aspects of snow-accumulation and ablation processes, were employed to identify the best model variant and to evaluate the improvement in the simulation of snow-cover distribution with minimal data input, i.e. design template for implementation in data scarce regions. All the variants mimicked the snow-cover distribution in both regions with high accuracy. Daily radiation was found to be the most influential additional variable in terms of model performance during simulation the snow-cover distribution. Any future implementation of the proposed methodology is not limited to the model variants used in this study as the approach is flexible enough to accommodate any snow-routine capable of simulating the snow-cover distribution. Furthermore, the parameters were found to be transferable to different regimes without much loss in performance. The model setup including the model inputs were designed to be minimalistic, thus incorporating only precipitation and temperature as the observational model drivers. All other model inputs including the net radiation were extracted or estimated with the DEM.

Thresholds for simulation

Due to the cloud contamination of the MODIS snow-cover images and the calibration design to accommodate binary dataset, different thresholds were set, identified and recommended in the study for a MODIS based model snow-melt model calibration. NDSI thresholds for MODIS and SWE thresholds for snow/no snow differentiation for simulated snow-cover, and the cloud percentage threshold critical for the selection of MODIS images for calibration

were identified. NDSI thresholds were the most sensitive and the globally accepted 0.4 works well in this methodology as well. However, the spatial detail and the uncertainties associated with MODIS snow-cover algorithms, do not allow the reliable detection of actual snow. Due to this and the precipitation interpolation uncertainties at higher elevations, a clear recommendation on threshold was not made, rather a range was put forward for these thresholds. The further advantage offered by this snow-cover based calibration was the lesser sensitivity towards cloud thresholds. This allows the flexibility to calibrate on patches of snow and no-snow in the images, with the model performance not so much affected by the cloud cover.

Selection of images for calibration

The selection of MODIS images based on different stages of the snow season for calibration is a crucial question as it governs the identifiability of the parameters in terms of understanding the relevant processes. The MODIS based standalone calibrated parameters were found to be more or less transferable to different seasons within a snow period. Depending upon the snow regimes, a set of MODIS images within a period during the snow season was observed to be adequate to adeptly simulate the snow-cover distribution for the whole season [Gyawali and Bárdossy, 2022].

Robustness and uncertainty reduction

The selection of calibration data, i.e. as binary MODIS information, and the spatial extent of snow cover bolsters the calibration at pixel level allowing relatively complex snow-melt modules to be calibrated with more robustness. This can be attributed to the reduction in the uncertainty associated with calibration data, as one is only dealing with '0' or '1', which is often a critical limitation with the case of snow-depth or snow-water equivalent based calibration. Furthermore, the uncertainty in the representation of snow-accumulation and melt processes can be reduced with the standalone calibration of the snow-melt models, as calibrating only on discharge generally permits parameter compensations with other non-snow parameters, even if the discharge simulation is found to be reliable leading to 'right for wrong reasons' conclusion. Estimation of the parameters solely from any RS based snow-cover information not only eliminates the reliance on a single calibration variable discharge which are not readily available in the higher altitudes, but also thereby preserves the spatial heterogeneity as well with the spatial information coming in from MODIS.

Furthermore, the melt outputs used as standalone input to the hydrological model increased the reliability of discharge prediction as highlighted by the hydrological model performance comparison. This improvement in model performance can be attributed to 'a right reason' with a better representation of the underlying snow processes With the reliable simulation of snow-cover distribution using the MODIS based calibration, the estimated parameters can be considered 'snow-processes informed' parameters and any improvement in the hydrological model performance can be deemed for 'a right reason' with a better representation of the underlying snow processes. The standalone calibration further makes it possible to add more relevant parameters into the snow model which if calibrated in conjunction with

the hydrological model would then lead to a much more complex and uncertain calibration procedure, due to these additional parameters. The reduced parameter space in separate snow-model and hydrological model calibrations, thus offers a subsequent reduction in modeling uncertainties as the equifinal set of calibrated parameters becomes small, which in turn leads to reliable discharge simulation. In addition, a better computational efficiency can be garnered with this approach as the model calibration with reduced parameterization requires lesser computational time. It is to be noted that calibration on binary information imparts additional efficiency as it is relatively quicker to calibrated on '0' and '1'.

In conclusion, this thesis showcased a novel approach of exploiting MODIS snow-cover information in calibrating snow-melt models on the snow/no-snow information using a modest input data demand. The solidity of the approach used in this thesis lies in the simplicity, spatial flexibility and global availability of the model input data which can be very useful for snow-melt and hydrological predictions in data scarce regions. The calibration using readily available images used in this method offers adequate flexibility to calibrate snow distribution in mountainous areas across a wide geographical extent with reasonably accurate precipitation and temperature data, especially in data scarce regions, with parameters estimated with MODIS [Gyawali and Bárdossy, 2022]. This independent calibration offers independent evaluation of snow processes without passing the snow simulation through a more complex hydrological model. In addition, this also allows immediate verification with point measurements. Future implementation can also include snow-depth information from geodetic approaches as well as cloud mask information from geostationary satellites.

It is a big and a highly imperative challenge to improve the snow-estimation in the mountains via improvement of the snow-melt routines in widely and successfully used hydrological models like HBV. The reduction in uncertainties regarding snow-cover estimation and discharge prediction with this methodology thus adds pertinent value to the improved conceptualization of the temperature-index model routines and further potential model updating in future works.

Bibliography

S. Ahmed and G. De Marsily. Comparison of geostatistical methods for estimating transmissivity using data on transmissivity and specific capacity. *Water resources research*, 23(9): 1717–1737, 1987.

S. Ahmed and K. Devi. *Kriging for Estimating Hydrogeological Parameters*, pages 172–178. Springer Netherlands, Dordrecht, 2008. ISBN 978-1-4020-6540-8. doi: 10.1007/978-1-4020-6540-8_13. URL 10.1007/978-1-4020-6540-8_13.

E. A. Anderson. A point energy and mass balance model of a snow cover. *NOAA technical report NWS*, (19), 1976. URL https://repository.library.noaa.gov/view/noaa/6392.

M. Anderson, J. Norman, J. Mecikalski, J. Otkin, and W. Kustas. A climatological study of evapotranspiration and moisture stress across the continental united states based on thermal remote sensing: 2. surface moisture climatology. *Journal of Geophysical Research: Atmospheres*, 112(D11), 2007. doi: 10.1029/2006JD007507. URL https://agupubs.onlinelibrary.wiley.com/doi/abs/10.1029/2006JD007507.

F. Avanzi, C. De Michele, S. Morin, C. M. Carmagnola, A. Ghezzi, and Y. Lejeune. Model complexity and data requirements in snow hydrology: seeking a balance in practical applications. *Hydrological Processes*, 30(13):2106–2118, 2016. doi: 10.1002/hyp.10782. URL https://onlinelibrary.wiley.com/doi/abs/10.1002/hyp.10782.

B. Bacchi and N. T. Kottegoda. Identification and calibration of spatial correlation patterns of rainfall. *Journal of Hydrology*, 165(1):311–348, 1995. ISSN 0022-1694. doi: 10.1016/0022-1694(94)02590-8. URL https://www.sciencedirect.com/science/article/pii/0022169494025908.

E. H. Bair, R. Davis, K. Rittger, and J. Dozier. Operational swe forecasts using a hybrid approach. In *Proceedings of the International Snow Science Workshop (ISSW 2013), Grenoble Chamonix-Mont-Blanc, France*, pages 1293–1297, 2013.

A. Bárdossy and G. Pegram. Interpolation of precipitation under topographic influence at different time scales. *Water Resources Research*, 49(8):4545–4565, 2013. doi: 10.1002/wrcr.20307. URL https://agupubs.onlinelibrary.wiley.com/doi/abs/10.1002/wrcr.20307.

A. Bárdossy and S. K. Singh. Robust estimation of hydrological model parameters. *Hydrology and Earth System Sciences*, 12(6):1273–1283, 2008. doi: 10.5194/hess-12-1273-2008. URL https://hess.copernicus.org/articles/12/1273/2008/.

A. Bárdossy, F. Anwar, and J. Seidel. Hydrological modelling in data sparse environment: Inverse modelling of a historical flood event. *Water*, 12(11), 2020. ISSN 2073-4441. doi: 10.3390/w12113242. URL https://www.mdpi.com/2073-4441/12/11/3242.

T. P. Barnett, J. C. Adam, and D. P. Lettenmaier. Potential impacts of a warming climate on water availability in snow-dominated regions. *Nature*, 438(6):303–309, 2005. doi: 10.1038/nature04141. URL 10.1038/nature04141.

D. Bavera and C. De Michele. Snow water equivalent estimation in the mallero basin using snow gauge data and modis images and fieldwork validation. *Hydrological Processes*, 23 (14):1961–1972, 2009. doi: 10.1002/hyp.7328. URL https://onlinelibrary.wiley.com/doi/abs/10.1002/hyp.7328.

K. E. Bennett, J. E. Cherry, B. Balk, and S. Lindsey. Using modis estimates of fractional snow cover area to improve streamflow forecasts in interior alaska. *Hydrology and Earth System Sciences*, 23(5):2439–2459, 2019. doi: 10.5194/hess-23-2439-2019. URL https://hess.copernicus.org/articles/23/2439/2019/.

S. Bergström. *The HBV model.*, chapter Computer models of watershed hydrology, pages 443–476. Water Resources Publications, Colorado, USA, 1995.

K. Beven. How far can we go in distributed hydrological modelling? *Hydrology and Earth System Sciences*, 5(1):1–12, 2001. doi: 10.5194/hess-5-1-2001. URL https://hess.copernicus.org/articles/5/1/2001/.

H. Bourennane, D. King, and A. Couturier. Comparison of kriging with external drift and simple linear regression for predicting soil horizon thickness with different sample densities. *Geoderma*, 97(3):255 – 271, 2000. ISSN 0016-7061. doi: 10.1016/S0016-7061(00)00042-2. URL http://www.sciencedirect.com/science/article/pii/S0016706100000422.

G. W. Brier. Verification of forecasts expressed in terms of probability. *Monthly Weather Review*, 78(1):1 – 3, 1950. doi: 10.1175/1520-0493(1950)078⟨0001:VOFEIT⟩2.0.CO;2. URL https://journals.ametsoc.org/view/journals/mwre/78/1/1520-0493_1950_078_0001_vofeit_2_0_co_2.xml.

P. R. Briggs and J. G. Cogley. Topographic bias in mesoscale precipitation networks. *Journal of Climate*, 9(1):205–218, 1996. ISSN 08948755, 15200442. URL http://www.jstor.org/stable/26200116.

K. Brubaker, A. Rango, and W. KUSTAS. Incorporating radiation inputs into the snowmelt runoff model. *Hydrological Processes*, 10(10):1329–1343, 1996. doi: 10.1002/(SICI)1099-1085(199610)10:10⟨1329::AID-HYP464⟩3.0.CO;2-W. URL https://onlinelibrary.wiley.com/doi/abs/10.1002/%28SICI%291099-1085%28199610%2910%3A10%3C1329%3A%3AAID-HYP464%3E3.0.CO%3B2-W.

A. Bárdossy and S. K. Singh. Regionalization of hydrological model parameters using data depth. *Hydrology Research*, 42(5):356–371, 10 2011. ISSN 0029-1277. doi: 10.2166/nh.2011.031. URL https://doi.org/10.2166/nh.2011.031.

D. R. Caicedo, J. M. C. Torres, and J. R. Cure. Comparison of eight degree-days estimation methods in four agroecological regions in colombia. *Bragantia*, 71:299–307, 2012. doi: 10.1590/S0006-87052012005000011R.

J. R. Carr. Order relation correction experiments for probability kriging. *Mathematical Geology*, 26(5):605–621, Jul 1994. ISSN 1573-8868. doi: 10.1007/BF02089244. URL 10.1007/BF02089244.

J. R. Carr and N.-h. Mao. A general form of probability kriging for estimation of the indicator and uniform transforms. *Mathematical Geology*, 25(4):425–438, May 1993. ISSN 1573-8868. doi: 10.1007/BF00894777. URL 10.1007/BF00894777.

C. Caruso and F. Quarta. Interpolation methods comparison. *Computers Mathematics with Applications*, 35(12):109–126, 1998. ISSN 0898-1221. doi: 10.1016/S0898-1221(98)00101-1. URL https://www.sciencedirect.com/science/article/pii/S0898122198001011.

F. Cazorzi and G. Dalla Fontana. Snowmelt modelling by combining air temperature and a distributed radiation index. *Journal of Hydrology*, 181(1):169–187, 1996. ISSN 0022-1694. doi: 10.1016/0022-1694(95)02913-3. URL https://www.sciencedirect.com/science/article/pii/0022169495029133.

F. Chebana and T. Ouarda. Multivariate quantiles in hydrological frequency analysis. *Environmetrics*, 22(1):63–78, 2011. doi: https://doi.org/10.1002/env.1027. URL https://onlinelibrary.wiley.com/doi/abs/10.1002/env.1027.

M. P. Clark, J. Hendrikx, A. G. Slater, D. Kavetski, B. Anderson, N. J. Cullen, T. Kerr, E. Örn Hreinsson, and R. A. Woods. Representing spatial variability of snow water equivalent in hydrologic and land-surface models: A review. *Water Resources Research*, 47(7), 2011. doi: 10.1029/2011WR010745. URL https://agupubs.onlinelibrary.wiley.com/doi/abs/10.1029/2011WR010745.

A. Colombi, C. De Michele, M. Pepe, and A. Rampini. Estimation of daily mean air temperature from modis lst in alpine areas. In *New Developments and Challenges in Remote Sensing, EARSeL eProceedings*, volume 6, pages 38–46, 2007. ISBN 978-90-5966-053-3.

C. Corbari, G. Ravazzani, J. Martinelli, and M. Mancini. Elevation based correction of snow coverage retrieved from satellite images to improve model calibration. *Hydrology and Earth System Sciences*, 13(5):639–649, 2009. doi: 10.5194/hess-13-639-2009. URL https://hess.copernicus.org/articles/13/639/2009/.

W. L. Crosson, M. Z. Al-Hamdan, S. N. Hemmings, and G. M. Wade. A daily merged modis aqua–terra land surface temperature data set for the conterminous united states. *Remote Sensing of Environment*, 119:315–324, 2012. ISSN 0034-4257. doi: 10.1016/j.rse.2011.12.019. URL https://www.sciencedirect.com/science/article/pii/S0034425712000077.

T. Das, A. Bárdossy, E. Zehe, and Y. He. Comparison of conceptual model performance using different representations of spatial variability. *Journal of Hydrology*, 356(1):106–118, 2008. ISSN 0022-1694. doi: 10.1016/j.jhydrol.2008.04.008. URL https://www.sciencedirect.com/science/article/pii/S002216940800173X.

B. Daya Sagar, Q. Cheng, and F. Agterberg. *Handbook of Mathematical Geosciences*. Springer Cham, 2018. ISBN 978-3-319-78999-6. doi: 10.1007/978-3-319-78999-6.

J. de Niet, D. C. Finger, A. Bring, D. Egilson, D. Gustafsson, and Z. Kalantari. Benefits of combining satellite-derived snow cover data and discharge data to calibrate a glaciated catchment in sub-arctic iceland. *Water*, 12(4), 2020. ISSN 2073-4441. doi: 10.3390/w12040975. URL https://www.mdpi.com/2073-4441/12/4/975.

B. Debele, R. Srinivasan, and A. Gosain. Comparison of process-based and temperature-index snowmelt modeling in swat. *Water Resources Management*, 24(6):1065–1088, 2009. doi: 10.1007/s11269-009-9486-2.

N. Di Marco, D. Avesani, M. Righetti, M. Zaramella, B. Majone, and M. Borga. Reducing hydrological modelling uncertainty by using modis snow cover data and a topography-based distribution function snowmelt model. *Journal of Hydrology*, 599:126020, 2021. ISSN 0022-1694. doi: 10.1016/j.jhydrol.2021.126020. URL https://www.sciencedirect.com/science/article/pii/S0022169421000676.

D. DiMiceli, R. Sohlberg, and J. Towsend. Modis/terra vegetation continuous fields yearly l3 global 250m sin grid. http://doi.org/10.5067/MODIS/MOD44B.061, 2022.

J. Dozier. Spectral signature of alpine snow cover from the landsat thematic mapper. *Remote Sensing of Environment*, 28:9–22, 1989. ISSN 0034-4257. doi: https://doi.org/10.1016/0034-4257(89)90101-6. URL https://www.sciencedirect.com/science/article/pii/0034425789901016.

J. Dozier, R. O. Green, A. W. Nolin, and T. H. Painter. Interpretation of snow properties from imaging spectrometry. *Remote Sensing of Environment*, 113:S25–S37, 2009. ISSN 0034-4257. doi: 10.1016/j.rse.2007.07.029. URL https://www.sciencedirect.com/science/article/pii/S0034425709000777. Imaging Spectroscopy Special Issue.

D. Duethmann, J. Peters, T. Blume, S. Vorogushyn, and A. Güntner. The value of satellite-derived snow cover images for calibrating a hydrological model in snow-dominated catchments in central asia. *Water Resources Research*, 50(3):2002–2021, 2014. doi: 10.1002/2013WR014382. URL https://agupubs.onlinelibrary.wiley.com/doi/abs/10.1002/2013WR014382.

E. Engman and R. Gurney. Remote sensing in hydrology, london. 17(6), 1991. doi: 10.1002/esp.3290170615.

X. Feng, A. Sahoo, K. Arsenault, P. Houser, Y. Luo, and T. J. Troy. The impact of snow model complexity at three clpx sites. *Journal of Hydrometeorology*, 9:1464–1481, 2008. doi: 10.1175/2008JHM860.1.

D. Finger, F. Pellicciotti, M. Konz, S. Rimkus, and P. Burlando. The value of glacier mass balance, satellite snow cover images, and hourly discharge for improving the performance of a physically based distributed hydrological model. *Water Resources Research*, 47(7), 2011. doi: 10.1029/2010WR009824. URL https://agupubs.onlinelibrary.wiley.com/doi/abs/10.1029/2010WR009824.

D. Finger, M. Vis, M. Huss, and J. Seibert. The value of multiple data set calibration versus model complexity for improving the performance of hydrological models in mountain catchments. *Water Resources Research*, 51(4):1939–1958, 2015. doi: 10.1002/2014WR015712. URL https://agupubs.onlinelibrary.wiley.com/doi/abs/10.1002/2014WR015712.

K. J. Franz and L. R. Karsten. Calibration of a distributed snow model using modis snow covered area data. *Journal of Hydrology*, 494:160–175, 2013. ISSN 0022-1694. doi: 10.1016/j.jhydrol.2013.04.026. URL https://www.sciencedirect.com/science/article/pii/S002216941300320X.

M. Friedl and D. Sulla-Menashe. Modis/terra+aqua land cover type yearly l3 global 500m sin grid, version 6. http://doi.org/10.5067/MODIS/MCD12Q1.006, 2015.

G. Fu, Z. Shen, X. Zhang, P. Shi, Y. Zhang, and J. Wu. Estimating air temperature of an alpine meadow on the northern tibetan plateau using modis land surface temperature. *Acta Ecologica Sinica*, 31(1):8–13, 2011. ISSN 1872-2032. doi: 10.1016/j.chnaes.2010.11.002. URL https://www.sciencedirect.com/science/article/pii/S1872203210000661.

J. Gabbi, M. Carenzo, F. Pellicciotti, A. Bauder, and M. Funk. A comparison of empirical and physically based glacier surface melt models for long-term simulations of glacier response. *Journal of Glaciology*, 60(224):1140–1154, 2014. doi: 10.3189/2014JoG14J011.

A. Gafurov. *Water Balance Modeling Using Remote Sensing Information - Focus on Central Asia*. Doctoral thesis, Institut für Wasserbau, Universität Stuttgart, Stuttgart, Germany, 2010. URL http://elib.uni-stuttgart.de/opus/volltexte/2011/6002.

A. Gafurov and A. Bárdossy. Cloud removal methodology from modis snow cover product. *Hydrology and Earth System Sciences*, 13(7):1361–1373, 2009. doi: 10.5194/hess-13-1361-2009. URL https://hess.copernicus.org/articles/13/1361/2009/.

Y. Gan, Y. Zhang, Y. Liu, C. Kongoli, and C. Grassotti. Assimilation of blended in situ-satellite snow water equivalent into the national water model for improving hydrologic simulation in two us river basins. *Science of The Total Environment*, 838:156567, 2022. ISSN 0048-9697. doi: 10.1016/j.scitotenv.2022.156567. URL https://www.sciencedirect.com/science/article/pii/S0048969722036646.

M. Girons Lopez, M. J. P. Vis, M. Jenicek, N. Griessinger, and J. Seibert. Assessing the degree of detail of temperature-based snow routines for runoff modelling in mountainous areas in central europe. *Hydrology and Earth System Sciences*, 24(9):4441–4461, 2020. doi: 10.5194/hess-24-4441-2020. URL https://hess.copernicus.org/articles/24/4441/2020/.

P. Goovaerts. Geostatistical approaches for incorporating elevation into the spatial interpolation of rainfall. *Journal of Hydrology*, 228(1):113 – 129, 2000. ISSN 0022-1694. doi: 10.1016/S0022-1694(00)00144-X. URL http://www.sciencedirect.com/science/article/pii/S002216940000144X.

J. Götzinger and A. Bárdossy. Comparison of four regionalisation methods for a distributed hydrological model. *Journal of Hydrology*, 333:374–384, 2007.

S. N. Goward, R. H. Waring, D. G. Dye, and J. Yang. Ecological remote sensing at otter: Satellite macroscale observations. *Ecological Applications*, 4(2):322–343, 1994. doi: 10.2307/1941937. URL https://esajournals.onlinelibrary.wiley.com/doi/abs/10.2307/1941937.

D. R. Gyawali and A. Bárdossy. Development and parameter estimation of snowmelt models using spatial snow-cover observations from modis. *Hydrology and Earth System Sciences*, 26(12):3055–3077, 2022. doi: 10.5194/hess-26-3055-2022. URL https://hess.copernicus.org/articles/26/3055/2022/.

D. K. Hall and G. A. Riggs. Accuracy assessment of the modis snow products. *Hydrological Processes*, 21(12):1534–1547, 2007. doi: https://doi.org/10.1002/hyp.6715. URL https://onlinelibrary.wiley.com/doi/abs/10.1002/hyp.6715.

D. K. Hall and G. A. Riggs. Modis/terra snow cover daily l3 global 500m sin grid, version 6. https://nsidc.org/data/MOD10A1/versions/6, 2016.

D. K. Hall, G. A. Riggs, V. V. Salomonson, N. E. DiGirolamo, and K. J. Bayr. Modis snow-cover products. *Remote Sensing of Environment*, 83(1):181–194, 2002. ISSN 0034-4257. doi: 10.1016/S0034-4257(02)00095-0. URL https://www.sciencedirect.com/science/article/pii/S0034425702000950. The Moderate Resolution Imaging Spectroradiometer (MODIS): a new generation of Land Surface Monitoring.

D. K. Hall, G. A. Riggs, N. E. DiGirolamo, and M. O. Román. Evaluation of modis and viirs cloud-gap-filled snow-cover products for production of an earth science data record. *Hydrology and Earth System Sciences*, 23(12):5227–5241, 2019. doi: 10.5194/hess-23-5227-2019. URL https://hess.copernicus.org/articles/23/5227/2019/.

D. M. Hannah, L. E. Brown, A. M. Milner, A. M. Gurnell, G. R. McGregor, G. E. Petts, B. P. Smith, and D. L. Snook. Integrating climate–hydrology–ecology for alpine river systems. *Aquatic Conservation: Marine and Freshwater Ecosystems*, 17(6):636–656, 2007. doi: 10.1002/aqc.800. URL https://onlinelibrary.wiley.com/doi/abs/10.1002/aqc.800.

S. Härer, M. Bernhardt, M. Siebers, and K. Schulz. On the need for a time- and location-dependent estimation of the ndsi threshold value for reducing existing uncertainties in snow cover maps at different scales. *The Cryosphere*, 12(5):1629–1642, 2018. doi: 10.5194/tc-12-1629-2018. URL https://tc.copernicus.org/articles/12/1629/2018/.

M. R. Haylock, N. Hofstra, A. M. G. Klein Tank, E. J. Klok, P. D. Jones, and M. New. A european daily high-resolution gridded data set of surface temperature and precipitation for 1950–2006. *Journal of Geophysical Research: Atmospheres*, 113(D20), 2008. doi: 10.1029/2008JD010201. URL https://agupubs.onlinelibrary.wiley.com/doi/abs/10.1029/2008JD010201.

Z. He, S. Vorogushyn, K. Unger-Shayesteh, A. Gafurov, O. Kalashnikova, E. Omorova, and B. Merz. The value of hydrograph partitioning curves for calibrating hydrological models in glacierized basins. *Water Resources Research*, 54(3):2336–2361, 2018. doi: 10.1002/2017WR021966. URL https://agupubs.onlinelibrary.wiley.com/doi/abs/10.1002/2017WR021966.

Z. H. He, J. Parajka, F. Q. Tian, and G. Blöschl. Estimating degree-day factors from modis for snowmelt runoff modeling. *Hydrology and Earth System Sciences*, 18(12):4773–4789, 2014. doi: 10.5194/hess-18-4773-2014. URL https://hess.copernicus.org/articles/18/4773/2014/.

T. Hengl, G. Geuvelink, and A. Stein. Comparison of kriging with external drift and regression-kriging. Technical report, ITC, 2003. URL Availableon-lineathttp://www.itc.nl/library/Academicoutput/.

T. Hengl, G. B. M. Heuvelink, M. Perčec Tadić, and E. J. Pebesma. Spatio-temporal prediction of daily temperatures using time-series of modis lst images. *Theoretical and Applied Climatology*, 107:265–277, 2012. doi: 10.1007/s00704-011-0464-2. URL 10.1007/s00704-011-0464-2.

R. J. Hijmans, S. E. Cameron, J. L. Parra, P. G. Jones, and A. Jarvis. Very high resolution interpolated climate surfaces for global land areas. *International Journal of Climatology*, 25 (15):1965–1978, 2005. doi: 10.1002/joc.1276. URL https://rmets.onlinelibrary.wiley.com/doi/abs/10.1002/joc.1276.

R. Hock. A distributed temperature-index ice- and snowmelt model including potential direct solar radiation. *Journal of Glaciology*, 45(149):101–111, 1999. doi: 10.3189/S0022143000003087.

R. Hock. Temperature index melt modelling in mountain areas. *Journal of Hydrology*, 282 (1):104–115, 2003. ISSN 0022-1694. doi: 10.1016/S0022-1694(03)00257-9. URL https://www.sciencedirect.com/science/article/pii/S0022169403002579. Mountain Hydrology and Water Resources.

J. Hofierka and M. Suri. The solar radiation model for open source gis: implementation and applications. *Proceedings of the Open source GIS - GRASS users conference 2002*, 2002.

X. Huang, J. Deng, W. Wang, Q. Feng, and T. Liang. Impact of climate and elevation on snow cover using integrated remote sensing snow products in tibetan plateau. *Remote Sensing of Environment*, 190:274–288, 2017. ISSN 0034-4257. doi: 10.1016/j.rse.2016.12.028. URL https://www.sciencedirect.com/science/article/pii/S0034425716305077.

G. Hudson and H. Wackernagel. Mapping temperature using kriging with external drift: Theory and an example from scotland. *International Journal of Climatology*, 14(1):77–91, 1994. doi: 10.1002/joc.3370140107. URL https://rmets.onlinelibrary.wiley.com/doi/abs/10.1002/joc.3370140107.

G. C. Hulley, D. Ghent, F. M. Göttsche, P. C. Guillevic, D. J. Mildrexler, and C. Coll. 3 - land surface temperature. In G. C. Hulley and D. Ghent, editors, *Taking the Temperature of the Earth*, pages 57–127. Elsevier, 2019. ISBN 978-0-12-814458-9. doi: 10.1016/B978-0-12-814458-9.00003-4. URL https://www.sciencedirect.com/science/article/pii/B9780128144589000034.

M. F. Hutchinson. Interpolating mean rainfall using thin plate smoothing splines. *International Journal of Geographical Information Systems*, 9(4):385–403, 1995. doi: 10.1080/02693799508902045. URL 10.1080/02693799508902045.

W. Immerzeel, P. Droogers, S. de Jong, and M. Bierkens. Large-scale monitoring of snow cover and runoff simulation in himalayan river basins using remote sensing. *Remote Sensing of Environment*, 113(1):40–49, 2009. ISSN 0034-4257. doi: 10.1016/j.rse.2008.08.010. URL https://www.sciencedirect.com/science/article/pii/S0034425708002575.

M. F. Ismail, B. S. Naz, M. Wortmann, M. Disse, L. C. Bowling, and B. Wolfgang. Comparison of two model calibration approaches and their influence on future projections under climate change in the upper indus basin. *Climatic Change*, 163:1227–1246, 2020. doi: 10.1007/s10584-020-02902-3. URL 10.1007/s10584-020-02902-3.

A. Jarvis, E. Guevara, H. Reuter, and A. Nelson. Hole-filled srtm for the globe : version 4 : data grid, 2008. Published by CGIAR-CSI on 19 August 2008.

M. Jenicek, H. Pevna, and O. Matejka. Canopy structure and topography effects on snow distribution at a catchment scale: Application of multivariate approaches. *Journal of Hydrology and Hydromechanics*, 66(1):43–54, 2018. doi: doi:10.1515/johh-2017-0027. URL 10.1515/johh-2017-0027.

Y. Jieru. *Nonlinear estimation of short time precipitation using weather radar and surface observations*. Doctoral thesis, Institut für Wasser- und Umweltsystemmodellierung, Universität Stuttgart, Stuttgart, Germany, 2018. URL https://elib.uni-stuttgart.de/bitstream/11682/10287/3/Diss_Jieru.pdf.

M. Jin and R. E. Dickinson. Land surface skin temperature climatology: benefitting from the strengths of satellite observations. *Environmental Research Letters*, 5(4):044004, nov 2010. doi: 10.1088/1748-9326/5/4/044004. URL https://dx.doi.org/10.1088/1748-9326/5/4/044004.

G. Jost, R. Dan Moore, R. Smith, and D. R. Gluns. Distributed temperature-index snowmelt modelling for forested catchments. *Journal of Hydrology*, 420-421:87–101, 2012. ISSN 0022-1694. doi: 10.1016/j.jhydrol.2011.11.045. URL https://www.sciencedirect.com/science/article/pii/S0022169411008304.

A. G. Journal and F. Alabert. Non-Gaussian data expansion in the Earth Sciences. *Terra Nova*, 1:123–134, Mar. 1989. doi: 10.1111/j.1365-3121.1989.tb00344.x.

Y. Julien and J. A. Sobrino. The yearly land cover dynamics (ylcd) method: An analysis of global vegetation from ndvi and lst parameters. *Remote Sensing of Environment*, 113 (2):329–334, 2009. ISSN 0034-4257. doi: 10.1016/j.rse.2008.09.016. URL https://www.sciencedirect.com/science/article/pii/S0034425708003131.

J. W. Kirchner. Getting the right answers for the right reasons: Linking measurements, analyses, and models to advance the science of hydrology. *Water Resources Research*, 42(3), 2006. doi: 10.1029/2005WR004362. URL https://agupubs.onlinelibrary.wiley.com/doi/abs/10.1029/2005WR004362.

J. D. Kirkham, I. Koch, T. M. Saloranta, M. Litt, E. E. Stigter, K. Møen, A. Thapa, K. Melvold, and W. W. Immerzeel. Near real-time measurement of snow water equivalent in the nepal

himalayas. *Frontiers in Earth Science*, 7:177, 2019. ISSN 2296-6463. doi: 10.3389/feart.2019.00177. URL https://www.frontiersin.org/article/10.3389/feart.2019.00177.

C. Kongoli, P. Romanov, and R. Ferraro. Snow cover monitoring from remote-sensing satellites: Possibilities for drought assessment. (554), 2012. URL https://digitalcommons.unl.edu/usdeptcommercepub/554/.

M. Konz and J. Seibert. On the value of glacier mass balances for hydrological model calibration. *Journal of Hydrology*, 385(1):238–246, 2010. ISSN 0022-1694. doi: 10.1016/j.jhydrol.2010.02.025. URL https://www.sciencedirect.com/science/article/pii/S0022169410000958.

W. P. Kustas, A. Rango, and R. Uijlenhoet. A simple energy budget algorithm for the snowmelt runoff model. *Water Resources Research*, 30(5):1515–1527, 1994. doi: 10.1029/94WR00152. URL https://agupubs.onlinelibrary.wiley.com/doi/abs/10.1029/94WR00152.

E. Kuusisto. On the values and variability of degree-day melting factor in finland. *Nord. Hydrol.*, 11(4):235–242, 1980.

E. F. Lambin and D. Ehrlich. Combining vegetation indices and surface temperature for land-cover mapping at broad spatial scales. *International Journal of Remote Sensing*, 16(3):573–579, 1995. doi: 10.1080/01431169508954423. URL 10.1080/01431169508954423.

C. Largeron, M. Dumont, S. Morin, A. Boone, M. Lafaysse, S. Metref, E. Cosme, T. Jonas, A. Winstral, and S. A. Margulis. Toward snow cover estimation in mountainous areas using modern data assimilation methods: A review. *Frontiers in Earth Science*, 8, 2020. ISSN 2296-6463. doi: 10.3389/feart.2020.00325. URL https://www.frontiersin.org/articles/10.3389/feart.2020.00325.

G. H. Leavesley. Problems of snowmelt runoff modelling for a variety of physiographic and climatic conditions. *Hydrological Sciences Journal*, 34(6):617–634, 1989. doi: 10.1080/02626668909491371. URL 10.1080/02626668909491371.

H. Lebrenz and A. Bárdossy. Geostatistical interpolation by quantile kriging. *Hydrology and Earth System Sciences*, 23(3):1633–1648, 2019. doi: 10.5194/hess-23-1633-2019. URL https://hess.copernicus.org/articles/23/1633/2019/.

S. Leinss, G. Parrella, and I. Hajnsek. Snow height determination by polarimetric phase differences in x-band sar data. *IEEE Journal of Selected Topics in Applied Earth Observations and Remote Sensing*, 7(9):3794–3810, 2014. doi: 10.1109/JSTARS.2014.2323199.

X. Li and M. W. Williams. Snowmelt runoff modelling in an arid mountain watershed, tarim basin, china. *Hydrological Processes*, 22(19):3931–3940, 2008. doi: 10.1002/hyp.7098. URL https://onlinelibrary.wiley.com/doi/abs/10.1002/hyp.7098.

X. Li, Y. Jing, H. Shen, and L. Zhang. The recent developments in cloud removal approaches of modis snow cover product. *Hydrology and Earth System Sciences*, 23(5):2401–2416, 2019. doi: 10.5194/hess-23-2401-2019. URL https://hess.copernicus.org/articles/23/2401/2019/.

Z.-L. Li, B.-H. Tang, H. Wu, H. Ren, G. Yan, Z. Wan, I. F. Trigo, and J. A. Sobrino. Satellite-derived land surface temperature: Current status and perspectives. *Remote Sensing of Environment*, 131:14–37, 2013. ISSN 0034-4257. doi: 10.1016/j.rse.2012.12.008. URL https://www.sciencedirect.com/science/article/pii/S0034425712004749.

R. Y. Liu, J. M. Parelius, and K. Singh. Multivariate analysis by data depth: Descriptive statistics, graphics and inference. *The Annals of Statistics*, 27(3):783–840, 2023/02/23/ 1999. ISSN 00905364. URL http://www.jstor.org/stable/120138. Full publication date: Jun., 1999.

T. Liu, P. Willems, X. W. Feng, Q. Li, Y. Huang, A. M. Bao, X. Chen, F. Veroustraete, and Q. H. Dong. On the usefulness of remote sensing input data for spatially distributed hydrological modelling: case of the tarim river basin in china. *Hydrological Processes*, 26 (3):335–344, 2012. doi: 10.1002/hyp.8129. URL https://onlinelibrary.wiley.com/doi/abs/10.1002/hyp.8129.

J. Martinec. The degree-day factor for snowmelt-runoff forecasting. *Surface Waters, in: IUGG Gen- eral Assembly of Helsinki*, pages 468–477, 1960.

J. Martinec. Snowmelt-Runoff model for stream flow forecasts. *Hydrology Research*, 6(3): 145–154, 06 1975. ISSN 0029-1277. doi: 10.2166/nh.1975.0010. URL 10.2166/nh.1975.0010.

J. Martinec and A. Rango. Areal distribution of snow water equivalent evaluated by snow cover monitoring. *Water Resources Research*, 17(5):1480–1488, 1981. doi: 10.1029/WR017i005p01480. URL https://agupubs.onlinelibrary.wiley.com/doi/abs/10.1029/WR017i005p01480.

A. Martínez-Cob. Multivariate geostatistical analysis of evapotranspiration and precipitation in mountainous terrain. *Journal of Hydrology*, 174(1):19–35, 1996. ISSN 0022-1694. doi: 10.1016/0022-1694(95)02755-6. URL https://www.sciencedirect.com/science/article/pii/0022169495027556.

G. Matheron. *Les variables régionalisées et leur estimation: Une application de la théorie de fonctions aléatoires aux sciences de la nature.* Paris: Masson et Cie, 1965.

F. Mattia, G. Satalino, V. R. N. Pauwels, and A. Loew. Soil moisture retrieval through a merging of multi-temporal l-band sar data and hydrologic modelling. *Hydrology and Earth System Sciences*, 13(3):343–356, 2009. doi: 10.5194/hess-13-343-2009. URL https://hess.copernicus.org/articles/13/343/2009/.

N. P. Molotch. Reconstructing snow water equivalent in the rio grande headwaters using remotely sensed snow cover data and a spatially distributed snowmelt model. *Hydrological Processes*, 23(7):1076–1089, 2009. doi: 10.1002/hyp.7206. URL https://onlinelibrary.wiley.com/doi/abs/10.1002/hyp.7206.

N. P. Molotch and S. A. Margulis. Estimating the distribution of snow water equivalent using remotely sensed snow cover data and a spatially distributed snowmelt model: A multi-resolution, multi-sensor comparison. *Advances in Water Resources*, 31(11):1503–1514, 2008.

ISSN 0309-1708. doi: 10.1016/j.advwatres.2008.07.017. URL https://www.sciencedirect.com/science/article/pii/S0309170808001255. Hydrologic Remote Sensing.

A. Moreno and H. Hasenauer. Spatial downscaling of european climate data. *International Journal of Climatology*, 36(3):1444–1458, 2016. doi: 10.1002/joc.4436. URL https://rmets.onlinelibrary.wiley.com/doi/abs/10.1002/joc.4436.

G. V. Mostovoy, R. L. King, K. R. Reddy, V. G. Kakani, and M. G. Filippova. Statistical estimation of daily maximum and minimum air temperatures from modis lst data over the state of mississippi. *GIScience & Remote Sensing*, 43(1):78–110, 2006. doi: 10.2747/1548-1603.43.1.78. URL 10.2747/1548-1603.43.1.78.

S. Muhammad and A. Thapa. An improved terra–aqua modis snow cover and randolph glacier inventory 6.0 combined product (moydgl06*) for high-mountain asia between 2002 and 2018. *Earth System Science Data*, 12(1):345–356, 2020. doi: 10.5194/essd-12-345-2020. URL https://essd.copernicus.org/articles/12/345/2020/.

C. Mullen, G. Penny, and M. F. Müller. A simple cloud-filling approach for remote sensing water cover assessments. *Hydrology and Earth System Sciences*, 25(5):2373–2386, 2021. doi: 10.5194/hess-25-2373-2021. URL https://hess.copernicus.org/articles/25/2373/2021/.

R. R. Nemani and S. W. Running. Estimation of regional surface resistance to evapotranspiration from ndvi and thermal-ir avhrr data. *Journal of Applied Meteorology and Climatology*, 28(4):276 – 284, 1989. doi: 10.1175/1520-0450(1989)028⟨0276:EORSRT⟩2.0.CO;2. URL https://journals.ametsoc.org/view/journals/apme/28/4/1520-0450_1989_028_0276_eorsrt_2_0_co_2.xml.

T. Nester, R. Kirnbauer, J. Parajka, and G. Blöschl. Evaluating the snow component of a flood forecasting model. *Hydrology Research*, 43(6):762–779, 05 2012. ISSN 0029-1277. doi: 10.2166/nh.2012.041. URL 10.2166/nh.2012.041.

M. Neteler and H. Mitasova. *Open source GIS: a GRASS GIS approach - Appendix*, volume 689. Kluwer Academic Pub, 2002.

V. Nourani, A. Afkhaminia, S. Andaryani, and Y. Zhang. Multi-station calibration strategy for evaluation and sensitivity analysis of the snowmelt runoff model using MODIS satellite images. *Hydrology Research*, 52(6):1389–1404, 10 2021. ISSN 0029-1277. doi: 10.2166/nh.2021.075. URL 10.2166/nh.2021.075.

NSIDC. Modis application in research. URL https://nsidc.org/data/modis/research.html.

I. Odeh, A. McBratney, and D. Chittleborough. Further results on prediction of soil properties from terrain attributes: heterotopic cokriging and regression-kriging. *Geoderma*, 67(3):215 – 226, 1995. ISSN 0016-7061. doi: 10.1016/0016-7061(95)00007-B. URL http://www.sciencedirect.com/science/article/pii/001670619500007B.

A. Ohmura. Physical basis for the temperature-based melt-index method. *Journal of Applied Meteorology*, 40(4):753 – 761, 2001. doi: 10.1175/1520-0450(2001)040⟨0753:PBFTTB⟩2.0.CO;2. URL https://journals.ametsoc.org/view/journals/apme/40/4/1520-0450_2001_040_0753_pbfttb_2.0.co_2.xml.

J. Parajka and G. Blöschl. Spatio-temporal combination of modis images – potential for snow cover mapping. *Water Resources Research*, 44(3), 2008(a). doi: 10.1029/2007WR006204. URL https://agupubs.onlinelibrary.wiley.com/doi/abs/10.1029/2007WR006204.

J. Parajka and G. Blöschl. The value of modis snow cover data in validating and calibrating conceptual hydrologic models. *Journal of Hydrology*, 358(3):240–258, 2008(b). ISSN 0022-1694. doi: 10.1016/j.jhydrol.2008.06.006. URL https://www.sciencedirect.com/science/article/pii/S0022169408002862.

J. Parajka and G. Blöschl. Modis-based snow cover products, validation, and hydrologic applications. In *Multiscale Hydrologic Remote Sensing*, pages 185–212. CRC Press, Taylor Francis Group, Boca Raton, FL, 1 edition, 2012.

J. Parajka, G. Blöschl, and R. Merz. Regional calibration of catchment models: Potential for ungauged catchments. *Water Resources Research*, 43(6), 2007. doi: 10.1029/2006WR005271. URL https://agupubs.onlinelibrary.wiley.com/doi/abs/10.1029/2006WR005271.

J. Parajka, V. Naeimi, G. Blöschl, and J. Komma. Matching ers scatterometer based soil moisture patterns with simulations of a conceptual dual layer hydrologic model over austria. *Hydrology and Earth System Sciences*, 13(2):259–271, 2009. doi: 10.5194/hess-13-259-2009. URL https://hess.copernicus.org/articles/13/259/2009/.

D. Parr, G. Wang, and D. Bjerklie. Integrating remote sensing data on evapotranspiration and leaf area index with hydrological modeling: Impacts on model performance and future predictions. *Journal of Hydrometeorology*, 16(5):2086–2100, 2015. ISSN 1525755X, 15257541. URL http://www.jstor.org/stable/24915519.

F. Pellicciotti, B. Brock, U. Strasser, P. Burlando, M. Funk, and J. Corripio. An enhanced temperature-index glacier melt model including the shortwave radiation balance: development and testing for haut glacier d'arolla, switzerland. *Journal of Glaciology*, 51(175): 573–587, 2005. doi: 10.3189/172756505781829124.

D. L. Phillips, J. Dolph, and D. Marks. A comparison of geostatistical procedures for spatial analysis of precipitation in mountainous terrain. *Agricultural and Forest Meteorology*, 58(1): 119–141, 1992. ISSN 0168-1923. doi: 10.1016/0168-1923(92)90114-J. URL https://www.sciencedirect.com/science/article/pii/016819239290114J.

J. Pomeroy and D. Marks. Hydrometeorlogical data from mountain and alpine research catchments. *Earth Syst. Sci. Data*, 2020. URL https://essd.copernicus.org/articles/special_issue871.html.

C. Prudhomme and D. W. Reed. Mapping extreme rainfall in a mountainous region using geostatistical techniques: a case study in Scotland. *International Journal of Climatology*, 19: 1337–1356, Oct. 1999. doi: 10.1002/(SICI)1097-0088(199910)19:12⟨1337::AID-JOC421⟩3.3.CO;2-7.

M. S. Raleigh and J. D. Lundquist. Comparing and combining swe estimates from the snow-17 model using prism and swe reconstruction. *Water Resources Research*, 48(1), 2012.

doi: 10.1029/2011WR010542. URL https://agupubs.onlinelibrary.wiley.com/doi/abs/10.1029/2011WR010542.

A. Rango and K. I. Itten. Satellite Potentials in Snowcover Monitoring and Runoff Prediction. *Hydrology Research*, 7(4):209–230, 08 1976. ISSN 0029-1277. doi: 10.2166/nh.1976.0014. URL 10.2166/nh.1976.0014.

J. C. Ritchie and A. Rango. Remote sensing applications to hydrology: introduction. *Hydrological Sciences Journal*, 41(4):429–431, 1996. doi: 10.1080/02626669609491518. URL 10.1080/02626669609491518.

K. Rittger, E. H. Bair, A. Kahl, and J. Dozier. Spatial estimates of snow water equivalent from reconstruction. *Advances in Water Resources*, 94:345–363, 2016. ISSN 0309-1708. doi: 10.1016/j.advwatres.2016.05.015. URL https://www.sciencedirect.com/science/article/pii/S0309170816301506.

M. Rodell and P. R. Houser. Updating a land surface model with modis-derived snow cover. *Journal of Hydrometeorology*, 5(6):1064 – 1075, 2004. doi: 10.1175/JHM-395.1. URL https://journals.ametsoc.org/view/journals/hydr/5/6/jhm-395_1.xml.

P. J. Rousseeuw and A. Struyf. Computing location depth and regression depth in higher dimensions. *Statistics and Computing*, 8(3):193–203, Aug 1998. ISSN 1573-1375. doi: 10.1023/A:1008945009397. URL https://doi.org/10.1023/A:1008945009397.

A. Roy, A. Royer, and R. Turcotte. Improvement of springtime streamflow simulations in a boreal environment by incorporating snow-covered area derived from remote sensing data. *Journal of Hydrology*, 390(1):35–44, 2010. ISSN 0022-1694. doi: 10.1016/j.jhydrol.2010.06.027. URL https://www.sciencedirect.com/science/article/pii/S0022169410003628.

N. Rutter, R. Essery, J. Pomeroy, N. Altimir, K. Andreadis, I. Baker, A. Barr, P. Bartlett, A. Boone, H. Deng, H. Douville, E. Dutra, K. Elder, C. Ellis, X. Feng, A. Gelfan, A. Goodbody, Y. Gusev, D. Gustafsson, R. Hellström, Y. Hirabayashi, T. Hirota, T. Jonas, V. Koren, A. Kuragina, D. Lettenmaier, W. Li, C. Luce, E. Martin, O. Nasonova, J. Pumpanen, R. Pyles, P. Samuelsson, M. Sandells, G. Schädler, A. Shmakin, T. Smirnova, M. Stähli, R. Stöckli, U. Strasser, H. Su, K. Suzuki, K. Takata, K. Tanaka, E. Thompson, T. Vesala, P. Viterbo, A. Wiltshire, K. Xia, Y. Xue, and T. Yamazaki. Evaluation of forest snow processes models (snowmip2). *Journal of Geophysical Research*, 2009. doi: 10.1029/2008JD011063. 12.01.03; LK 01; 114(D06111), 2009.

V. Salomonson and I. Appel. Estimating fractional snow cover from modis using the normalized difference snow index. *Remote Sensing of Environment*, 89(3):351–360, 2004. ISSN 0034-4257. doi: 10.1016/j.rse.2003.10.016. URL https://www.sciencedirect.com/science/article/pii/S0034425703002864.

B. Schaefli and M. Huss. Integrating point glacier mass balance observations into hydrologic model identification. *Hydrology and Earth System Sciences*, 15(4):1227–1241, 2011. doi: 10.5194/hess-15-1227-2011. URL https://hess.copernicus.org/articles/15/1227/2011/.

B. Schaefli, B. Hingray, M. Niggli, and A. Musy. A conceptual glacio-hydrological model for high mountainous catchments. *Hydrology and Earth System Sciences*, 9(1/2):95–109, 2005. doi: 10.5194/hess-9-95-2005. URL https://hess.copernicus.org/articles/9/95/2005/.

E. Schmucki, C. Marty, C. Fierz, and M. Lehning. Evaluation of modelled snow depth and snow water equivalent at three contrasting sites in switzerland using snowpack simulations driven by different meteorological data input. *Cold Regions Science and Technology*, 99:27–37, 2014. ISSN 0165-232X. doi: 10.1016/j.coldregions.2013.12.004. URL https://www.sciencedirect.com/science/article/pii/S0165232X13002036.

J. Seibert. Estimation of parameter uncertainty in the hbv model. *Nordic Hydrology*, 28: 247–262, 1996.

J. Seibert. Multi-criteria calibration of a conceptual runoff model using a genetic algorithm. *Hydrology and Earth System Sciences*, 4(2):215–224, 2000. doi: 10.5194/hess-4-215-2000. URL https://hess.copernicus.org/articles/4/215/2000/.

E. Shamir and K. P. Georgakakos. Estimating snow depletion curves for american river basins using distributed snow modeling. *Journal of Hydrology*, 334(1):162–173, 2007. ISSN 0022-1694. doi: 10.1016/j.jhydrol.2006.10.007. URL https://www.sciencedirect.com/science/article/pii/S0022169406005361.

S. Shen and G. G. Leptoukh. Estimation of surface air temperature over central and eastern eurasia from modis land surface temperature. *Environmental Research Letters*, 6(4): 045206, nov 2011. doi: 10.1088/1748-9326/6/4/045206. URL https://dx.doi.org/10.1088/1748-9326/6/4/045206.

M. Shrestha, L. Wang, T. Koike, H. Tsutsui, Y. Xue, and Y. Hirabayashi. Correcting basin-scale snowfall in a mountainous basin using a distributed snowmelt model and remote-sensing data. *Hydrology and Earth System Sciences*, 18(2):747–761, 2014. doi: 10.5194/hess-18-747-2014. URL https://hess.copernicus.org/articles/18/747/2014/.

S. Singh. *Robust Parameter Estimation in Gauged and Ungauged Basins*. Doctoral thesis, Institut für Wasserbau, Universitaẗ Stuttgart, Stuttgart, Germany, 2010. URL http://elib.uni-stuttgart.de/handle/11682/377.

S. K. Singh and A. Bárdossy. Calibration of hydrological models on hydrologically unusual events. *Advances in Water Resources*, 38:81–91, 2012. ISSN 0309-1708. doi: https://doi.org/10.1016/j.advwatres.2011.12.006. URL https://www.sciencedirect.com/science/article/pii/S0309170811002351.

S. K. Singh, H. McMillan, and A. Bárdossy. Use of the data depth function to differentiate between case of interpolation and extrapolation in hydrological model prediction. *Journal of Hydrology*, 477:213–228, 2013. ISSN 0022-1694. doi: https://doi.org/10.1016/j.jhydrol.2012.11.034. URL https://www.sciencedirect.com/science/article/pii/S002216941201013X.

T. A. J. G. Sirisena, S. Maskey, and R. Ranasinghe. Hydrological model calibration with streamflow and remote sensing based evapotranspiration data in a data poor basin.

Remote Sensing, 12(22), 2020. ISSN 2072-4292. doi: 10.3390/rs12223768. URL https://www.mdpi.com/2072-4292/12/22/3768.

K. Stahl, R. D. Moore, J. M. Shea, D. Hutchinson, and A. J. Cannon. Coupled modelling of glacier and streamflow response to future climate scenarios. *Water Resources Research*, 44 (2), 2008. doi: 10.1029/2007WR005956. URL https://agupubs.onlinelibrary.wiley.com/doi/abs/10.1029/2007WR005956.

W. Sun, H. Ishidaira, S. Bastola, and J. Yu. Estimating daily time series of streamflow using hydrological model calibrated based on satellite observations of river water surface width: Toward real world applications. *Environmental Research*, 139:36–45, 2015. ISSN 0013-9351. doi: 10.1016/j.envres.2015.01.002. URL https://www.sciencedirect.com/science/article/pii/S0013935115000031. Environmental Research on Hydrology and Water Resources.

B. Széles, J. Parajka, P. Hogan, R. Silasari, L. Pavlin, P. Strauss, and G. Blöschl. The added value of different data types for calibrating and testing a hydrologic model in a small catchment. *Water Resources Research*, 56(10):e2019WR026153, 2020. doi: 10.1029/2019WR026153. URL https://agupubs.onlinelibrary.wiley.com/doi/abs/10.1029/2019WR026153. e2019WR026153 2019WR026153.

A. A. Tahir, P. Chevallier, Y. Arnaud, L. Neppel, and B. Ahmad. Modeling snowmelt-runoff under climate scenarios in the hunza river basin, karakoram range, northern pakistan. *Journal of Hydrology*, 409(1):104–117, 2011. ISSN 0022-1694. doi: 10.1016/j.jhydrol.2011.08.035. URL https://www.sciencedirect.com/science/article/pii/S0022169411005816.

R. Tang, Z.-L. Li, and B. Tang. An application of the ts–vi triangle method with enhanced edges determination for evapotranspiration estimation from modis data in arid and semi-arid regions: Implementation and validation. *Remote Sensing of Environment*, 114(3):540–551, 2010. ISSN 0034-4257. doi: 10.1016/j.rse.2009.10.012. URL https://www.sciencedirect.com/science/article/pii/S0034425709003216.

L. Tarasova, M. Knoche, J. Dietrich, and R. Merz. Effects of input discretization, model complexity, and calibration strategy on model performance in a data-scarce glacierized catchment in central asia. *Water Resources Research*, 52(6):4674–4699, 2016. doi: 10.1002/2015WR018551. URL https://agupubs.onlinelibrary.wiley.com/doi/abs/10.1002/2015WR018551.

A. E. Tekeli, Z. Akyürek, A. Arda Şorman, A. Şensoy, and A. Ünal Şorman. Using modis snow cover maps in modeling snowmelt runoff process in the eastern part of turkey. *Remote Sensing of Environment*, 97(2):216–230, 2005. ISSN 0034-4257. doi: 10.1016/j.rse.2005.03.013. URL https://www.sciencedirect.com/science/article/pii/S0034425705001379.

G. Thirel, P. Salamon, P. Burek, and M. Kalas. Assimilation of modis snow cover area data in a distributed hydrological model using the particle filter. *Remote Sensing*, 5(11):5825–5850, 2013. ISSN 2072-4292. doi: 10.3390/rs5115825. URL https://www.mdpi.com/2072-4292/5/11/5825.

M. Todd Walter, E. S. Brooks, D. K. McCool, L. G. King, M. Molnau, and J. Boll. Process-based snowmelt modeling: does it require more input data than temperature-index modeling?

Journal of Hydrology, 300(1):65–75, 2005. ISSN 0022-1694. doi: 10.1016/j.jhydrol.2004.05.002. URL https://www.sciencedirect.com/science/article/pii/S0022169404002550.

J. Tong, S. J. Déry, and P. L. Jackson. Topographic control of snow distribution in an alpine watershed of western canada inferred from spatially-filtered modis snow products. *Hydrology and Earth System Sciences*, 13(3):319–326, 2009a. doi: 10.5194/hess-13-319-2009. URL https://hess.copernicus.org/articles/13/319/2009/.

J. Tong, S. J. Déry, and P. L. Jackson. Interrelationships between modis/terra remotely sensed snow cover and the hydrometeorology of the quesnel river basin, british columbia, canada. *Hydrology and Earth System Sciences*, 13(8):1439–1452, 2009b. doi: 10.5194/hess-13-1439-2009. URL https://hess.copernicus.org/articles/13/1439/2009/.

R. Tong, J. Parajka, J. Komma, and G. Blöschl. Mapping snow cover from daily collection 6 modis products over austria. *Journal of Hydrology*, 590:125548, 2020. ISSN 0022-1694. doi: 10.1016/j.jhydrol.2020.125548. URL https://www.sciencedirect.com/science/article/pii/S0022169420310088.

H. Tran, P. Nguyen, M. Ombadi, K. lin Hsu, S. Sorooshian, and X. Qing. A cloud-free modis snow cover dataset for the contiguous united states from 2000 to 2017. *Sci Data*, 6, 2019. doi: 10.1038/sdata.2018.300.

J. W. Tukey. Mathematics and the picturing of data. 1975.

H.-C. Udnæs, E. Alfnes, and L. M. Andreassen. Improving runoff modelling using satellite-derived snow covered area? *Hydrology Research*, 38:21–32, 2007.

T. Virdee and N. Kottegoda. A brief review of kriging and its application to optimal interpolation and observation well selection. *Hydrological Sciences Journal*, 29(4):367–387, 1984. doi: 10.1080/02626668409490957. URL 10.1080/02626668409490957.

D. Viviroli, D. R. Archer, W. Buytaert, H. J. Fowler, G. B. Greenwood, A. F. Hamlet, Y. Huang, G. Koboltschnig, M. I. Litaor, J. I. López-Moreno, S. Lorentz, B. Schädler, H. Schreier, K. Schwaiger, M. Vuille, and R. Woods. Climate change and mountain water resources: overview and recommendations for research, management and policy. *Hydrology and Earth System Sciences*, 15(2):471–504, 2011. doi: 10.5194/hess-15-471-2011. URL https://hess.copernicus.org/articles/15/471/2011/.

W. Wagner, N. E. C. Verhoest, R. Ludwig, and M. Tedesco. Editorial remote sensing in hydrological sciences". *Hydrology and Earth System Sciences*, 13(6):813–817, 2009. doi: 10.5194/hess-13-813-2009. URL https://hess.copernicus.org/articles/13/813/2009/.

Z. Wan, P. Wang, and X. Li. Using modis land surface temperature and normalized difference vegetation index products for monitoring drought in the southern great plains, usa. *International Journal of Remote Sensing*, 25(1):61–72, 2004. doi: 10.1080/0143116031000115328. URL 10.1080/0143116031000115328.

Z. Wan, S. Hook, and G. Hulley. Modis/terra land surface temperature/emissivity daily l3 global 1km sin grid v061 [data set]. Technical report, NASA EOSDIS Land Processes DAAC, 2021. URL 10.5067/MODIS/MOD11A1.061.

X. Wang and H. Xie. New methods for studying the spatiotemporal variation of snow cover based on combination products of modis terra and aqua. *Journal of Hydrology*, 371(1): 192–200, 2009. ISSN 0022-1694. doi: 10.1016/j.jhydrol.2009.03.028. URL https://www.sciencedirect.com/science/article/pii/S0022169409001966.

Y. Yang, T. Onishi, and K. Hiramatsu. Improving the performance of temperature index snowmelt model of swat by using modis land surface temperature data. *The Scientific World Journal*, 2014(4):045206, 2014. doi: 10.1155/2014/823424. URL 10.1155/2014/823424.

B. F. Zaitchik and M. Rodell. Forward-looking assimilation of modis-derived snow-covered area into a land surface model. *Journal of Hydrometeorology*, 10(1):130 – 148, 2009. doi: 10.1175/2008JHM1042.1. URL https://journals.ametsoc.org/view/journals/hydr/10/1/2008jhm1042_1.xml.

H. Zhang, F. Zhang, G. Zhang, T. Che, W. Yan, M. Ye, and N. Ma. Ground-based evaluation of modis snow cover product v6 across china: Implications for the selection of ndsi threshold. *Science of The Total Environment*, 651:2712–2726, 2019. ISSN 0048-9697. doi: 10.1016/j.scitotenv.2018.10.128. URL https://www.sciencedirect.com/science/article/pii/S0048969718340099.

G. Zhou, M. Cui, J. Wan, and S. Zhang. A review on snowmelt models: Progress and prospect. *Sustainability*, 13(20), 2021. ISSN 2071-1050. doi: 10.3390/su132011485. URL https://www.mdpi.com/2071-1050/13/20/11485.

W. Zhu, A. Lű, and S. Jia. Estimation of daily maximum and minimum air temperature using modis land surface temperature products. *Remote Sensing of Environment*, 130:62–73, 2013. ISSN 0034-4257. doi: 10.1016/j.rse.2012.10.034. URL https://www.sciencedirect.com/science/article/pii/S0034425712004221.

Y. Zuo and R. Serfling. General notions of statistical depth function. *Annals of Statistics*, 28: 461–482, 2000.

J. F. Zuzel and L. M. Cox. Relative importance of meteorological variables in snowmelt. *Water Resources Research*, 11(1):174–176, 1975. doi: 10.1029/WR011i001p00174. URL https://agupubs.onlinelibrary.wiley.com/doi/abs/10.1029/WR011i001p00174.

A. Şorman, Arda, A. Şensoy, A. E. Tekeli, A. Şorman, and Z. Akyürek. Modelling and forecasting snowmelt runoff process using the hbv model in the eastern part of turkey. *Hydrological Processes*, 23(7):1031–1040, 2009. doi: 10.1002/hyp.7204. URL https://onlinelibrary.wiley.com/doi/abs/10.1002/hyp.7204.

A. Snow-melt model results

Annex A.1 and A.2 show the temporal validation of all the employed models on different cloud-free days in Switzerland and Baden-Württemberg respectively. The red highlights show the best performance in terms of Brier scores among the models for the day. Annex A.3 shows the normalized confusion matrices for all the models calibrated against a single day image (2012-01-18) in Switzerland.

Likewise, Annex A.4 compares the MODIS inferred and reference model simulated cumulative snow covered areas (in percentage) for different validation days. Annex A.5 shows the number of days with snow for different years as calculated from MODIS and with reference model.

Annex A.1.: Brier scores for all models on different validation days in Switzerland

	Model1	Model2	Model3	Model4	Model5	Model6
2010-03-08	0.1006	0.0971	0.0840	0.0893	0.0937	0.0914
2010-03-19	0.0449	0.0446	0.0508	0.0453	0.0413	0.0403
2011-01-03	0.1033	0.1133	0.1277	0.0941	0.0840	0.0821
2011-02-09	0.0679	0.0646	0.0800	0.0662	0.0617	0.0591
2011-03-08	0.0457	0.0468	0.0523	0.0496	0.0472	0.0478
2011-11-17	0.0649	0.0649	0.0770	0.0683	0.0640	0.0630
2011-12-26	0.0531	0.0516	0.0815	0.0509	0.0483	0.0478
2012-01-14	0.0352	0.0362	0.0481	0.0418	0.0362	0.0364
2012-01-18	0.0422	0.0409	0.0441	0.0381	0.0373	0.0367
2012-03-01	0.0421	0.0418	0.0577	0.0465	0.0430	0.0425
2012-03-14	0.0400	0.0399	0.0415	0.0381	0.0385	0.0385
2012-03-26	0.0402	0.0392	0.0413	0.0386	0.0378	0.0372
2012-10-30	0.0957	0.0965	0.0990	0.0909	0.0870	0.0872
2012-12-12	0.0375	0.0380	0.0431	0.0425	0.0398	0.0397
2013-01-08	0.0830	0.0829	0.1063	0.0894	0.0818	0.0805
2013-03-04	0.0689	0.0643	0.0586	0.0693	0.0941	0.0723
2013-10-17	0.0456	0.0469	0.0475	0.0462	0.0453	0.0459
2013-11-27	0.1008	0.0856	0.0568	0.0599	0.0728	0.0675
2013-12-10	0.1418	0.1399	0.1636	0.1488	0.1361	0.1341
2014-02-24	0.0346	0.0367	0.0474	0.0413	0.0355	0.0355
2014-03-17	0.0421	0.0411	0.0405	0.0390	0.0392	0.0387
2014-12-23	0.0378	0.0375	0.0504	0.0435	0.0376	0.0377
2015-01-13	0.0597	0.0606	0.0729	0.0647	0.0606	0.0590
2015-03-13	0.0493	0.0485	0.0549	0.0459	0.0473	0.0468
2015-10-20	0.0488	0.0485	0.0471	0.0495	0.0524	0.0511
2015-12-20	0.1893	0.1903	0.2083	0.1795	0.1644	0.1585
2016-01-25	0.0888	0.0891	0.0994	0.0970	0.0912	0.0894
2016-03-10	0.1000	0.0920	0.0768	0.0774	0.0846	0.0782
2016-11-30	0.0623	0.0618	0.0655	0.0560	0.0574	0.0566
2017-02-16	0.0492	0.0494	0.0658	0.0547	0.0518	0.0514
2017-10-25	0.0625	0.0586	0.0652	0.0638	0.0625	0.0624
2018-02-13	0.1120	0.0976	0.0696	0.0741	0.0905	0.0865
2018-03-14	0.0380	0.0386	0.0443	0.0385	0.0371	0.0371
2018-12-07	0.0980	0.1009	0.1343	0.1127	0.1000	0.0977
2018-12-26	0.1532	0.1553	0.2039	0.1704	0.1588	0.1571

Annex A.2.: Brier scores for all models on different validation days in Baden-Württemberg

	Mod1	Mod2	Mod3	Mod4	Mod5	Mod6
2010-02-04	0.098	0.081	0.080	0.083	0.081	0.081
2010-02-16	0.005	0.005	0.005	0.005	0.005	0.005
2010-02-27	0.113	0.110	0.106	0.107	0.106	0.106
2010-03-01	0.119	0.111	0.119	0.119	0.119	0.119
2010-03-08	0.073	0.095	0.073	0.073	0.073	0.073
2010-03-23	0.024	0.024	0.024	0.024	0.024	0.024
2010-10-26	0.235	0.236	0.236	0.236	0.236	0.235
2010-11-30	0.002	0.003	0.002	0.002	0.002	0.002
2010-12-13	0.145	0.180	0.285	0.292	0.289	0.230
2011-01-05	0.012	0.012	0.012	0.012	0.012	0.012
2011-01-16	0.185	0.154	0.157	0.161	0.158	0.165
2011-02-06	0.149	0.160	0.183	0.184	0.185	0.182
2011-02-23	0.426	0.357	0.404	0.398	0.402	0.425
2011-03-05	0.127	0.075	0.073	0.074	0.073	0.076
2011-11-21	0.251	0.251	0.251	0.251	0.251	0.251
2012-01-16	0.234	0.277	0.246	0.250	0.246	0.223
2012-02-12	0.257	0.257	0.257	0.257	0.257	0.257
2012-02-22	0.069	0.148	0.100	0.103	0.100	0.083
2012-03-09	0.106	0.109	0.108	0.108	0.108	0.108
2012-10-31	0.274	0.344	0.374	0.372	0.373	0.361
2012-12-12	0.025	0.026	0.026	0.026	0.026	0.025
2012-12-29	0.264	0.262	0.269	0.275	0.270	0.273
2013-03-04	0.178	0.100	0.086	0.086	0.085	0.096
2013-10-30	0.224	0.224	0.224	0.224	0.224	0.224
2013-12-17	0.263	0.276	0.278	0.276	0.278	0.279
2014-03-07	0.053	0.061	0.062	0.062	0.062	0.062
2014-10-24	0.124	0.124	0.124	0.124	0.124	0.124
2015-01-05	0.172	0.160	0.163	0.177	0.166	0.148
2015-02-07	0.081	0.122	0.079	0.083	0.080	0.072
2015-03-20	0.021	0.020	0.020	0.019	0.020	0.020
2015-12-07	0.253	0.253	0.253	0.253	0.253	0.253
2015-12-19	0.302	0.302	0.302	0.302	0.302	0.302
2015-12-28	0.209	0.209	0.209	0.209	0.209	0.209

Annex A.3.: Confusion matrices for all models in Switzerland

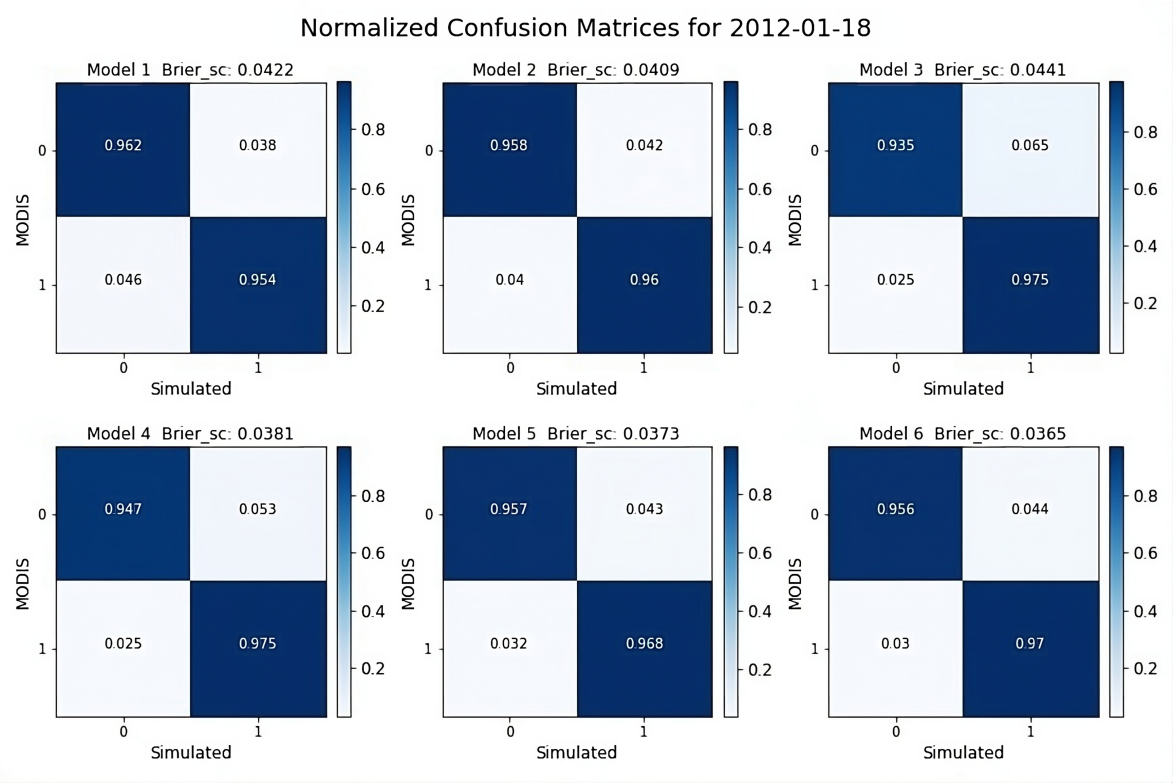

Annex A.4.: MODIS-inferred and simulated SCAs (in %) for selected validation days in Switzerland

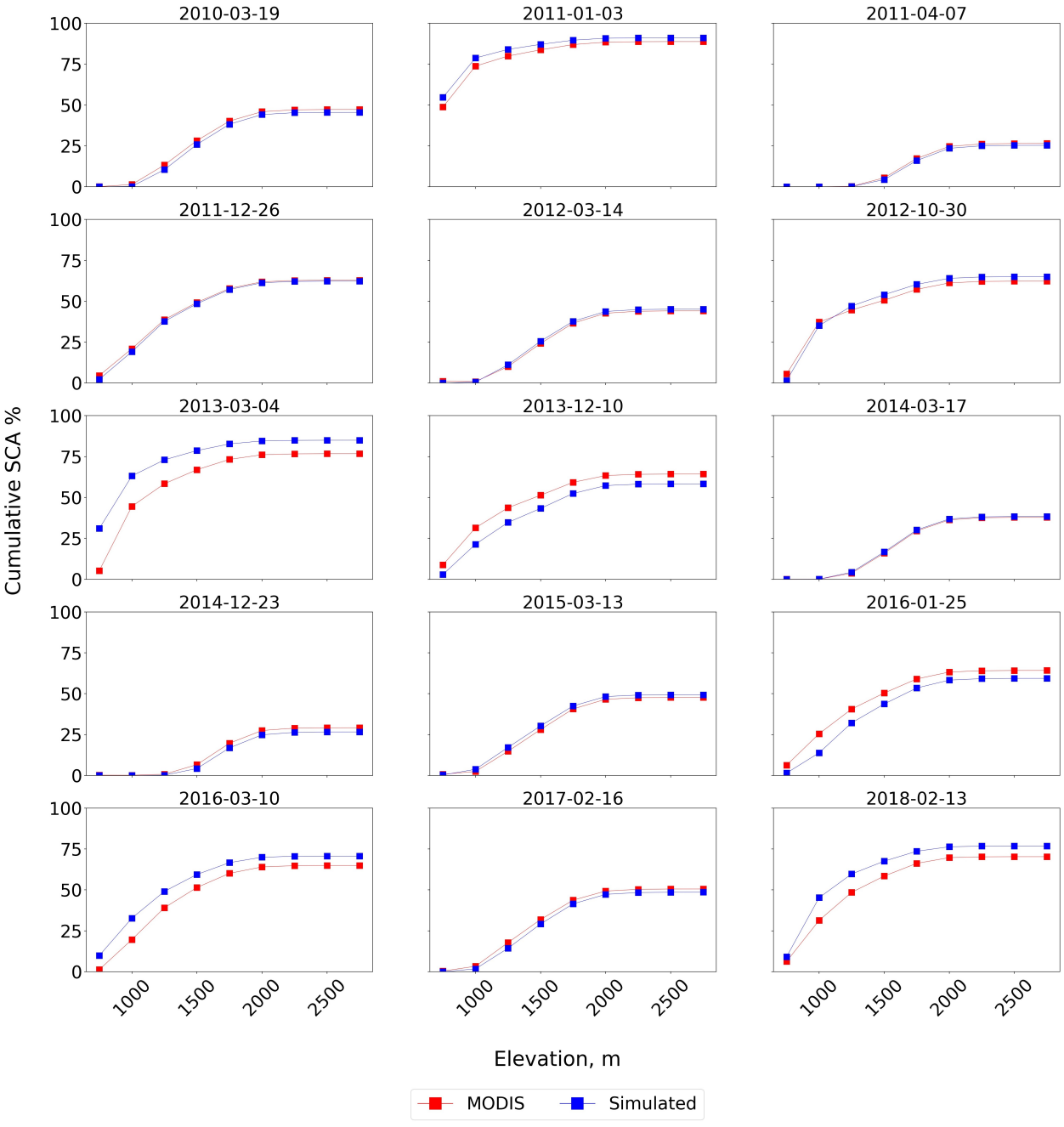

Annex A.5.: MODIS-inferred and simulated snow covered days for different years in Switzerland

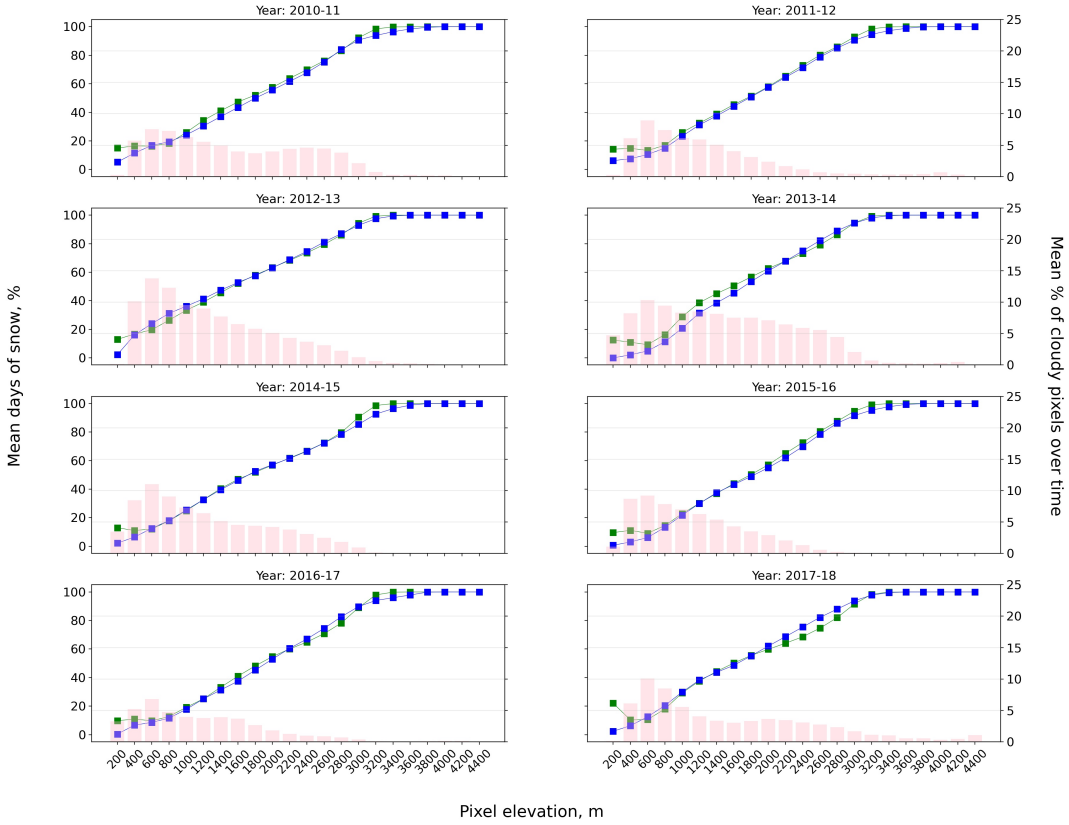

B. Sensitivity analysis of different adopted thresholds for simulation

Annex B.1 and B.2 show the performance of the reference model in terms of Brier scores for different thresholds adopted in the study, respectively for Switzerland and Baden-Württemberg. Detection threshold in the figures refers to the SWE thresholds assumed to differentiate the simulated SWE as 'snow' or 'no-snow'.

Annex B.1.: Sensitivity analysis results for NDSI, cloud percentage, and SWE thresholds in Switzerland

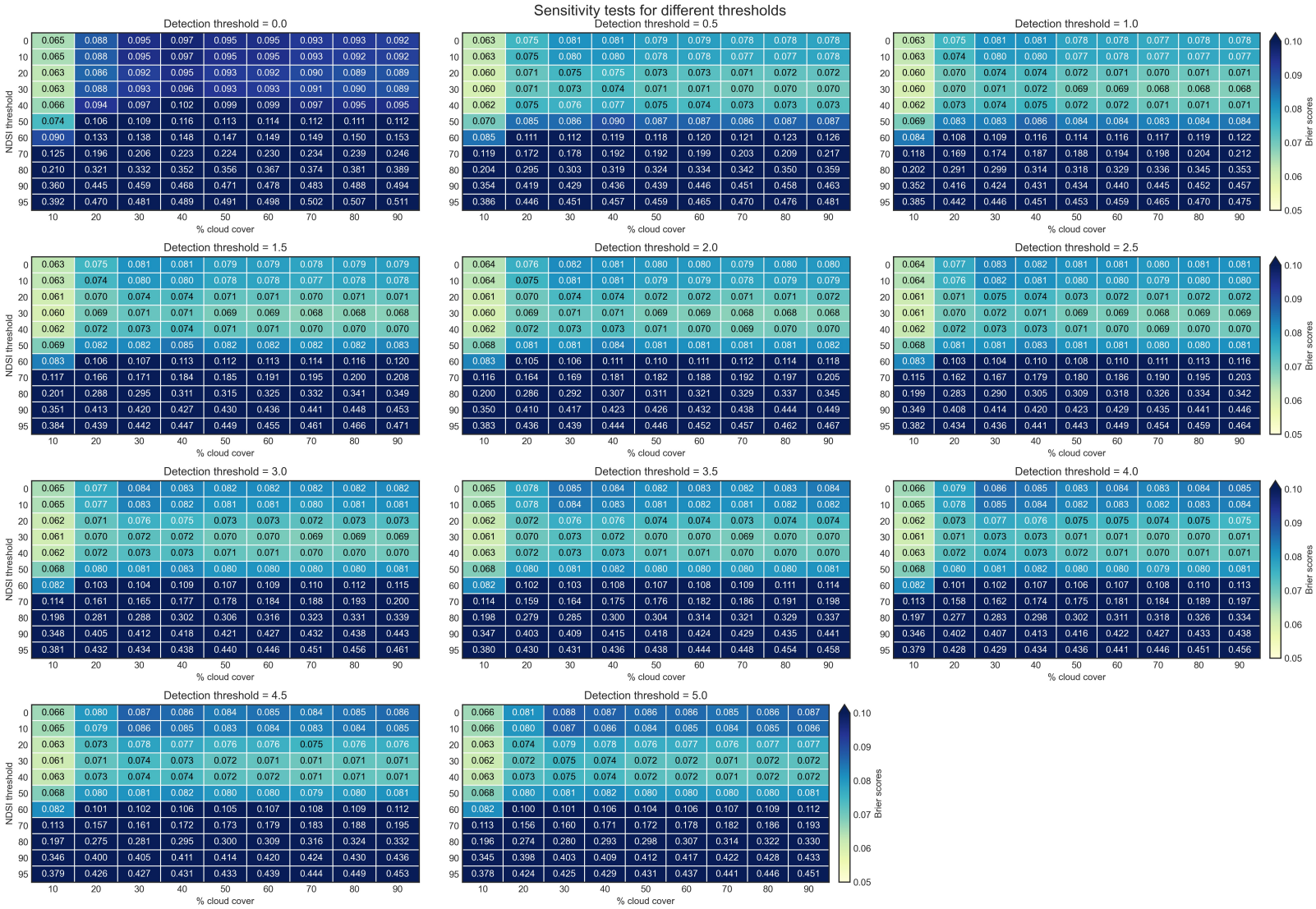

Annex B.2.: Sensitivity analysis results for NDSI, cloud percentage, and SWE thresholds in Baden-Württemberg

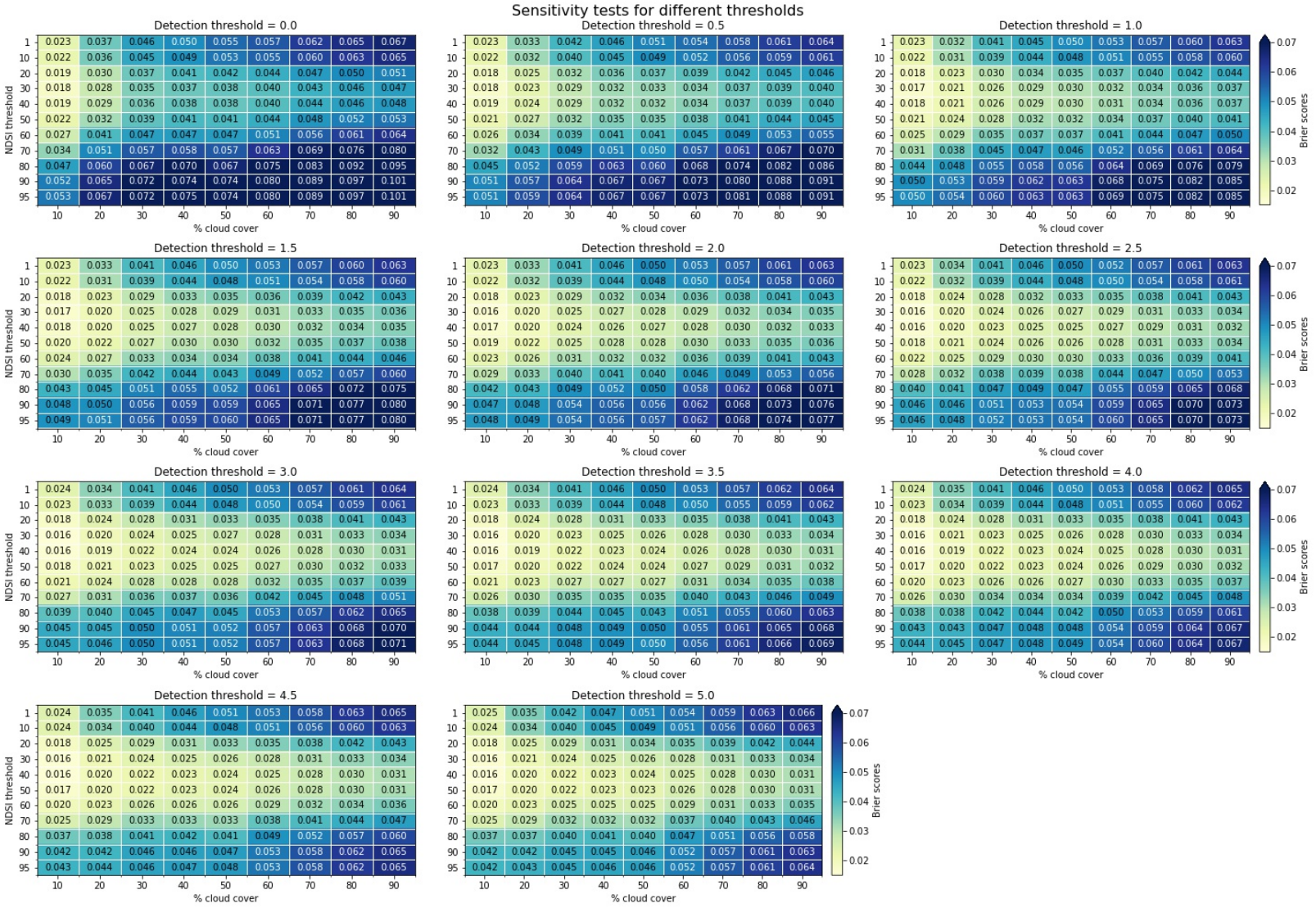

Institut für Wasser- und Umweltsystemmodellierung
Universität Stuttgart

Pfaffenwaldring 61
70569 Stuttgart (Vaihingen)
Telefon (0711) 685 - 60156
Telefax (0711) 685 - 51073
E-Mail: iws@iws.uni-stuttgart.de
http://www.iws.uni-stuttgart.de

Direktoren
Prof. Dr.-Ing. Rainer Helmig
Prof. Dr.-Ing. Wolfgang Nowak
Prof. Dr.-Ing. Silke Wieprecht

Emeriti
Prof. Dr.-Ing. habil. Dr.-Ing. E.h. Jürgen Giesecke
Prof. Dr.h.c. Dr.-Ing. E.h. Helmut Kobus, PhD

Lehrstuhl für Wasserbau und Wassermengenwirtschaft
Leiterin: Prof. Dr.-Ing. Silke Wieprecht
Stellv.: Dr.-Ing. Kristina Terheiden
Versuchsanstalt für Wasserbau
Leiter: Stefan Haun, PhD

Lehrstuhl für Hydromechanik und Hydrosystemmodellierung
Leiter: Prof. Dr.-Ing. Rainer Helmig
Stellv.: apl. Prof. Dr.-Ing. Holger Class

Lehrstuhl für Stochastische Simulation und Sicherheitsforschung für Hydrosysteme
Leiter: Prof. Dr.-Ing. Wolfgang Nowak
Stellv.: apl. Prof. Dr.-Ing. Sergey Oladyshkin
Hydrogeophysik der Vadosen Zone
(mit Forschungszentrum Jülich)
Leiter: Prof. Dr. J.A. Sander Huisman

***VEGAS,* Versuchseinrichtung zur Grundwasser- und Altlastensanierung**
Leiter: Dr.-Ing. Simon Kleinknecht
PD Dr.-Ing. Claus Haslauer

Verzeichnis der Mitteilungshefte

7 *Sonderheft anläßlich des 65. Geburtstages von Prof. Arthur Röhnisch mit Beiträgen von* Benk, Dieter; Breitling, J.; Gurr, Siegfried; Haberhauer, Robert; Honekamp, Hermann; Kuz, Klaus Dieter; Marotz, Günter; Mayer-Vorfelder, Hans-Jörg; Miller, Rudolf; Plate, Erich J.; Radomski, Helge; Schwarz, Helmut; Vollmer, Ernst; Wildenhahn, Eberhard; 1967

8 Jumikis, Alfred: *Beitrag zur experimentellen Untersuchung des Wassernachschubs in einem gefrierenden Boden und die Beurteilung der Ergebnisse*, 1968

9 Marotz, Günter: *Technische Grundlagen einer Wasserspeicherung im natürlichen Untergrund*, 1968

10 Radomski, Helge: *Untersuchungen über den Einfluß der Querschnittsform wellenförmiger Spundwände auf die statischen und rammtechnischen Eigenschaften*, 1968

11 Schwarz, Helmut: *Die Grenztragfähigkeit des Baugrundes bei Einwirkung vertikal gezogener Ankerplatten als zweidimensionales Bruchproblem*, 1969

12 Erbel, Klaus: *Ein Beitrag zur Untersuchung der Metamorphose von Mittelgebirgsschneedecken unter besonderer Berücksichtigung eines Verfahrens zur Bestimmung der thermischen Schneequalität*, 1969

13 Westhaus, Karl-Heinz: *Der Strukturwandel in der Binnenschiffahrt und sein Einfluß auf den Ausbau der Binnenschiffskanäle*, 1969

14 Mayer-Vorfelder, Hans-Jörg: *Ein Beitrag zur Berechnung des Erdwiderstandes unter Ansatz der logarithmischen Spirale als Gleitflächenfunktion*, 1970

15 Schulz, Manfred: *Berechnung des räumlichen Erddruckes auf die Wandung kreiszylindrischer Körper*, 1970

16 Mobasseri, Manoutschehr: *Die Rippenstützmauer. Konstruktion und Grenzen ihrer Standsicherheit*, 1970

17 Benk, Dieter: *Ein Beitrag zum Betrieb und zur Bemessung von Hochwasserrückhaltebecken*, 1970

18 Gàl, Attila: *Bestimmung der mitschwingenden Wassermasse bei überströmten Fischbauchklappen mit kreiszylindrischem Staublech*, 1971, *vergriffen*

19 Kuz, Klaus Dieter: *Ein Beitrag zur Frage des Einsetzens von Kavitationserscheinungen in einer Düsenströmung bei Berücksichtigung der im Wasser gelösten Gase*, 1971, *vergriffen*

20 Schaak, Hartmut: *Verteilleitungen von Wasserkraftanlagen*, 1971

21 *Sonderheft zur Eröffnung der neuen Versuchsanstalt des Instituts für Wasserbau der Universität Stuttgart mit Beiträgen von* Brombach, Hansjörg; Dirksen, Wolfram; Gàl, Attila; Gerlach, Reinhard; Giesecke, Jürgen; Holthoff, Franz-Josef; Kuz, Klaus Dieter; Marotz, Günter; Minor, Hans-Erwin; Petrikat, Kurt; Röhnisch, Arthur; Rueff, Helge; Schwarz, Helmut; Vollmer, Ernst; Wildenhahn, Eberhard; 1972

22 Wang, Chung-su: *Ein Beitrag zur Berechnung der Schwingungen an Kegelstrahlschiebern*, 1972

23 Mayer-Vorfelder, Hans-Jörg: *Erdwiderstandsbeiwerte nach dem Ohde-Variationsverfahren*, 1972

24 Minor, Hans-Erwin: *Beitrag zur Bestimmung der Schwingungsanfachungsfunktionen überströmter Stauklappen*, 1972, *vergriffen*

25 Brombach, Hansjörg: *Untersuchung strömungsmechanischer Elemente (Fluidik) und die Möglichkeit der Anwendung von Wirbelkammerelementen im Wasserbau*, 1972, *vergriffen*

26 Wildenhahn, Eberhard: *Beitrag zur Berechnung von Horizontalfilterbrunnen*, 1972

27 Steinlein, Helmut: *Die Eliminierung der Schwebstoffe aus Flußwasser zum Zweck der unterirdischen Wasserspeicherung, gezeigt am Beispiel der Iller*, 1972

28 Holthoff, Franz Josef: *Die Überwindung großer Hubhöhen in der Binnenschiffahrt durch Schwimmerhebewerke*, 1973

29 Röder, Karl: *Einwirkungen aus Baugrundbewegungen auf trog- und kastenförmige Konstruktionen des Wasser- und Tunnelbaues*, 1973

30 Kretschmer, Heinz: *Die Bemessung von Bogenstaumauern in Abhängigkeit von der Talform*, 1973

31 Honekamp, Hermann: *Beitrag zur Berechnung der Montage von Unterwasserpipelines*, 1973

32 Giesecke, Jürgen: *Die Wirbelkammertriode als neuartiges Steuerorgan im Wasserbau*, und Brombach, Hansjörg: *Entwicklung, Bauformen, Wirkungsweise und Steuereigenschaften von Wirbelkammerverstärkern*, 1974

33 Rueff, Helge: *Untersuchung der schwingungserregenden Kräfte an zwei hintereinander angeordneten Tiefschützen unter besonderer Berücksichtigung von Kavitation*, 1974

34 Röhnisch, Arthur: *Einpreßversuche mit Zementmörtel für Spannbeton - Vergleich der Ergebnisse von Modellversuchen mit Ausführungen in Hüllwellrohren*, 1975

35 *Sonderheft anläßlich des 65. Geburtstages von Prof. Dr.-Ing. Kurt Petrikat mit Beiträgen von*: Brombach, Hansjörg; Erbel, Klaus; Flinspach, Dieter; Fischer jr., Richard; Gàl, Attila; Gerlach, Reinhard; Giesecke, Jürgen; Haberhauer, Robert; Hafner Edzard; Hausenblas, Bernhard; Horlacher, Hans-Burkhard; Hutarew, Andreas; Knoll, Manfred; Krummet, Ralph; Marotz, Günter; Merkle, Theodor; Miller, Christoph; Minor, Hans-Erwin; Neumayer, Hans; Rao, Syamala; Rath, Paul; Rueff, Helge; Ruppert, Jürgen; Schwarz, Wolfgang; Topal-Gökceli, Mehmet; Vollmer, Ernst; Wang, Chung-su; Weber, Hans-Georg; 1975

36 Berger, Jochum: *Beitrag zur Berechnung des Spannungszustandes in rotationssymmetrisch belasteten Kugelschalen veränderlicher Wandstärke unter Gas- und Flüssigkeitsdruck durch Integration schwach singulärer Differentialgleichungen*, 1975

37 Dirksen, Wolfram: *Berechnung instationärer Abflußvorgänge in gestauten Gerinnen mittels Differenzenverfahren und die Anwendung auf Hochwasserrückhaltebecken*, 1976

38 Horlacher, Hans-Burkhard: *Berechnung instationärer Temperatur- und Wärmespannungsfelder in langen mehrschichtigen Hohlzylindern*, 1976

39 Hafner, Edzard: *Untersuchung der hydrodynamischen Kräfte auf Baukörper im Tiefwasserbereich des Meeres*, 1977, ISBN 3-921694-39-6

40 Ruppert, Jürgen: *Über den Axialwirbelkammerverstärker für den Einsatz im Wasserbau*, 1977, ISBN 3-921694-40-X

41 Hutarew, Andreas: *Beitrag zur Beeinflußbarkeit des Sauerstoffgehalts in Fließgewässern an Abstürzen und Wehren*, 1977, ISBN 3-921694-41-8, *vergriffen*

42 Miller, Christoph: *Ein Beitrag zur Bestimmung der schwingungserregenden Kräfte an unterströmten Wehren*, 1977, ISBN 3-921694-42-6

43 Schwarz, Wolfgang: *Druckstoßberechnung unter Berücksichtigung der Radial- und Längsverschiebungen der Rohrwandung*, 1978, ISBN 3-921694-43-4

44 Kinzelbach, Wolfgang: *Numerische Untersuchungen über den optimalen Einsatz variabler Kühlsysteme einer Kraftwerkskette am Beispiel Oberrhein*, 1978, ISBN 3-921694-44-2

45 Barczewski, Baldur: *Neue Meßmethoden für Wasser-Luftgemische und deren Anwendung auf zweiphasige Auftriebsstrahlen*, 1979, ISBN 3-921694-45-0

46 Neumayer, Hans: *Untersuchung der Strömungsvorgänge in radialen Wirbelkammerverstärkern*, 1979, ISBN 3-921694-46-9

47 Elalfy, Youssef-Elhassan: *Untersuchung der Strömungsvorgänge in Wirbelkammerdioden und -drosseln*, 1979, ISBN 3-921694-47-7

48 Brombach, Hansjörg: *Automatisierung der Bewirtschaftung von Wasserspeichern*, 1981, ISBN 3-921694-48-5

49 Geldner, Peter: *Deterministische und stochastische Methoden zur Bestimmung der Selbstdichtung von Gewässern*, 1981, ISBN 3-921694-49-3, *vergriffen*

50 Mehlhorn, Hans: *Temperaturveränderungen im Grundwasser durch Brauchwassereinleitungen*, 1982, ISBN 3-921694-50-7, *vergriffen*

51 Hafner, Edzard: *Rohrleitungen und Behälter im Meer*, 1983, ISBN 3-921694-51-5

52 Rinnert, Bernd: *Hydrodynamische Dispersion in porösen Medien: Einfluß von Dichteunterschieden auf die Vertikalvermischung in horizontaler Strömung*, 1983, ISBN 3-921694-52-3, *vergriffen*

53 Lindner, Wulf: *Steuerung von Grundwasserentnahmen unter Einhaltung ökologischer Kriterien*, 1983, ISBN 3-921694-53-1, *vergriffen*

54 Herr, Michael; Herzer, Jörg; Kinzelbach, Wolfgang; Kobus, Helmut; Rinnert, Bernd: *Methoden zur rechnerischen Erfassung und hydraulischen Sanierung von Grundwasserkontaminationen*, 1983, ISBN 3-921694-54-X

55 Schmitt, Paul: *Wege zur Automatisierung der Niederschlagsermittlung*, 1984, ISBN 3-921694-55-8, *vergriffen*

56 Müller, Peter: *Transport und selektive Sedimentation von Schwebstoffen bei gestautem Abfluß*, 1985, ISBN 3-921694-56-6

57 El-Qawasmeh, Fuad: *Möglichkeiten und Grenzen der Tropfbewässerung unter besonderer Berücksichtigung der Verstopfungsanfälligkeit der Tropfelemente*, 1985, ISBN 3-921694-57-4, *vergriffen*

58 Kirchenbaur, Klaus: *Mikroprozessorgesteuerte Erfassung instationärer Druckfelder am Beispiel seegangsbelasteter Baukörper*, 1985, ISBN 3-921694-58-2

59 Kobus, Helmut (Hrsg.): *Modellierung des großräumigen Wärme- und Schadstofftransports im Grundwasser*, Tätigkeitsbericht 1984/85 (DFG-Forschergruppe an den Universitäten Hohenheim, Karlsruhe und Stuttgart), 1985, ISBN 3-921694-59-0, *vergriffen*

60 Spitz, Karlheinz: *Dispersion in porösen Medien: Einfluß von Inhomogenitäten und Dichteunterschieden*, 1985, ISBN 3-921694-60-4, *vergriffen*

61 Kobus, Helmut: *An Introduction to Air-Water Flows in Hydraulics*, 1985, ISBN 3-921694-61-2

62 Kaleris, Vassilios: *Erfassung des Austausches von Oberflächen- und Grundwasser in horizontalebenen Grundwassermodellen*, 1986, ISBN 3-921694-62-0

63 Herr, Michael: *Grundlagen der hydraulischen Sanierung verunreinigter Porengrundwasserleiter*, 1987, ISBN 3-921694-63-9

64 Marx, Walter: *Berechnung von Temperatur und Spannung in Massenbeton infolge Hydratation*, 1987, ISBN 3-921694-64-7

65 Koschitzky, Hans-Peter: *Dimensionierungskonzept für Sohlbelüfter in Schußrinnen zur Vermeidung von Kavitationsschäden*, 1987, ISBN 3-921694-65-5

66 Kobus, Helmut (Hrsg.): *Modellierung des großräumigen Wärme- und Schadstofftransports im Grundwasser*, Tätigkeitsbericht 1986/87 (DFG-Forschergruppe an den Universitäten Hohenheim, Karlsruhe und Stuttgart) 1987, ISBN 3-921694-66-3

67 Söll, Thomas: *Berechnungsverfahren zur Abschätzung anthropogener Temperaturanomalien im Grundwasser*, 1988, ISBN 3-921694-67-1

68 Dittrich, Andreas; Westrich, Bernd: *Bodenseeufererosion, Bestandsaufnahme und Bewertung*, 1988, ISBN 3-921694-68-X, *vergriffen*

69 Huwe, Bernd; van der Ploeg, Rienk R.: *Modelle zur Simulation des Stickstoffhaushaltes von Standorten mit unterschiedlicher landwirtschaftlicher Nutzung*, 1988, ISBN 3-921694-69-8, *vergriffen*

70 Stephan, Karl: *Integration elliptischer Funktionen*, 1988, ISBN 3-921694-70-1

71 Kobus, Helmut; Zilliox, Lothaire (Hrsg.): *Nitratbelastung des Grundwassers, Auswirkungen der Landwirtschaft auf die Grundwasser- und Rohwasserbeschaffenheit und Maßnahmen zum Schutz des Grundwassers*. Vorträge des deutsch-französischen Kolloquiums am 6. Oktober 1988, Universitäten Stuttgart und Louis Pasteur Strasbourg (Vorträge in deutsch oder französisch, Kurzfassungen zweisprachig), 1988,

ISBN 3-921694-71-X

72 Soyeaux, Renald: *Unterströmung von Stauanlagen auf klüftigem Untergrund unter Berücksichtigung laminarer und turbulenter Fließzustände*,1991, ISBN 3-921694-72-8

73 Kohane, Roberto: *Berechnungsmethoden für Hochwasserabfluß in Fließgewässern mit überströmten Vorländern*, 1991, ISBN 3-921694-73-6

74 Hassinger, Reinhard: *Beitrag zur Hydraulik und Bemessung von Blocksteinrampen in flexibler Bauweise*, 1991, ISBN 3-921694-74-4, *vergriffen*

75 Schäfer, Gerhard: *Einfluß von Schichtenstrukturen und lokalen Einlagerungen auf die Längsdispersion in Porengrundwasserleitern*, 1991, ISBN 3-921694-75-2

76 Giesecke, Jürgen: *Vorträge, Wasserwirtschaft in stark besiedelten Regionen; Umweltforschung mit Schwerpunkt Wasserwirtschaft*, 1991, ISBN 3-921694-76-0

77 Huwe, Bernd: *Deterministische und stochastische Ansätze zur Modellierung des Stickstoffhaushalts landwirtschaftlich genutzter Flächen auf unterschiedlichem Skalenniveau*, 1992, ISBN 3-921694-77-9, *vergriffen*

78 Rommel, Michael: *Verwendung von Kluftdaten zur realitätsnahen Generierung von Kluftnetzen mit anschließender laminar-turbulenter Strömungsberechnung*, 1993, ISBN 3-92 1694-78-7

79 Marschall, Paul: *Die Ermittlung lokaler Stofffrachten im Grundwasser mit Hilfe von Einbohrloch-Meßverfahren*, 1993, ISBN 3-921694-79-5, *vergriffen*

80 Ptak, Thomas: *Stofftransport in heterogenen Porenaquiferen: Felduntersuchungen und stochastische Modellierung*, 1993, ISBN 3-921694-80-9, *vergriffen*

81 Haakh, Frieder: *Transientes Strömungsverhalten in Wirbelkammern,* 1993, ISBN 3-921694-81-7

82 Kobus, Helmut; Cirpka, Olaf; Barczewski, Baldur; Koschitzky, Hans-Peter: *Versuchseinrichtung zur Grundwasser- und Altlastensanierung VEGAS, Konzeption und Programmrahmen*, 1993, ISBN 3-921694-82-5

83 Zang, Weidong: *Optimaler Echtzeit-Betrieb eines Speichers mit aktueller Abflußregenerierung*, 1994, ISBN 3-921694-83-3, *vergriffen*

84 Franke, Hans-Jörg: *Stochastische Modellierung eines flächenhaften Stoffeintrages und Transports in Grundwasser am Beispiel der Pflanzenschutzmittelproblematik*, 1995, ISBN 3-921694-84-1

85 Lang, Ulrich: *Simulation regionaler Strömungs- und Transportvorgänge in Karstaquiferen mit Hilfe des Doppelkontinuum-Ansatzes: Methodenentwicklung und Parameteridenti-fikation*, 1995, ISBN 3-921694-85-X, *vergriffen*

86 Helmig, Rainer: *Einführung in die Numerischen Methoden der Hydromechanik*, 1996, ISBN 3-921694-86-8, *vergriffen*

87 Cirpka, Olaf: *CONTRACT: A Numerical Tool for Contaminant Transport and Chemical Transformations - Theory and Program Documentation -*, 1996, ISBN 3-921694-87-6

88 Haberlandt, Uwe: *Stochastische Synthese und Regionalisierung des Niederschlages für Schmutzfrachtberechnungen*, 1996, ISBN 3-921694-88-4

89 Croisé, Jean: *Extraktion von flüchtigen Chemikalien aus natürlichen Lockergesteinen mittels erzwungener Luftströmung*, 1996, ISBN 3-921694-89-2, *vergriffen*

90 Jorde, Klaus: *Ökologisch begründete, dynamische Mindestwasserregelungen bei Ausleitungskraftwerken*, 1997, ISBN 3-921694-90-6, *vergriffen*

91 Helmig, Rainer: *Gekoppelte Strömungs- und Transportprozesse im Untergrund - Ein Beitrag zur Hydrosystemmodellierung-*, 1998, ISBN 3-921694-91-4, *vergriffen*

92 Emmert, Martin: *Numerische Modellierung nichtisothermer Gas-Wasser Systeme in porösen Medien,* 1997, ISBN 3-921694-92-2

93 Kern, Ulrich: *Transport von Schweb- und Schadstoffen in staugeregelten Fließgewässern am Beispiel des Neckars*, 1997, ISBN 3-921694-93-0, *vergriffen*

94 Förster, Georg: *Druckstoßdämpfung durch große Luftblasen in Hochpunkten von Rohrleitungen 1997*, ISBN 3-921694-94-9

95 Cirpka, Olaf: *Numerische Methoden zur Simulation des reaktiven Mehrkomponententransports im Grundwasser*, 1997, ISBN 3-921694-95-7, *vergriffen*

96 Färber, Arne: *Wärmetransport in der ungesättigten Bodenzone: Entwicklung einer thermischen In-situ-Sanierungstechnologie*, 1997, ISBN 3-921694-96-5

97 Betz, Christoph: *Wasserdampfdestillation von Schadstoffen im porösen Medium: Entwicklung einer thermischen In-situ-Sanierungstechnologie*, 1998, SBN 3-921694-97-3

98 Xu, Yichun: *Numerical Modeling of Suspended Sediment Transport in Rivers*, 1998, ISBN 3-921694-98-1, *vergriffen*

99 Wüst, Wolfgang: *Geochemische Untersuchungen zur Sanierung CKW-kontaminierter Aquifere mit Fe(0)-Reaktionswänden,* 2000, ISBN 3-933761-02-2

100 Sheta, Hussam: *Simulation von Mehrphasenvorgängen in porösen Medien unter Einbeziehung von Hysterese-Effekten*, 2000, ISBN 3-933761-03-4

101 Ayros, Edwin: *Regionalisierung extremer Abflüsse auf der Grundlage statistischer Verfahren*, 2000, ISBN 3-933761-04-2, *vergriffen*

102 Huber, Ralf: *Compositional Multiphase Flow and Transport in Heterogeneous Porous Media*, 2000, ISBN 3-933761-05-0

103 Braun, Christopherus: *Ein Upscaling-Verfahren für Mehrphasenströmungen in porösen Medien*, 2000, ISBN 3-933761-06-9

104 Hofmann, Bernd: *Entwicklung eines rechnergestützten Managementsystems zur Beurteilung von Grundwasserschadensfällen*, 2000, ISBN 3-933761-07-7

105 Class, Holger: *Theorie und numerische Modellierung nichtisothermer Mehrphasenprozesse in NAPL-kontaminierten porösen Medien,* 2001, ISBN 3-933761-08-5

106 Schmidt, Reinhard: *Wasserdampf- und Heißluftinjektion zur thermischen Sanierung kontaminierter Standorte*, 2001, ISBN 3-933761-09-3

107 Josef, Reinhold: *Schadstoffextraktion mit hydraulischen Sanierungsverfahren unter Anwendung von grenzflächenaktiven Stoffen*, 2001, ISBN 3-933761-10-7

108 Schneider, Matthias: *Habitat- und Abflussmodellierung für Fließgewässer mit unscharfen Berechnungsansätzen*, 2001, ISBN 3-933761-11-5

109 Rathgeb, Andreas: *Hydrodynamische Bemessungsgrundlagen für Lockerdeckwerke an überströmbaren Erddämmen*, 2001, ISBN 3-933761-12-3

110 Lang, Stefan: *Parallele numerische Simulation instätionärer Probleme mit adaptiven Methoden auf unstrukturierten Gittern*, 2001, ISBN 3-933761-13-1

111 Appt, Jochen; Stumpp Simone: *Die Bodensee-Messkampagne 2001, IWS/CWR Lake Constance Measurement Program 2001*, 2002, ISBN 3-933761-14-X

112 Heimerl, Stephan: *Systematische Beurteilung von Wasserkraftprojekten,* 2002, ISBN 3-933761-15-8, *vergriffen*

113 Iqbal, Amin: *On the Management and Salinity Control of Drip Irrigation,* 2002, ISBN 3-933761-16-6

114 Silberhorn-Hemminger, Annette: *Modellierung von Kluftaquifersystemen: Geostatistische Analyse und deterministisch-stochastische Kluftgenerierung,* 2002, ISBN 3-933761-17-4

115 Winkler, Angela: *Prozesse des Wärme- und Stofftransports bei der In-situ-Sanierung mit festen Wärmequellen,* 2003, ISBN 3-933761-18-2

116 Marx, Walter: *Wasserkraft, Bewässerung, Umwelt - Planungs- und Bewertungsschwerpunkte der Wasserbewirtschaftung,* 2003, ISBN 3-933761-19-0

117 Hinkelmann, Reinhard: *Efficient Numerical Methods and Information-Processing Techniques in Environment Water,* 2003, ISBN 3-933761-20-4

118 Samaniego-Eguiguren, Luis Eduardo: *Hydrological Consequences of Land Use / Land Cover and Climatic Changes in Mesoscale Catchments*, 2003, ISBN 3-933761-21-2

119 Neunhäuserer, Lina: *Diskretisierungsansätze zur Modellierung von Strömungs- und Transportprozessen in geklüftet-porösen Medien*, 2003, ISBN 3-933761-22-0

120 Paul, Maren: *Simulation of Two-Phase Flow in Heterogeneous Poros Media with Adaptive Methods*, 2003, ISBN 3-933761-23-9

121 Ehret, Uwe: *Rainfall and Flood Nowcasting in Small Catchments using Weather Radar*, 2003, ISBN 3-933761-24-7

122 Haag, Ingo: *Der Sauerstoffhaushalt staugeregelter Flüsse am Beispiel des Neckars - Analysen, Experimente, Simulationen -,* 2003, ISBN 3-933761-25-5

123 Appt, Jochen: *Analysis of Basin-Scale Internal Waves in Upper Lake Constance,* 2003, ISBN 3-933761-26-3

124 Hrsg.: Schrenk, Volker; Batereau, Katrin; Barczewski, Baldur; Weber, Karolin und Koschitzky, Hans-Peter: *Symposium Ressource Fläche und VEGAS - Statuskolloquium 2003, 30. September und 1. Oktober 2003,* 2003, ISBN 3-933761-27-1

125 Omar Khalil Ouda: *Optimisation of Agricultural Water Use: A Decision Support System for the Gaza Strip,* 2003, ISBN 3-933761-28-0

126 Batereau, Katrin: *Sensorbasierte Bodenluftmessung zur Vor-Ort-Erkundung von Schadensherden im Untergrund*, 2004, ISBN 3-933761-29-8

127 Witt, Oliver: *Erosionsstabilität von Gewässersedimenten mit Auswirkung auf den Stofftransport bei Hochwasser am Beispiel ausgewählter Stauhaltungen des Oberrheins*, 2004, ISBN 3-933761-30-1

128 Jakobs, Hartmut: *Simulation nicht-isothermer Gas-Wasser-Prozesse in komplexen Kluft-Matrix-Systemen*, 2004, ISBN 3-933761-31-X

129 Li, Chen-Chien: *Deterministisch-stochastisches Berechnungskonzept zur Beurteilung der Auswirkungen erosiver Hochwasserereignisse in Flussstauhaltungen,* 2004, ISBN 3-933761-32-8

130 Reichenberger, Volker; Helmig, Rainer; Jakobs, Hartmut; Bastian, Peter; Niessner, Jennifer: *Complex Gas-Water Processes in Discrete Fracture-Matrix Systems: Up-scaling, Mass-Conservative Discretization and Efficient Multilevel Solution,* 2004, ISBN 3-933761-33-6

131 Hrsg.: Barczewski, Baldur; Koschitzky, Hans-Peter; Weber, Karolin; Wege, Ralf: *VEGAS - Statuskolloquium 2004,* Tagungsband zur Veranstaltung am 05. Oktober 2004 an der Universität Stuttgart, Campus Stuttgart-Vaihingen, 2004, ISBN 3-933761-34-4

132 Asie, Kemal Jabir: *Finite Volume Models for Multiphase Multicomponent Flow through Porous Media*. 2005, ISBN 3-933761-35-2

133 Jacoub, George: *Development of a 2-D Numerical Module for Particulate Contaminant Transport in Flood Retention Reservoirs and Impounded Rivers,* 2004, ISBN 3-933761-36-0

134 Nowak, Wolfgang: *Geostatistical Methods for the Identification of Flow and Transport Parameters in the Subsurface,* 2005, ISBN 3-933761-37-9

135 Süß, Mia: *Analysis of the influence of structures and boundaries on flow and transport processes in fractured porous media*, 2005, ISBN 3-933761-38-7

136 Jose, Surabhin Chackiath: *Experimental Investigations on Longitudinal Dispersive Mixing in Heterogeneous Aquifers,* 2005, ISBN: 3-933761-39-5

137 Filiz, Fulya: *Linking Large-Scale Meteorological Conditions to Floods in Mesoscale Catchments,* 2005, ISBN 3-933761-40-9

138 Qin, Minghao: *Wirklichkeitsnahe und recheneffiziente Ermittlung von Temperatur und Spannungen bei großen RCC-Staumauern*, 2005, ISBN 3-933761-41-7

139 Kobayashi, Kenichiro: *Optimization Methods for Multiphase Systems in the Subsurface - Application to Methane Migration in Coal Mining Areas*, 2005, ISBN 3-933761-42-5

140 Rahman, Md. Arifur: *Experimental Investigations on Transverse Dispersive Mixing in Heterogeneous Porous Media,* 2005, ISBN 3-933761-43-3

141 Schrenk, Volker: *Ökobilanzen zur Bewertung von Altlastensanierungsmaßnahmen,* 2005, ISBN 3-933761-44-1

142 Hundecha, Hirpa Yeshewatesfa: *Regionalization of Parameters of a Conceptual Rainfall-Runoff Model*, 2005, ISBN: 3-933761-45-X

143 Wege, Ralf: *Untersuchungs- und Überwachungsmethoden für die Beurteilung natürlicher Selbstreinigungsprozesse im Grundwasser,* 2005, ISBN 3-933761-46-8

144 Breiting, Thomas: *Techniken und Methoden der Hydroinformatik - Modellierung von komplexen Hydrosystemen im Untergrund*, 2006, ISBN 3-933761-47-6

145 Hrsg.: Braun, Jürgen; Koschitzky, Hans-Peter; Müller, Martin: *Ressource Untergrund: 10 Jahre VEGAS: Forschung und Technologieentwicklung zum Schutz von Grundwasser und Boden,* Tagungsband zur Veranstaltung am 28. und 29. September 2005 an der Universität Stuttgart, Campus Stuttgart-Vaihingen, 2005, ISBN 3-933761-48-4

146 Rojanschi, Vlad: *Abflusskonzentration in mesoskaligen Einzugsgebieten unter Berücksichtigung des Sickerraumes,* 2006, ISBN 3-933761-49-2

147 Winkler, Nina Simone: *Optimierung der Steuerung von Hochwasserrückhaltebeckensystemen,* 2006, ISBN 3-933761-50-6

148 Wolf, Jens: *Räumlich differenzierte Modellierung der Grundwasserströmung alluvialer Aquifere für mesoskalige Einzugsgebiete*, 2006, ISBN: 3-933761-51-4

149 Kohler, Beate: *Externe Effekte der Laufwasserkraftnutzung*, 2006, ISBN 3-933761-52-2

150 Hrsg.: Braun, Jürgen; Koschitzky, Hans-Peter; Stuhrmann, Matthias: *VEGAS-Statuskolloquium 2006,* Tagungsband zur Veranstaltung am 28. September 2006 an der Universität Stuttgart, Campus Stuttgart-Vaihingen, 2006, ISBN 3-933761-53-0

151 Niessner, Jennifer: *Multi-Scale Modeling of Multi-Phase - Multi-Component Processes in Heterogeneous Porous Media*, 2006, ISBN 3-933761-54-9

152 Fischer, Markus: *Beanspruchung eingeerdeter Rohrleitungen infolge Austrocknung bindiger Böden,* 2006, ISBN 3-933761-55-7

153 Schneck, Alexander: *Optimierung der Grundwasserbewirtschaftung unter Berücksichtigung der Belange der Wasserversorgung, der Landwirtschaft und des Naturschutzes*, 2006, ISBN 3-933761-56-5

154 Das, Tapash: *The Impact of Spatial Variability of Precipitation on the Predictive Uncertainty of Hydrological Models,* 2006, ISBN 3-33761-57-3

155 Bielinski, Andreas: *Numerical Simulation of CO_2 sequestration in geological formations*, 2007, ISBN 3-933761-58-1

156 Mödinger, Jens: *Entwicklung eines Bewertungs- und Entscheidungsunterstützungssystems für eine nachhaltige regionale Grundwasserbewirtschaftung*, 2006, ISBN 3-933761-60-3

157 Manthey, Sabine: *Two-phase flow processes with dynamic effects in porous media - parameter estimation and simulation,* 2007, ISBN 3-933761-61-1

158 Pozos Estrada, Oscar: *Investigation on the Effects of Entrained Air in Pipelines,* 2007, ISBN 3-933761-62-X

159 Ochs, Steffen Oliver: *Steam injection into saturated porous media – process analysis including experimental and numerical investigations*, 2007, ISBN 3-933761-63-8

160 Marx, Andreas: *Einsatz gekoppelter Modelle und Wetterradar zur Abschätzung von Niederschlagsintensitäten und zur Abflussvorhersage, 2007,* ISBN 3-933761-64-6

161 Hartmann, Gabriele Maria: *Investigation of Evapotranspiration Concepts in Hydrological Modelling for Climate Change Impact Assessment*, 2007, ISBN 3-933761-65-4

162 Kebede Gurmessa, Tesfaye: *Numerical Investigation on Flow and Transport Characteristics to Improve Long-Term Simulation of Reservoir Sedimentation*, 2007, ISBN 3-933761-66-2

163 Trifković, Aleksandar: *Multi-objective and Risk-based Modelling Methodology for Planning, Design and Operation of Water Supply Systems*, 2007, ISBN 3-933761-67-0

164 Götzinger, Jens: *Distributed Conceptual Hydrological Modelling - Simulation of Climate, Land Use Change Impact and Uncertainty Analysis*, 2007, ISBN 3-933761-68-9

165 Hrsg.: Braun, Jürgen; Koschitzky, Hans-Peter; Stuhrmann, Matthias: *VEGAS – Kolloquium 2007,* Tagungsband zur Veranstaltung am 26. September 2007 an der Universität Stuttgart, Campus Stuttgart-Vaihingen, 2007, ISBN 3-933761-69-7

166 Freeman, Beau: *Modernization Criteria Assessment for Water Resources Planning; Klamath Irrigation Project, U.S.*, 2008, ISBN 3-933761-70-0

167 Dreher, Thomas: *Selektive Sedimentation von Feinstschwebstoffen in Wechselwirkung mit wandnahen turbulenten Strömungsbedingungen*, 2008, ISBN 3-933761-71-9

168 Yang, Wei: *Discrete-Continuous Downscaling Model for Generating Daily Precipitation Time Series*, 2008, ISBN 3-933761-72-7

169 Kopecki, Ianina: *Calculational Approach to FST-Hemispheres for Multiparametrical Benthos Habitat Modelling,* 2008*,* ISBN 3-933761-73-5

170 Brommundt, Jürgen: *Stochastische Generierung räumlich zusammenhängender Niederschlagszeitreihen*, 2008, ISBN 3-933761-74-3

171 Papafotiou, *Alexandros: Numerical Investigations of the Role of Hysteresis in Heterogeneous Two-Phase Flow Systems*, 2008, ISBN 3-933761-75-1

172 He, Yi: *Application of a Non-Parametric Classification Scheme to Catchment Hydrology*, 2008, ISBN 978-3-933761-76-7

173 Wagner, Sven: *Water Balance in a Poorly Gauged Basin in West Africa Using Atmospheric Modelling and Remote Sensing Information*, 2008, ISBN 978-3-933761-77-4

174 Hrsg.: Braun, Jürgen; Koschitzky, Hans-Peter; Stuhrmann, Matthias; Schrenk, Volker: *VEGAS-Kolloquium 2008 Ressource Fläche III*, Tagungsband zur Veranstaltung am 01. Oktober 2008 an der Universität Stuttgart, Campus Stuttgart-Vaihingen, 2008, ISBN 978-3-933761-78-1

175 Patil, Sachin: *Regionalization of an Event Based Nash Cascade Model for Flood Predictions in Ungauged Basins*, 2008, ISBN 978-3-933761-79-8

176 Assteerawatt, Anongnart: *Flow and Transport Modelling of Fractured Aquifers based on a Geostatistical Approach,* 2008, ISBN 978-3-933761-80-4

177 Karnahl, Joachim Alexander: *2D numerische Modellierung von multifraktionalem Schwebstoff- und Schadstofftransport in Flüssen*, 2008, ISBN 978-3-933761-81-1

178 Hiester, Uwe: *Technologieentwicklung zur In-situ-Sanierung der ungesättigten Bodenzone mit festen Wärmequellen,* 2009, ISBN 978-3-933761-82-8

179 Laux, Patrick: *Statistical Modeling of Precipitation for Agricultural Planning in the Volta Basin of West Africa,* 2009, ISBN 978-3-933761-83-5

180 Ehsan, Saqib: *Evaluation of Life Safety Risks Related to Severe Flooding,* 2009, ISBN 978-3-933761-84-2

181 Prohaska, Sandra: *Development and Application of a 1D Multi-Strip Fine Sediment Transport Model for Regulated Rivers,* 2009, ISBN 978-3-933761-85-9

182 Kopp, Andreas: *Evaluation of CO_2 Injection Processes in Geological Formations for Site Screening,* 2009, ISBN 978-3-933761-86-6

183 Ebigbo, Anozie: *Modelling of biofilm growth and its influence on CO_2 and water (two-phase) flow in porous media,* 2009, ISBN 978-3-933761-87-3

184 Freiboth, Sandra: *A phenomenological model for the numerical simulation of multiphase multicomponent processes considering structural alterations of porous media*, 2009, ISBN 978-3-933761-88-0

185 Zöllner, Frank: *Implementierung und Anwendung netzfreier Methoden im Konstruktiven Wasserbau und in der Hydromechanik*, 2009, ISBN 978-3-933761-89-7

186 Vasin, Milos: *Influence of the soil structure and property contrast on flow and transport in the unsaturated zone*, 2010, ISBN 978-3-933761-90-3

187 Li, Jing: *Application of Copulas as a New Geostatistical Tool*, 2010, ISBN 978-3-933761-91-0

188 AghaKouchak, Amir: *Simulation of Remotely Sensed Rainfall Fields Using Copulas*, 2010, ISBN 978-3-933761-92-7

189 Thapa, Pawan Kumar: *Physically-based spatially distributed rainfall runoff modelling for soil erosion estimation*, 2010, ISBN 978-3-933761-93-4

190 Wurms, Sven: *Numerische Modellierung der Sedimentationsprozesse in Retentionsanlagen zur Steuerung von Stoffströmen bei extremen Hochwasserabflussereignissen*, 2011, ISBN 978-3-933761-94-1

191 Merkel, Uwe: *Unsicherheitsanalyse hydraulischer Einwirkungen auf Hochwasserschutzdeiche und Steigerung der Leistungsfähigkeit durch adaptive Strömungsmodellierung*, 2011, ISBN 978-3-933761-95-8

192 Fritz, Jochen: *A Decoupled Model for Compositional Non-Isothermal Multiphase Flow in Porous Media and Multiphysics Approaches for Two-Phase Flow*, 2010, ISBN 978-3-933761-96-5

193 Weber, Karolin (Hrsg.): *12. Treffen junger WissenschaftlerInnen an Wasserbauinstituten*, 2010, ISBN 978-3-933761-97-2

194 Bliefernicht, Jan-Geert: *Probability Forecasts of Daily Areal Precipitation for Small River Basins,* 2011, ISBN 978-3-933761-98-9

195 Hrsg.: Koschitzky, Hans-Peter; Braun, Jürgen: *VEGAS-Kolloquium 2010 In-situ-Sanierung - Stand und Entwicklung Nano und ISCO -,* Tagungsband zur Veranstaltung am 07. Oktober 2010 an der Universität Stuttgart, Campus Stuttgart-Vaihingen*,* 2010*,* ISBN 978-3-933761-99-6

196 Gafurov, Abror: *Water Balance Modeling Using Remote Sensing Information - Focus on Central Asia,* 2010, ISBN 978-3-942036-00-9

197 Mackenberg, Sylvia: *Die Quellstärke in der Sickerwasserprognose: Möglichkeiten und Grenzen von Labor- und Freilanduntersuchungen,* 2010, ISBN 978-3-942036-01-6

198 Singh, Shailesh Kumar: *Robust Parameter Estimation in Gauged and Ungauged Basins,* 2010, ISBN 978-3-942036-02-3

199 Doğan, Mehmet Onur: *Coupling of porous media flow with pipe flow,* 2011, ISBN 978-3-942036-03-0

200 Liu, Min: *Study of Topographic Effects on Hydrological Patterns and the Implication on Hydrological Modeling and Data Interpolation,* 2011, ISBN 978-3-942036-04-7

201 Geleta, Habtamu Itefa: *Watershed Sediment Yield Modeling for Data Scarce Areas,* 2011, ISBN 978-3-942036-05-4

202 Franke, Jörg: *Einfluss der Überwachung auf die Versagenswahrscheinlichkeit von Staustufen,* 2011, ISBN 978-3-942036-06-1

203 Bakimchandra, Oinam: *Integrated Fuzzy-GIS approach for assessing regional soil erosion risks,* 2011, ISBN 978-3-942036-07-8

204 Alam, Muhammad Mahboob: *Statistical Downscaling of Extremes of Precipitation in Mesoscale Catchments from Different RCMs and Their Effects on Local Hydrology,* 2011, ISBN 978-3-942036-08-5

205 Hrsg.: Koschitzky, Hans-Peter; Braun, Jürgen: *VEGAS-Kolloquium 2011 Flache Geothermie - Perspektiven und Risiken,* Tagungsband zur Veranstaltung am 06. Oktober 2011 an der Universität Stuttgart, Campus Stuttgart-Vaihingen*,* 2011*,* ISBN 978-3-933761-09-2

206 Haslauer, Claus: *Analysis of Real-World Spatial Dependence of Subsurface Hydraulic Properties Using Copulas with a Focus on Solute Transport Behaviour,* 2011,

ISBN 978-3-942036-10-8

207 Dung, Nguyen Viet: *Multi-objective automatic calibration of hydrodynamic models – development of the concept and an application in the Mekong Delta,* 2011, ISBN 978-3-942036-11-5

208 Hung, Nguyen Nghia: *Sediment dynamics in the floodplain of the Mekong Delta, Vietnam,* 2011, ISBN 978-3-942036-12-2

209 Kuhlmann, Anna: *Influence of soil structure and root water uptake on flow in the unsaturated zone,* 2012, ISBN 978-3-942036-13-9

210 Tuhtan, Jeffrey Andrew: *Including the Second Law Inequality in Aquatic Ecodynamics: A Modeling Approach for Alpine Rivers Impacted by Hydropeaking,* 2012, ISBN 978-3-942036-14-6

211 Tolossa, Habtamu: *Sediment Transport Computation Using a Data-Driven Adaptive Neuro-Fuzzy Modelling Approach,* 2012, ISBN 978-3-942036-15-3

212 Tatomir, Alexandru-Bodgan: *From Discrete to Continuum Concepts of Flow in Fractured Porous Media,* 2012, ISBN 978-3-942036-16-0

213 Erbertseder, Karin: *A Multi-Scale Model for Describing Cancer-Therapeutic Transport in the Human Lung,* 2012, ISBN 978-3-942036-17-7

214 Noack, Markus: *Modelling Approach for Interstitial Sediment Dynamics and Reproduction of Gravel Spawning Fish,* 2012, ISBN 978-3-942036-18-4

215 De Boer, Cjestmir Volkert: *Transport of Nano Sized Zero Valent Iron Colloids during Injection into the Subsurface*, 2012, ISBN 978-3-942036-19-1

216 Pfaff, Thomas: *Processing and Analysis of Weather Radar Data for Use in Hydrology*, 2013, ISBN 978-3-942036-20-7

217 Lebrenz, Hans-Henning: *Addressing the Input Uncertainty for Hydrological Modeling by a New Geostatistical Method*, 2013, ISBN 978-3-942036-21-4

218 Darcis, Melanie Yvonne: *Coupling Models of Different Complexity for the Simulation of CO_2 Storage in Deep Saline Aquifers*, 2013, ISBN 978-3-942036-22-1

219 Beck, Ferdinand: *Generation of Spatially Correlated Synthetic Rainfall Time Series in High Temporal Resolution - A Data Driven Approach*, 2013, ISBN 978-3-942036-23-8

220 Guthke, Philipp: *Non-multi-Gaussian spatial structures: Process-driven natural genesis, manifestation, modeling approaches, and influences on dependent processes*, 2013, ISBN 978-3-942036-24-5

221 Walter, Lena: *Uncertainty studies and risk assessment for CO_2 storage in geological formations*, 2013, ISBN 978-3-942036-25-2

222 Wolff, Markus: *Multi-scale modeling of two-phase flow in porous media including capillary pressure effects,* 2013, ISBN 978-3-942036-26-9

223 Mosthaf, Klaus Roland: *Modeling and analysis of coupled porous-medium and free flow with application to evaporation processes,* 2014, ISBN 978-3-942036-27-6

224 Leube, Philipp Christoph: *Methods for Physically-Based Model Reduction in Time: Analysis, Comparison of Methods and Application*, 2013, ISBN 978-3-942036-28-3

225 Rodríguez Fernández, Jhan Ignacio: *High Order Interactions among environmental variables: Diagnostics and initial steps towards modeling*, 2013, ISBN 978-3-942036-29-0

226 Eder, Maria Magdalena: *Climate Sensitivity of a Large Lake*, 2013, ISBN 978-3-942036-30-6

227 Greiner, Philipp: *Alkoholinjektion zur In-situ-Sanierung von CKW Schadensherden in Grundwasserleitern: Charakterisierung der relevanten Prozesse auf unterschiedlichen Skalen*, 2014, ISBN 978-3-942036-31-3

228 Lauser, Andreas: *Theory and Numerical Applications of Compositional Multi-Phase Flow in Porous Media*, 2014, ISBN 978-3-942036-32-0

229 Enzenhöfer, Rainer: *Risk Quantification and Management in Water Production and Supply Systems*, 2014, ISBN 978-3-942036-33-7

230 Faigle, Benjamin: *Adaptive modelling of compositional multi-phase flow with capillary pressure*, 2014, ISBN 978-3-942036-34-4

231 Oladyshkin, Sergey: *Efficient modeling of environmental systems in the face of complexity and uncertainty*, 2014, ISBN 978-3-942036-35-1

232 Sugimoto, Takayuki: *Copula based Stochastic Analysis of Discharge Time Series*, 2014, ISBN 978-3-942036-36-8

233 Koch, Jonas: *Simulation, Identification and Characterization of Contaminant Source Architectures in the Subsurface*, 2014, ISBN 978-3-942036-37-5

234 Zhang, Jin: *Investigations on Urban River Regulation and Ecological Rehabilitation Measures, Case of Shenzhen in China*, 2014, ISBN 978-3-942036-38-2

235 Siebel, Rüdiger: *Experimentelle Untersuchungen zur hydrodynamischen Belastung und Standsicherheit von Deckwerken an überströmbaren Erddämmen,* 2014, ISBN 978-3-942036-39-9

236 Baber, Katherina: *Coupling free flow and flow in porous media in biological and technical applications: From a simple to a complex interface description,* 2014, ISBN 978-3-942036-40-5

237 Nuske, Klaus Philipp: *Beyond Local Equilibrium — Relaxing local equilibrium assumptions in multiphase flow in porous media,* 2014, ISBN 978-3-942036-41-2

238 Geiges, Andreas: *Efficient concepts for optimal experimental design in nonlinear environmental systems*, 2014, ISBN 978-3-942036-42-9

239 Schwenck, Nicolas: *An XFEM-Based Model for Fluid Flow in Fractured Porous Media*, 2014, ISBN 978-3-942036-43-6

240 Chamorro Chávez, Alejandro: *Stochastic and hydrological modelling for climate change prediction in the Lima region, Peru*, 2015, ISBN 978-3-942036-44-3

241 Yulizar: *Investigation of Changes in Hydro-Meteorological Time Series Using a Depth-Based Approach*, 2015, ISBN 978-3-942036-45-0

242 Kretschmer, Nicole: *Impacts of the existing water allocation scheme on the Limarí watershed – Chile, an integrative approach*, 2015, ISBN 978-3-942036-46-7

243 Kramer, Matthias: *Luftbedarf von Freistrahlturbinen im Gegendruckbetrieb*, 2015, ISBN 978-3-942036-47-4

244 Hommel, Johannes: *Modeling biogeochemical and mass transport processes in the subsurface: Investigation of microbially induced calcite precipitation*, 2016, ISBN 978-3-942036-48-1

245 Germer, Kai: *Wasserinfiltration in die ungesättigte Zone eines makroporösen Hanges und deren Einfluss auf die Hangstabilität*, 2016, ISBN 978-3-942036-49-8

246 Hörning, Sebastian: *Process-oriented modeling of spatial random fields using copulas*, 2016, ISBN 978-3-942036-50-4

247 Jambhekar, Vishal: *Numerical modeling and analysis of evaporative salinization in a coupled free-flow porous-media system,* 2016, ISBN 978-3-942036-51-1

248 Huang, Yingchun: *Study on the spatial and temporal transferability of conceptual hydrological models*, 2016, ISBN 978-3-942036-52-8

249 Kleinknecht, Simon Matthias: *Migration and retention of a heavy NAPL vapor and remediation of the unsaturated zone*, 2016, ISBN 978-3-942036-53-5

250 Kwakye, Stephen Oppong: *Study on the effects of climate change on the hydrology of the West African sub-region*, 2016, ISBN 978-3-942036-54-2

251 Kissinger, Alexander: *Basin-Scale Site Screening and Investigation of Possible Impacts of CO_2 Storage on Subsurface Hydrosystems*, 2016, ISBN 978-3-942036-55-9

252 Müller, Thomas: *Generation of a Realistic Temporal Structure of Synthetic Precipitation Time Series for Sewer Applications*, 2017, ISBN 978-3-942036-56-6

253 Grüninger, Christoph: *Numerical Coupling of Navier-Stokes and Darcy Flow for Soil-Water Evaporation*, 2017, ISBN 978-3-942036-57-3

254 Suroso: *Asymmetric Dependence Based Spatial Copula Models: Empirical Investigations and Consequences on Precipitation Fields*, 2017, ISBN 978-3-942036-58-0

255 Müller, Thomas; Mosthaf, Tobias; Gunzenhauser, Sarah; Seidel, Jochen; Bárdossy, András: *Grundlagenbericht Niederschlags-Simulator (NiedSim3)*, 2017, ISBN 978-3-942036-59-7

256 Mosthaf, Tobias: *New Concepts for Regionalizing Temporal Distributions of Precipitation and for its Application in Spatial Rainfall Simulation,* 2017, ISBN 978-3-942036-60-3

257 Fenrich, Eva Katrin: *Entwicklung eines ökologisch-ökonomischen Vernetzungsmodells für Wasserkraftanlagen und Mehrzweckspeicher,* 2018, ISBN 978-3-942036-61-0

258 Schmidt, Holger: *Microbial stabilization of lotic fine sediments*, 2018, ISBN 978-3-942036-62-7

259 Fetzer, Thomas: *Coupled Free and Porous-Medium Flow Processes Affected by Turbulence and Roughness – Models, Concepts and Analysis*, 2018, ISBN 978-3-942036-63-4

260 Schröder, Hans Christoph: *Large-scale High Head Pico Hydropower Potential Assessment*, 2018, ISBN 978-3-942036-64-1

261 Bode, Felix: *Early-Warning Monitoring Systems for Improved Drinking Water Resource Protection*, 2018, ISBN 978-3-942036-65-8

262 Gebler, Tobias: *Statistische Auswertung von simulierten Talsperrenüberwachungsdaten zur Identifikation von Schadensprozessen an Gewichtsstaumauern*, 2018, ISBN 978-3-942036-66-5

263 Harten, Matthias von: *Analyse des Zuppinger-Wasserrades – Hydraulische Optimierungen unter Berücksichtigung ökologischer Aspekte*, 2018, ISBN 978-3-942036-67-2

264 Yan, Jieru: *Nonlinear estimation of short time precipitation using weather radar and surface observations*, 2018, ISBN 978-3-942036-68-9

265 Beck, Martin: *Conceptual approaches for the analysis of coupled hydraulic and geomechanical processes*, 2019, ISBN 978-3-942036-69-6

266 Haas, Jannik: *Optimal planning of hydropower and energy storage technologies for fully renewable power systems*, 2019, ISBN 978-3-942036-70-2

267 Schneider, Martin: *Nonlinear Finite Volume Schemes for Complex Flow Processes and Challenging Grids*, 2019, ISBN 978-3-942036-71-9

268 Most, Sebastian Christopher: *Analysis and Simulation of Anomalous Transport in Porous Media*, 2019, ISBN 978-3-942036-72-6

269 Buchta, Rocco: *Entwicklung eines Ziel- und Bewertungssystems zur Schaffung nachhaltiger naturnaher Strukturen in großen sandgeprägten Flüssen des norddeutschen Tieflandes*, 2019, ISBN 978-3-942036-73-3

270 Thom, Moritz: *Towards a Better Understanding of the Biostabilization Mechanisms of Sediment Beds*, 2019, ISBN 978-3-942036-74-0

271 Stolz, Daniel: *Die Nullspannungstemperatur in Gewichtsstaumauern unter Berücksichtigung der Festigkeitsentwicklung des Betons*, 2019, ISBN 978-3-942036-75-7

272 Rodriguez Pretelin, Abelardo: *Integrating transient flow conditions into groundwater well protection*, 2020, ISBN: 978-3-942036-76-4

273 Weishaupt, Kilian: *Model Concepts for Coupling Free Flow with Porous Medium Flow at the Pore-Network Scale: From Single-Phase Flow to Compositional Non-Isothermal Two-Phase Flow*, 2020, ISBN: 978-3-942036-77-1

274 Koch, Timo: *Mixed-dimension models for flow and transport processes in porous media with embedded tubular network systems*, 2020, ISBN: 978-3-942036-78-8

275 Gläser, Dennis: *Discrete fracture modeling of multi-phase flow and deformation in fractured poroelastic media*, 2020, ISBN: 978-3-942036-79-5

276 Seitz, Lydia: *Development of new methods to apply a multi-parameter approach – A first step towards the determination of colmation*, 2020, ISBN: 978-3-942036-80-1

277 Ebrahim Bakhshipour, Amin: *Optimizing hybrid decentralized systems for sustainable ur-ban drainage infrastructures planning*, 2021, ISBN: 978-3-942036-81-8

278 Seitz, Gabriele: *Modeling Fixed-Bed Reactors for Thermochemical Heat Storage with the Reaction System CaO/Ca(OH)$_2$*, 2021, ISBN: 978-3-942036-82-5

279 Emmert, Simon: *Developing and Calibrating a Numerical Model for Microbially Enhanced Coal-Bed Methane Production*, 2021, ISBN: 978-3-942036-83-2

280 Heck, Katharina Klara: *Modelling and analysis of multicomponent transport at the interface between free- and porous-medium flow - influenced by radiation and roughness*, 2021, ISBN: 978-3-942036-84-9

281 Ackermann, Sina: *A multi-scale approach for drop/porous-medium interaction*, 2021, ISBN: 978-3-942036-85-6

282 Beckers, Felix: *Investigations on Functional Relationships between Cohesive Sediment Erosion and Sediment Characteristics*, 2021, ISBN: 978-3-942036-86-3

283 Schlabing, Dirk: *Generating Weather for Climate Impact Assessment on Lakes*, 2021, ISBN: 978-3-942036-87-0

284 Becker, Beatrix: *Efficient multiscale multiphysics models accounting for reversible flow at various subsurface energy storage sites*, 2021, ISBN: 978-3-942036-88-7

285 Reuschen, Sebastian: *Bayesian Inversion and Model Selection of Heterogeneities in Geo-statistical Subsurface Modeling*, 2021, ISBN: 978-3-942036-89-4

286 Michalkowski, Cynthia: *Modeling water transport at the interface between porous GDL and gas distributor of a PEM fuel cell cathode*, 2022, ISBN: 978-3-942036-90-0

287 Koca, Kaan: *Advanced experimental methods for investigating flow-biofilm-sediment interactions*, 2022, ISBN: 978-3-942036-91-7

288 Modiri, Ehsan: *Clustering simultaneous occurrences of extreme floods in the Neckar catchment*, 2022, ISBN: 978-3-942036-92-4

289 Mayar, Mohammad Assem: *High-resolution spatio-temporal measurements of the colmation phenomenon under laboratory conditions*, 2022, ISBN: 978-3-942036-93-1

290 Schäfer Rodrigues Silva, Aline: *Quantifying and Visualizing Model Similarities for Multi-Model Methods*, 2022, ISBN: 978-3-942036-94-8

291 Moreno Leiva, Simón: *Optimal planning of water and renewable energy systems for copper production processes with sector coupling and demand flexibility*, 2022, ISBN 978-3-942036-95-5

292 Schönau, Steffen: *Modellierung von Bodenerosion und Sedimentaustrag bei Hochwasserereignissen am Beispiel des Einzugsgebiets der Rems*, 2022, ISBN 978-3-942036-96-2

293 Glatz, Kumiko: *Upscaling of Nanoparticle Transport in Porous Media,* 2022, ISBN 978-3-942036-97-9

294 Pavía Santolamazza, Daniela: *Event-based flood estimation using a random forest algorithm for the regionalization in small catchments*, 2022, ISBN 978-3-942036-98-6

295 Haun, Stefan: *Advanced Methods for a Sustainable Sediment Management of Reservoirs*, 2022, ISBN 978-3-942036-99-3

296 Herma, Felix: *Data Processing and Model Choice for Flood Prediction*, 2022, ISBN 978-3-910293-00-7

297 Weinhardt, Felix: *Porosity and permeability alterations in processes of biomineralization in porous media - microfluidic investigations and their interpretation*, 2022, ISBN 978-3-910293-01-4

298 Sadid, Najibullah: *Bedload Transport Estimation in Mountainous Intermittent Rivers and Streams*, 2023, ISBN 978-3-910293-02-1

299 Mohammadi, Farid: *A Surrogate-Assisted Bayesian Framework for Uncertainty-Aware Validation Benchmarks*, 2023, ISBN 978-3-910293-03-8

300 Praditia, Timothy: *Physics-informed Neural Networks for Learning Dynamic, Distributed and Uncertain Systems*, 2023, ISBN 978-3-910293-04-5

301 Gyawali, Dhiraj Raj: *Development and parameter estimation of conceptual snow-melt models using MODIS snow-cover distribution*, 2023, ISBN 978-3-910293-05-2

Die Mitteilungshefte ab der Nr. 134 (Jg. 2005) stehen als pdf-Datei über die Homepage des Instituts: www.iws.uni-stuttgart.de zur Verfügung.